Regenerative Electric Actuators for Active Control of Civil Structures

by

Allan C. Nerves

Dissertation submitted to the Faculty of the

Virginia Polytechnic Institute and State University

in partial fulfillment of the requirements for the degree of

DOCTOR OF PHILOSOPHY

IN

ELECTRICAL ENGINEERING

APPROVED:

Krishnan Ramu, Chair

Hugh F. VanLandingham

Mahendra P. Singh

William T. Baumann

John S. Bay

December 10, 1996
Blacksburg, Virginia

Keywords: Regenerative, Actuator, Control, Structure, Wind, Earthquake

REGENERATIVE ELECTRIC ACTUATORS FOR ACTIVE CONTROL OF CIVIL STRUCTURES

by

Allan C. Nerves

Prof. Krishnan Ramu, Chairman

Electrical Engineering

(ABSTRACT)

A novel technique is investigated for utilizing the motion caused by environmental forces on a civil structure to generate electrical energy when the structure's response is within safety limits. When strong winds and earthquakes occur, the utility power source which supply energy to the actuator in an active control system is usually not reliable. With a regenerative electric actuator, recovered energy can be used to reduce the peak oscillations of the structure by applying forces (through actuators which use the recovered energy) counter to the environmental forces even if the utility power is not available. The use of a regenerative electric actuator allows a precise control of the amount of damping being provided by the actuator. Another advantage of using regenerative electric actuators is the reduction of the required energy capacity of the electrical source. This translates into lower energy ratings for the electrical source, and lower equipment and maintenance costs. This study is the first of its kind to propose and investigate active control of civil structures using regenerative electric actuators. This study is also the first of its kind to investigate the applicability of sliding mode control to civil structures using regenerative electric actuators. Sliding mode control provides a natural synthesis of the on-off nature of pulse width modulation control and control force saturation, and guarantees stability for the control law. It is also invariant to parameter changes and external disturbances. New direct-control schemes for neural network and adaptive fuzzy control of civil structures using regenerative electric actuators are proposed and investigated. These allow on-line control of the structure without the need for either an accurate model of the system or a specific learning stage. Since the error at the output of these controllers will be unknown in the direct-control scheme, the error at the system output is used to train or update the controller parameters. Simulations are conducted for wind and earthquake excitations using linear and nonlinear models. It is shown that the use of regenerative electric actuators is a viable and a reliable alternative for active control of civil structures.

To Maria Nona and Alana Rae

Acknowledgments

I would like to thank my advisor, Prof. Krishnan Ramu, for his guidance and encouragement. My thanks to all members of my academic committee, Prof. VanLandingham, Prof. Singh, Prof. Baumann, and Prof. Bay, for their interest and enthusiasm for my work.

I would like to express my gratitude for the financial support provided by the Philippine Department of Science and Technology.

I would like to thank the members of the Motion Control Systems Research Group for their help and support in the completion of this work.

My sincere thanks to my family and friends who provided moral support and encouragement.

Above everything else, I thank Him Who is the Source of all knowledge.

Table of Contents

List of Figures

List of Tables

Nomenclature

m_s	mass of the structure
k_s	spring or stiffness coefficient of the structure
c_s	damping coefficient of the structure
$u(t)$	control force
$f(t)$	external excitation force
y_s	structure's displacement with respect to an inertial reference frame
z_s	structure's displacement with respect to the ground
$\mathbf{A}$	system matrix
$\mathbf{B}$	control coefficient matrix
$\mathbf{H}$	disturbance coefficient matrix
$\mathbf{w}$	external disturbance vector
$\mathbf{x}$	state vector
$\mathbf{u}$	vector of control forces
$\ddot{y}_0$	ground acceleration
F_k	restoring force due to the spring/stiffness element
α	ratio of postyielding to preyielding stiffness
D_y	yielding displacement
v	nondimensional auxiliary variable
$\lambda, \beta, \gamma, \eta$	hysteresis parameters of stiffness element
y_d	damper's displacement with respect to an inertial reference frame
z_d	damper's displacement with respect to the structure
y_0	ground displacement with respect to an inertial reference frame
m_i	mass of floor i
c_i	damping coefficient of floor i
k_i	stiffness or spring coefficient of floor i
y_i	displacement of floor i with respect to an inertial reference frame
f_i	wind force exerted on floor i
u_i	control force exerted on floor i
$\mathbf{M}$	mass matrix
$\mathbf{C}$	damping coefficient matrix
$\mathbf{K}$	stiffness coefficient matrix

$\mathbf{y}$	vector of displacements with respect to an inertial reference frame
z_i	relative displacement between floor i and floor i-1 or between floor i and the ground
$\mathbf{m}$	vector of masses
$\mathbf{f}$	vector of wind forces
m_b	mass of the base floor
c_b	damping coefficient of the base floor
k_b	stiffness coefficient of the base floor
z_b	displacement of the base floor with respect to the ground
m_d, m_g	mass of the damper
c_d, c_g	damping coefficient of the damper
k_d, k_g	stiffness coefficient of the damper
$\mathbf{G}$	actuator infuence matrix
$\mathbf{F}_c$	vector of nonlinear damping forces
$\mathbf{F}_k$	vector of nonlinear stiffness forces
$\mathbf{K}_e$	elastic stiffness coefficient matrix
$\mathbf{K}_i$	inelastic stiffness coefficient matrix
$\mathbf{v}$	vector of auxiliary variables
u_k	control force exerted by active variable-stiffness device
$k(z)$	variable stiffness coefficient
z	interstory deformation
c_c	viscous damping coefficient of active variable damper
u_c	control force exerted by active variable-damping device
n	positive number
f_w	wind force
p	magnitude parameter of wind force
ω	frequency parameter of wind force
K	proportional feedback gain
T_d	actuator time delay
T_m	measurement time delay
$p_a(t)$	actuator instantaneous power
$e_a(t)$	energy drawn by the actuator from the electrical source
Z_{pas}	maximum interstory drift for passive control
Z_{pro}	maximum interstory drift for proportional control

R_{pas}	root-mean-square value of interstory drift for passive control
R_{pro}	root-mean-square value of interstory drift for proportional control
Y_{pas}	maximum displacement with respect to the ground for passive control
Y_{pro}	maximum displacement with respect to the ground for proportional control
$\mathbf{A}_d$	discrete-time system matrix
$\mathbf{E}_d$	discrete-time input matrix
$\mathbf{r}(k)$	discrete-time input vector
$\mathbf{a}(\mathbf{x},\mathbf{u},t)$	n-vector function
$\mathbf{u}^*(t)$	admissible control
$\mathbf{x}^*(t)$	admissible state trajectory
J	performance index
$h(\mathbf{x},t)$	scalar function
$g(\mathbf{x},\mathbf{u},t)$	scalar function
t_0	initial time
t_f	final time
$\mathcal{H}$	Hamiltonian function
$\mathbf{p}(t)$	vector of Lagrange multipliers or costate variables
δx_f	variations in the final state
δt_f	variations in the final time
$\mathbf{x}_0$	final state
H, **Q**	real, symmetric, positive semi-definite weighting matrix
R	real, symmetric, positive definite weighting matrix
$\mathbf{p}^*$	admissible costate trajectory
P	Riccati matrix
K	feedback gain matrix
α, β	scalar weights
I	identity matrix
Q11	first diagonal element of **Q**-matrix for single-degree-of-freedom system
Z_{lq}	maximum interstory drift for linear quadratic control
R_{lq}	root-mean-square value of interstory drift for linear quadratic control
Y_{lq}	maximum displacement with respect to the ground for linear quadratic control
q_{11}, q_{22}	scalar factor in **Q**-matrix
$\mathbf{f}(\mathbf{x},t)$	vector of nonlinear state functions
σ	switching manifold

σ_i	ith switching surface
$\mathbf{S}$	coefficient matrix of switching surface
$\mathbf{u}_{eq}$	equivalent control
$\mathbf{v}$	external disturbance
$\Delta\mathbf{A}$, $\Delta\mathbf{B}$	system perturbation
$\mathbf{T}$	orthonormal transformation matrix
$\mathbf{z}$	transformed state vector
$\mathbf{A}_{11}$, $\mathbf{A}_{12}$	partition of transformed system matrix
$\mathbf{A}_{21}$, $\mathbf{A}_{22}$	partition of transformed system matrix
$\mathbf{0}$	null matrix
$\mathbf{B}_2$	partition of transformed control matrix
$\mathbf{S}_1$, $\mathbf{S}_2$	partition of coefficient matrix for switching surface
$\mathbf{z}_1$, $\mathbf{z}_2$	partition of the transformed state vector
$\mathbf{Q}$	constant, symmetric, positive definite weighting matrix
t_s	time it takes to reach the sliding manifold
$\mathbf{Q}_{11}$, $\mathbf{Q}_{12}$	partition of weighting matrix $\mathbf{Q}$
$\mathbf{Q}_{11}$, $\mathbf{Q}_{12}$	partition of weighting matrix $\mathbf{Q}$
q_i	diagonal element of weighting matrix $\mathbf{Q}$
s_{ij}	element of switching surface coefficient matrix $\mathbf{S}$
$\mathbf{K}$	switched feedback-gain matrix
k_{ij}	element of feedback-gain matrix $\mathbf{K}$
Ψ	matrix of boundary values for switched feedback gains
ψ_{ij}	boundary values of switched feedback-gains
Z_{sm}	maximum interstory drift for sliding mode control
R_{sm}	root-mean-square value of interstory drift for sliding mode control
Y_{sm}	maximum displacement with respect to the ground for sliding mode control
d	desired plant output
y	plant output
u_k	kth output of the neural network controller
y_q	qth plant output
e_q	error at the qth plant output
d_q	qth desired plant output
n_q	weighted-sum of inputs to the plant's output unit q
a_q	output of neuron unit q

$f(n_k)$	activation function
w_{ij}	connection weight between units i and j
η	learning rate
K_i	input scaling factor
G, K_o	output gain factor
E_u	squared-error at output of fuzzy controller
u_d	desired output of fuzzy controller
E_y	squared-error at system output
e_y	system output error
θ	fuzzy controller parameter
μ_{ji}	degree of membership of jth input for rule i
$\bar{u}_i$	center of the output membership function for rule i
$\bar{x}_{ji}$	center of the jth-input's membership function for rule i
σ_{ji}	spread of the jth-input's membership function for rule i
m_c	momentum factor
n_t, n_{tg}, n_{td}	linear-to-rotational transformation ratio
T_L	load torque
T_e, T_{eg}, T_{ed}	actuator electromagnetic torque
J	moment of inertia of actuator
B	rotational damping coefficient of actuator
ω	angular speed
e	efficiency
p	pitch
v_{ks}	voltage of phase k
i_{ks}	current of phase k
R_s	stator phase resistance
L_{ii}	self-inductance of phase i
L_{ij}	mutual inductance between phases i and j
e_{ks}	induced electromotive force (emf) for phase k
E_p	peak value of induced emf
K_b	induced-emf constant
ω_r	rotor speed in electrical radians per second
P	number of poles

ω_m	rotor speed in mechanical radians per second
$f(\theta_r)$	position-dependent function
θ_r	rotor position in electrical radians
I_p^*	current magnitude command
T_e^*	torque command

CHAPTER 1

Introduction

1.1 THE PRINCIPLE OF REGENERATIVE ELECTRIC ACTUATION

Mitigation of wind- and earthquake-induced oscillations in civil structures, such as buildings, is of crucial importance for the safety of the people in the building and for the protection of the structural integrity of the building itself. Passive damping in the form of tuned mass dampers (TMD) is a widely prevalent practice for tall buildings. Basically, a TMD consists of a mass attached to a structure such that it oscillates at the same frequency as the structure but with a phase shift. It is found that the TMDs have better performance with wind forces than with earthquake excitations. To counter this high frequency excitation of the earthquake, various semi-active control methodologies have come to fore recently. All of these rely on energy for actuation from an external supply which most likely is the utility power supply. As the utility power supply itself may be under threat and therefore unavailable during strong-wind and earthquake episodes, it is important that the energy source to counter the oscillations of the building must itself be derived from these oscillations. The energy from the environmental forces could be converted into electrical energy and stored for re-use by an actuator which produces a counter-force to the environmental forces. Therefore, the actuator has to be an electrical one as it can handle energy flow in both directions, i.e., it can generate electrical energy when given a mechanical input (generation mode) as well as produce mechanical energy when given an electrical input (motoring mode). The interconnection between the building and the electric actuator is through the medium of the tuned mass damper. It must be noted that during generating and motoring modes, the energy taken out of the TMD can be precisely controlled. That indirectly amounts to a controlled damping of the building. This is a significant factor because the controlled damping is able to accommodate most safety criteria for the building displacement, velocity, acceleration, inter-story shift and its velocity, etc.

The electric actuation being proposed has the unique advantage of being able to operate even in the absence of a power source such as the utility power supply. This is unlike other or most of the semi-active and active control systems being proposed for civil structures. Therefore, the reliability of the control system is increased manifold, hitherto considered impossible both in concept and in practice. Furthermore, the electric actuation has the advantage of controlling the damping during both the energy-acquisition mode and in the force-application mode. Therefore,

control is guaranteed at all times, unlike other systems. The space and volume requirements for the electric actuator seem to be feasible and within the constraints of the housing required for most of the other control systems. Hence, it should not be of any concern from the point of view of implementation.

1.2 OBJECTIVES OF THE STUDY

The study makes the following original contributions: (1) The study is the first of its kind, to propose and investigate active control of civil structures using regenerative electric actuators. (2) The study investigates a sliding mode controller for regenerative electric actuators (REA), with a control structure composed of linear feedback with switched gains. Other researchers have concentrated on a control structure composed of a sum of the equivalent control and an augmentation of this equivalent control. The performance of the proposed sliding-mode controller is evaluated for both wind and earthquake excitation. Previous studies considered only earthquake excitation. (3) While other studies have focused on indirect-learning or generalized-learning architectures, the present study proposes a neural network controller for the REA with a specialized-learning architecture. This allows the controller to be trained on-line and fine-tuned while performing its function. Hence, it is able to operate even in the presence of nonlinear or time-varying system parameters or operating conditions. Investigations are made for both wind and earthquake excitation. (4) Lastly, an adaptive fuzzy controller for the REA is proposed. It uses a steepest-descent algorithm as the adaptation mechanism. Previous investigations considered only nonadaptive schemes or neuro-fuzzy structures.

A novel technique is investigated for utilizing the motion caused by environmental forces on a civil structure to generate electrical energy when the structure's response is within safety limits. When strong winds and earthquakes occur, the utility power source which supply energy to the actuator in an active control system is usually not reliable. It is during these instances that active control is needed most. With a regenerative electric actuator, the recovered energy is used to reduce the peak oscillations of the structure by applying forces (through actuators which use the recovered energy) counter to the environmental forces even if the utility power is not available. To achieve this, a tuned mass damper is used as the intermediary for the energy transfer between the structure and the actuator. The use of a regenerative electric actuator allows a precise control of the amount of damping being provided by the actuator. Another advantage of using regenerative electric actuators is the reduction of the required energy capacity of the electrical source. This translates into lower energy ratings for the electrical source, and lower

equipment and maintenance costs. This study is the first of its kind to propose and investigate active control of civil structures using regenerative electric actuators.

Although no original contribution is being claimed for proportional control, it can be used as a benchmark against which controllers for the regenerative electric actuator are evaluated. The effect of variations in gain, actuator time delay, and measurement time delay on the structural response is investigated. Differences between the results of a linear and a nonlinear simulation and the effect of control force saturation are also studied.

For wind excitation, it is shown that proportional feedback control can provide effective control. However, the reduction in the structure's displacement is accompanied by an increase in the control force and the stroke length. The use of feedback control generally reduces the damping of the mass damper which, in turn, increases the stroke length. A certain amount of gain variation can be tolerated without any significant increase in the displacement. Critical values of the actuator time delay and measurement time delay have to be determined. Feedforward control can also be used for wind-excited structures. Critical values for the gain, actuator time delay, and measurement time delay determine the limits of effectiveness for this type of control. Simulations are conducted for a single-degree-of-freedom system , a fixed-base multistory building, and a base-isolated multistory building.

Feedback and feedforward proportional control of the single-degree-of-freedom system under earthquake excitation is not effective. It is only slightly effective for a base-isolated multistory building. It is shown that regeneration can be achieved while under proportional control.

Although no original contribution is being claimed for linear quadratic (LQ) control, it provides a benchmark against which controllers for the regenerative electric actuator are evaluated. Since environmental disturbances are seldom known *a priori*, the regulator solution presented is used to search for the best closed-loop control law for structures subjected to unknown disturbances. This is done by determining the response of the controlled structure when subjected to some assumed disturbances. The best regulator is one which performs well for most of the assumed excitations and those excitations which closely resemble the actual disturbances.

The LQ controller is tested on a single-degree-of-freedom system, a fixed-base multistory building, and a base-isolated multistory building. Increasing the weight on the displacement produces a reduction in the displacement at the cost of increasing the control force and damper stroke. The LQ controller is shown to be effective for both wind and earthquake excitations. However, peak reduction seems to be a problem in earthquake-excited cases. Various criteria are suggested for choosing the weighting matrices.

To improve control efficiency, limits can be set on the control force to reduce stroke length without compromising the displacement response. The LQ controller provides opportunity for regeneration. In some cases with sufficient duration of the excitation, there is even a net gain in the source energy

This study is the first of its kind to investigate the applicability of sliding mode control to civil structures, with special emphasis on the mitigation of wind- and earthquake-induced motion in tall buildings using regenerative electric actuators. The rationale for using sliding mode control is the fact that regenerative electric actuators use a form of on-off control based on pulse width modulation (PWM). Sliding mode control provides a synthesis of this on-off nature of PWM control and guarantees stability for the on-off control law. Furthermore, sliding mode control naturally fits the nonlinear, on-off nature of control force saturation which is always present in the active control of civil structures. Again, sliding mode provides a natural synthesis of the on-off nature of control force saturation and guarantees stability for the on-off control law.

Both linear and nonlinear models of the structure are considered in this study to assess the sliding mode controller's performance during disturbances. It is shown that the controller is able to overcome sensitivity to structural parameter variations, particularly structural stiffness. Systematic procedures for the design of the sliding surface, using both pole-placement and quadratic-minimization methods, are presented together with simulation results obtained by using linear and nonlinear models of the structure. These controllers are also shown to be effective even in the presence of control force saturation. With sliding mode control, the regenerative electric actuator is able to recover energy and store it for later use. This reduces the net energy drawn from the supply by the actuator. In some cases, there is even a net gain in the energy of the supply.

A new direct-control scheme for neural network control of civil structures using regenerative electric actuators is proposed. This allows on-line control of the structure without the need for either an accurate model of the system or a specific learning stage. Unlike the controllers that have previously been considered, the neural network controller is able to address changes in system parameters and changes in the operating point and external disturbances. A modified backpropagation algorithm is used to train the neural network. Since the error at the output of the neural network controller will be unknown in the direct-control scheme, the error at the system output is instead backpropagated through the system by considering the system as an additional layer of the neural network. Simulations are conducted for wind and earthquake excitation using a two-layer network composed of neurons with tangent-sigmoid activation functions. It is shown that the controller can tolerate large variations in the input scaling factor,

output gain factor, and maximum control force. It is also equally effective for both linear and nonlinear models of the structure.

A new on-line, direct-control scheme for active control of civil structures using an adaptive fuzzy controller is proposed. The advantage of using an adaptive fuzzy controller is that it does not require an accurate model of the system. The controller learns the system dynamics by adapting its parameters on-line. It is proposed that a modified gradient descent method be used as the adaptation mechanism. In order to adapt the parameters of the fuzzy system, the error at the output of the fuzzy controller must be known. In the proposed direct-control scheme, this error is unknown. Thus, it is proposed that the updating be based on the output error of the system directly. The update equations are derived for the controller. Simulations are performed for a structure with a regenerative electric actuator.

After investigating the feasibility of various controllers for application in structures with regenerative electric actuators, a comparison is made of the different controllers based on various criteria. The major factors that have to be considered when choosing a controller for the regenerative electric actuator include maximum displacement, stroke length, control force, actuator power, and actuator energy. Control force saturation has to be considered in order to obtain the most effective type of control. When choosing a controller for the regenerative electric actuator, the final decision has to consider all of the above-mentioned factors. A compromise may be required if conflicting objectives have to be satisfied.

The actuator proposed for this study is a permanent-magnet brushless DC machine which can provide a higher instantaneous torque in a compact frame size. The actuator can either operate in the passive mode, 4-quadrant mode, or 2-quadrant generation mode. In the 4-quadrant mode, the performance of various controllers are compared based on the maximum displacement, stroke, control torque, actuator power, and source energy. It is desired that the controller require a smaller actuator power rating so that the cost of the machine will be lower. A lower actuator energy is also desired so that the capacity of the electrical source will be lower. Furthermore, a lower energy requirement means that a lower capacity for the energy storage device is needed. In majority of the test cases, sliding mode control often has the lowest power and energy requirement. The use of regenerative electric actuators reduce the required source capacity as compared to using non-regenerative actuators which simply dissipate energy as heat. The amount of reduction is often significant. This can translate to savings in equipment and maintenance costs. Single-degree-of-freedom and multidegree-of-freedom structures are simulated. In the regeneration mode, the system response must always fall within the safety margins for the

structure. The amount of energy that can be recovered is limited by the power rating of the actuator and the energy capacity of the electrical source and storage device.

The dynamics of the electrical subsystem can be incorporated into the actuator-structure system to determine the transient behavior of the entire system. The equations of motion are derived for the combined system. In order to obtain a preliminary estimate of the system response, it is initially assumed that the commanded control T_e^* is also the actual control T_e. It is shown that this assumption is valid, due to the faster time constants of the electrical subsystem compared to those of the mechanical subsystem. This is one of the advantages of using an electrical actuator. More accurate models of the electrical source and storage device can also be included in the simulation to determine the variation of the voltage at the terminals of the source. In this study, the electrical source is modeled as an ideal voltage source in series with a source resistance.

This study shows that the use of regenerative electric actuators is a viable and a reliable alternative for active control of civil structures.

1.3 SCOPE OF THE STUDY

The present study has the following scope: (a) The study is limited to discretized, deterministic structural systems with lumped parameters. (b) The study focuses on active control schemes that use active or semi-active mass damper systems. This is a prerequisite for implementing regenerative electric actuators. (c) Although this study focuses only on mass damper systems the control laws that are being proposed can still be applied to systems with other forms of actuation, aside from REA. (d) Only feedback control is emphasized due to problems with time delay and phase in feedforward control.

1.4 METHODOLOGY

Since the proper implementation of regenerative electric actuators for active control of civil structures has to take into account the nature of the load it is controlling, i.e. the civil structure, the design process entails a systematic survey of various controllers. These include classical linear, nonlinear, and intelligent controllers. Hence, benchmarks have to be established against which any proposed controller is evaluated. Although no original contributions are being made in proportional or linear quadratic control, these control types are investigated in order to provide the necessary benchmarks.

In simulating a civil structure's response under control, it is considered necessary to include both mechanical and electrical dynamics of the REA. Thus, coupled sets of equations are

eventually used in the investigation. To obtain an initial estimate of the response, actuator dynamics is neglected. Then the mechanical dynamics of the actuator is introduced. Finally, the machine drive dynamics (electrical) are included to obtain a more accurate simulation.

1.5 ORGANIZATION OF THE STUDY

Chapter 2 provides a survey of various passive, active, and semi-active control schemes. The system equations are derived in Chapter 3. Chapter 4 addresses the problem of determining the effect of variations in gain, time delay, and measurement time on proportional feedback controllers. The significance of control saturation is also tackled. Chapter 5 applies linear quadratic control to civil structures. Chapter 6 introduces sliding mode control which addresses the problem of uncertain, time-varying, and nonlinear system characteristics. Neural and fuzzy control are explored in Chapter 7 and Chapter 8 as model-free controllers which require minimal system information. Only feedback forms of the preceding controllers are emphasized. This is due to problems in time delay and phase shifts encountered in feedforward control schemes. Chapter 9 compares the merits and demerits of the different controllers being considered. After looking at these various candidates for the controller in the regenerative electric actuation scheme, the entire system is simulated and analyzed in Chapter 10.

CHAPTER 2

Active Control of Civil Structures

2.1 INTRODUCTION

This chapter presents a survey of the existing technology and research in the area of active control of civil structures. This provides a broader view of the problem being addressed by regenerative electric actuation. The ever-increasing demand for tall structures is due to considerations in cost, convenience of having almost every office or residential function under one roof, lack of land space, congestion due to increasing population in many parts of the world, etc. Tall structures bring with them a good number of problems to be solved. This chapter presents the need for control of tall civil structures, and the role and importance of modern control theory in this endeavor to modify the structural characteristics so that the structure can overcome and survive the impact of environmental disturbances. Broadly, three types of control systems emerge in this arena: passive, active, and hybrid control systems. The merits and demerits of each of these control systems are discussed; then methods for their implementation are presented. A qualitative discussion of the various subsystems which comprise the control system is provided. These subsystems can be base isolation systems, mass-effect systems, energy absorption systems, active variable-stiffness systems, active bracing systems, tuned liquid dampers, electrorheological dampers, and various kinds of actuators which produce the active force required. Finally, problems facing the use of various control strategies in the implementation of active and hybrid control are highlighted. These control strategies constitute the central theme of this monograph.

2.2 THE NEED FOR CONTROL IN TALL STRUCTURES

In the past, it was considered acceptable for buildings and infrastructures to incur damage and their functions as facilities to be affected, as long as they resisted collapse to protect human life. However, this design philosophy for structures is no longer adequate for the demands of society in the present times [1]. Today's society must be able to efficiently transport people, goods, energy, and information. We now live in a society which requires highly sophisticated information. A total loss of important data or vital information would create panic and chaos. Today's society must be able to provide clean air and water, control disease, and conduct commerce. Therefore, the fundamental requirement that structures protect human lives is no

longer sufficient. It is getting more important that the fundamental function of society be protected as well, especially in the event of a natural disaster [2].

In recent years, significant advances in construction technology and materials have brought about the design and construction of light-weight and flexible structures, such as high-rise buildings and long-span bridges. It is expected that building heights and bridge lengths will gradually increase in the near future. These structures are characterized by lower stiffness and higher strength-to-mass ratios. Unfortunately, such characteristics make these structures extremely susceptible to environmental loads, such as earthquakes and strong winds. These random loadings usually produce large deflections and accelerations on these structures. Once oscillations in the structure have started, they will usually continue on for considerable periods with very little additional input from the environmental excitation. This can be attributed to the fact that a structure's inherent damping is very low. In some cases, the structure's motion can induce additional aerodynamic forces which could lead to a phenomenon with positive feedback called flutter [3].

This trend towards taller and lighter structures with increased flexibility and minimal damping will produce structures that are highly sensitive to environmental excitation. Aside from the possible failure and damage in various structural members, occupant comfort is becoming an even more important issue as the number of tall business and residential buildings increase. Although not necessarily a threat to the safety of the structure, excessive accelerations in the higher levels of a tall building during a wind storm or a weak to medium earthquake can cause considerable discomfort or even illness to occupants. Therefore, a design for one of these structures must provide safety and integrity to the structure, while also providing a measure of comfort for its occupants. Additional constraints on the design include the demand for extreme reliability under highly uncertain loading conditions, the differences in the strength and behavior of the actual structural components as opposed to their design characteristics, and the errors introduced during construction [4]. To safeguard against the above uncertainties and the potential for extensive physical damage and loss of life, past designs have traditionally adopted a very conservative approach. However, adopting the conventional design methods used for shorter buildings usually results in unacceptably high costs. Alternatives have to be found to satisfy safety requirements, comfort considerations, and economic constraints.

Driven by the demand for higher safety levels and more stringent performance requirements, engineers have turned to control theory to provide solutions to cost-effective protection of tall civil structures against earthquakes, winds, and other environmental disturbances. At the same time, recent advances in electronic data acquisition, transmission,

processing, and storage have increased the economic viability of performing real-time monitoring and control of structural systems.

Although it is impossible to precisely predict the ground motion during an earthquake or the wind force during a hurricane, the structure itself can be adjusted in a positive manner to protect it from these environmental forces. Therefore, the basic concept of structural control is the artificial adjustment of a structure's dynamic properties, such as stiffness and damping [2]. By regulating the pertinent structural characteristics, a desirable structural response is ensured whenever the structure is subjected to random disturbances. The desired response is obtained by supplementing the basic structure with mechanisms that generate control forces which cancel the effect of a disturbance.

2.3 METHODS OF CONTROL

Structural response can be controlled by (a) cutting off the input energy from the disturbance, which is highly impossible because the structure cannot be completely isolated from the ground or shielded from wind disturbances, (b) modifying the natural frequencies of the structure from the predominant power components of the disturbance, (c) providing nonlinear structural characteristics to establish a nonstationary state and a nonresonant system, (d) supplying a control force to suppress the structural response induced by the disturbance, and (e) utilizing an energy absorption mechanism [5]. Structural control systems can be classified into passive, active, or hybrid control systems. This general classification is based on whether or not they require an external energy supply to restrain and control the response of a structure to external disturbances.

Passive control systems do not require an external power source in order to operate. In most cases, the mechanical properties of systems of this type cannot be modified. Most of these systems are aimed at augmenting structural damping or shifting the natural frequencies of the structure. Energy dissipating devices are introduced into the structure to absorb energy. The motion of the structure produces relative motion within these damping devices which, in turn, dissipate the energy. Energy is dissipated through various mechanisms like yielding of mild steel, viscoelastic action in rubber-like materials, sloshing of fluid, shearing of viscous fluid, orificing of fluid, and sliding friction [6]. The advantage of the passive control system is that it does not need an external power supply and is therefore maintenance-free and mechanically simple. The energy dissipating devices can also be replaced if they suffer extensive damage. A disadvantage of the passive system is that it is effective only for excitation frequencies within a narrow band and is not very effective for transient vibrations caused by nonstationary excitation [7]. In

addition, the passive control mechanisms are only able to control the structural response up to a certain limit. The cost of the system also increases when more stringent requirements have to be satisfied above those required for optimum design [8].

Active control systems require a significant amount of external power in order to operate. They also require continuous monitoring of the structural response and/or the environmental load disturbance. With a chosen control algorithm, these measurements are used to determine an appropriate control action. Active systems can be divided into fully-active systems and semi-active systems. Fully-active systems use the supply energy to generate control forces which directly resist the external disturbance, while semi-active systems use the supply energy to change the parameters of the structure to counteract the disturbance [9]. A number of advantages can be cited for active control systems. Active systems have superior effectiveness in reducing vibration amplitudes; the degree of effectiveness being limited only by the capacity of the control system. Compared to passive systems, active systems are more flexible because they are able to control the structure for a broader range of loadings, wider range of excitation frequencies, and transient vibrations. Thus, active systems can be used for motion control during both earthquakes and strong winds. Also, existing structures can be retrofitted with active controllers without any substantial modification to the structures. Depending on the control algorithm being used, the control objectives can be chosen to suit the functions of the structure and the needs of its occupants. This has the distinct advantage of having custom-made control software being used for standardized hardware, which leads to higher reliability and a lower cost for system design, development, integration, and application. Furthermore, the control hardware can be employed in a distributed manner, resulting in smaller and compact motion-control hardware subsystems. This is immensely important for large-scale deployment of such control systems due to its low cost and the high reliability afforded by large-scale manufacturing of these systems. Such is not the case with passive control systems which require specific hardware designs for each and every structure. Therefore, the passive approach to control of structures results in higher engineering costs. At present, active control systems also have their drawbacks. The amount of energy required to generate the control forces within a small time interval may be too great to be economical and practical. In addition, the time at which the control power is most needed often coincides with the time at which most utility systems fail. The availability of adequate energy sources is therefore a real concern. At the same time, the high level of maintenance for the control system makes the cost of the structure expensive. There is also the question of reliability of infrequently-used equipment since an active control system may remain in standby mode for a long time due to the rare occurrence of earthquakes or strong winds. The

large control forces can also be as detrimental as the environmental forces if the control system does not function properly. Finally, occupants of the structure may have some psychological reservations about the concept of active control [10]. Global stability must be assured for this type of control.

Hybrid control systems incorporates the best features of both passive and active control in a rational manner so as to reduce the disadvantages of both solutions. They have reduced power demands and improved reliability compared to a purely active system, and better control effectiveness and efficiency compared to a purely passive system. The energy required to generate control forces is smaller because of the suppressed structural response due to passive control devices. As in an active system, the mechanical properties of the structure are adjusted based on measurements of the structural response and/or excitation. The motion of the structure is used to develop control forces through the appropriate adjustment of the damping and stiffness characteristics, as in a passive system. Since the control forces are always directed opposite to the direction of structural motion, the stability of the system is ensured. In the event of a complete power failure, the hybrid system devices can be designed to exhibit either prescribed damping or stiffness characteristics and thereby making the system fail-safe [6].

Base Isolation Systems

Base isolation systems (BIS) have been shown to be an effective passive method for mitigating the transmission of horizontal seismic forces to a structure. However, they are not as effective in isolating the structure from any vertical component of seismic forces. Passive base isolation systems can be classified as either elastomeric bearing systems or sliding systems. In these schemes, the structure is mounted on either very flexible supports or sliding supports which effectively isolates the superstructure from the foundation. This decreases the natural frequencies of the structure and shifts them outside the range of excitation frequencies which have high energy content. Fig. 2.1 shows a passive base isolation system using elastomeric bearings. The lead-rubber bearings used for base isolation in elastomeric systems are flexible in the horizontal direction but stiff in the vertical direction [11]. However, since the natural frequencies of a structure are fixed quantities, passive base isolation will be effective only for a limited range of earthquake disturbances. There is also the possibility of producing strong uplift forces especially in the isolation system of tall structures. This could cause instability and eventual failure of the structure. Inelastic and permanent deformation can also accumulate after several seismic episodes in some base isolation systems using lead-core elastomeric bearings. An advantage of the sliding system over the elastomeric system is that the degree of isolation it provides is

dependent only on the coefficient of friction on the sliding interface, i.e. smaller coefficients give better isolation. Isolation performance is not dependent on the intensity nor the frequency of the earthquake excitation [11]. However, this type of isolation system is rendered impractical by its unavoidable residual displacement and excessive sliding displacement. Therefore, passive base isolation can become inadequate for earthquake protection of tall civil structures, aside from being ineffective against strong winds.

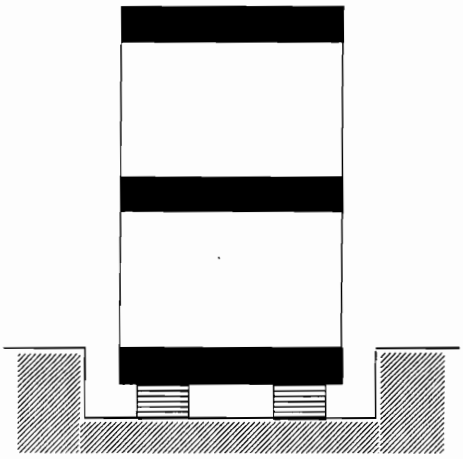

Fig. 2.1 Passive BIS using Elastomeric Bearings

There has been a growing interest in a hybrid system which combines base isolators with an active system that applies control forces on the base [11][12]. By itself, passive base isolation can reduce inter-story drifts and absolute accelerations in the structure which, in turn, causes the structure to behave like a rigid body. Although the shear force on the superstructure is small, the absolute displacement of the base itself is quite large. Active control forces applied at the base can reduce this displacement in both elastomeric and sliding systems. These control forces do not have to be large because the base isolators are either highly flexible or slides with minimal friction. Active elastomeric and sliding isolation systems are shown in Fig. 2.2 and Fig. 2.3 where A indicates an actuator. Hybrid systems which connect the base isolation system to either a tuned mass damper or an active mass damper [13] are also able to preserve the advantages of base isolation and protect the isolation system's integrity. Although typically installed on the top floor, setting the mass damper on the base of the structure makes it possible to dissipate the seismic energy before it is transmitted to the superstructure. Installation will also be easier and practical at the base level. Fig. 2.4 and Fig. 2.5 illustrate such hybrid systems. Sliding systems using variable-friction bearings, shown in Fig. 2.6, have been proposed wherein the coefficient of friction at the sliding interface is actively controlled. In these systems, the structure is supported

by a number of sliding bearings; each bearing is a carved-out steel disk with a sliding interface outside (circular perimeter) and a fluid chamber inside [14][15][16]. The chamber is sealed by a rubber O-ring around the circular perimeter just inside the sliding surface. A sliding material, such as a Teflon-based material, is placed on the sliding surface. A pressure-control system, composed of a pump, an accumulator, and a servo valve, is connected to the fluid chambers of all the bearings. The friction force on the sliding interface between the bearing and the ground is controlled by adjusting the fluid pressure in the chamber.

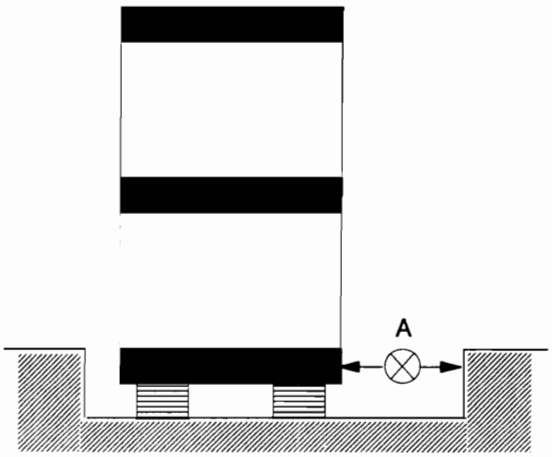

Fig. 2.2 Active Elastomeric BIS

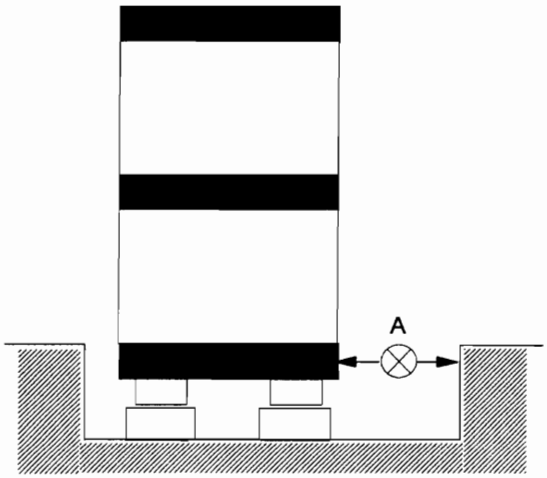

Fig. 2.3 Active Sliding BIS

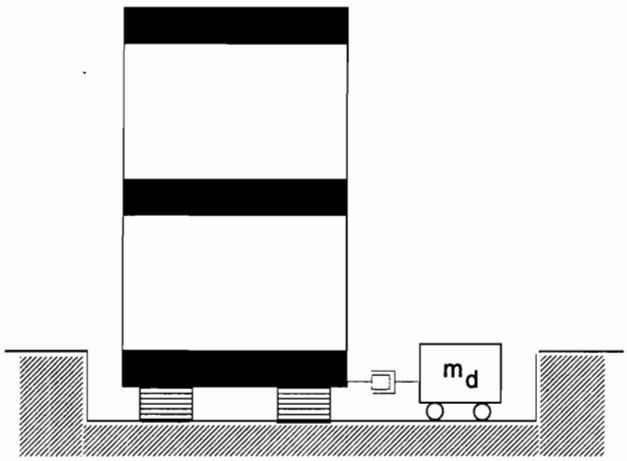

Fig. 2.4 Hybrid BIS with Tuned Mass Damper

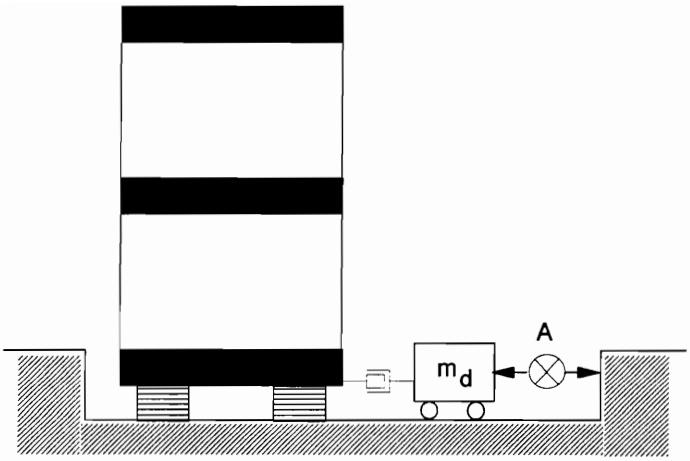

Fig. 2.5 Hybrid BIS with Hybrid Mass Damper

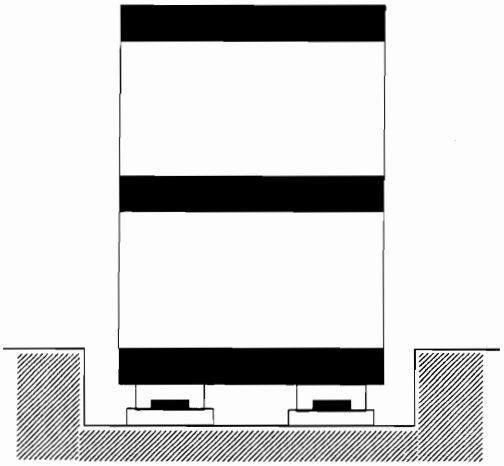

Fig. 2.6 Hybrid Sliding BIS with Friction-Controllable Bearings

Mass-Effect Systems

Mass-effect systems transform the input energy of a disturbance into the kinetic energy of a vibration mechanism added to a structure. This reduces the response of the structure and the energy with which the structure itself is forced to cope. The transformation of input energy to kinetic energy is achieved through the motion of an auxiliary mass. The moving mass produces inertia forces that gives the main structure large viscous damping. Therefore, it is important to keep the phase of the auxiliary mass opposite to that of the main structure. Mass-effect systems are primarily expected to reduce the first natural-mode vibration. The mass ratio, which is the ratio of the added mass to the effective mass of the structure, determines the system's damping effect. As the ratio gets higher, the control efficiency improves. Mass-effect systems can be

classified into passive, semi-active, active, and hybrid mass damper systems [17] as shown in Fig. 2.7, Fig. 2.8, Fig. 2.9, and Fig. 2.10, respectively. In these figures, the mass, stiffness, and damping of the structure are indicated as m_s, k_s, and c_s, respectively. m_d, k_d, and c_d are the corresponding damper parameters. The external excitation force is given as F_e. S and C are sensors and controllers, respectively. The actuator is labeled as A.

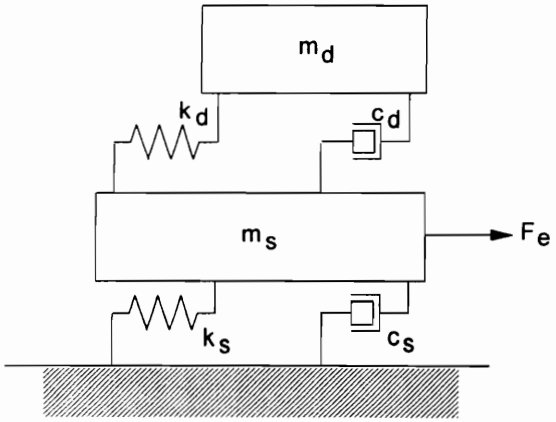

Fig. 2.7 Passive Damper System

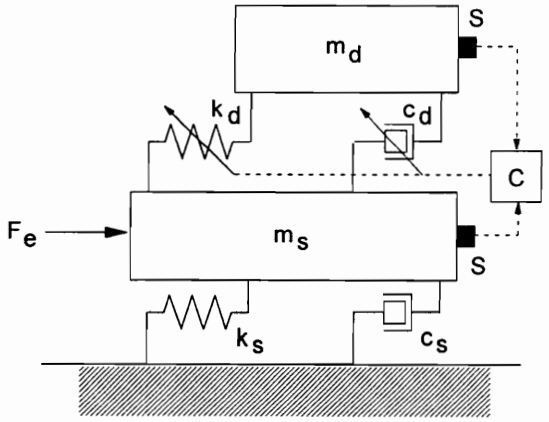

Fig. 2.8 Semiactive Damper System

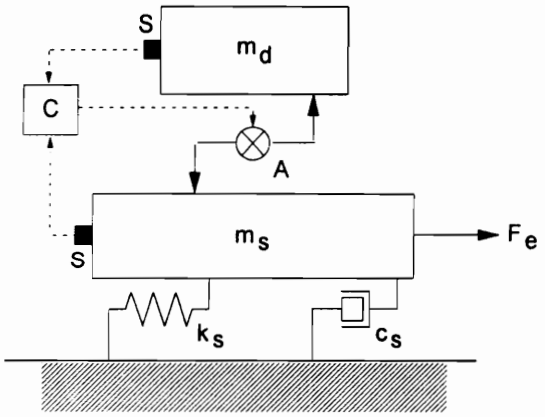

Fig. 2.9 Active Damper System

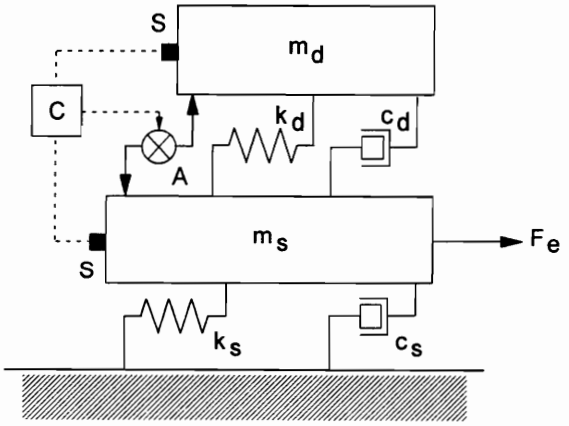

Fig. 2.10 Hybrid Damper System

The passive mass damper, which is commonly referred to as a tuned mass damper (TMD), is able to provide excellent control by optimum adjustment of its mass, spring, and damper elements. Most TMD systems have a 1% mass ratio for economic viability and construction simplicity. Tuned mass dampers are usually tuned to the first fundamental frequency of the primary structure. Therefore, they are only effective for structural control when the first mode is the dominant mode. Tuned mass dampers have been found to be effective in

reducing wind-induced vibrations in tall buildings. Since the input energy of an earthquake excitation is spread over a wider frequency band, the effectiveness of TMDs in reducing the response of tall buildings to severe earthquakes is still not completely settled at this time [18]. Another shortcoming of the passive mass damper system is its slow start-up. It can only become effective once the structure it is supposed to control has started moving. Therefore, it may not be able to provide the peak control force at the same instant that the peak response occurs. The amount of damping that a TMD can provide is determined by its stroke and the amount of added mass [19]. The stroke is the mass's relative displacement. As the natural period of the structure becomes longer and the input disturbance becomes stronger, the amplitude of vibration of the auxiliary mass also becomes larger. This means that a larger stroke would be required to reduce the response. Therefore, the stroke length could limit the TMD's usefulness. A variation of the tuned mass damper system is the doubly tuned mass damper (DTMD) consisting of two masses in series interconnected by springs and dampers to the main structure [20]. As in the TMD, it is also used to control a specific mode of vibration of a structure.

Since the tuned mass damper system does not have a response-monitoring system, it is unable to adapt and keep itself tuned to changes in the characteristics of the structure or the damper system itself. The semi-active mass damper system has its own set of sensors which enable it to make appropriate changes in the characteristics of its own spring and/or damper elements.

An active mass damper (AMD) system can reduce both the transient response of the structure and the mass stroke by introducing control forces using an external energy supply. In the AMD system, the spring and damper elements of a TMD system are replaced by an actuator, a controller and a set of sensors. Compared to a TMD, the AMD (a) has a better capability in reducing vibration amplitudes, (b) can reduce torsional vibrations, and (c) is effective for a wider frequency range. However, it requires a large amount of power to be able to control a tall structure. Equipment maintenance and the large capacities of the actuators also make the system expensive. Reliability of the energy supply and of the AMD system itself is an additional concern.

The hybrid mass damper (HMD) system combines the tuned mass damper with an actuator that generates a much smaller force than in an AMD. The HMD is more effective in vibration suppression than a TMD and much more energy-efficient and economical than an AMD. Since hybrid control systems can be considered as active control of passive systems, then control algorithms for AMDs can be directly applied to HMDs. Furthermore, the system is fail-safe to a certain degree since vibration energy will still be absorbed and dissipated by the spring

and damper elements even if the active subsystem fails. One implementation of an HMD system consists of an auxiliary mass being supported by multistage rubber bearings and an actuator being driven by an AC servomotor [21]. Another implementation, shown in Fig. 2.11, involves mounting a small AMD on top of a conventional TMD, which is in turn mounted on hollowed laminated rubber bearings [22]. The AMD weight is about 10% to 15% of the TMD weight. The bearings provide the passive TMD with adequate lateral stiffness. Vibration energy is dissipated by oil dampers connected between the TMD mass and the structure. The AMD actuator consists of an AC servomotor and a ballscrew mechanism.

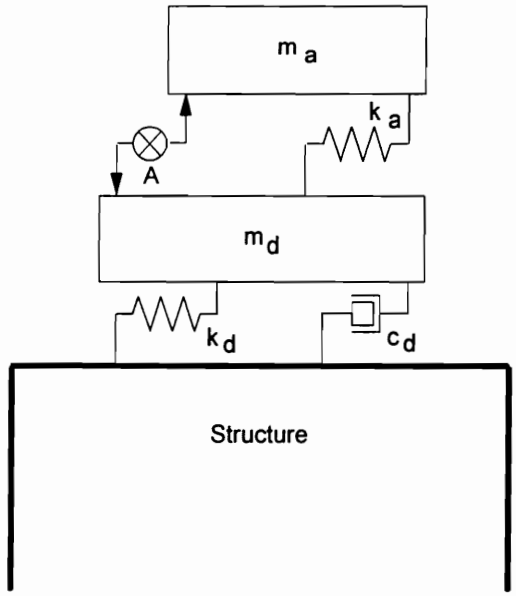

Fig. 2.11 Hybrid TMD/AMD System

Energy Absorption Systems

An energy absorption system or damping system reduces the response of a structure to an external excitation by absorbing the input energy of the disturbance and transforming it into thermal energy. In some respects, it is similar to a mass effect system without the auxiliary mass. The displacement or velocity response of the structure is used by the damping devices to dissipate the energy.

Passive viscoelastic (VE) dampers are usually installed on the diagonal braces between two floors of a structure. They can be used for retrofit or new structures. The damper absorbs and dissipates the vibrational energy through the shearing deformation produced by the structural

motion on the viscoelastic material [23]. The heat generated by the hysteretic behavior of the material is dissipated by conduction through the steel members of the damper.

Active Variable Stiffness System

The active variable stiffness (AVS) system controls the structural response due to an environmental disturbance by actively controlling the structural stiffness characteristics. Through a special bracing mechanism and a variable stiffness device (VSD), the AVS system switches and selects an appropriate stiffness distribution within the structure so that resonance does not occur with external excitation. Fig. 2.12 shows an AVS system.

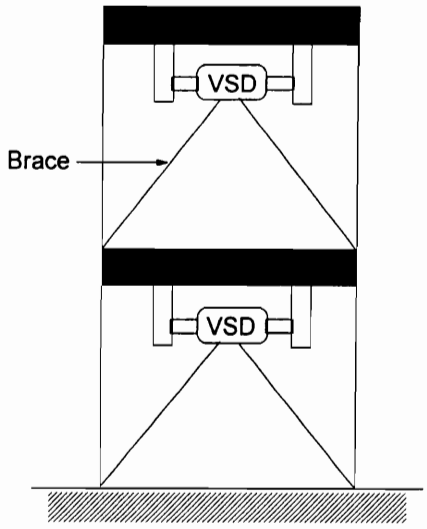

Fig. 2.12 Active Variable Stiffness System

Active Bracing System

The active bracing system (ABS), which is sometimes called the active tendon system (ATS), is composed of a set of prestressed tendons or braces connected to a structure. The tensions on these braces are actively controlled by actuators such as electrohydraulic mechanisms or electrical machines [24]. The system applies a horizontal control force at each floor of the structure. The ABS system is suitable for retrofitting an existing structure. Various ABS schemes are shown in Fig. 2.13, Fig, 2.14, Fig. 2.15, and Fig. 2.16.

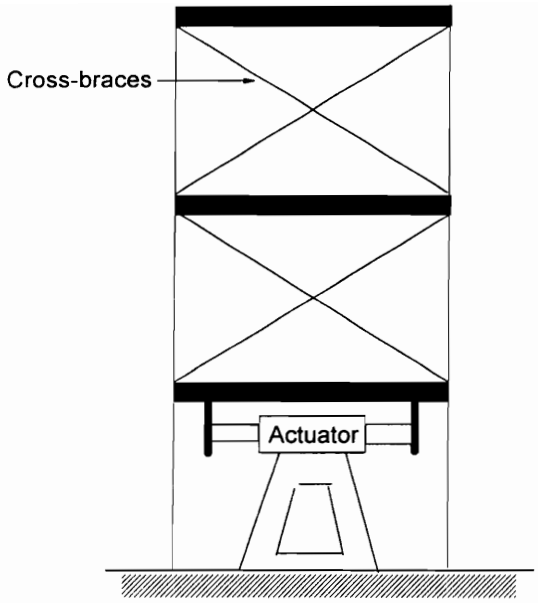

Fig. 2.13 Active Bracing System

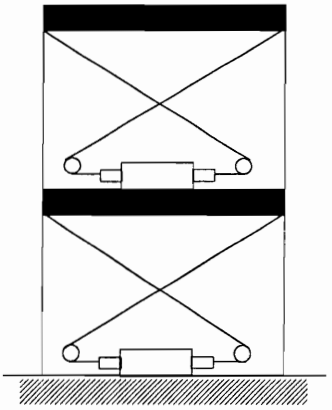

Fig. 2.14 Active Tendon System

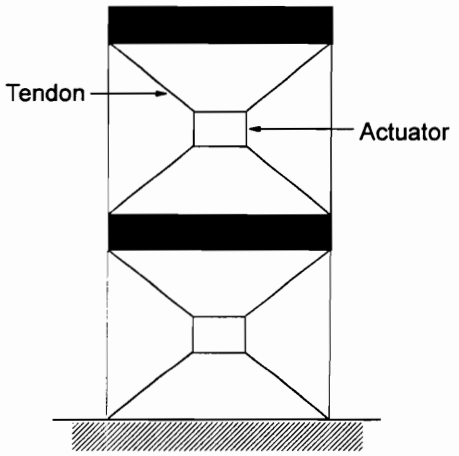

Fig. 2.15 Active Tendon System

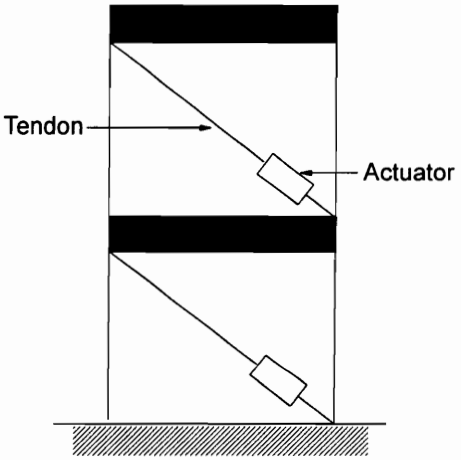

Fig. 2.16 Active Bracing System

Tuned Liquid Dampers

The tuned liquid damper (TLD) utilizes the motion of shallow liquid inside a rigid tank (shown in Fig. 2.17) to change the dynamic characteristics of a structure and dissipate its vibration energy [25]. The TLD provides indirect damping to the system through the sloshing liquid's absorption of the structural energy and its dissipation by the viscous action of the fluid, wave breaking, contamination of the free surface with beads, and container geometry at the surface [26]. Some of its advantages include: (a) simple construction at a relatively low cost, (b)

easy installation even in structures with space constraints, (c) easy adjustment, (d) can be used temporarily, (d) almost-zero trigger level, (e) no external damping device is required because the liquid provides inherent damping, (f) can be effective omnidirectionally, (g) possibly effective over a range of frequencies even in the passive mode since the TLD is a multi-degree-of-freedom system which can provide damping in several directions instead of just one direction , and (h) minimal maintenance is required. As in the TMD, the TLD is primarily tuned to the fundamental frequency of the structure. Therefore, it is effective when the predominant excitation is in that particular mode. In the TLD, the sloshing liquid mass serves as the secondary mass analogous to the TMD mass. With minimum power, active control can extend its effectiveness to a wider range of excitation frequencies.

A column of liquid mass in a U-tube container attached to the primary structure serves as the secondary inertial system in a tuned liquid column damper (TLCD) system shown in Fig. 2.18. The vibration of the primary structure is reduced by the inertial restoring force of the liquid mass and by the damping introduced by liquid's passage through an orifice which has inherent head-loss characteristics. A hybrid system can be obtained by actively-controlling the opening and closing of the orifice, thereby controlling the damping provided by the TLCD. Similar to a mass effect system, the magnitude and phase of the counter force exerted by the liquid can be controlled by adjusting the orifice opening and container geometry.

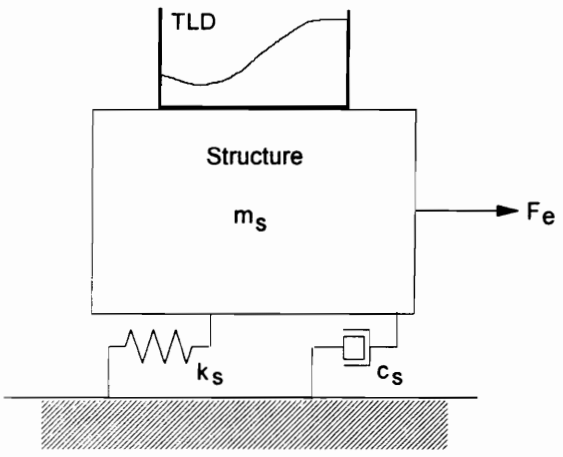

Fig. 2.17 Tuned Liquid Damper System

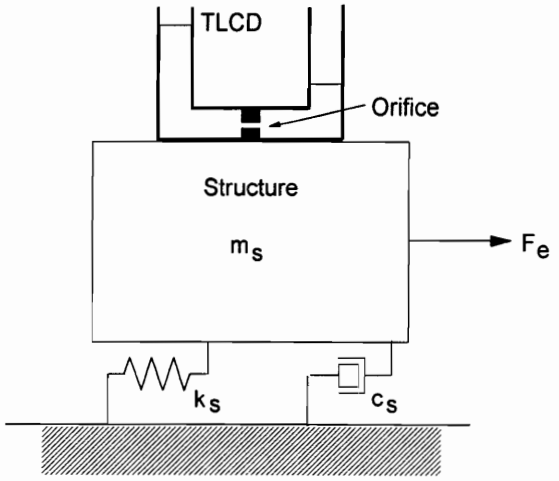

Fig. 2.18 Tuned Liquid Column Damper System

Electrorheological Dampers

Electrorheological (ER) fluids exhibit the characteristics of a yielding solid when subjected to an electric field. Actively-controlled ER dampers have been proposed for use as substitutes for such damping devices as viscoelastic dampers and elastomeric bearings [27]. The application of these ER dampers will be constrained by the attendant problems in maintaining a high-voltage power supply.

2.4 ACTUATORS

Hydraulic actuators have been used in AMD and HMD systems for controlling wind- and earthquake-induced oscillations in tall structures. Due to the complexity of the system, its application is limited by equipment and maintenance costs. Hydraulic actuators have also been proposed for use in ABS systems. Pneumatic actuators have been tested in the laboratory in conjunction with pulse control of structures.

AC and DC motors have been used as electric actuators in various mass damper systems. Electric actuators are used because the control theory for electric machines is already well-developed and their reliability is proven. Pneumatic and hydraulic actuators have greater failure rates than electric actuators because they are composed of a greater number of subsystems. Electric actuators can also be controlled with greater precision than pneumatic or hydraulic actuators. Furthermore, they cost less and are easier and less expensive to maintain.

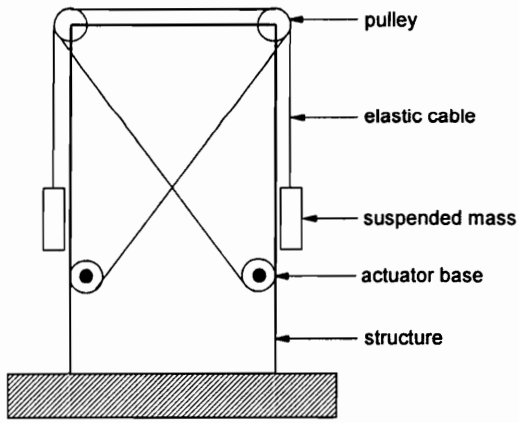

Fig. 2.19 Gravity actuator system

The use of gravity actuators have been proposed as a solution to the problem of energy availability during the occurrence of a natural disaster [28]. The actuator system consists of suspended masses which are free to move in the vertical direction, as shown in Fig. 2.19. These

masses are attached to a system of pulleys and cables, and are anchored by mechanisms which drive, release, and catch the masses.

A novel technique has been proposed [29] for utilizing the displacement caused by environmental forces on a tall structure to generate electrical energy when the structure's displacement is within the safety limits. This recovered energy is used to reduce the peak oscillations of the structure. To achieve this, a tuned mass damper is used as the intermediary for the energy transfer between the structure and the actuator. A permanent-magnet brushless DC machine is chosen as the actuator for the setup. This regenerative electric actuator will subsequently be described.

2.5 PROBLEMS IN THE IMPLEMENTATION OF ACTIVE AND HYBRID CONTROL

Although there has been a significant amount of research, testing, and evaluation done in the area of active and hybrid control of structures, full implementation of these control systems in actual structures is still faced with a number of problems.

A primary concern is the reliability of the external energy supply needed to generate the control forces, especially during strong earthquakes and hurricanes. There is a great probability that the energy supply will fail at the same time that energy will be required by the control system. Therefore, there is a need to devise fail-safe alternatives which will not require the use of external power at critical instants of time.

Another major obstacle to active or hybrid control of earthquake-excited structures is the proportionate increase in energy requirement as structures increase their height, length, or mass. More efficient control algorithms have to be developed that would reduce the control effort but maintain the same level of effectiveness.

Most of the available control algorithms require an accurate model of the system. Uncertainties in structural parameters and their variation over time increase the difficulty of applying these active control algorithms. Since structures are basically distributed-parameter systems, control algorithms based on lumped-parameter models can also become inaccurate. Furthermore, extreme loads on a structure produce a strongly nonlinear response due to the geometry or material behavior of system components. Control algorithms that use inaccurate models to calculate control forces can destabilize the actual structure. Therefore, there is a need to develop model-free algorithms for structural control. A global stability guarantee for all the proposed controllers is a prerequisite for implementation in civil structures; otherwise, a large number of residents' lives may be put at risk. The model-free controllers that are emerging are of the intelligent type, i.e., neural, fuzzy, or neural-fuzzy controllers. These controllers defy the

conventional concept of stability and therefore necessitate significant theoretical breakthroughs in control theory for their eventual implementation.

System robustness and overall reliability of the actuators and controllers have to be maintained at a high level acceptable for use in this application, in order to promote public acceptance of active or hybrid control of structures.

All the challenges confronting the implementation of active control could be boldly tackled by bringing together experts in all fields of engineering in a multi-disciplinary way in order to cross-fertilize the field with their ideas, concepts, and experimental work. Such an effort has been launched at the national level in 1991 and continues successfully. Education of the engineering community, high-level management personnel in construction industries, and the public at large is an absolute necessity in order to highlight the advantages, feasibility, and robustness of active control of structures. This will develop a backdrop with which their reservations for these systems are overcomed. Such a step will ultimately lead to a large-scale deployment of these systems in tall civil structures to provide comfort and safety from the impact of environmental forces.

CHAPTER 3

Modeling of Civil Structures, System Components, and Disturbances

3.1 INTRODUCTION

This chapter derives the systems equations for a discrete, lumped-parameter model of civil structures. The form of the equations consider simultaneous excitation due to wind and earthquake. Previous formulations considered only one type of excitation at a time.

Closed-form analytical solutions to engineering problems can only be obtained for a few simple cases. Idealizations have to be made in order to make an engineering problem mathematically manageable without compromising safety and economy. This mathematical model substitutes an idealized system, together with a set of assumptions, for the actual physical system.

3.2 LINEAR, SINGLE-DEGREE-OF-FREEDOM MODEL OF STRUCTURES

The number of independent coordinates needed to completely specify the configuration or position of a structural system at any given time is referred to as the number of degrees of freedom [1]. Although the continuous structure has an infinite number of degrees of freedom, idealization permits the reduction of the number of degrees of freedom to a discrete number. In some cases, the structure is reduced to having just a single degree of freedom. A single-degree-of-freedom model represents the structure as a system with one displacement coordinate. The model shown in Fig. 3.1 has the following elements [1]: (1) a mass element m_s which represents the mass and inertial characteristics of the structure; (2) a spring element k_s which represents the elastic restoring force and potential energy capacity of the structure; (3) a damping element c_s which represents the frictional characteristics and energy losses of the structure; (4) an excitation force $f(t)$ which represents the external forces acting on the structure; and (5) a control force $u(t)$ which represents the control forces applied to the structure to mitigate the structural response.

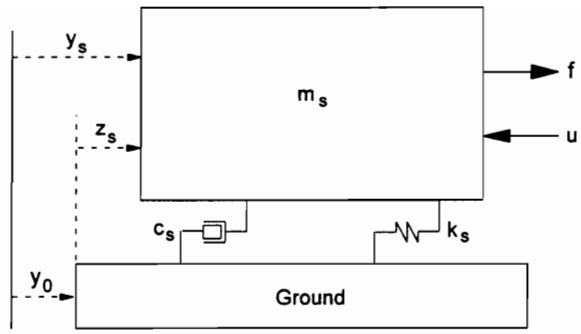

Fig. 3.1 Linear Single-Degree-of-Freedom Model

The equation of motion for the single-degree-of-freedom model is given by

$$m_s\ddot{y}_s + c_s(\dot{y}_s - \dot{y}_0) + k_s(y_s - y_0) = f(t) - u(t) \tag{3.1}$$

where the displacement y_s is with respect to an inertial reference frame. Since $y_s = y_0 + z_s$, the equation can be written in terms of the displacement with respect to the ground z_s as,

$$m_s(\ddot{z}_s + \ddot{y}_0) + c_s\dot{z}_s + k_s z_s = f(t) - u(t) \tag{3.2}$$

or

$$m_s\ddot{z}_s + c_s\dot{z}_s + k_s z_s = f(t) - u(t) - m_s\ddot{y}_0 \tag{3.3}$$

In order to get a state-space representation of the system, (3.3) can be manipulated to obtain

$$\ddot{z}_s = -\frac{c_s}{m_s}\dot{z}_s - \frac{k_s}{m_s}z_s + \frac{f}{m_s} - \frac{u}{m_s} - \ddot{y}_0 \tag{3.4}$$

If the state variables are chosen as,

$$\mathbf{x} = \begin{bmatrix} x_1 \\ x_2 \end{bmatrix} = \begin{bmatrix} z_s \\ \dot{z}_s \end{bmatrix} \tag{3.5}$$

then the state equations can be written as,

$$\begin{bmatrix} \dot{x}_1 \\ \dot{x}_2 \end{bmatrix} = \begin{bmatrix} \dot{z}_s \\ \ddot{z}_s \end{bmatrix} = \begin{bmatrix} 0 & 1 \\ -\frac{c_s}{m_s} & -\frac{k_s}{m_s} \end{bmatrix}\begin{bmatrix} z_s \\ \dot{z}_s \end{bmatrix} + \begin{bmatrix} 0 \\ -\frac{1}{m_s} \end{bmatrix}u + \begin{bmatrix} 0 & 0 \\ \frac{1}{m_s} & -1 \end{bmatrix}\begin{bmatrix} f \\ \ddot{y}_0 \end{bmatrix} \tag{3.6}$$

or

$$\dot{\mathbf{x}} = \mathbf{A}\mathbf{x} + \mathbf{B}u + \mathbf{H}\mathbf{w} \tag{3.7}$$

where

$$\mathbf{A} = \begin{bmatrix} 0 & 1 \\ -\frac{c_s}{m_s} & -\frac{k_s}{m_s} \end{bmatrix} \qquad \mathbf{B} = \begin{bmatrix} 0 \\ -\frac{1}{m_s} \end{bmatrix} \tag{3.8}$$

$$\mathbf{H} = \begin{bmatrix} 0 & 0 \\ \dfrac{1}{m_s} & -1 \end{bmatrix} \qquad \mathbf{w} = \begin{bmatrix} f \\ \ddot{y}_0 \end{bmatrix} \tag{3.9}$$

3.3 NONLINEAR, SINGLE-DEGREE-OF-FREEDOM MODEL OF STRUCTURES

The restoring force due to the spring element k_s in Fig. 3.1 is given by

$$F_k = k_s z_s \tag{3.10}$$

To model the inelastic behavior of structural components, this restoring force is modified as a superposition of a linear and a nonlinear component [2]

$$F_k = \alpha k_s z_s + (1-\alpha) k_s D_y v \tag{3.11}$$

where k_s is the elastic stiffness as given in Section 3.2; α is the ratio of postyielding to preyielding stiffness ($0 < \alpha < 1$); z_s is the principal displacement associated with the force F_k. D_y is the yielding displacement; and v is a nondimensional auxiliary variable introduced to take into account the inelastic and hysteretic behavior of the structural stiffness. The hysteretic behavior is included through the nonlinear relationship between v and z_s given by

$$\dot{v} = \frac{1}{D_y}\left\{\lambda \dot{z}_s - \beta v |\dot{z}_s| |v|^{\eta-1} - \gamma \dot{z}_s |v|^{\eta}\right\} \tag{3.12}$$

where λ, β, and γ determine the scale and general shape of the hysteresis, and η determines the smoothness of the force-displacement (F_k vs. z_s) curve. This hysteretic model of the building stiffness provides an explicit mathematical expression with enough flexible parameters to accurately model various hysteretic behaviors in inelastic systems.

The equation of motion for the single-degree-of-freedom model shown in Fig. 3.1 is then modified as,

$$m_s \ddot{z}_s + c_s \dot{z}_s + F_k = f(t) - u(t) - m_s \ddot{y}_0 \tag{3.13}$$

Substituting (3.11) into (3.13), the equation of motion can now be expressed as,

$$m_s \ddot{z}_s + c_s \dot{z}_s + \alpha k_s z_s + (1-\alpha) k_s D_y v = f(t) - u(t) - m_s \ddot{y}_0 \tag{3.14}$$

To obtain a state-space representation, (3.14) can be rearranged such that

$$\ddot{z}_s = -\frac{c_s}{m_s}\dot{z}_s - \alpha \frac{k_s}{m_s} z_s - (1-\alpha)\frac{k_s}{m_s} D_y v + \frac{1}{m_s} f(t) - \frac{1}{m_s} u(t) - \ddot{y}_0 \tag{3.15}$$

If the state variables are chosen as,

$$\mathbf{x} = \begin{bmatrix} x_1 \\ x_2 \\ x_3 \end{bmatrix} = \begin{bmatrix} z_s \\ \dot{z}_s \\ v \end{bmatrix} \tag{3.16}$$

then the state equations are obtained as,

$$\dot{x}_1 = \dot{z}_s = x_2 \tag{3.17}$$

$$\dot{x}_2 = \ddot{z}_s = -\frac{c_s}{m_s} x_2 - \alpha \frac{k_s}{m_s} x_1 - (1-\alpha)\frac{k_s}{m_s} D_y x_3 + \frac{1}{m_s} f(t) - \frac{1}{m_s} u(t) - \ddot{y}_0 \tag{3.18}$$

$$\dot{x}_3 = \dot{v} = \frac{1}{D_y}\left\{\lambda x_2 - \beta x_3 |x_2| |x_3|^{\eta-1} - \gamma x_2 |x_3|^{\eta}\right\} \tag{3.19}$$

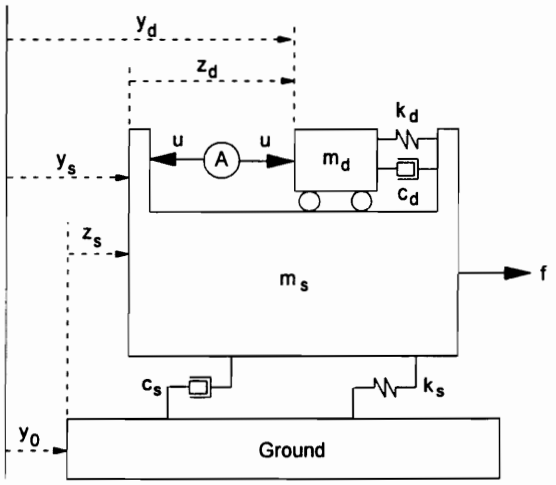

Fig. 3.2 Single-Degree-of-Freedom Structure with Mass Damper

3.4 SINGLE-DEGREE-OF-FREEDOM STRUCTURES WITH A MASS DAMPER

A mass damper is a mass attached to a structure such that it oscillates at the same frequency as the structure but with a phase shift. A hydraulic or electric actuator may be included in the set-up to provide a control force $u(t)$. A building with a mass damper at the top floor can be modeled as shown in Fig. 3.2.

Initially assuming a linear structure, the equations of motion for the building-mass damper system are given by [3]

$$m_s \ddot{y}_s + c_s(\dot{y}_s - \dot{y}_0) + k_s(y_s - y_0) + c_d(\dot{y}_s - \dot{y}_d) + k_d(y_s - y_d) = f(t) - u(t) \tag{3.20}$$

$$m_d\ddot{y}_d + c_d(\dot{y}_d - \dot{y}_s) + k_d(y_d - y_s) = u(t) \tag{3.21}$$

where the subscripts s and d refer to building and damper elements, respectively. However,

$$y_s = y_0 + z_s \tag{3.22}$$

$$y_d = y_0 + z_s + z_d \tag{3.23}$$

Substituting (3.22) and (3.23) into the state equations yield

$$m_s(\ddot{y}_0 + \ddot{z}_s) + c_s\dot{z}_s + k_s z_s - c_d\dot{z}_d - k_d z_d = f(t) - u(t) \tag{3.24}$$

$$m_d(\ddot{y}_0 + \ddot{z}_s + \ddot{z}_d) + c_d\dot{z}_d + k_d z_d = u(t) \tag{3.25}$$

To obtain a state-space representation, (3.24) and (3.25) can be manipulated such that

$$\ddot{z}_s = -\frac{c_s}{m_s}\dot{z}_s - \frac{k_s}{m_s}z_s + \frac{c_d}{m_s}\dot{z}_d + \frac{k_d}{m_s}z_d + \frac{1}{m_s}f(t) - \frac{1}{m_s}u(t) - \ddot{y}_0 \tag{3.26}$$

$$\ddot{z}_d = -\frac{c_d}{m_d}\dot{z}_d - \frac{k_d}{m_d}z_d - \frac{1}{m_d}u(t) - \ddot{y}_0 - \ddot{z}_s \tag{3.27}$$

Substituting the expression for $\ddot{z}_s$ given by (3.26) into (3.27) yields

$$\ddot{z}_d = \frac{c_s}{m_s}\dot{z}_s + \frac{k_s}{m_s}z_s - \left(\frac{c_d}{m_d} + \frac{c_d}{m_s}\right)\dot{z}_d - \left(\frac{k_d}{m_d} + \frac{k_d}{m_s}\right)z_d - \frac{1}{m_s}f(t) + \left(\frac{1}{m_s} + \frac{1}{m_d}\right)u(t) \tag{3.28}$$

If the state variables are chosen as,

$$\mathbf{x} = \begin{bmatrix} x_1 \\ x_2 \\ x_3 \\ x_4 \end{bmatrix} = \begin{bmatrix} z_s \\ z_d \\ \dot{z}_s \\ \dot{z}_d \end{bmatrix} \tag{3.29}$$

then state equations can be written in matrix form as,

$$\dot{\mathbf{x}}(t) = \mathbf{A}\mathbf{x}(t) + \mathbf{B}u(t) + \mathbf{H}\mathbf{w}(t) \tag{3.30}$$

where

$$\mathbf{A} = \begin{bmatrix} 0 & 0 & 1 & 0 \\ 0 & 0 & 0 & 1 \\ -\frac{k_s}{m_s} & \frac{k_d}{m_s} & -\frac{c_s}{m_s} & \frac{c_d}{m_s} \\ \frac{k_s}{m_s} & -\left(\frac{k_d}{m_d} + \frac{k_d}{m_s}\right) & \frac{c_s}{m_s} & -\left(\frac{c_d}{m_d} + \frac{c_d}{m_s}\right) \end{bmatrix} \tag{3.31}$$

$$\mathbf{B}=\begin{bmatrix} 0 \\ 0 \\ -\dfrac{1}{m_s} \\ \dfrac{1}{m_s}+\dfrac{1}{m_d} \end{bmatrix} \qquad \mathbf{H}=\begin{bmatrix} 0 & 0 \\ 0 & 0 \\ \dfrac{1}{m_s} & -1 \\ -\dfrac{1}{m_s} & 0 \end{bmatrix} \qquad \mathbf{w}=\begin{bmatrix} f \\ \ddot{y}_0 \end{bmatrix} \tag{3.32}$$

If the structure's stiffness force is nonlinear, the motion equation for the structure is modified as,

$$m_s(\ddot{y}_0+\ddot{z}_s)+c_s\dot{z}_s+\alpha k_s z_s+(1-\alpha)k_s D_y v-c_d\dot{z}_d-k_d z_d=f(t)-u(t) \tag{3.33}$$

Thus,

$$\ddot{z}_s=-\frac{c_s}{m_s}\dot{z}_s-\alpha\frac{k_s}{m_s}z_s-(1-\alpha)\frac{k_s}{m_s}D_y v+\frac{c_d}{m_s}\dot{z}_d+\frac{k_d}{m_s}z_d+\frac{1}{m_s}f(t)-\frac{1}{m_s}u(t)-\ddot{y}_0 \tag{3.34}$$

Substituting (3.34) into (3.28) gives

$$\ddot{z}_d=\frac{c_s}{m_s}\dot{z}_s+\alpha\frac{k_s}{m_s}z_s+(1-\alpha)\frac{k_s}{m_s}D_y v-\left(\frac{c_d}{m_d}+\frac{c_d}{m_s}\right)\dot{z}_d-\left(\frac{k_d}{m_d}+\frac{k_d}{m_s}\right)z_d-\frac{1}{m_s}f(t)+\left(\frac{1}{m_s}+\frac{1}{m_d}\right)u(t) \tag{3.35}$$

Choosing the state variables to be

$$\mathbf{x}=\begin{bmatrix} x_1 \\ x_2 \\ x_3 \\ x_4 \\ x_5 \end{bmatrix}=\begin{bmatrix} z_s \\ z_d \\ \dot{z}_s \\ \dot{z}_d \\ v \end{bmatrix} \tag{3.36}$$

will result in the following state equations:

$$\dot{x}_1=\dot{z}_s=x_3 \tag{3.37}$$

$$\dot{x}_2=\dot{z}_d=x_4 \tag{3.38}$$

$$\dot{x}_3 = \ddot{z}_s = -\frac{c_s}{m_s}x_3 - \alpha\frac{k_s}{m_s}x_1 - (1-\alpha)\frac{k_s}{m_s}D_y x_5 + \frac{c_d}{m_s}x_4 + \frac{k_d}{m_s}x_2 + \frac{1}{m_s}f(t) - \frac{1}{m_s}u(t) - \ddot{y}_0 \quad (3.39)$$

$$\dot{x}_4 = \ddot{z}_d = \frac{c_s}{m_s}x_3 + \alpha\frac{k_s}{m_s}x_1 + (1-\alpha)\frac{k_s}{m_s}D_y x_5 - \left(\frac{c_d}{m_d} + \frac{c_d}{m_s}\right)x_4 - \left(\frac{k_d}{m_d} + \frac{k_d}{m_s}\right)x_2 - \frac{1}{m_s}f(t) + \left(\frac{1}{m_s} + \frac{1}{m_d}\right)u(t) \quad (3.40)$$

$$\dot{x}_5 = \dot{v} = \frac{1}{D_y}\left\{\lambda x_2 - \beta x_5 |x_2||x_5|^{\eta-1} - \gamma x_2 |x_5|^{\eta}\right\} \quad (3.41)$$

3.5 LINEAR, MULTIDEGREE-OF-FREEDOM STRUCTURES

To obtain a better representation of the actual structure, a multiple degree of freedom model can be used to describe its dynamic behavior. Although continuous models are available, these are usually too complex and require considerable mathematical analysis. These models are applicable to only a few relatively-simple structures with uniform material properties and regular geometry. Finite-element models are also available for structures with much simpler geometries. A discrete model with multiple degrees of freedom can provide a near-exact characterization of the actual structure. The multistory shear building is one of the most instructive and practical of these models. A shear building is characterized by the absence of any displacement in the vertical and torsional directions. This model assumes that the structure is deflected by shear forces only. To limit the structure to shear deflections, it is assumed that (a) masses are lumped at the floor levels, (b) the girders on the floors are infinitely rigid compared to the columns, and (c) any horizontal deflection in the structure is independent of axial forces in the column. Fig. 3.3 shows a multistory fixed-base building.

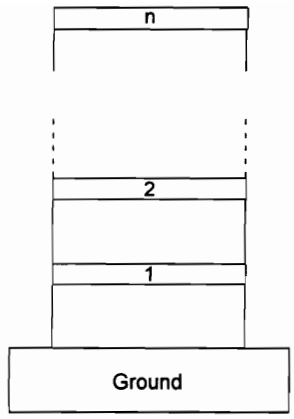

Fig. 3.3 Fixed-base Building Structure

Various reference frames can be used to formulate the shear-building model of this structure. One can either use displacements relative to an inertial reference, displacements between floors, or displacements relative to the ground. Although the formulation in the different reference frames are equivalent, a particular formulation may be more appropriate for a given set of measurement data without the need for additional data preparation.

3.5.1 Using the Displacement with Respect to an Inertial Refence Frame (Absolute Coordinates)

Fig. 3.4 shows a shear-building model of the n-story fixed-base structure using displacements relative to an inertial reference frame. The equation of motion for the different floors can be written as

$$m_1\ddot{y}_1 + c_1(\dot{y}_1 - \dot{y}_0) + k_1(y_1 - y_0) + c_2(\dot{y}_1 - \dot{y}_2) + k_2(y_1 - y_2) = f_1 + u_1 \tag{3.42}$$

$$m_i\ddot{y}_i + c_i(\dot{y}_i - \dot{y}_{i-1}) + k_i(y_i - y_{i-1}) + c_{i+1}(\dot{y}_i - \dot{y}_{i+1}) + k_{i+1}(y_i - y_{i+1}) = f_i + u_i \tag{3.43}$$

$$i = 2,\ldots,n-1$$

$$m_n\ddot{y}_n + c_n(\dot{y}_n - \dot{y}_{n-1}) + k_n(y_n - y_{n-1}) = f_n + u_n \tag{3.44}$$

where y_0 and y_i are the displacement of the ground and the displacement of the ith floor, respectively, relative to an inertial reference frame. It is seen that the ground-motion-induced disturbance $c_1\dot{y}_0 + k_1 y_0$ appears only in the first (base) floor equation.

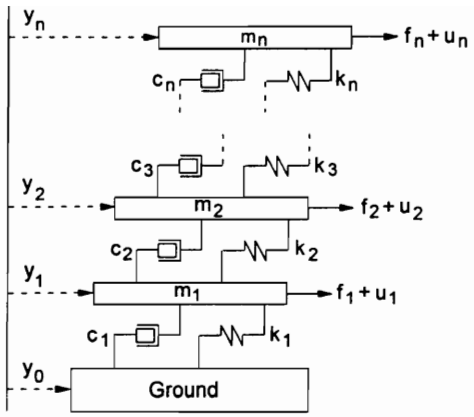

Fig. 3.4 Shear-Building Model using Absolute Displacements

The equations of motion can be written in matrix form as

$$\mathbf{M}\ddot{\mathbf{y}} + \mathbf{C}\dot{\mathbf{y}} + \mathbf{K}\mathbf{y} = \mathbf{w} + \mathbf{u} \tag{3.45}$$

where

$$\mathbf{y} = [y_1 \quad y_2 \quad . \quad . \quad . \quad y_n]^T \tag{3.46}$$

$$\mathbf{M} = \begin{bmatrix} m_1 & & & & \\ & m_2 & & & \\ & & . & & \\ & & & . & \\ & & & & . \\ & & & & m_n \end{bmatrix} \tag{3.47}$$

$$\mathbf{C} = \begin{bmatrix} c_1 + c_2 & -c_2 & & & & & \\ -c_2 & c_2 + c_3 & -c_3 & & & & \\ & . & . & . & & & \\ & & . & . & . & & \\ & & & . & . & . & \\ & & & & -c_{n-1} & c_{n-1} + c_n & -c_n \\ & & & & & -c_n & c_n \end{bmatrix} \tag{3.48}$$

$$\mathbf{K} = \begin{bmatrix} k_1 + k_2 & -k_2 & & & & & \\ -k_2 & k_2 + k_3 & -k_3 & & & & \\ & \cdot & \cdot & \cdot & & & \\ & & \cdot & \cdot & \cdot & & \\ & & & \cdot & \cdot & \cdot & \\ & & & & -k_{n-1} & k_{n-1} + k_n & -k_n \\ & & & & & -k_n & k_n \end{bmatrix} \tag{3.49}$$

$$\mathbf{w} = \begin{bmatrix} f_1 + c_1 \dot{y}_0 + k_1 y_0 & f_2 & \cdot & \cdot & \cdot & f_n \end{bmatrix}^T \tag{3.50}$$

$$\mathbf{u} = \begin{bmatrix} u_1 & u_2 & \cdot & \cdot & \cdot & u_n \end{bmatrix}^T \tag{3.51}$$

All elements that are not indicated in the above matrices are equal to zero. In state-space form:

$$\dot{\mathbf{x}} = \begin{bmatrix} \mathbf{0} & \mathbf{I} \\ -\mathbf{M}^{-1}\mathbf{K} & -\mathbf{M}^{-1}\mathbf{C} \end{bmatrix} \mathbf{x} + \begin{bmatrix} \mathbf{0} \\ \mathbf{M}^{-1} \end{bmatrix} \mathbf{u} + \begin{bmatrix} \mathbf{0} \\ \mathbf{M}^{-1} \end{bmatrix} \mathbf{w} \tag{3.52}$$

or

$$\dot{\mathbf{x}}(t) = \mathbf{A}\mathbf{x}(t) + \mathbf{B}\mathbf{u}(t) + \mathbf{H}\mathbf{w}(t) \tag{3.53}$$

3.5.2 Using the Relative Displacement Between Floors

The equation of motion for the model of the multistory building indicated in Fig. 3.4 can be expressed as

$$m_1 \ddot{y}_1 + c_1(\dot{y}_1 - \dot{y}_0) + k_1(y_1 - y_0) + c_2(\dot{y}_1 - \dot{y}_2) + k_2(y_1 - y_2) = f_1 + u_1 \tag{3.54}$$

$$m_i \ddot{y}_i + c_i(\dot{y}_i - \dot{y}_{i-1}) + k_i(y_i - y_{i-1}) + c_{i+1}(\dot{y}_i - \dot{y}_{i+1}) + k_{i+1}(y_i - y_{i+1}) = f_i + u_i \tag{3.55}$$

$$i = 2, \ldots, n-1$$

$$m_n \ddot{y}_n + c_n(\dot{y}_n - \dot{y}_{n-1}) + k_n(y_n - y_{n-1}) = f_n + u_n \tag{3.56}$$

where m_i is the mass of the ith floor, c_i is the damping coefficient of the ith floor, k_i is the stiffness of the ith floor, y_i is the displacement of the ith floor, u_i is the control force on the ith floor, and f_i is the external excitation at the ith floor.

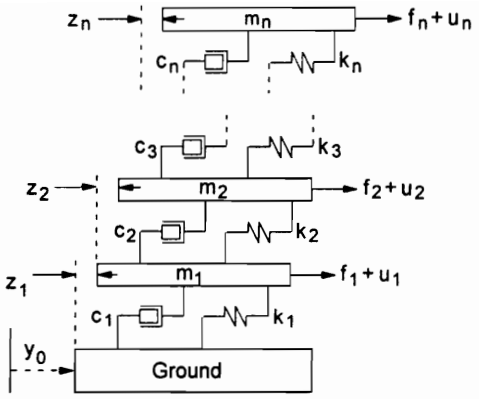

Fig. 3.5 Shear-Building Model using Displacements between Floors

Rewriting in terms of the relative displacement z_j as indicated in Fig. 3.5,

$$m_i \sum_{j=1}^{i} \ddot{z}_j + c_i \dot{z}_i + k_i z_i - c_{i+1} \dot{z}_{i+1} - k_{i+1} z_{i+1} = f_i + u_i - m_i \ddot{y}_0 \tag{3.57}$$

$$j = 1, 2, \ldots, n$$

where

$$z_i = y_i - y_{i-1} \tag{3.58}$$

$$y_i = \sum_{j=1}^{i} z_j + y_0 \tag{3.59}$$

$$c_{n+1} = k_{n+1} = 0 \tag{3.60}$$

Writing in matrix form,

$$\mathbf{M}\ddot{\mathbf{z}} + \mathbf{C}\dot{\mathbf{z}} + \mathbf{K}\mathbf{z} = \mathbf{f} + \mathbf{u} - \mathbf{m}\ddot{y}_0 \tag{3.61}$$

or

$$\ddot{\mathbf{z}} = -\mathbf{M}^{-1}\mathbf{C}\dot{\mathbf{z}} - \mathbf{M}^{-1}\mathbf{K}\mathbf{z} + \mathbf{M}^{-1}\mathbf{f} + \mathbf{M}^{-1}\mathbf{u} - \mathbf{M}^{-1}\mathbf{m}\ddot{y}_0 \tag{3.62}$$

where

$$\mathbf{M} = \begin{bmatrix} m_1 & & & & & & \\ m_2 & m_2 & & & & & \\ m_3 & m_3 & m_3 & & & & \\ . & & & . & & & \\ . & & & & . & & \\ . & & & & & . & \\ m_n & m_n & m_n & . & . & . & m_n \end{bmatrix} \tag{3.63}$$

$$\mathbf{C} = \begin{bmatrix} c_1 & -c_2 & & & & & \\ & c_2 & -c_3 & & & & \\ & & . & . & & & \\ & & & . & . & & \\ & & & & . & . & \\ & & & & & c_{n-1} & -c_n \\ & & & & & & c_n \end{bmatrix} \tag{3.64}$$

$$\mathbf{K} = \begin{bmatrix} k_1 & -k_2 & & & & & \\ & k_2 & -k_3 & & & & \\ & & . & . & & & \\ & & & . & . & & \\ & & & & . & . & \\ & & & & & k_{n-1} & -k_n \\ & & & & & & k_n \end{bmatrix} \tag{3.65}$$

$$\mathbf{m} = \begin{bmatrix} m_1 & m_2 & m_3 & . & . & . & m_n \end{bmatrix}^T \tag{3.66}$$

$$\mathbf{u} = \begin{bmatrix} u_1 & u_2 & u_3 & . & . & . & u_n \end{bmatrix}^T \tag{3.67}$$

$$\mathbf{f} = \begin{bmatrix} f_1 & f_2 & f_3 & . & . & . & f_n \end{bmatrix}^T \tag{3.68}$$

If we let

$$\mathbf{x}(t)=\begin{bmatrix}\mathbf{z}\\ \dot{\mathbf{z}}\end{bmatrix} \qquad \mathbf{w}=\begin{bmatrix}\mathbf{f}\\ \ddot{y}_0\end{bmatrix} \tag{3.69}$$

then combining (3.34) and (3.41),

$$\dot{\mathbf{x}}=\begin{bmatrix}\mathbf{0} & \mathbf{I}\\ -\mathbf{M}^{-1}\mathbf{K} & -\mathbf{M}^{-1}\mathbf{C}\end{bmatrix}\mathbf{x}+\begin{bmatrix}\mathbf{0}\\ \mathbf{M}^{-1}\end{bmatrix}\mathbf{u}+\begin{bmatrix}\mathbf{0} & \mathbf{0}\\ \mathbf{M}^{-1} & -\mathbf{M}^{-1}\mathbf{m}\end{bmatrix}\mathbf{w} \tag{3.70}$$

or

$$\dot{\mathbf{x}}(t)=\mathbf{A}\mathbf{x}(t)+\mathbf{B}\mathbf{u}(t)+\mathbf{H}\mathbf{w}(t) \tag{3.71}$$

3.5.3 Using the Displacement with Respect to the Ground

A shear-building model of the fixed-base structure using displacements relative to the ground is shown in Fig. 3.6. One horizontal degree of freedom is assigned to each of the floors. Taking each floor as a free body, the equations of motion of this n-story tall building can be expressed as

$$m_1(\ddot{y}_0+\ddot{z}_1)+c_1\dot{z}_1+k_1z_1-c_2(\dot{z}_2-\dot{z}_1)-k_2(z_2-z_1)=f_1+u_1 \tag{3.72}$$

$$m_i(\ddot{y}_0+\ddot{z}_i)+c_i(\dot{z}_i-\dot{z}_{i-1})+k_i(z_i-z_{i-1})+c_{i+1}(\dot{z}_i-\dot{z}_{i+1})+k_{i+1}(z_i-z_{i+1})=f_i+u_i$$

$$i=2,\ldots,n-1 \tag{3.73}$$

$$m_n(\ddot{y}_0+\ddot{z}_n)+c_n(\dot{z}_n-\dot{z}_{n-1})+k_n(z_n-z_{n-1})=f_n+u_n \tag{3.74}$$

where $\ddot{y}_0$ is the ground acceleration relative to an inertial reference frame; $z_i,\dot{z}_i,\ddot{z}_i$ are the relative displacement, velocity, and acceleration of the ith story with respect to the ground, respectively; and f_i and u_i are the external horizontal force and the control force applied to the ith story, respectively. It is seen that the ground-motion-induced disturbance $m_i\ddot{y}_0$ appears in the equation for every floor.

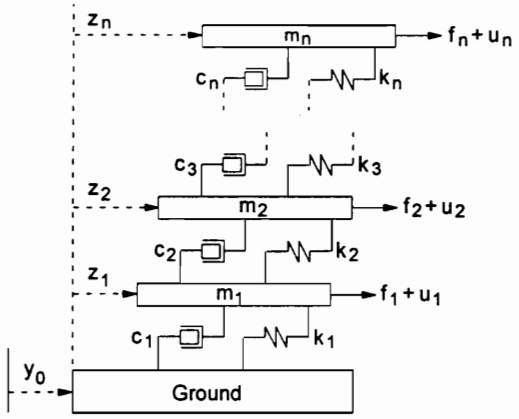

Fig. 3.6. Shear-Building Model using Displacements Relative to the Ground

In matrix form,

$$\mathbf{M}\ddot{\mathbf{z}} + \mathbf{C}\dot{\mathbf{z}} + \mathbf{K}\mathbf{z} = \mathbf{f} + \mathbf{u} - \mathbf{m}\ddot{y}_0 \tag{3.75}$$

where **M, C, K, z, f,** and **u** are the matrices for masses, damping coefficients, stiffnesses and vectors for displacements, external forces, and control forces, respectively. They have the form

$$\mathbf{M} = \begin{bmatrix} m_1 & & & & \\ & m_2 & & & \\ & & \ddots & & \\ & & & \ddots & \\ & & & & m_n \end{bmatrix} \tag{3.76}$$

$$\mathbf{C} = \begin{bmatrix} c_1 + c_2 & -c_2 & & & & & \\ -c_2 & c_2 + c_3 & -c_3 & & & & \\ & \ddots & \ddots & \ddots & & & \\ & & \ddots & \ddots & \ddots & & \\ & & & \ddots & \ddots & \ddots & \\ & & & & -c_{n-1} & c_{n-1} + c_n & -c_n \\ & & & & & -c_n & c_n \end{bmatrix} \tag{3.77}$$

$$\mathbf{K} = \begin{bmatrix} k_1 + k_2 & -k_2 & & & & & \\ -k_2 & k_2 + k_3 & -k_3 & & & & \\ & \ddots & \ddots & \ddots & & & \\ & & \ddots & \ddots & \ddots & & \\ & & & \ddots & \ddots & \ddots & \\ & & & & -k_{n-1} & k_{n-1} + k_n & -k_n \\ & & & & & -k_n & k_n \end{bmatrix} \tag{3.78}$$

$$\mathbf{z} = \begin{bmatrix} z_1 & z_2 & \cdots & z_n \end{bmatrix}^T \tag{3.79}$$

$$\mathbf{f} = \begin{bmatrix} f_1 & f_2 & \cdots & f_n \end{bmatrix}^T \tag{3.80}$$

$$\mathbf{u} = [u_1 \quad u_2 \quad . \quad . \quad . \quad u_n]^T \tag{3.81}$$

$$\mathbf{m} = [m_1 \quad m_2 \quad . \quad . \quad . \quad m_n]^T \tag{3.82}$$

If the state and disturbance vectors are defined as,

$$\mathbf{x}(t) = \begin{bmatrix} \mathbf{z} \\ \dot{\mathbf{z}} \end{bmatrix} \qquad \mathbf{w} = \begin{bmatrix} \mathbf{f} \\ \ddot{y}_0 \end{bmatrix} \tag{3.83}$$

then the state equation can be written as,

$$\dot{\mathbf{x}} = \begin{bmatrix} \mathbf{0} & \mathbf{I} \\ -\mathbf{M}^{-1}\mathbf{K} & -\mathbf{M}^{-1}\mathbf{C} \end{bmatrix} \mathbf{x} + \begin{bmatrix} \mathbf{0} \\ \mathbf{M}^{-1} \end{bmatrix} \mathbf{u} + \begin{bmatrix} \mathbf{0} & \mathbf{0} \\ \mathbf{M}^{-1} & -\mathbf{M}^{-1}\mathbf{m} \end{bmatrix} \mathbf{w} \tag{3.84}$$

or

$$\dot{\mathbf{x}}(t) = \mathbf{A}\mathbf{x}(t) + \mathbf{B}\mathbf{u}(t) + \mathbf{H}\mathbf{w}(t) \tag{3.85}$$

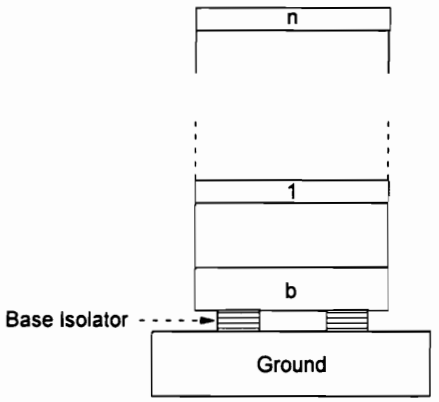

Fig. 3.7. Base-Isolated Structure

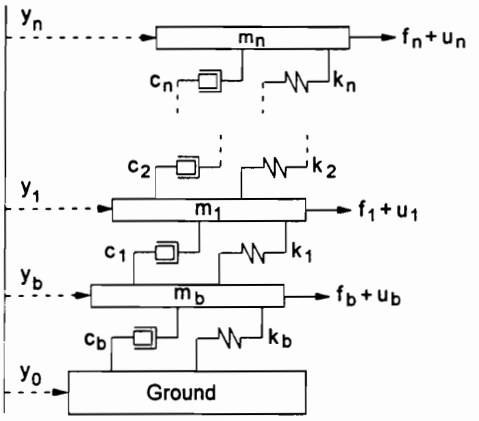

Fig. 3.8. Shear-Building Model of Base-Isolated Structure using an Inertial Reference

3.6 BASE-ISOLATED STRUCTURES

For the base-isolated structure shown in Fig. 3.7, the equations of motion can be formulated using an inertial reference frame (as in Section 3.5.1) as shown in Fig. 3.8 such that

$$\mathbf{M}\ddot{\mathbf{y}} + \mathbf{C}\dot{\mathbf{y}} + \mathbf{K}\mathbf{y} = \mathbf{w} + \mathbf{u} \tag{3.86}$$

where

$$\mathbf{y} = \begin{bmatrix} y_b & y_1 & . & . & . & y_n \end{bmatrix}^T \tag{3.87}$$

$$\mathbf{M} = \begin{bmatrix} m_b & & & & & \\ & m_1 & & & & \\ & & . & & & \\ & & & . & & \\ & & & & . & \\ & & & & & m_n \end{bmatrix} \tag{3.88}$$

$$\mathbf{C} = \begin{bmatrix} c_b + c_1 & -c_1 & & & & & \\ -c_1 & c_1 + c_2 & -c_2 & & & & \\ & . & . & . & & & \\ & & . & . & . & & \\ & & & . & . & . & \\ & & & & -c_{n-1} & c_{n-1} + c_n & -c_n \\ & & & & & -c_n & c_n \end{bmatrix} \tag{3.89}$$

$$\mathbf{K} = \begin{bmatrix} k_b + k_1 & -k_1 & & & & & \\ -k_1 & k_1 + k_2 & -k_2 & & & & \\ & . & . & . & & & \\ & & . & . & . & & \\ & & & . & . & . & \\ & & & & -k_{n-1} & k_{n-1} + k_n & -k_n \\ & & & & & -k_n & k_n \end{bmatrix} \tag{3.90}$$

$$\mathbf{w} = \begin{bmatrix} f_b + c_b\dot{y}_0 + k_b y_0 & f_1 & . & . & . & f_n \end{bmatrix}^T \tag{3.91}$$

$$\mathbf{u} = \begin{bmatrix} u_b & u_1 & \cdots & u_n \end{bmatrix}^T \tag{3.92}$$

y_0 is the ground displacement with respect to an inertial reference frame. y_b and y_i are the displacements of the base and ith floor relative to the inertial reference frame. In state-space form,

$$\dot{\mathbf{x}} = \begin{bmatrix} \mathbf{0} & \mathbf{I} \\ -\mathbf{M}^{-1}\mathbf{K} & -\mathbf{M}^{-1}\mathbf{C} \end{bmatrix} \mathbf{x} + \begin{bmatrix} \mathbf{0} \\ \mathbf{M}^{-1} \end{bmatrix} \mathbf{u} + \begin{bmatrix} \mathbf{0} \\ \mathbf{M}^{-1} \end{bmatrix} \mathbf{w} \tag{3.93}$$

or

$$\dot{\mathbf{x}}(t) = \mathbf{A}\mathbf{x}(t) + \mathbf{B}\mathbf{u}(t) + \mathbf{H}\mathbf{w}(t) \tag{3.94}$$

where

$$\mathbf{x} = \begin{bmatrix} \mathbf{y} \\ \dot{\mathbf{y}} \end{bmatrix} \tag{3.95}$$

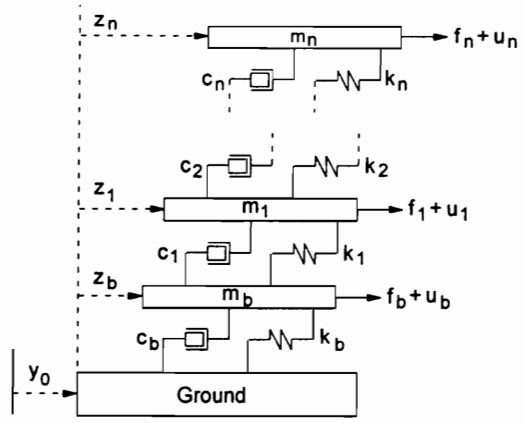

Fig. 3.9. Shear-Building Model of BIS using Displacements Relative to the Ground

Using relative displacements with respect to the ground (as in Section 3.5.3), the equations of motion for the model shown in Fig. 3.9 can be written as

$$\mathbf{M}\ddot{\mathbf{z}} + \mathbf{C}\dot{\mathbf{z}} + \mathbf{K}\mathbf{z} = \mathbf{f} + \mathbf{u} - \mathbf{m}\ddot{y}_0 \tag{3.96}$$

where

$$\mathbf{z} = \begin{bmatrix} z_b & z_1 & \cdots & z_n \end{bmatrix}^T \tag{3.97}$$

$$\mathbf{M} = \begin{bmatrix} m_b & & & & \\ & m_1 & & & \\ & & \cdot & & \\ & & & \cdot & \\ & & & & m_n \end{bmatrix} \tag{3.98}$$

$$\mathbf{C} = \begin{bmatrix} c_b + c_1 & -c_1 & & & & & \\ -c_1 & c_1 + c_2 & -c_2 & & & & \\ & \cdot & \cdot & \cdot & & & \\ & & \cdot & \cdot & \cdot & & \\ & & & \cdot & \cdot & \cdot & \\ & & & & -c_{n-1} & c_{n-1} + c_n & -c_n \\ & & & & & -c_n & c_n \end{bmatrix} \tag{3.99}$$

$$\mathbf{K} = \begin{bmatrix} k_b + k_1 & -k_1 & & & & & \\ -k_1 & k_1 + k_2 & -k_2 & & & & \\ & \cdot & \cdot & \cdot & & & \\ & & \cdot & \cdot & \cdot & & \\ & & & \cdot & \cdot & \cdot & \\ & & & & -k_{n-1} & k_{n-1} + k_n & -k_n \\ & & & & & -k_n & k_n \end{bmatrix} \tag{3.100}$$

$$\mathbf{f} = \begin{bmatrix} f_b & f_1 & \cdot & \cdot & \cdot & f_n \end{bmatrix}^T \tag{3.101}$$

$$\mathbf{u} = \begin{bmatrix} u_b & u_1 & \cdot & \cdot & \cdot & u_n \end{bmatrix}^T \tag{3.102}$$

$$\mathbf{m} = \begin{bmatrix} m_b & m_1 & \cdot & \cdot & \cdot & m_n \end{bmatrix}^T \tag{3.103}$$

$\ddot{y}_0$ is the ground acceleration with respect to an inertial reference frame. z_b and z_i are the relative displacements of the base and ith floor with respect to the ground. In state-space form,

$$\dot{\mathbf{x}} = \begin{bmatrix} \mathbf{0} & \mathbf{I} \\ -\mathbf{M}^{-1}\mathbf{K} & -\mathbf{M}^{-1}\mathbf{C} \end{bmatrix} \mathbf{x} + \begin{bmatrix} \mathbf{0} \\ \mathbf{M}^{-1} \end{bmatrix} \mathbf{u} + \begin{bmatrix} \mathbf{0} & \mathbf{0} \\ \mathbf{M}^{-1} & \mathbf{M}^{-1}\mathbf{m} \end{bmatrix} \mathbf{w} \tag{3.104}$$

or

$$\dot{\mathbf{x}}(t) = \mathbf{A}\mathbf{x}(t) + \mathbf{B}\mathbf{u}(t) + \mathbf{H}\mathbf{w}(t) \tag{3.105}$$

where

$$\mathbf{x}(t) = \begin{bmatrix} \mathbf{z} \\ \dot{\mathbf{z}} \end{bmatrix} \qquad \mathbf{w}(t) = \begin{bmatrix} \mathbf{f} \\ \ddot{y}_0 \end{bmatrix} \tag{3.106}$$

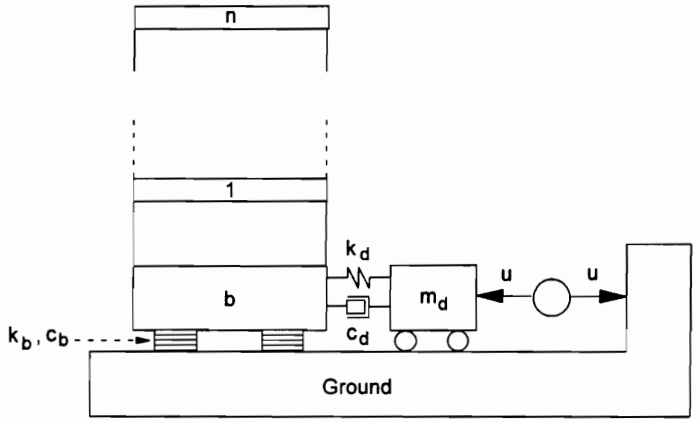

Fig. 3.10 Base-Isolated Building with Hybrid Mass Damper

3.7 STRUCTURES WITH MASS DAMPERS

Consider a base-isolated building structure with a hybrid mass damper system as shown in Fig. 3.10. Using relative displacements with respect to the ground, the (n+2) equations of motion for the entire system can be written as

$$\mathbf{M}\ddot{\mathbf{z}} + \mathbf{C}\dot{\mathbf{z}} + \mathbf{K}\mathbf{z} = \mathbf{f} + \mathbf{G}u - \mathbf{m}\ddot{y}_0 \tag{3.107}$$

where

$$\mathbf{z} = \begin{bmatrix} z_d & z_b & z_1 & \cdots & z_n \end{bmatrix}^T \tag{3.108}$$

$$\mathbf{M} = \begin{bmatrix} m_d & & & & & \\ & m_b & & & & \\ & & m_1 & & & \\ & & & . & & \\ & & & & . & \\ & & & & & . \\ & & & & & & m_n \end{bmatrix} \tag{3.109}$$

$$\mathbf{f} = \begin{bmatrix} 0 & f_b & f_1 & . & . & . & f_n \end{bmatrix}^T \tag{3.110}$$

$$\mathbf{G} = \begin{bmatrix} -1 & 0 & 0 & . & . & . & 0 \end{bmatrix}^T \tag{3.111}$$

$$\mathbf{m} = \begin{bmatrix} m_d & m_b & m_1 & . & . & . & m_n \end{bmatrix}^T \tag{3.112}$$

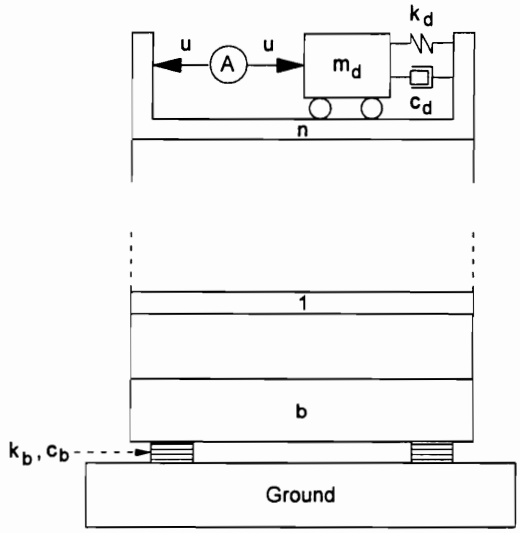

Fig. 3.11 Base-Isolated Structure with HMD on the Top Floor

For the base-isolated building with a hybrid mass damper at the top floor as shown in Fig. 3.11, the (n+2) equations of motion is modified by having

$$\mathbf{M} = \begin{bmatrix} m_b & & & & & \\ & m_1 & & & & \\ & & \cdot & & & \\ & & & \cdot & & \\ & & & & m_n & \\ & & & & & m_d \end{bmatrix} \tag{3.113}$$

$$\mathbf{f} = \begin{bmatrix} f_b & f_1 & \cdot & \cdot & \cdot & f_n & 0 \end{bmatrix}^T \tag{3.114}$$

$$\mathbf{G} = \begin{bmatrix} 0 & 0 & \cdot & \cdot & \cdot & -1 & 1 \end{bmatrix}^T \tag{3.115}$$

$$\mathbf{m} = \begin{bmatrix} m_b & m_1 & \cdot & \cdot & \cdot & m_n & m_d \end{bmatrix}^T \tag{3.116}$$

3.8 NONLINEAR, MULTIDEGREE-OF-FREEDOM STRUCTURES

If the building structure shown in Fig. 3.5 was nonlinear or hysteretic, the equations of motion for the structure can be obtained by modifying the equations for the linear structure such that

$$\mathbf{M}\ddot{\mathbf{z}} + \mathbf{F}_c + \mathbf{F}_k = \mathbf{f} + \mathbf{u} - \mathbf{m}\ddot{y}_0 \tag{3.117}$$

where $\mathbf{z}$ is the n-vector of interstory deformations; $\mathbf{F}_c$ is the n-vector of nonlinear damping forces; $\mathbf{F}_k$ is the n-vector of nonlinear or hysteretic stiffness forces; and

$$\mathbf{M} = \begin{bmatrix} m_1 & 0 & 0 & 0 & \cdot & \cdot & 0 \\ m_2 & m_2 & 0 & 0 & & & 0 \\ m_3 & m_3 & m_3 & 0 & & & \cdot \\ \cdot & & & \cdot & & & \cdot \\ \cdot & & & & \cdot & & \cdot \\ m_{n-1} & m_{n-1} & \cdot & \cdot & \cdot & m_{n-1} & 0 \\ m_n & m_n & \cdot & \cdot & \cdot & m_n & m_n \end{bmatrix} \tag{3.118}$$

$$\mathbf{z} = \begin{bmatrix} z_1 & z_2 & \cdot & \cdot & \cdot & z_n \end{bmatrix}^T \tag{3.119}$$

$$\mathbf{f} = \begin{bmatrix} f_1 & f_2 & . & . & . & f_n \end{bmatrix}^T \tag{3.120}$$

$$\mathbf{u} = \begin{bmatrix} u_1 & u_2 & . & . & . & u_n \end{bmatrix}^T \tag{3.121}$$

$$\mathbf{m} = \begin{bmatrix} m_1 & m_2 & . & . & . & m_n \end{bmatrix}^T \tag{3.122}$$

For most building structures, the damping and stiffness forces can be expressed as

$$\mathbf{F}_c = \mathbf{C}\dot{\mathbf{z}} \tag{3.123}$$

$$\mathbf{F}_k = \mathbf{K}_e\mathbf{z} + \mathbf{K}_i\mathbf{v} \tag{3.124}$$

where

$$\mathbf{C} = \begin{bmatrix} c_1 & -c_2 & 0 & 0 & . & . & 0 \\ 0 & c_2 & -c_3 & 0 & & & 0 \\ . & & . & . & & & . \\ . & & & . & . & & . \\ . & & & & . & . & . \\ 0 & . & . & . & 0 & c_{n-1} & -c_n \\ 0 & . & . & . & 0 & 0 & c_n \end{bmatrix} \tag{3.125}$$

$$\mathbf{K}_e = \begin{bmatrix} \alpha_1 k_1 & -\alpha_2 k_2 & 0 & 0 & . & . & 0 \\ 0 & \alpha_2 k_2 & -\alpha_3 k_3 & 0 & & & 0 \\ . & & . & . & & & . \\ . & & & . & . & & . \\ . & & & & . & . & . \\ 0 & . & . & . & 0 & \alpha_{n-1} k_{n-1} & -\alpha_n k_n \\ 0 & . & . & . & 0 & 0 & \alpha_n k_n \end{bmatrix} \tag{3.126}$$

$$\mathbf{K}_i = \begin{bmatrix} \sigma_1 k_1 & -\sigma_2 k_2 & 0 & 0 & . & . & 0 \\ 0 & \sigma_2 k_2 & -\sigma_3 k_3 & 0 & & & 0 \\ . & & . & . & & & . \\ . & & & . & . & & . \\ . & & & & . & . & . \\ 0 & . & . & . & 0 & \sigma_{n-1} k_{n-1} & -\sigma_n k_n \\ 0 & . & . & . & 0 & 0 & \sigma_n k_n \end{bmatrix} \tag{3.127}$$

$$\sigma_j = (1 - \alpha_j) D_{yj} \tag{3.128}$$

$$\mathbf{v} = [v_1 \quad v_2 \quad . \quad . \quad . \quad v_n]^T \tag{3.129}$$

v is an n-vector of auxiliary variables as described in Section 3.3. The equations of motion can now be written as,

$$\mathbf{M}\ddot{\mathbf{z}} + \mathbf{C}\dot{\mathbf{z}} + \mathbf{K}_e\mathbf{z} + \mathbf{K}_i\mathbf{v} = \mathbf{f} + \mathbf{u} - \mathbf{m}\ddot{y}_0 \tag{3.130}$$

In state-space form,

$$\dot{\mathbf{x}} = \begin{bmatrix} \dot{\mathbf{z}} \\ \dot{\mathbf{v}} \\ \ddot{\mathbf{z}} \end{bmatrix} \tag{3.131}$$

where

$$\mathbf{x} = [\mathbf{z} \quad \mathbf{v} \quad \dot{\mathbf{z}}]^T \tag{3.132}$$

$$\dot{\mathbf{z}} = [\mathbf{0} \quad \mathbf{0} \quad \mathbf{I}]\mathbf{x} \tag{3.133}$$

$$\dot{\mathbf{v}} = [\dot{v}_1 \quad \dot{v}_2 \quad . \quad . \quad . \quad \dot{v}_n]^T \tag{3.134}$$

$$\dot{v}_j = \frac{1}{D_{yj}} \{\lambda_j \dot{z}_j - \beta_j v_j |\dot{z}_j| |v_j|^{\eta_j - 1} - \gamma_j \dot{z}_j |v_j|^{\eta_j}\} \tag{3.135}$$

$$\ddot{\mathbf{z}} = -\mathbf{M}^{-1}[\mathbf{K}_e \quad \mathbf{K}_i \quad \mathbf{C}]\mathbf{x} + \mathbf{M}^{-1}\mathbf{f} + \mathbf{M}^{-1}\mathbf{u} - \mathbf{M}^{-1}\mathbf{m}\ddot{y}_0 \tag{3.136}$$

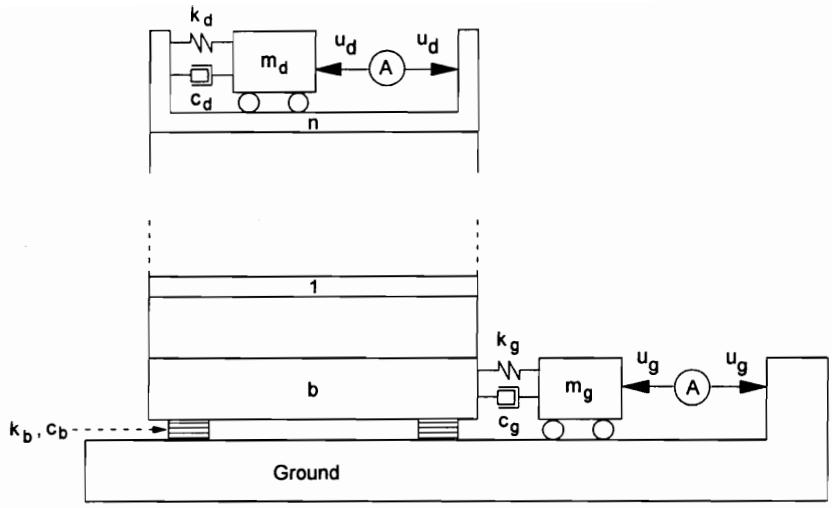

Fig. 3.12 Base-isolated structure with mass dampers

Consider the base-isolated structure in Fig. 3.12, with mass dampers in the base and top floors. If the system is initially assumed to be linear, then the equations of motion can be written as,

$$m_g\ddot{y}_g + c_g(\dot{y}_g - \dot{y}_b) + k_g(y_g - y_b) = -u_g \tag{3.137}$$

$$m_b\ddot{y}_b + c_b(\dot{y}_b - \dot{y}_0) + k_b(y_b - y_0) + c_1(\dot{y}_b - \dot{y}_1) + k_1(y_b - y_1) + c_g(\dot{y}_b - \dot{y}_g) + k_g(y_b - y_g) = 0 \tag{3.138}$$

$$m_1\ddot{y}_1 + c_1(\dot{y}_1 - \dot{y}_b) + k_1(y_1 - y_b) + c_2(\dot{y}_1 - \dot{y}_2) + k_2(y_1 - y_2) = f_1 \tag{3.139}$$

$$m_i\ddot{y}_i + c_i(\dot{y}_i - \dot{y}_{i-1}) + k_i(y_i - y_{i-1}) + c_{i+1}(\dot{y}_i - \dot{y}_{i+1}) + k_{i+1}(y_i - y_{i+1}) = f_i \tag{3.140}$$

$$i = 2,3,\ldots,n\text{-}1$$

$$m_n\ddot{y}_n + c_n(\dot{y}_n - \dot{y}_{n-1}) + k_n(y_n - y_{n-1}) + c_d(\dot{y}_n - \dot{y}_d) + k_d(y_n - y_d) = f_n + u_d \tag{3.141}$$

$$m_d\ddot{y}_d + c_d(\dot{y}_d - \dot{y}_n) + k_d(y_d - y_n) = -u_d \tag{3.142}$$

In terms of the interstory drifts,

$$y_g = y_0 + z_b + z_g \quad \text{where } z_g = y_g - y_b$$

$$y_b = y_0 + z_b$$

$$y_1 = y_0 + z_b + z_1$$

$$y_2 = y_0 + z_b + z_1 + z_2$$

....

$$y_n = y_0 + z_b + z_1 + z_2 + \ldots + z_n$$

$$y_d = y_0 + z_b + z_1 + z_2 + \ldots + z_n + z_d \tag{3.143}$$

Substituting into the motion equations,

$$m_g(\ddot{y}_0 + \ddot{z}_b + \ddot{z}_g) + c_g\dot{z}_g + k_g z_g = -u_g \tag{3.144}$$

$$m_b(\ddot{y}_0 + \ddot{z}_b) + c_b\dot{z}_b + k_b z_b - c_1\dot{z}_1 - k_1 z_1 - c_g\dot{z}_g - k_g z_g = 0 \tag{3.145}$$

$$m_1(\ddot{y}_0 + \ddot{z}_b + \ddot{z}_1) + c_1\dot{z}_1 + k_1 z_1 - c_2\dot{z}_2 - k_2 z_2 = f_1 \tag{3.146}$$

. . . .

$$m_n(\ddot{y}_0 + \ddot{z}_b + \ddot{z}_1 + \ddot{z}_n) + c_n\dot{z}_n + k_n z_n - c_d\dot{z}_d - k_d z_d = f_n + u_d \tag{3.147}$$

$$m_d(\ddot{y}_0 + \ddot{z}_b + \ddot{z}_1 + \ddot{z}_n + \ddot{z}_d) + c_d\dot{z}_d + k_d z_d = -u_d \tag{3.148}$$

In matrix form,

$$\mathbf{M}\ddot{\mathbf{z}} + \mathbf{C}\dot{\mathbf{z}} + \mathbf{K}\mathbf{z} = \mathbf{f} + \mathbf{G}\mathbf{u} - \mathbf{m}\ddot{y}_0 \tag{3.149}$$

where

$$\mathbf{z} = [z_g \quad z_b \quad z_1 \quad . \quad . \quad . \quad z_n \quad z_d]^T \tag{3.150}$$

$$\mathbf{M} = \begin{bmatrix} m_g & m_g & 0 & 0 & 0 & . & . & . & 0 \\ 0 & m_b & 0 & 0 & 0 & & & & 0 \\ 0 & m_1 & m_1 & 0 & 0 & & & & . \\ 0 & m_2 & m_2 & m_2 & 0 & & & & . \\ . & & & & . & & & & . \\ . & & & & & . & & & . \\ . & & & & & & . & & . \\ 0 & m_n & m_n & . & . & . & . & m_n & 0 \\ 0 & m_d & m_d & . & . & . & . & m_d & m_d \end{bmatrix} \tag{3.151}$$

$$\mathbf{C} = \begin{bmatrix} c_g & 0 & 0 & 0 & 0 & 0 & . & . & 0 \\ -c_g & c_b & -c_1 & 0 & 0 & 0 & & & 0 \\ 0 & 0 & c_1 & -c_2 & 0 & 0 & & & . \\ 0 & 0 & 0 & c_2 & -c_3 & 0 & & & . \\ . & & & & . & & & & . \\ . & & & & & . & & & . \\ . & & & & & & . & & . \\ 0 & 0 & 0 & . & . & . & 0 & c_n & -c_d \\ 0 & 0 & 0 & . & . & . & 0 & 0 & c_d \end{bmatrix} \tag{3.152}$$

$$\mathbf{K} = \begin{bmatrix} k_g & 0 & 0 & 0 & 0 & 0 & . & . & 0 \\ -k_g & k_b & -k_1 & 0 & 0 & 0 & & & 0 \\ 0 & 0 & k_1 & -k_2 & 0 & 0 & & & . \\ 0 & 0 & 0 & k_2 & -k_3 & 0 & & & . \\ . & & & & . & & & & . \\ . & & & & & . & & & . \\ . & & & & & & . & & . \\ 0 & 0 & 0 & . & . & . & 0 & k_n & -k_d \\ 0 & 0 & 0 & . & . & . & 0 & 0 & k_d \end{bmatrix} \tag{3.153}$$

$$\mathbf{G} = \begin{bmatrix} -1 & 0 \\ 0 & 0 \\ 0 & 0 \\ 0 & 0 \\ . & . \\ . & . \\ . & . \\ 0 & 0 \\ 0 & 1 \\ 0 & -1 \end{bmatrix} \tag{3.154}$$

$$\mathbf{f} = [0 \quad 0 \quad f_1 \quad f_2 \quad . \quad . \quad . \quad f_{n-1} \quad f_n \quad 0]^T \tag{3.155}$$

$$\mathbf{u} = \begin{bmatrix} u_g & u_d \end{bmatrix}^T \tag{3.156}$$

$$\mathbf{m} = [m_g \quad m_b \quad m_1 \quad m_2 \quad . \quad . \quad . \quad m_{n-1} \quad m_n \quad m_d]^T \tag{3.157}$$

For the nonlinear case (but assuming that k_g and k_d are linear), the stiffness force is modified as

$$\mathbf{F}_k = \mathbf{K}_e\mathbf{z} + \mathbf{K}_i\mathbf{v} \tag{3.158}$$

where

$$\mathbf{K}_e = \begin{bmatrix} k_g & 0 & 0 & 0 & 0 & 0 & . & . & 0 \\ -k_g & \alpha_b k_b & -\alpha_1 k_1 & 0 & 0 & 0 & & & 0 \\ 0 & 0 & \alpha_1 k_1 & -\alpha_2 k_2 & 0 & 0 & & & 0 \\ 0 & 0 & 0 & \alpha_2 k_2 & -\alpha_3 k_3 & 0 & & & 0 \\ . & & & & . & & & & . \\ . & & & & & . & & & . \\ . & & & & & & . & & . \\ 0 & 0 & 0 & . & . & . & 0 & \alpha_n k_n & -k_d \\ 0 & 0 & 0 & . & . & . & 0 & 0 & k_d \end{bmatrix} \tag{3.159}$$

$$\mathbf{K}_i = \begin{bmatrix} 0 & 0 & 0 & 0 & . & . & . & 0 \\ \sigma_b k_b & -\sigma_1 k_1 & 0 & 0 & & & & 0 \\ 0 & \sigma_1 k_1 & -\sigma_2 k_2 & 0 & & & & 0 \\ & & & . & & & & . \\ & & & & . & & & . \\ & & & & & . & & . \\ 0 & 0 & . & . & 0 & \sigma_{n-1} k_{n-1} & -\sigma_n k_n & \\ 0 & 0 & . & . & 0 & 0 & \sigma_n k_n & \\ 0 & 0 & . & . & 0 & 0 & 0 & \end{bmatrix}$$

(3.160)

$$\mathbf{v} = [v_b \quad v_1 \quad v_2 \quad . \quad . \quad . \quad v_{n-1} \quad v_n]^T \tag{3.161}$$

Since k_g and k_d are assumed to be linear, $\mathbf{v}$ is two elements less than $\mathbf{z}$. Consequently, $\mathbf{K}_i$ has two columns less than $\mathbf{K}_e$. The state-space equations are finally given by (3.131), (3.132), (3.133), (3.135), and

$$\dot{\mathbf{v}} = [\dot{v}_b \quad \dot{v}_1 \quad \dot{v}_2 \quad . \quad . \quad . \quad \dot{v}_{n-1} \quad \dot{v}_n]^T \tag{3.162}$$

$$\ddot{\mathbf{z}} = -\mathbf{M}^{-1}[\mathbf{K}_e \quad \mathbf{K}_i \quad \mathbf{C}]\mathbf{x} + \mathbf{M}^{-1}\mathbf{f} + \mathbf{M}^{-1}\mathbf{G}\mathbf{u} - \mathbf{M}^{-1}\mathbf{m}\ddot{y}_0 \tag{3.163}$$

3.9 ACTIVE VARIABLE STIFFNESS AND ACTIVE VARIABLE DAMPERS

For active control using variable stiffness devices, the control force can be expressed as

$$u_k = k(z)z \tag{3.164}$$

where $k(z)$ is a variable stiffness coefficient whose value generally depends on the interstory deformation z. For active control using variable dampers, the control force can usually be expressed as

$$u_c = c_c|\dot{z}|^n sign(\dot{z}) \tag{3.165}$$

where c_c is the viscous damping coefficient and n is a positive number ranging from 0.5 to 2. n has a value of 1 for linear viscous damping and a typical value of 0.5 for nonlinear dampers.

3.10 DISTURBANCES

For single-degree-of-freedom structures, a simplified model of the wind force can be written as [3]

$$f_w = p(3\sin\omega t + 7\sin 2\omega t + 5\sin 3\omega t + 4\sin 4\omega t) \tag{3.166}$$

where ω is the excitation fundamental frequency and p is the excitation magnitude. Fig. 3.13 shows an example of this wind force model. This model has been used in various studies to investigate the application of tuned mass dampers in a number of existing buildings in the U.S.

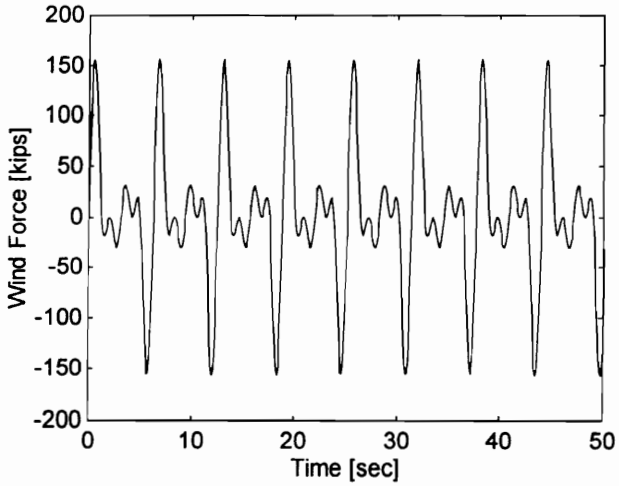

Fig. 3.13. Wind force

Earthquake excitation is typically specified as a time history of the ground acceleration. An example of the ground acceleration due to an earthquake is shown in Fig. 3.14.

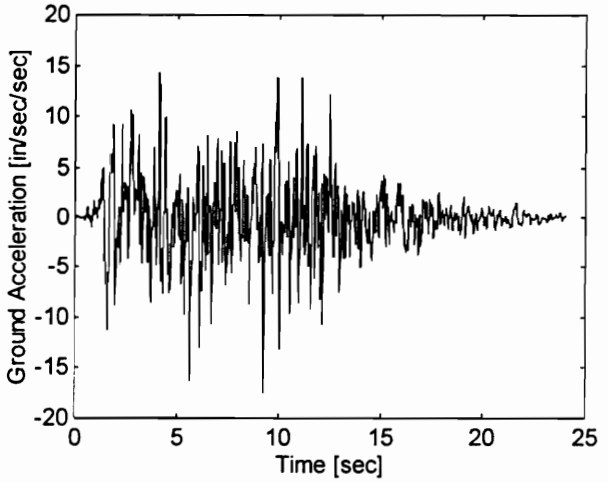

Fig. 3.14. Earthquake ground acceleration

A power spectral density plot of the ground acceleration is shown in Fig. 3.15. It shows the energy content at various frequencies. Most of the excitation energies are contained within 0 and 80 Hz.

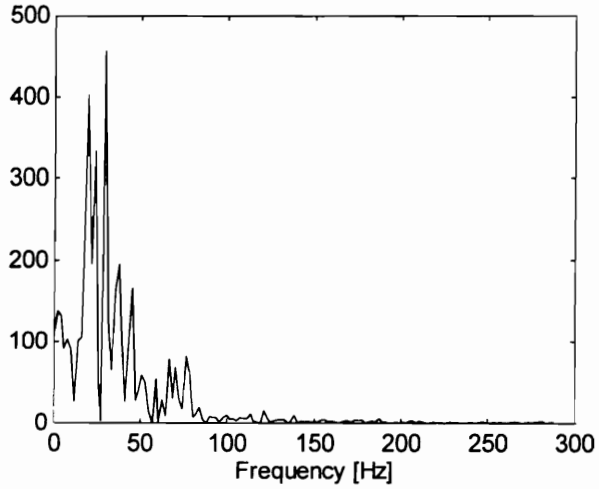

Fig. 3.15 Power spectral density of earthquake excitation

3.11 SUMMARY

The equations describing single-degree-of-freedom and multidegree-of-freedom models of structures are derived. Both fixed-base and base-isolated structures are considered. The equations are derived for various reference frames. The choice of which reference frame to use will depend on the available measurement data. Linear and nonlinear models are presented. Both wind and earthquake excitations are considered in the formulation of the equations. The wind force is modeled as a sum of sinusoids. An earthquake excitation is modeled by a time history of the ground acceleration.

CHAPTER 4

Proportional Control

4.1 INTRODUCTION

Classical control, represented by proportional-integral-derivative (PID) controllers, continues to provide great utility in practical applications for conventional systems. Although it is still usefulness in systems with one or two degrees-of-freedom, it does not suit the control of multi-degree-of-freedom systems because the PID control law is more difficult to formulate for these multivariable systems. However, the simplicity of the approach may outweigh any additional gains in performance that are possible for more-advanced modern control methods.

No original contribution is being claimed in this chapter. The reason for its inclusion is to provide a benchmark against which controllers for the regenerative electric actuator are evaluated. This chapter studies the effect of variations in gain, actuator time delay, and measurement time delay on the structural response. Differences between the results of a linear and a nonlinear simulation and the effect of control force saturation are also studied in this chapter.

For wind excitation, it is shown that proportional feedback control can provide effective control. However, the reduction in the structure's displacement is accompanied by an increase in the control force and the stroke length. The use of feedback control generally increases the control force to reduce the displacement. The increased force requirement, in turn, increases the stroke length. A certain amount of feedback gain variation can be tolerated without degrading the response. Critical values of actuator time delay and measurement time delay have to be determined. Feedforward control can also be used for wind-excited structures. Critical values for the gain, time delay, and sampling time determine the limits of effectiveness for this type of control. Simulations are conducted for a single-degree-of-freedom system and a fixed-base multistory building. Feedback and feedforward proportional control of the single-degree-of-freedom system under earthquake excitation is not effective. It is only slightly effective for a base-isolated multistory building. Regeneration can be achieved while under proportional control.

4.2 DISPLACEMENT FEEDBACK CONTROL

Fig. 4.1 shows a block diagram of a structural system where the displacement y, due to an external disturbance w, is used to generate the control input u . K is a proportional gain applied to the feedback y.

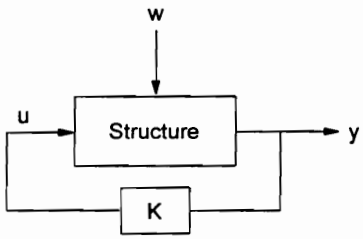

Fig. 4.1 Displacement-Feedback Control Scheme

The state equations of the system can be written as,

$$\dot{\mathbf{x}} = \mathbf{A}\mathbf{x} + \mathbf{B}u + \mathbf{H}\mathbf{w} \tag{4.1}$$

$$y = \mathbf{C}\mathbf{x} \tag{4.2}$$

If the control force is chosen to be of the form

$$u = Ky = K\mathbf{C}\mathbf{x} \tag{4.3}$$

then the state equations can be modified as

$$\dot{\mathbf{x}} = \mathbf{A}\mathbf{x} + \mathbf{B}K\mathbf{C}\mathbf{x} + \mathbf{H}\mathbf{w} = (\mathbf{A} + \mathbf{B}K\mathbf{C})\mathbf{x} + \mathbf{H}\mathbf{w} \tag{4.4}$$

or

$$\dot{\mathbf{x}} = \hat{\mathbf{A}}\mathbf{x} + \mathbf{H}\mathbf{w} \tag{4.5}$$

where

$$\hat{\mathbf{A}} = \mathbf{A} + \mathbf{B}K\mathbf{C} \tag{4.6}$$

Classical techniques, such as a root locus diagram, will show the effect of K on the poles of the system. This is equivalent to determining the eigenvalues of $\hat{\mathbf{A}}$ for various K.

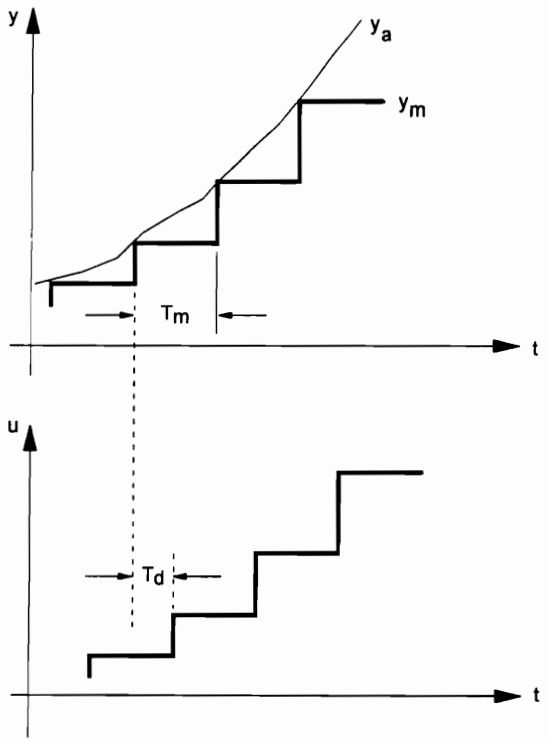

Fig. 4.2 Illustration of the actuator time delay (T_d) and measurement time delay (T_m)

A time delay (T_d) will always exist between the issuance of the control command by the controller and the application of the control force by the actuator. This is shown in Fig. 4.2. Therefore, the control expression is modified as

$$u(t) = Ky(t - T_d) = K\mathbf{C}\mathbf{x}(t - T_d) \tag{4.7}$$

The effect of time delay on the response of the system is determined in the test cases.

To reconstruct the feedback data, a zero-order hold (ZOH) is used. It assumes that the feedback is approximately constant within the sampling interval T_m as shown in Fig. 4.2. y_a is the actual displacement, while y_m is the reconstructed displacement. Obviously, the effectiveness of control is affected by the sampling time or measurement time (T_m). During this period, it is assumed that the control force u is kept constant at the value commanded at the start of the interval. The effect of measurement time on the system response is also investigated in the cases considered.

The instantaneous actuator power is calculated as the product of the control force and the stroke velocity. Thus,

$$p_a(t) = u(t)\dot{z}(t) \tag{4.8}$$

The energy supplied by the electrical source to the actuator is expressed as,

$$e_a(t) = \int p_a(t)dt \tag{4.9}$$

The simulations in this chapter assume that the effect of the actuator dynamics are negligible. This affords faster evaluation of the controller. The actuator operates in the 4-quadrant mode, acting as both a motor and a generator. Negative power indicates that it is the recovered power and it is stored for later use, instead of simply being dissipated as heat in other actuator types.

Example 4.1 SDOF Structure with Mass Damper

Consider a building structure with a mass damper on the top floor. The damper is used primarily to suppress the first fundamental mode of motion induced by external disturbances. A single-degree-of-freedom model of the structure with the mass damper is shown in Fig. 4.3. Assume the parameters of the system to be m_s = 104 kips-sec^2/in., c_s = 2.08 kips-sec/in., k_s = 104 kips/in., m_d = 2.08 kips-sec^2/in., c_d = 0.137 kips-sec/in., and k_d = 1.73 kips/in. The nonlinear structural stiffness is assumed to be characterized by the parameters α = 0.1, λ = 1.0, β = 0.18, γ = 0.18, and D_y = 1.0 in.

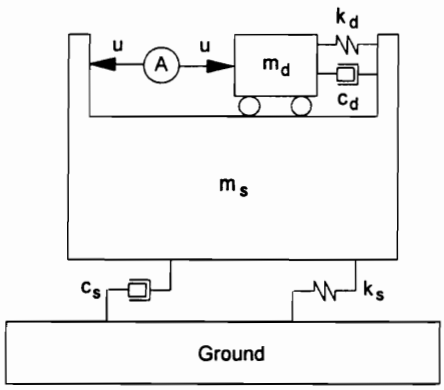

Fig. 4.3 Single-degree-of-freedom structure with mass damper

A root locus plot for a linear model of the system, with proportional feedback control, is shown in Fig. 4.4. The structure's displacement with respect to the ground is used as the feedback quantity, i.e. $u = Ky_s$. Two of the poles cross over to the right half plane at a gain K = -2.54. The plot shows that optimum damping is obtained just before the poles breakaway towards $K = +\infty$. After breakaway, only minimal changes in the damping ratio is obtained. This implies that increasing the gain further does not provide any significant improvement in the system response.

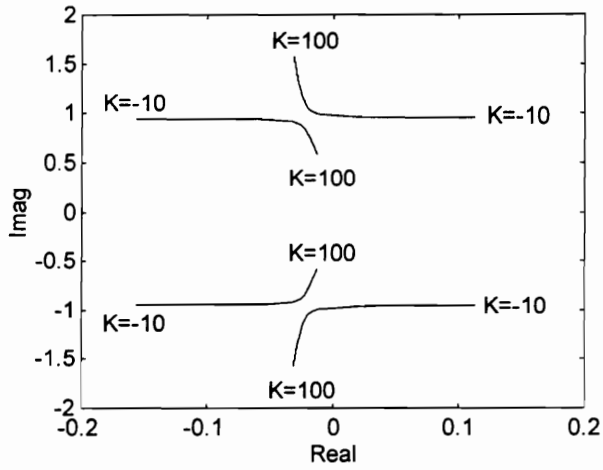

Fig. 4.4 Root locus for varying gain

Suppose that a wind excitation with parameters p = 9.75 kips and ω =1.0 rad/sec is applied to the structure. The resulting displacement for various gain values are shown in Fig. 4.5. In these simulations, it is assumed that the excitation is applied indefinitely. In the actual case, the excitation has a finite duration and eventually reduces to zero. The simulations use a nonlinear model for the structural stiffness. The time delay and measurement time are fixed at 0.0 seconds and 0.1 seconds, respectively. These plots show that after a gain of about K = 5 there is no significant reduction in the displacement. Thus, control efficiency is maximum near this value of gain.

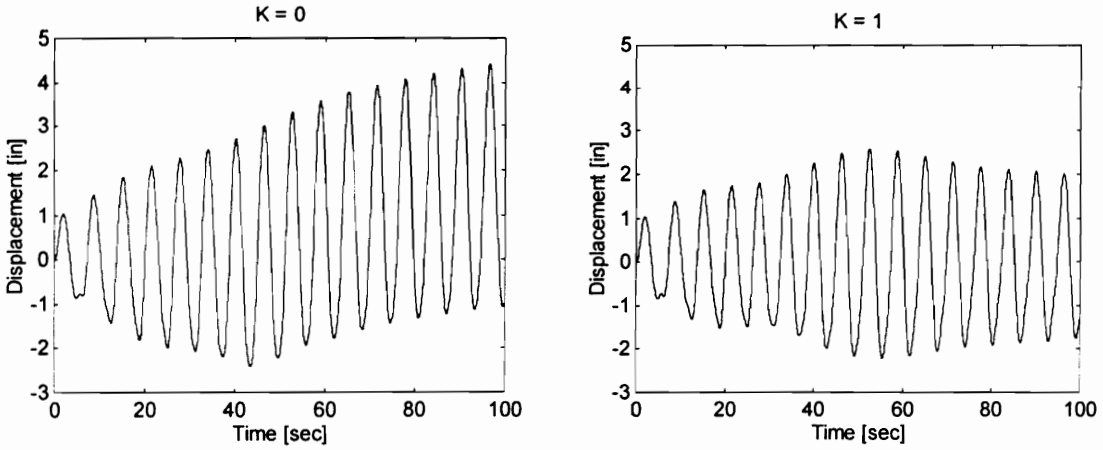

Fig. 4.5 Displacement for various gain (K) values

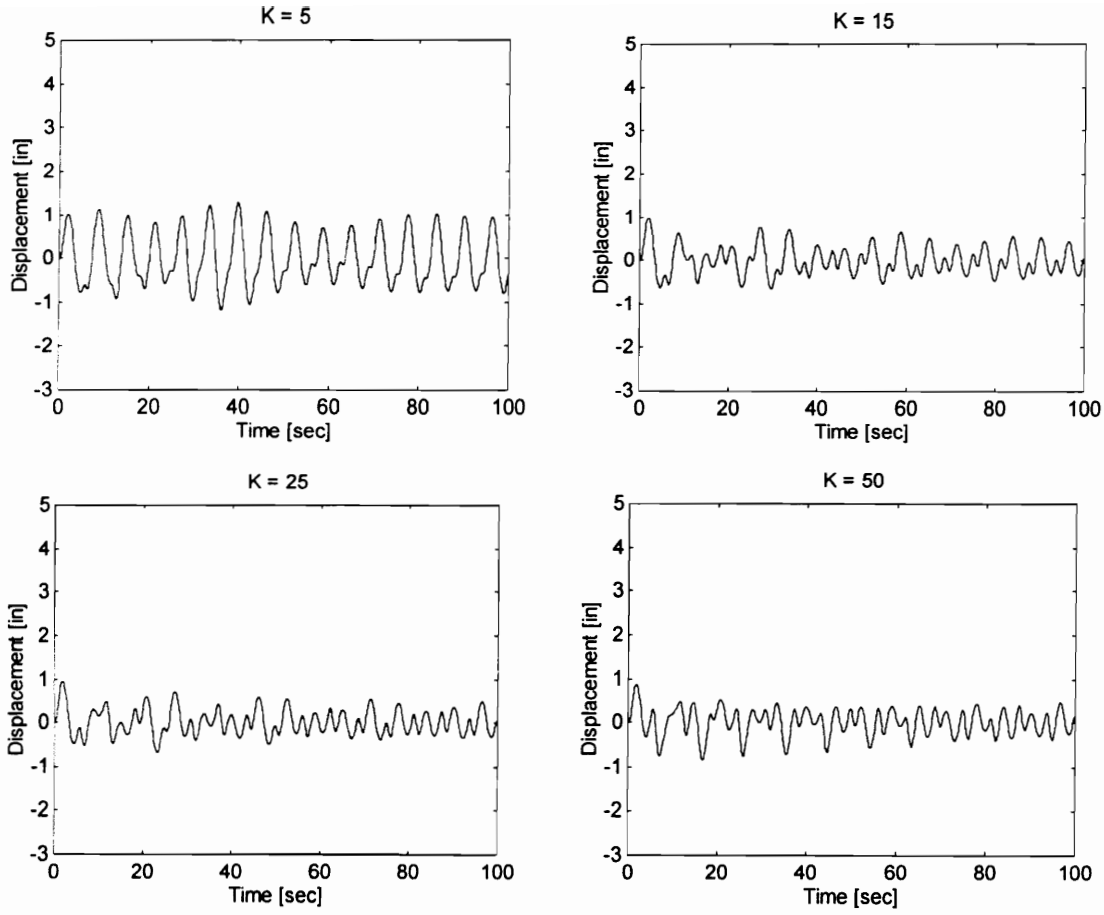

Fig. 4.5 (cont.) Displacement for various gain (K) values

A comparison of the structure's response with (K = 15) and without proportional control is shown in Table 4.1. There is a 79 % decrease in the peak displacement of the structure. However, this is accompanied by a 68 % increase in the peak stroke length. Thus, reducing the peak displacement will require an increase in the stroke length.

TABLE 4.1 Comparison of Response for Passive and Proportional Control

CONTROL TYPE	y_s(peak)	y_s(rms)	z(peak)	z(rms)
Passive	4.6275	1.8895	15.4839	9.3422
Proportional Control	0.9765	0.3342	26.0389	11.5849

where y_s is the structure's displacement with respect to the ground (in.) and z is the relative displacement between the structure and the damper (in.). z is also called the stroke length.

Fig. 4.6 shows the required actuator force, power, and energy for K = 15. Note that there are periods of negative actuator power. This means that power flows from the regenerative actuator to its electrical supply. The recovered energy is stored for later use, instead of being dissipated as heat. Therefore, the energy supplied by the source to the actuator is not monotonically increasing as one would expect for purely-motoring operation. Regeneration is achieved whenever negative power becomes available.

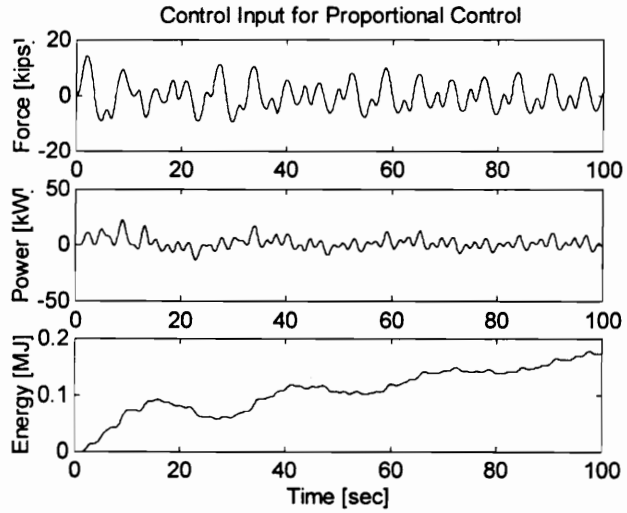

Fig. 4.6 Actuator force, power, and energy for K = 15

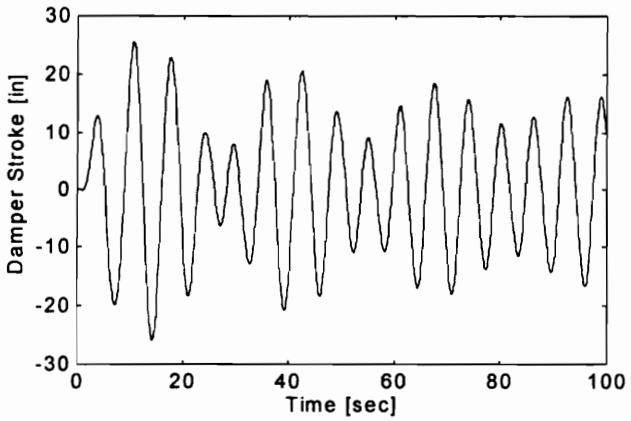

Fig. 4.7 Damper stroke length for K = 15

Fig. 4.7 shows a plot of the damper stroke length when the gain is K = 15. When the stroke velocity has the same polarity or direction as the control force, then positive power is obtained. This corresponds to motoring action in the regenerative actuator. Energy is being drawn from the electrical supply. If the stroke velocity is in the opposite direction as the actuator force, then

generator action occurs and negative power is obtained. In this case, energy is returned to the actuator electrical supply source.

Linear versus Nonlinear Model Response

A comparison is made between the resulting displacement for a linear and a nonlinear model of the structure. The difference between the results is shown in Fig. 4.8. Clearly, the use of a linear model will not affect the results significantly. It is assumed, however, that control is applied immediately at the start of the disturbance. Otherwise, the initial conditions will become different for the two simulations. It is noticed that there is zero difference between the two simulations at the beginning of the simulation. This simply means that the nonlinear simulation keeps the displacement within the elastic (linear) region of the stiffness characteristics.

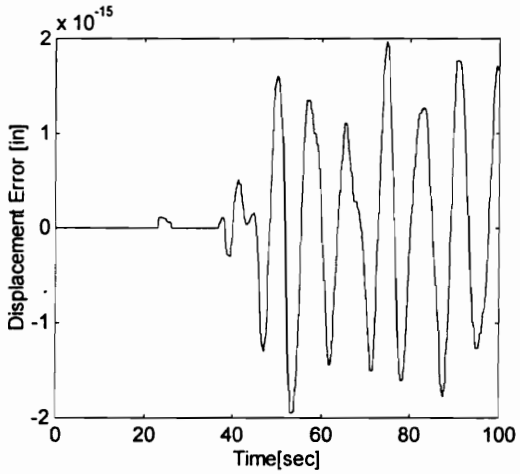

Fig. 4.8 Difference between a linear and a nonlinear simulation

Gain Variation

The sensitivities of the maximum displacement, control force, and damper stroke-length to variations in gain (K) are shown in figures 4.9, 4.10, and 4.11, respectively. Increasing the gain above $K = 7$ does not produce any significant reduction in the maximum displacement. Thus, the larger control force being provided by the larger gains does not necessarily translate to a proportional decrease in the peak displacement. In fact, the maximum displacement starts to increase after $K = 50$. Looking at the root locus of the linear system, the increase in the displacement peak can be attributed to the decrease in the damping ratio of two system poles with increasing K. As expected, the maximum control force increases with the gain. The stroke-length also increases with increasing gain to provide the larger control force.

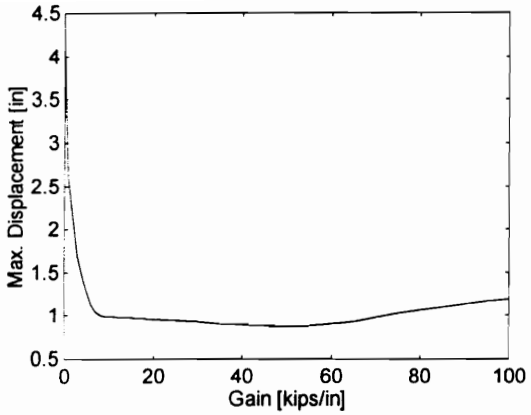

Fig. 4.9 Sensitivity of the maximum displacement to variations in feedback gain

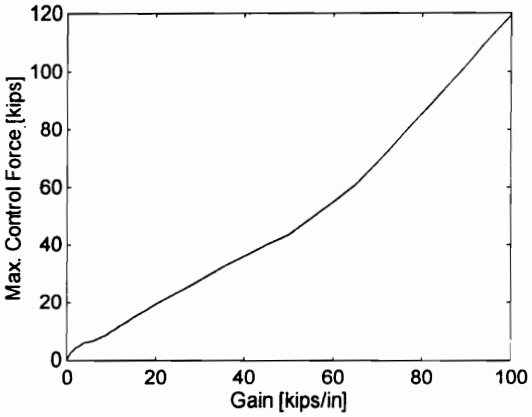

Fig. 4.10 Sensitivity of the maximum control force to variations in feedback gain

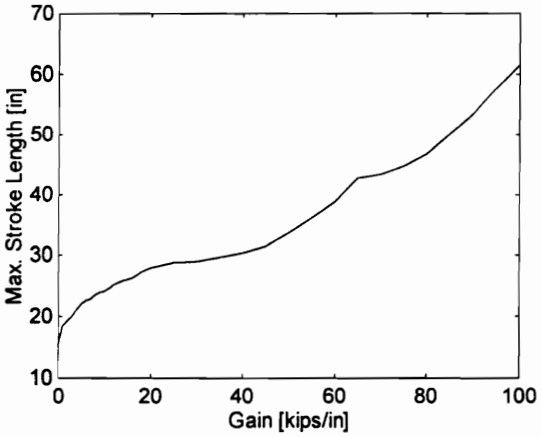

Fig. 4.11 Sensitivity of the maximum stroke length to variations in feedback gain

Effect of Actuator Time Delay

Fig. 4.12 shows the resulting displacement of the structure as the time delay is gradually increased. A gain of 15 kips/in. and a measurement time of 0.05 seconds are used. There is no significant degradation of the displacement response up to T_d = 0.35 second. However, the system abruptly becomes unstable after that. This means that the time delay has exceeded the critical delay time.

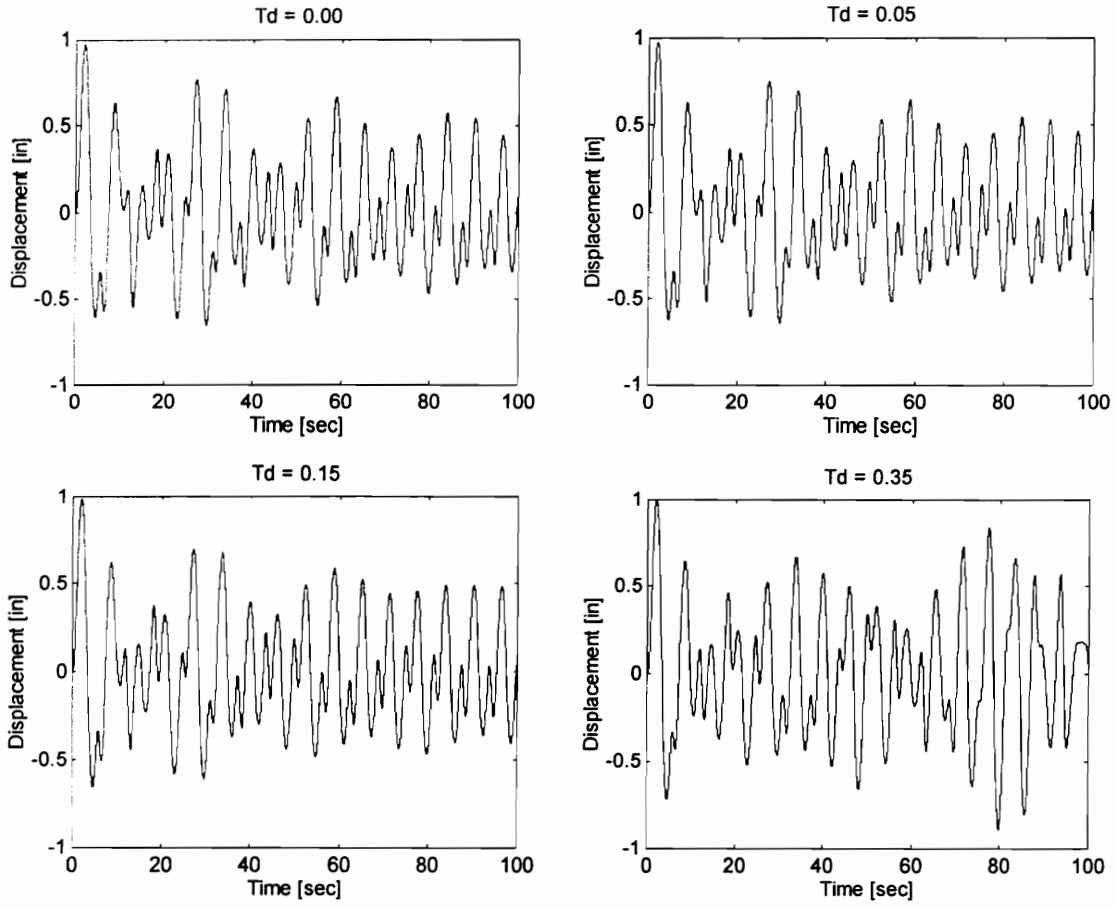

Fig. 4.12 Displacement for various actuator time delays (T_d seconds) for $K = 15$.

Sensitivity to Actuator Time Delay

The sensitivities of the maximum displacement, maximum control force, and maximum stroke length to variations in the actuator time delay are given in figures 4.13, 4.14, and 4.15, respectively. These plots show that the critical delay time is about 0.35 seconds, after which the system could become excited by the control force and even become unstable. Although the maximum control force and maximum displacement only start to increase at a delay of 0.35 seconds, the stroke length starts to increase at a delay of 0.10 second. Therefore, it would be desirable to keep the actuator time delay at about 0.10 second to obtain the minimum stroke length.

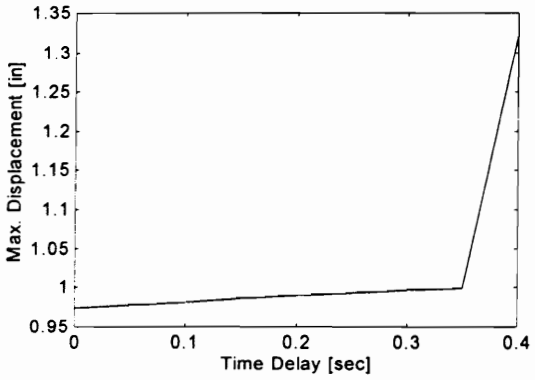

Fig. 4.13 Sensitivity of the maximum displacement to variation in time delay

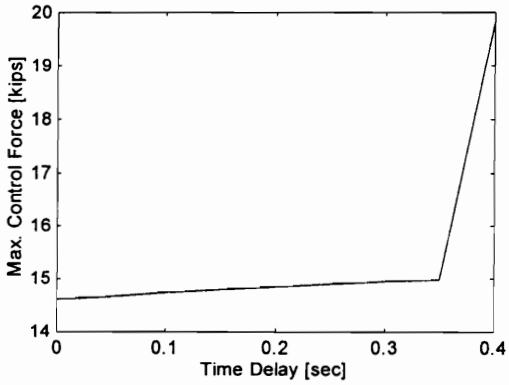

Fig. 4.14 Sensitivity of the maximum control force to variation in time delay

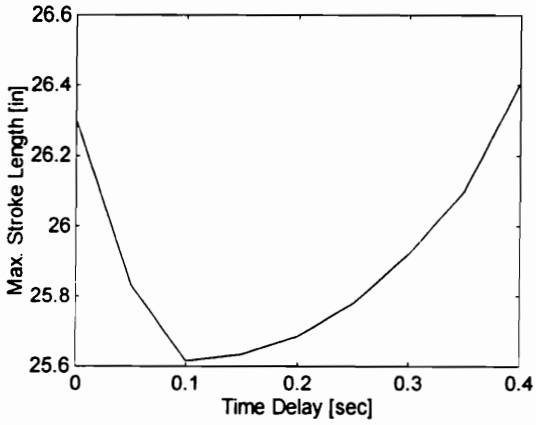

Fig. 4.15 Sensitivity of the maximum stroke length to variations in time delay

Effect of Measurement Time Delay

Fig. 4.16 shows the displacement of the structure for various measurement time delays. A gain of 15 kips/in. and an actuator time delay of 0.0 seconds are used in these simulations. There is no significant degradation in the displacement response until T_m = 0.20 second, after which the system becomes unstable. This corresponds to the critical value for stability. In terms of an equivalent discrete-time system, at this value of the sampling time one root of the system has moved out of the unit circle and causing instability.

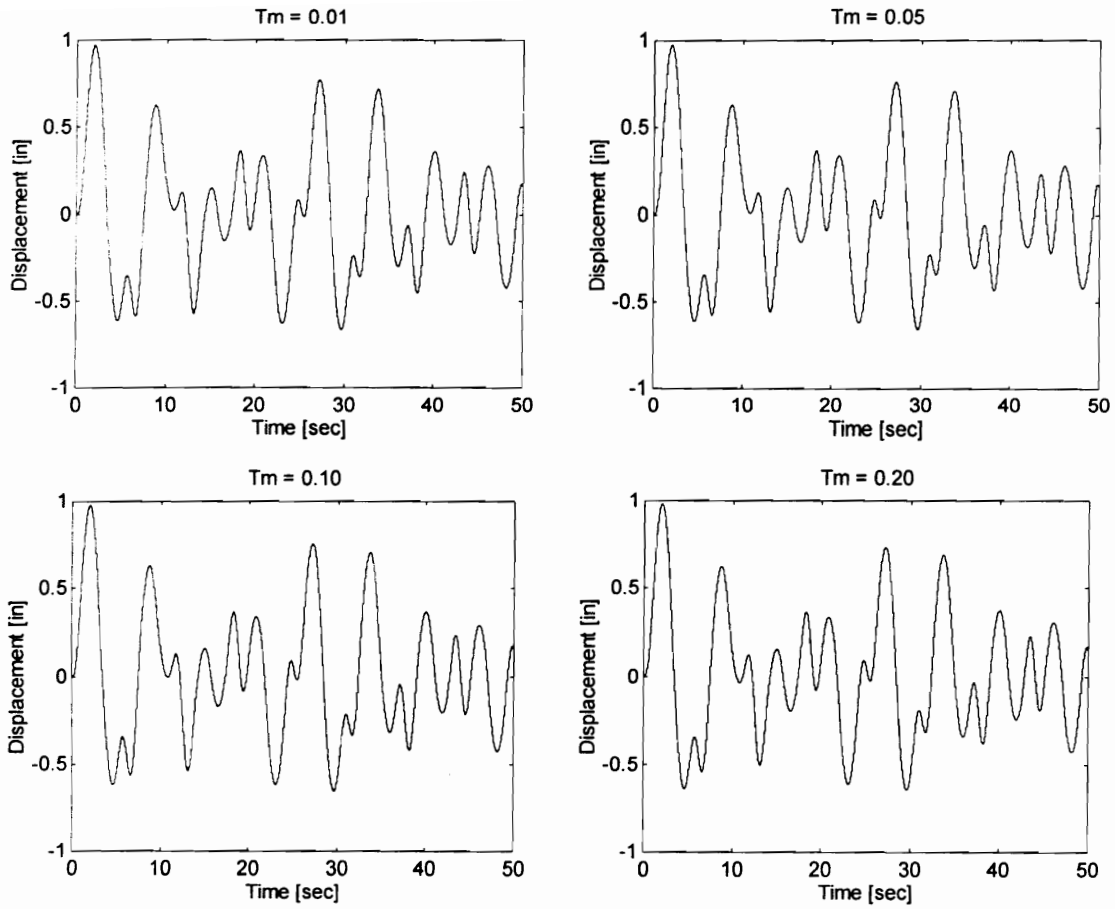

Fig. 4.16 Displacement for various measurement time delays (T_m seconds) using $K = 15$

Sensitivity to Measurement Time Delay

The effect of varying the measurement time delay on the maximum displacement, maximum control force, and maximum stroke length are exhibited in figures 4.17, 4.18, and 4.19, respectively. There is a negligible amount of variation in these quantities up to the critical value $T_m = 0.20$ second. After that, instability sets in.

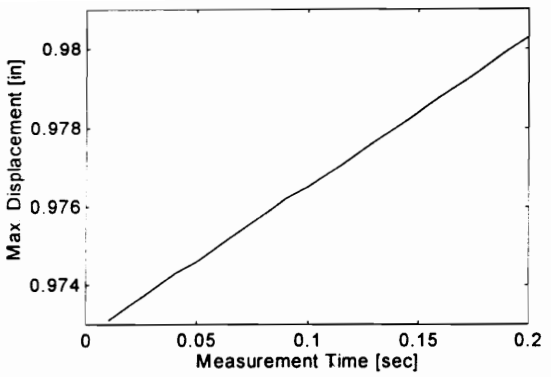

Fig. 4.17 Sensitivity of the maximum displacement to variation in measurement time delay

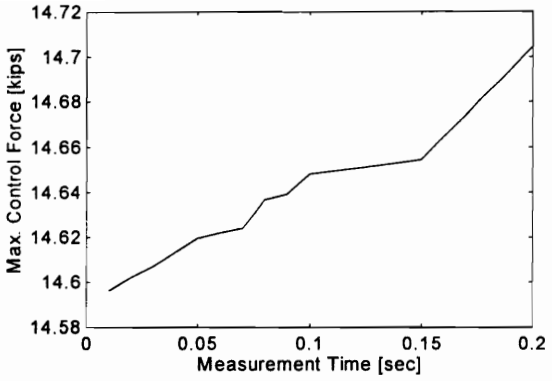

Fig. 4.18 Sensitivity of the maximum control force to variation in measurement time delay

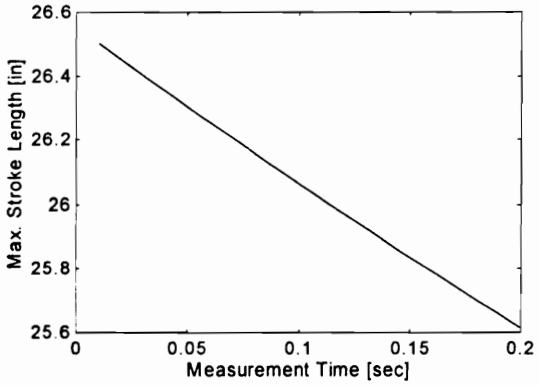

Fig. 4.19 Sensitivity of the maximum stroke length to variation in measurement time delay

Example 4.2 Earthquake-excited Structure

An earthquake excitation (see Fig. 3.14) is applied to the system in Example 4.1. The ground acceleration has a maximum value of 17.53 in/sec^2. Without any control, the displacement is shown in Fig. 4.20. The displacement given by Fig. 4.21 is obtained when a displacement-feedback controller with a gain of 15 kips/in is used. This controller, which is found to be effective for wind excitation, is ineffective for the given earthquake excitation. This can be attributed to the high frequency components of the excitation which make feedback of the displacement insufficient to achieve control of the structure.

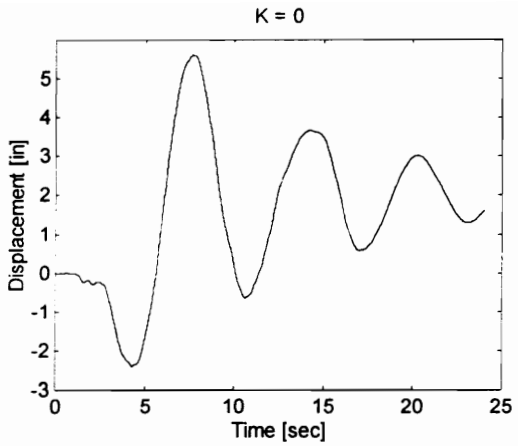

Fig. 4.20 Displacement without control

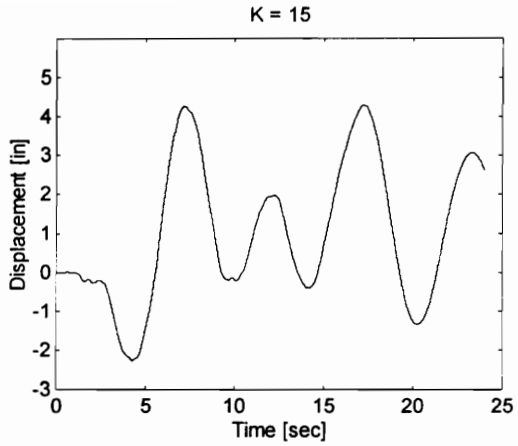

Fig. 4.21 Displacement with feedback control

Example 4.3 Linear, Fixed-Base, 8-Story Building with a Mass Damper on the Top Floor

Fig. 4.22 shows a linear, fixed-base, 8-story building with a mass damper on the top floor.

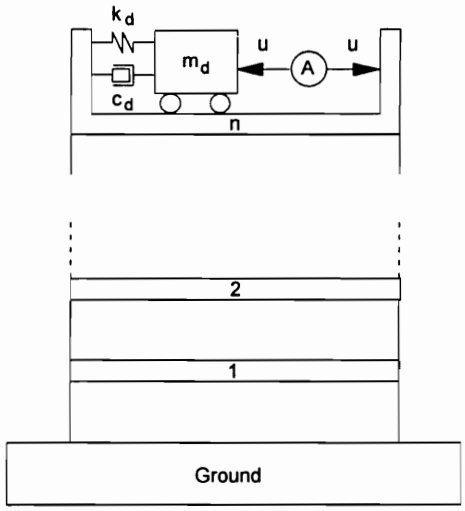

Fig. 4.22 Linear, fixed-base, eight-story structure

The structure has the parameters given in Table 4.2.

TABLE 4.2 Parameters of the Structure

Floor	m [metric tons]	c [kN-sec/m]	k [kN/m]
1	345.6	490	3.40×10^5
2	345.6	467	3.26×10^5
3	345.6	410	2.85×10^5
4	345.6	386	2.69×10^5
5	345.6	348	2.43×10^5
6	345.6	298	2.07×10^5
7	345.6	243	1.69×10^5
8	345.6	196	1.37×10^5
Damper	172.8	76.98	843.97

Without any form of active control, the response of the structure to a wind excitation is shown in Fig. 4.23. The wind force acting on each floor is given by

$$f_i = \frac{i}{8} p(3\sin\omega t + 7\sin 2\omega t + 5\sin 3\omega t + 4\sin 4\omega t)$$
$$i = 1,2,3,4,5,6,7,8$$

where p = 43.37 kN and ω = 1.0 rad/sec.

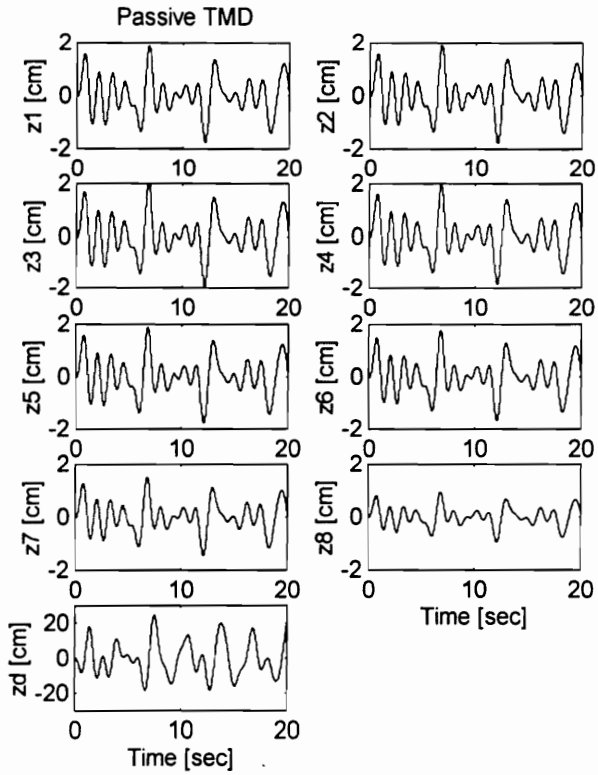

Fig. 4.23 Interstory displacements with passive control

Using a feedback of the displacement of the 8th floor with respect to the ground, a proportional controller with a gain of 10000 kN/m is used to provide active control to the structure. The resulting interstory displacements are shown in Fig. 4.24.

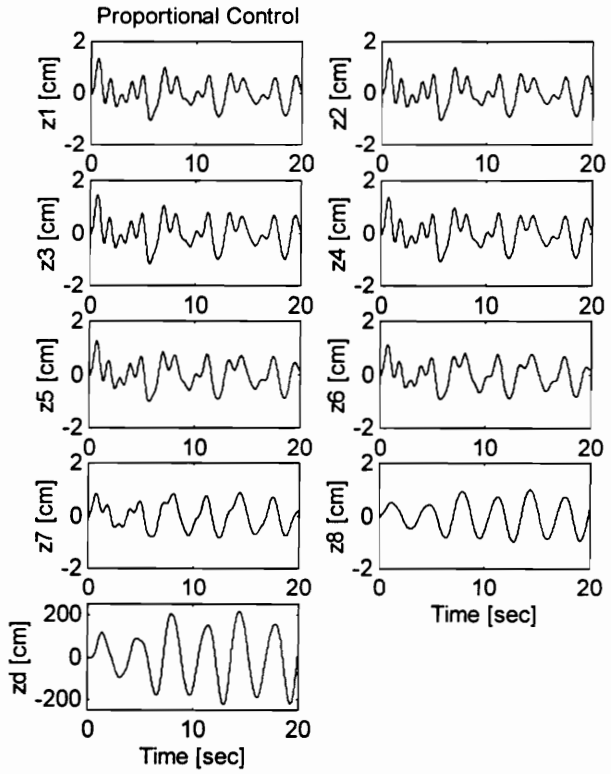

Fig. 4.24 Interstory displacements with proportional control

A comparison of the building response with passive control and with proportional control is shown in Table 4.3. The third story experiences the largest interstory drift. A 31% reduction in this floor's peak displacement is achieved with proportional control. However, this is accompanied by a 820% increase in the peak damper stroke. As expected, the eighth floor experiences the largest displacement with respect to ground. This peak displacement is reduced by 36% with proportional control applied.

TABLE 4.3 Comparison of Response for Passive and Proportional Control

FLOOR	Z_{pas}	Z_{pro}	R_{pas}	R_{pro}	Y_{pas}	Y_{pro}
1	1.9067	1.3400	0.7100	0.4867	1.9067	1.3400
2	1.9321	1.3520	0.7197	0.4926	3.8388	2.6920
3	2.0803	1.4422	0.7755	0.5295	5.9191	4.1342
4	1.9949	1.3603	0.7447	0.5082	7.9140	5.4945
5	1.8995	1.2591	0.7107	0.4892	9.8134	6.7536
6	1.7791	1.1207	0.6684	0.4796	11.5925	7.8730
7	1.5231	0.9006	0.5773	0.4860	13.1156	8.7249
8	0.9532	1.0235	0.3720	0.5537	14.0672	9.0484
Damper	24.4881	225.2129	9.9176	121.1703	21.3250	225.2893

where Z is the maximum interstory drift (cm), R is the RMS value of the interstory drift (cm), Y is the maximum displacement with respect to the ground (cm), *pas* is a subscript denoting passive control response, and *pro* is a subscript denoting proportional control response

The actuator force, power, and energy is shown in Fig. 4.25. The peak actuator force is 905 kN, which is 29% of the peak disturbance force (3128 kN) applied to the structure. Again, there are periods where the regenerative actuator's power is negative. This means that the actuator is able to regenerate and store this energy. The net energy flow is, however, from the source to the actuator.

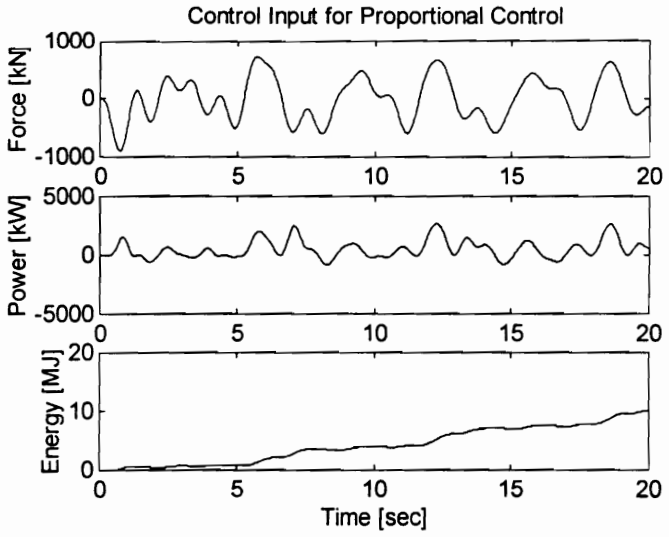

Fig. 4.25 Actuator force, power, and energy for proportional control

The damper stroke length is shown in Fig. 4.26. When the stroke velocity is in the same direction as the applied control force, then positive power is drawn from the electrical source. Motoring action occurs in the actuator. When the stroke velocity and control force are in opposite direction, then generator action occurs and energy is recovered and stored for later use.

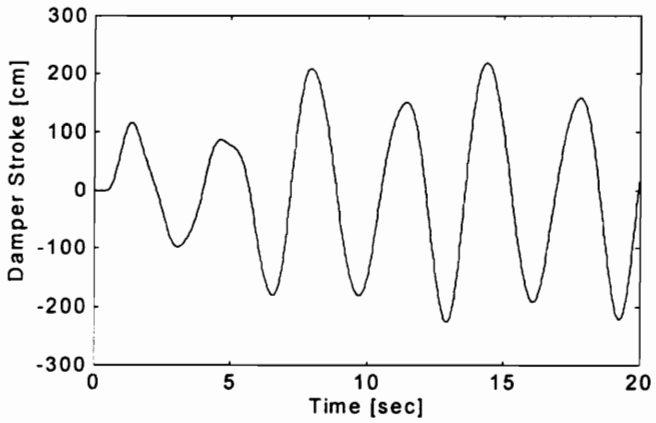

Fig. 4.26 Damper stroke length for proportional control

The effect of variations in the gain on the maximum interstory drift, the maximum damper stroke, the maximum displacement with respect to ground, and the maximum control force is shown in figures 4.27, 4.28, 4.29, and 4.30. Increasing the gain reduces the interstory drifts, but increases the required control force. The increase in the control force causes a corresponding increase in the damper stroke. Because only one feedback variable is used, a very limited amount of adjustment in the system characteristics is attainable. At a gain of about 1000, the interstory drifts start to decrease but, at the same time, the damper stroke and control force show a significant increase.

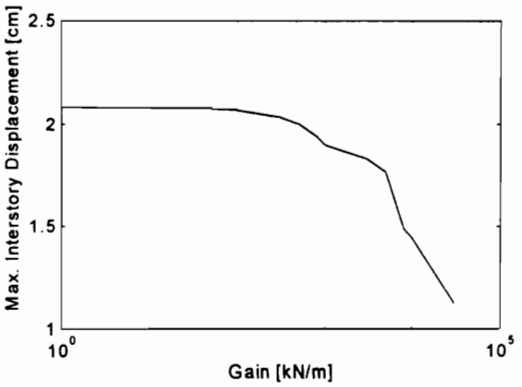

Fig. 4.27 Effect of gain variation on the maximum interstory drift

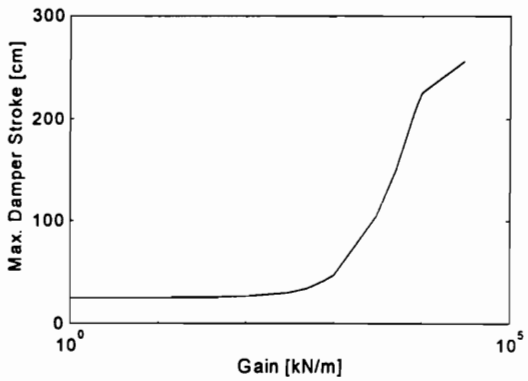

Fig. 4.28 Effect of gain variation on the maximum damper stroke

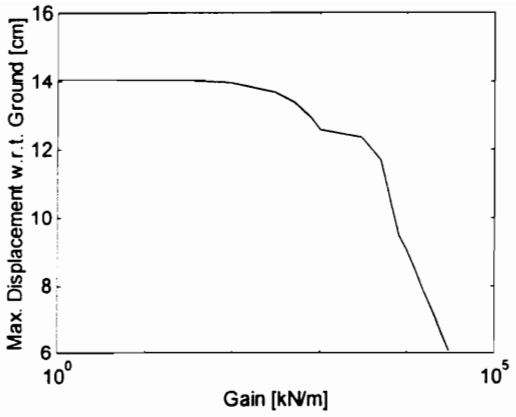

Fig. 4.29 Effect of gain variation on the maximum displacement with respect to the ground

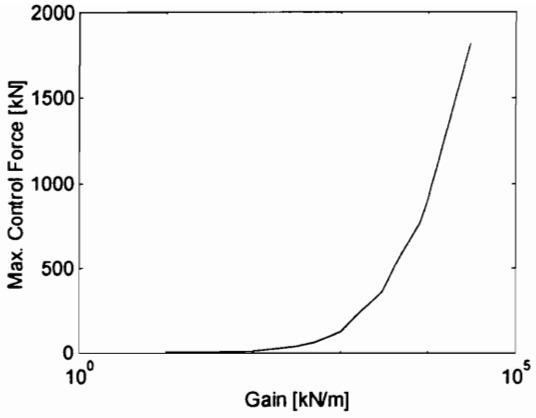

Fig. 4.30 Effect of gain variation on the maximum control force

Example 4.4 Linear, Base-Isolated, 8-Story Building with a Mass Damper on the Base Floor

Fig. 4.31 shows a linear, base-isolated, 8-story building with a mass damper on the base floor.

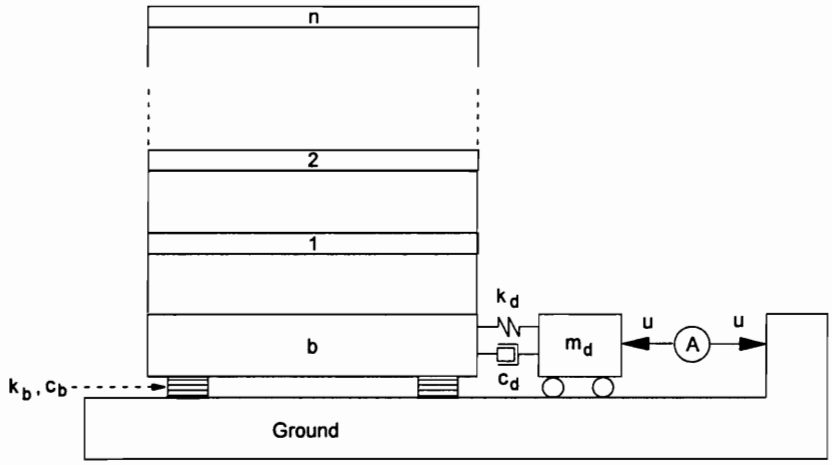

Fig. 4.31 Linear, base-isolated, eight--story structure

Table 4.4 gives the parameters of the structure.

TABLE 4.4 Parameters of the Structure

Floor	m [metric tons]	c [kN-sec/m]	k [kN/m]
Damper	172.8	76.38	843.97
Base	450.0	26.17	18050
1	345.6	490	3.40×10^5
2	345.6	467	3.26×10^5
3	345.6	410	2.85×10^5
4	345.6	386	2.69×10^5
5	345.6	348	2.43×10^5
6	345.6	298	2.07×10^5
7	345.6	243	1.69×10^5
8	345.6	196	1.37×10^5

With the mass damper acting in the passive mode, the structure's response to an earthquake excitation (see Fig. 3.14) is shown in Fig. 4.30.

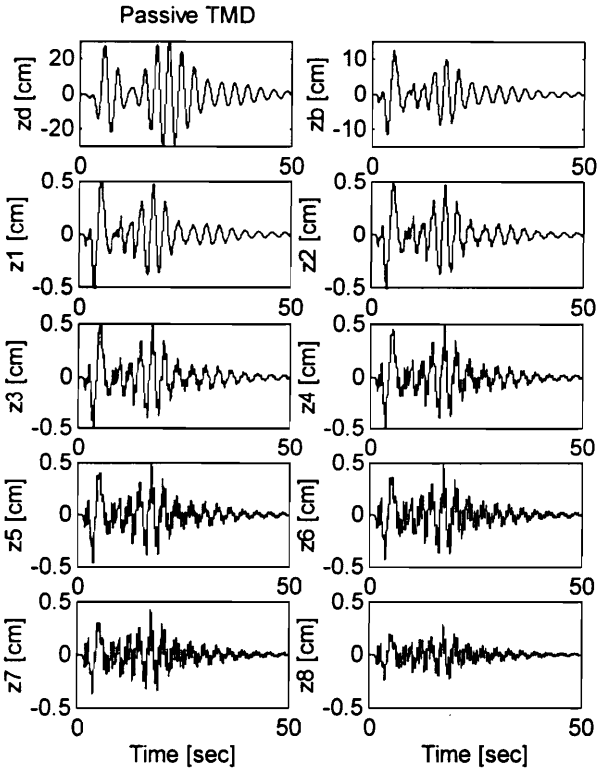

Fig. 4.32 Interstory displacements with passive control

To provide active control, a proportional controller with a gain K_p of 1000 uses a feedback of the base displacement. The resulting interstory displacements are shown in Fig. 4.33.

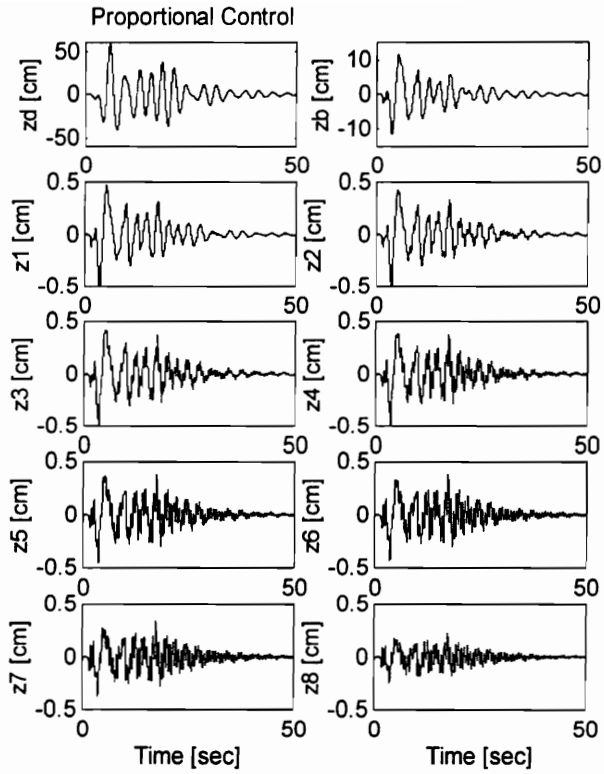

Fig. 4.33 Interstory displacements with proportional control

Table 4.5 gives a comparison of the response of the structure in the passive mode and with proportional control. For this case, the first floor has the largest interstory deformation. Proportional control is able to reduce this displacement by 4%. As with any base-isolated system, interstory displacement is minimal while base displacement is sizable. A 7% reduction in the base displacement is afforded by proportional control. This controller, however, also causes a 91% increase in the stroke length (from 35 cm to 68cm). Thus, the introduction of the feedback gain increases the damping on poles corresponding to all masses, except the damper mass where damping is reduced.

TABLE 4.5 Comparison of Responses for Passive and Proportional Control

FLOOR	Z_{pas}	Z_{pro}	R_{pas}	R_{pro}	Y_{pas}	Y_{pro}
Damper	31.4095	58.9167	10.8387	15.4515	35.4893	67.6722
Base	12.5719	11.6516	3.4460	3.0121	12.5719	11.6516
1	0.5401	0.5182	0.1492	0.1265	13.1090	12.1500

2	0.5120	0.4978	0.1399	0.1191	13.5905	12.6351
3	0.5326	0.5185	0.1426	0.1226	14.0548	13.1300
4	0.5094	0.4857	0.1326	0.1154	14.4606	13.5950
5	0.4984	0.4559	0.1250	0.1105	14.8198	14.0418
6	0.4846	0.4292	0.1181	0.1060	15.1363	14.4684
7	0.4349	0.3763	0.1037	0.0944	15.3955	14.8445
8	0.2891	0.2428	0.0681	0.0627	15.5620	15.0866

where Z is the maximum interstory drift (cm), R is the RMS value of the interstory drift (cm), Y is the maximum displacement with respect to the ground (cm), *pas* is a subscript denoting passive control response, *pro* is a subscript denoting proportional control response

The actuator force, power, and energy are shown in Fig. 4.34. The peak control force (117 kN) is only about 1% of the total force (7541 kN) acting on the structure. Therefore, proportional control is slightly effective for this particular structure and excitation. Although there are periods of negative power which allow the regenerative actuator to recover energy, the actuator is mostly operating as a motor and consuming energy.

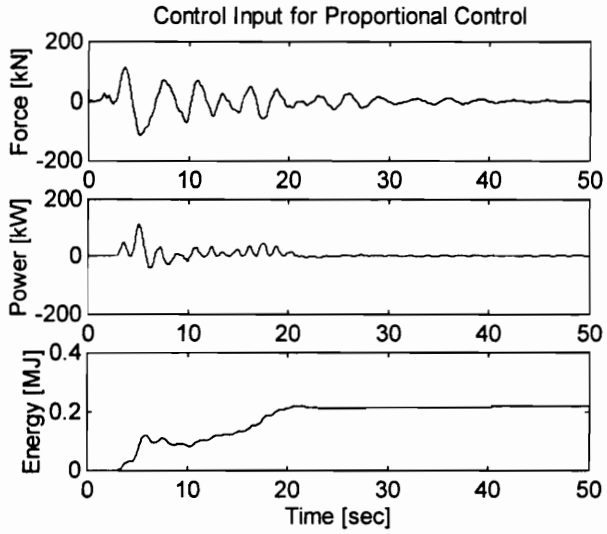

Fig. 4.34 Regenerative actuator force, power, and energy for proportional control

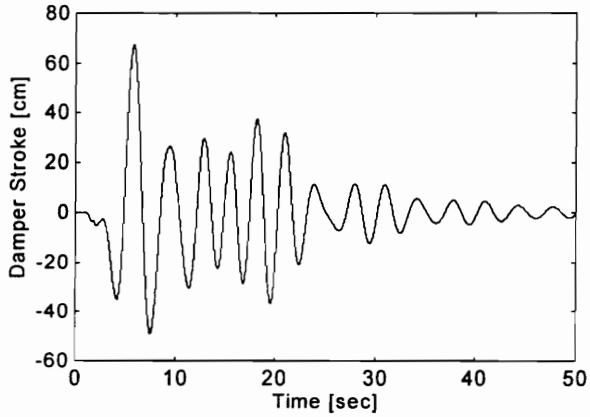

Fig. 4.35 Damper stroke length for proportional control

The damper stroke length when proportional control is applied is shown in Fig. 4.35. The stroke length is the displacement of the damper with respect to the ground. The peak stroke occurs during the early part of the disturbance. Motoring occurs when the stroke velocity and the control force are in the same direction. Otherwise, generator action is obtained and energy is recovered.

The effect of gain variation on the maximum damper stroke, maximum base displacement, maximum interstory drift, and maximum control force is shown in figures 4.36, 4.37, 4.38, and 4.39. Minimum base displacement occurs at a gain of 1000, before it starts to increase with increasing gain. The interstory displacement also keeps decreasing until a gain of 1000 is reached. Therefore, this is a critical gain value after which instability starts to set in. Some of the excitation frequencies could also be approaching one or more of the system pole frequencies, contributing to the tendency to be unstable after a gain of 1000.

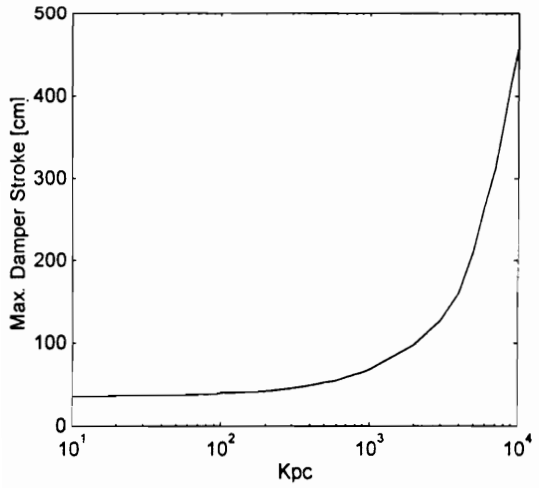

Fig. 4.36 Effect of gain variation on the maximum damper stroke

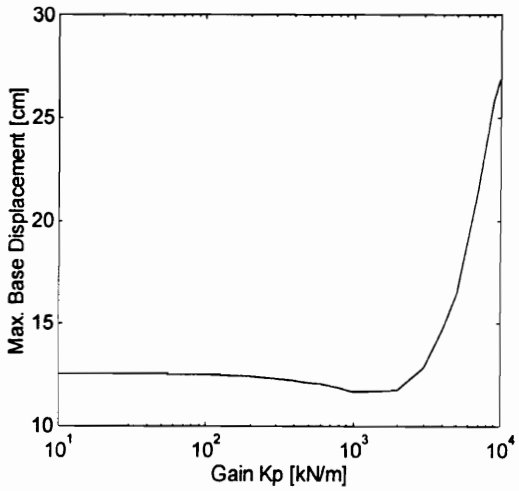

Fig. 4.37 Effect of gain variation on the maximum base displacement

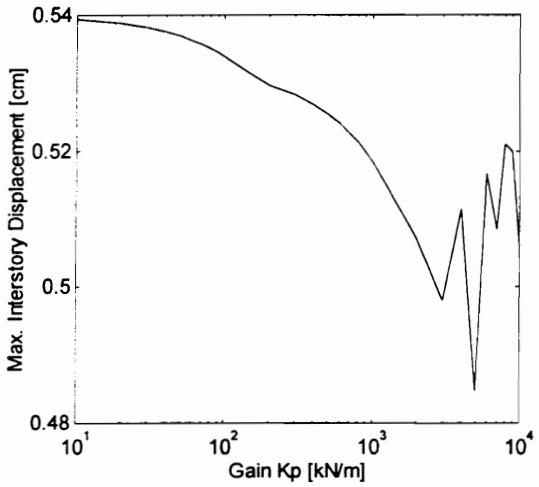

Fig. 4.38 Effect of gain variation on the maximum interstory drift

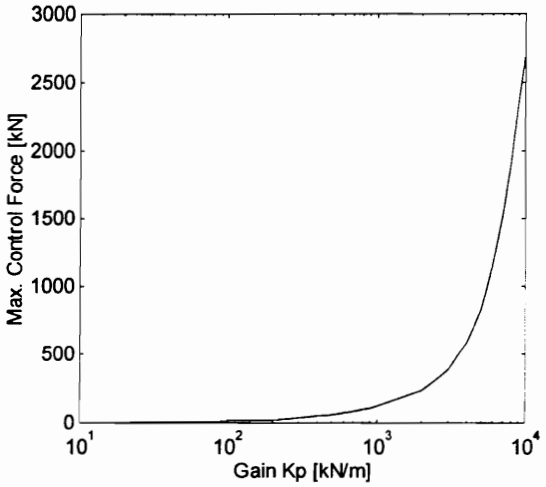

Fig. 4.39 Effect of gain variation on the maximum control force

4.3 FEEDFORWARD CONTROL

Fig. 4.40 shows a block diagram of a structure employing feedforward control, where a measurement of the external excitation w is used to generate the control force u. A gain K is applied to the measured excitation value to obtain the control input u. It is assumed that the disturbance can be measured without any distortion or significant time delay. Otherwise, the system can become unstable when the distortion or delay causes an incorrect phase shift.

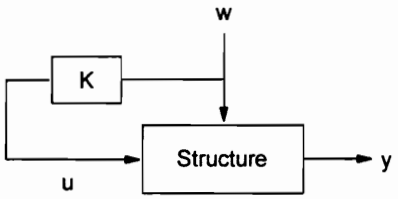

Fig. 4.40 Feedforward control scheme

The control input is of the form

$$u = Kw \tag{4.10}$$

The state equations are modified as

$$\dot{\mathbf{x}} = \mathbf{A}\mathbf{x} + \mathbf{B}(Kw) + \mathbf{H}w = \mathbf{A}\mathbf{x} + (\mathbf{B}K + \mathbf{H})w \tag{4.11}$$

It can be observed that feedforward control does not affect the system poles.

Example 4.5

Using the nonlinear system of Example 4.1 under wind excitation, plots of the resulting displacements when various gain values are employed are given in Fig. 4.41. A gain $K = 0.12$ produces the least displacements.

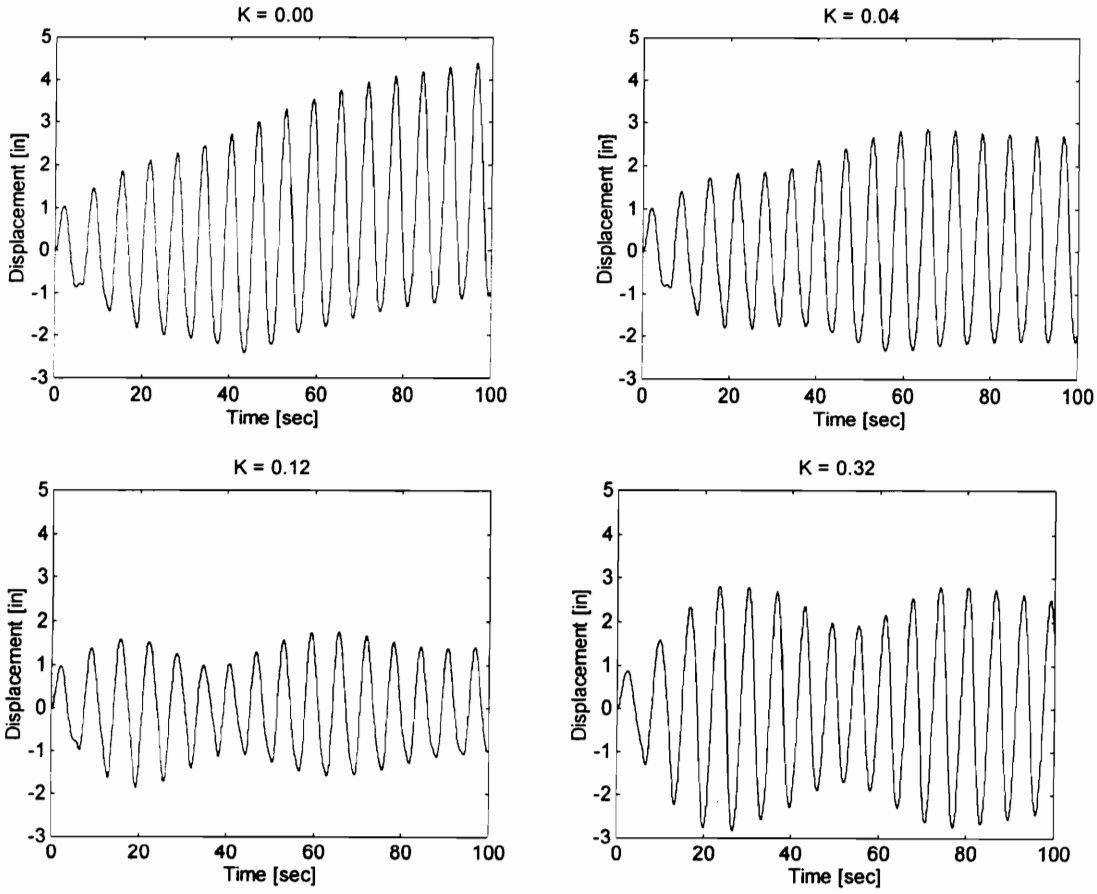

Fig. 4.41 Displacement for various feedforward gains (K)

A comparison of the responses for the passive case and a case with proportional feedforward control ($K = 0.12$) is shown in Table 4.6. A 60% reduction in the peak displacement is achieved through a 19% increase in the damper stroke.

TABLE 4.6 Comparison of Response for Passive and Proportional Control

CONTROL TYPE	y_s(peak)	y_s(rms)	z(peak)	z(rms)
Passive	4.6275	1.8895	15.4839	9.3422
Proportional Control	1.8679	0.9773	18.4036	10.0204

where y_s is the structure's displacement with respect to the ground (in.) and z is the relative displacement between the structure and the damper (in.).

Fig. 4.42 shows the actuator force, power, and energy required for K = 0.12. The negative power values indicate that the regenerative actuator is able to recover energy from the excitation. Note that the net energy flow is from the actuator to the source. This means that during the duration of the excitation, the source has gained energy instead of losing it.

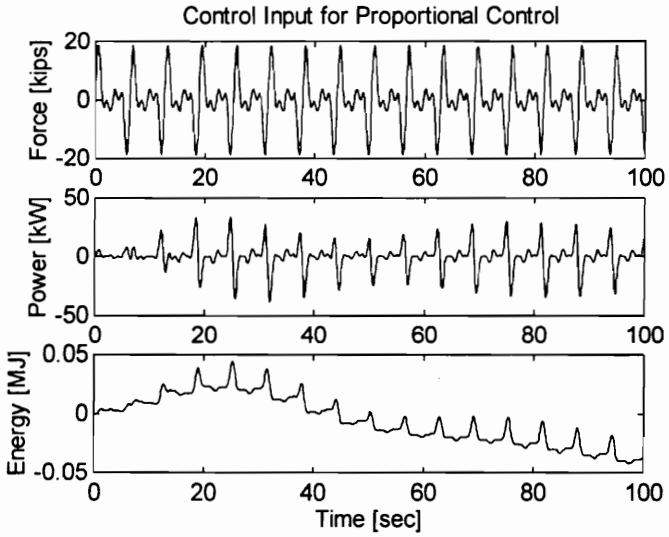

Fig. 4.42 Actuator force, power, and energy for K = 0.12

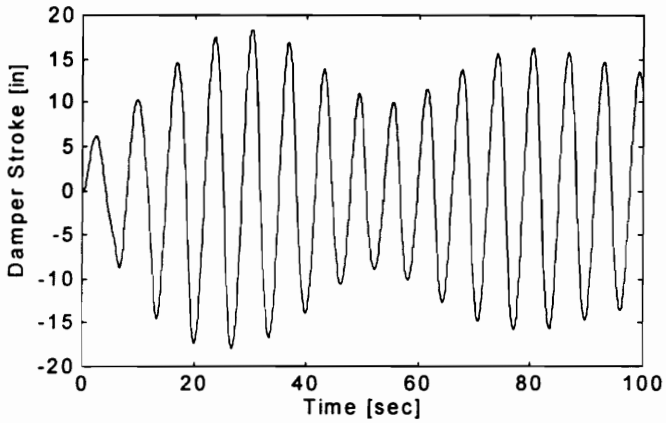

Fig. 4.43 Damper stroke length for feedforward control

The damper stroke length is shown in Fig. 4.43. The stroke has the same waveform as the displacement. When the stroke velocity is in the same direction as the control force, then motoring occurs and energy is drawn from the electrical source.

Sensitivity to Gain

The sensitivity of the maximum displacement, maximum control force, and maximum stroke length to variations in the feedforward gain are indicated by figures 4.44, 4.45, and 4.46, respectively. Note the critical gain of 0.12, after which the displacement starts to increase. The value of the critical gain will be dependent on the excitation and how close are its frequency content to the system frequencies. The stroke length and control force increase proportionately with gain.

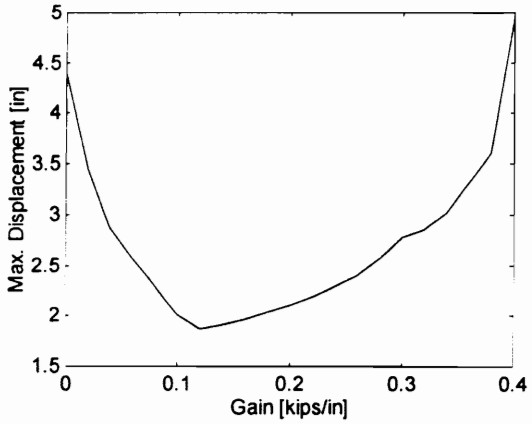

Fig. 4.44 Sensitivity of the maximum control force to gain variations

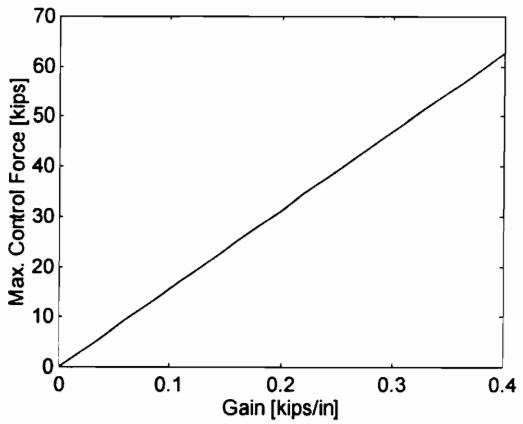

Fig. 4.45 Sensitivity of the maximum control force to gain variations

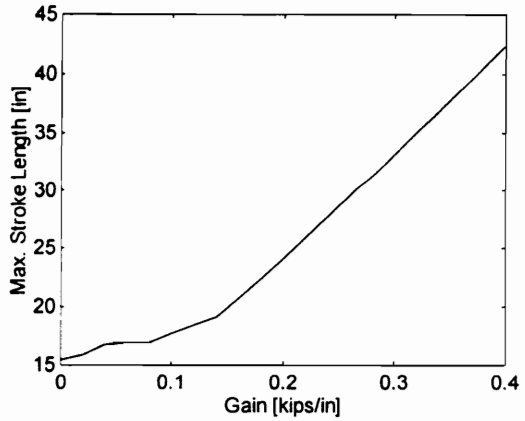

Fig. 4.46 Sensitivity of the maximum stroke length to gain variations

Effect of Time Delay

The effect of time delay on the displacement response of the feedforward-controlled system is shown in Fig. 4.47. The critical delay time is approximately 0.35 second, greater than which the response starts to increase again. The gain is kept at 0.12.

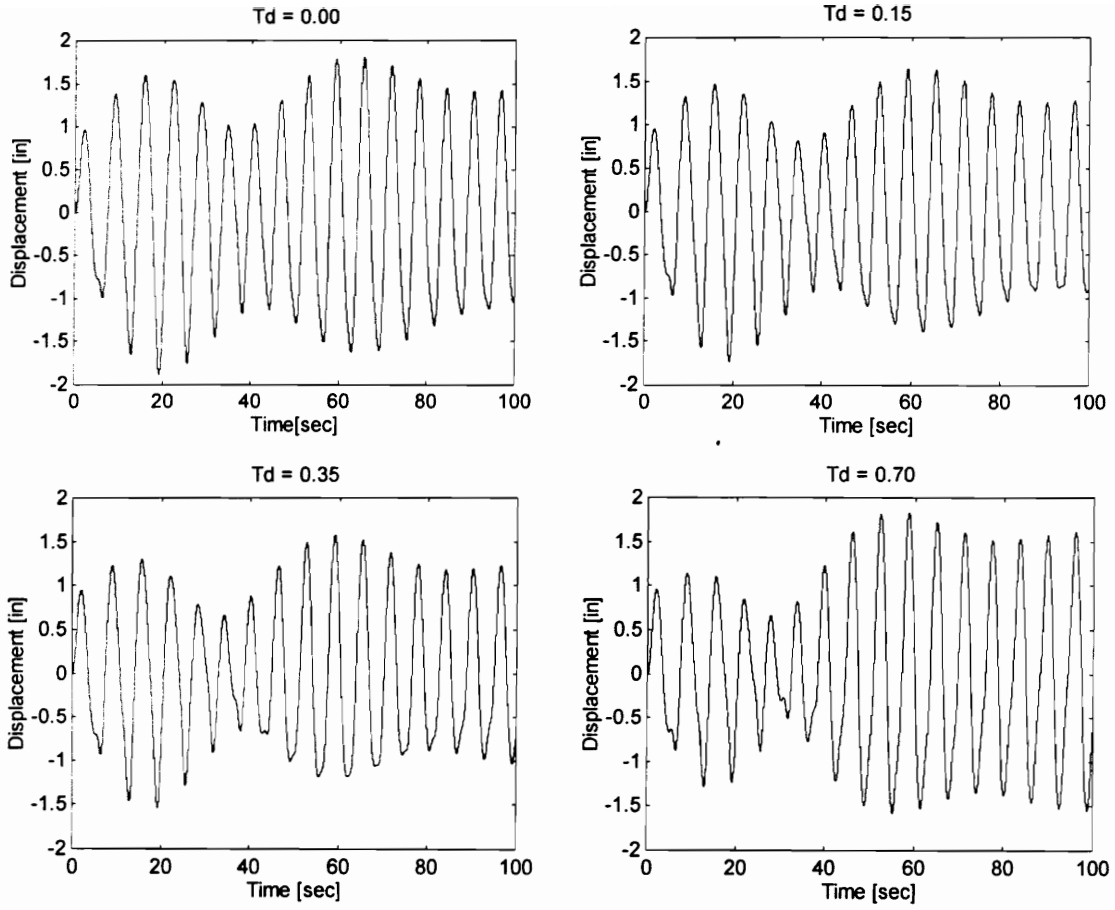

Fig. 4.47 Displacement for various actuator time delays (T_d seconds)

Sensitivity to Time Delay

The sensitivities of the maximum displacement, maximum control force, and maximum stroke length to changes in the actuator time delay are shown in figures 4.48, 4.49, and 4.50. The critical delay time is about 0.35 seconds. Larger time delays cause the system to become unstable. The maximum control force is determined by the excitation, which in this case has a fixed peak.

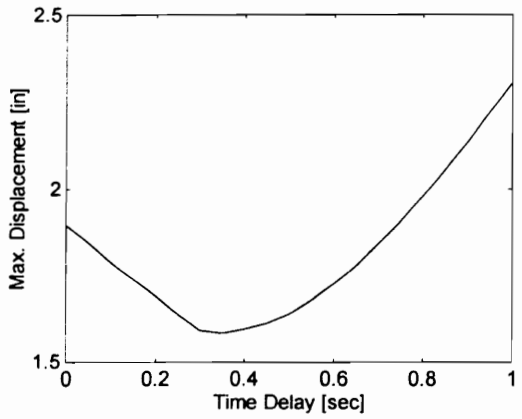

Fig. 4.48 Sensitivity of the maximum displacement to changes in the time delay

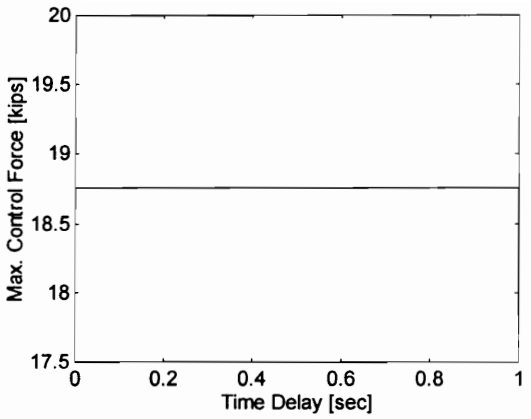

Fig. 4.49 Sensitivity of the maximum control force to changes in the time delay

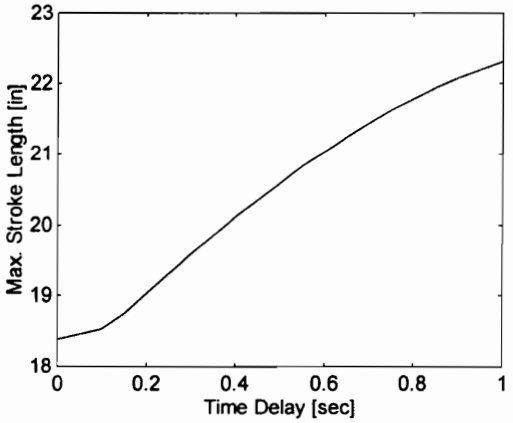

Fig. 4.50 Sensitivity of the maximum stroke length to changes in the time delay

Effect of Measurement Time Delay

When the measurement time delay is altered, the resulting displacements are shown in Fig. 4.51. The critical measurement time delay appears to be 0.70 seconds. The gain is fixed at 0.12. The maximum displacement decreases until a delay of 0.70 seconds is reached.

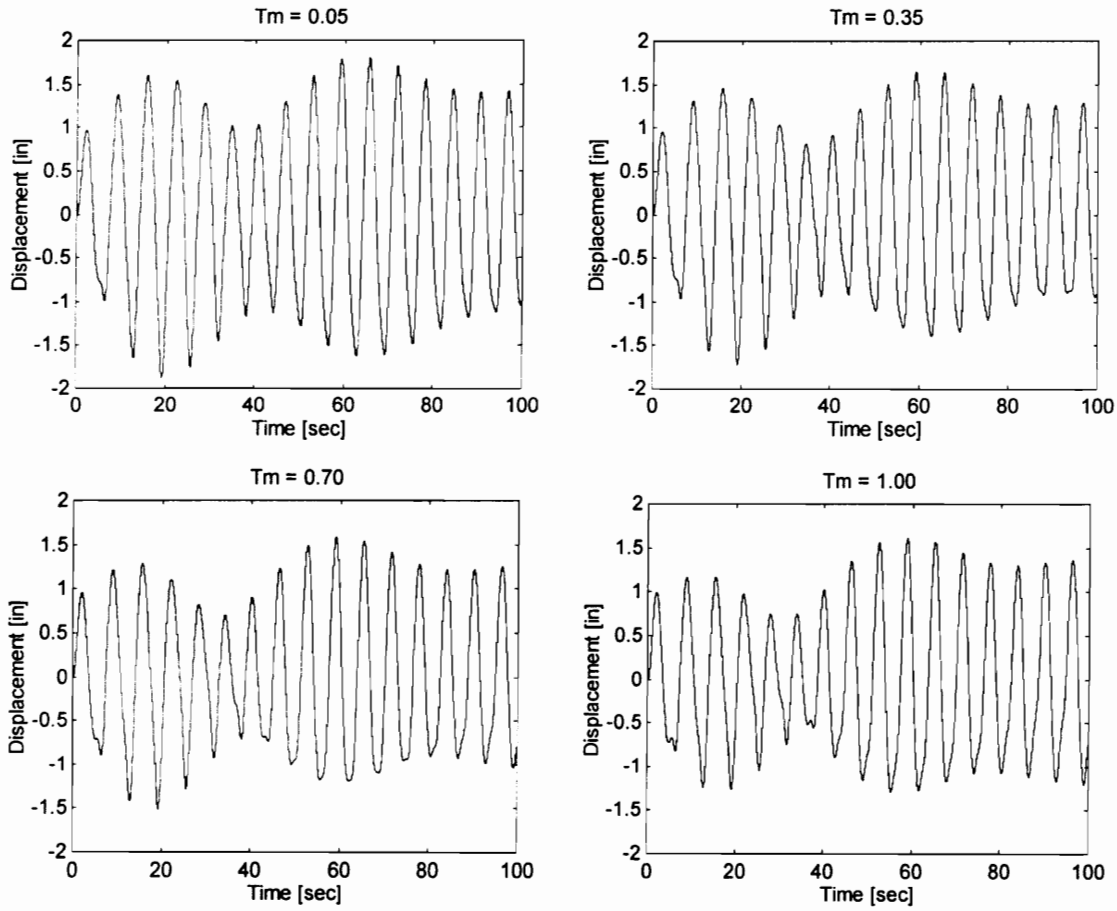

Fig. 4.51 Displacement for various measurement time delays (T_m seconds)

The effect of the measurement time delay on the maximum displacement, maximum control force, and maximum stroke length are shown in figures 4.52, 4.53, and 4.54. From the plot of the maximum displacement versus measurement time delay, the critical measurement time delay is found as the one corresponding to the minimum displacement-maximum. The plot for the maximum displacement gives the critical measurement time delay at about 0.7 second. Increasing the measurement time delay above 0.7 second causes an increase in the displacement, control force, and stroke length.

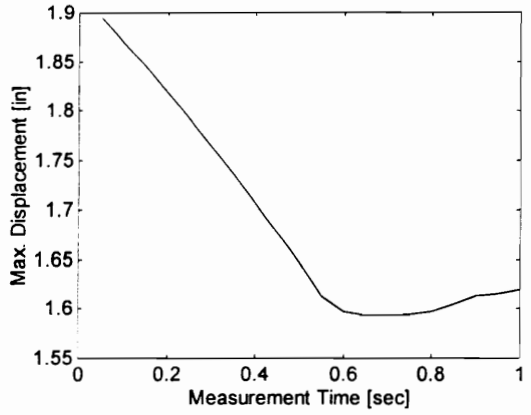

Fig. 4.52 Sensitivity of the maximum displacement to variations in measurement time delay

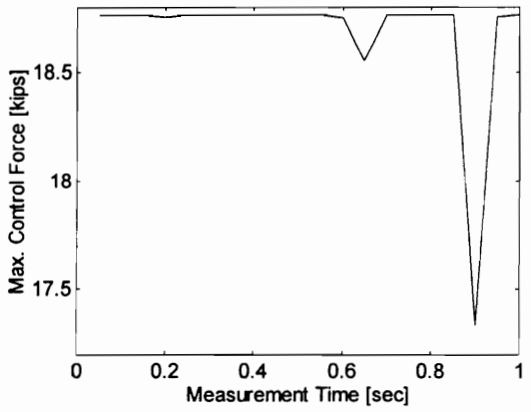

Fig. 4.53 Sensitivity of the maximum control force to variations in measurement time delay

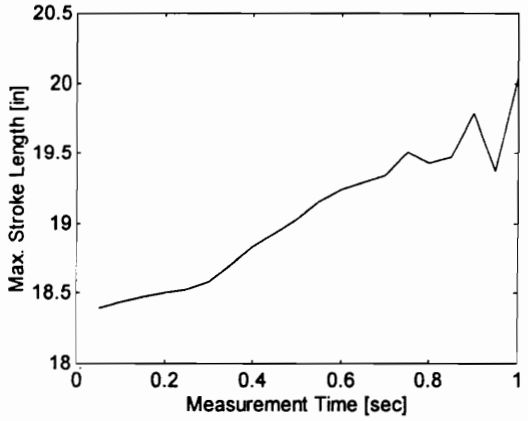

Fig. 4.54 Sensitivity of the maximum stroke length to variations in measurement time delay

Example 4.6 Earthquake-excited Structure

With the same system and earthquake excitation in Example 4.2, a feedforward controller with gain of 0.12 kips/in/sec^2 is used to provide control. The resulting displacement is shown in Fig. 4.55. As with feedback control, feedforward control is unable to reduce the peak displacements. The controller is unable to contain the response within the elastic limits. The response is very much similar to the uncontrolled case.

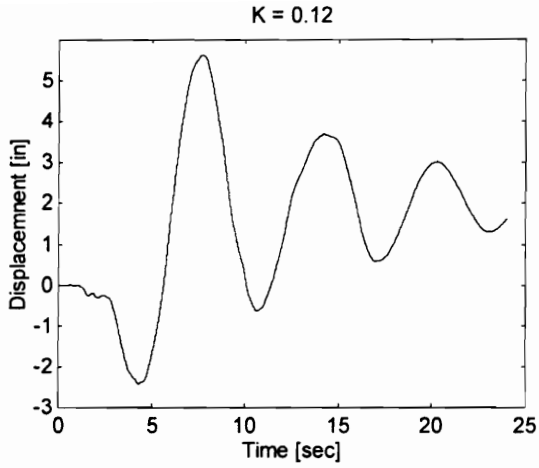

Fig. 4.55 Displacement with feedforward control

4.4 PROPORTIONAL CONTROL IN DISCRETE-TIME

To be able to apply digital control to a continuous system, the continuous system must be converted into an equivalent discrete-time system. Several techniques are available for discretizing a continuous system. Each technique has its own advantages and disadvantages. Examples of continuous-to-discrete transformations include the zero-order-hold (ZOH) or step-invariant transformation and the bilinear or Tustin transformation.

After discretization, the state equations will be of the form

$$\mathbf{x}(k+1) = \mathbf{A}_d\mathbf{x}(k) + \mathbf{E}_d\mathbf{r}(k) \tag{4.12}$$

where

$$\mathbf{E}_d = [\mathbf{B} \quad \mathbf{H}]_d \tag{4.13}$$

$$\mathbf{r}(k) = \begin{bmatrix} \mathbf{u}(k) \\ \mathbf{f}(k) \\ \ddot{y}_0(k) \end{bmatrix} \tag{4.14}$$

Example 4.7

Using a sampling time (T_S) of 0.10 sec, the system of Example 4.1 is discretized using the zero-order-hold transformation. It is assumed that the system is completely linear and is being subjected to a wind excitation. Without any control being exerted, the structure's displacement is shown in Fig. 4.56. The displacement response given in Fig. 4.57 is for the case when a feedback gain of 15 kips/in is applied to the displacement to generate the control force u. Feedforward control, using a gain of 0.12 kips/kips, results in the displacement response shown in Fig. 4.58.

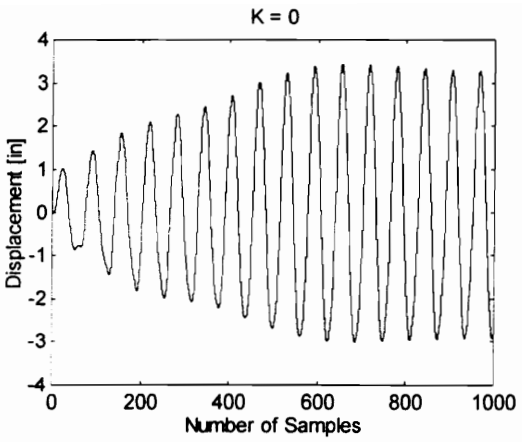

Fig. 4.56 Displacement without control

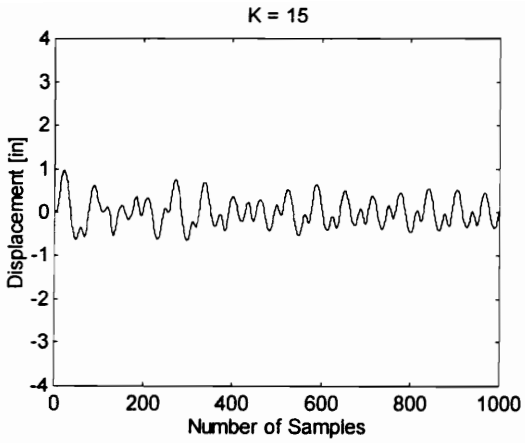

Fig. 4.57 Displacement with displacement-feedback control

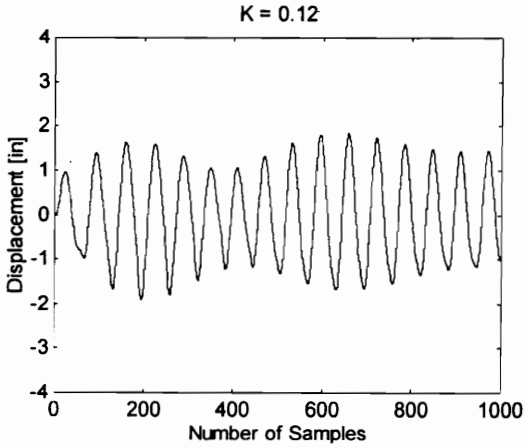

Fig. 4.58 Displacement with feedforward control

These results show that there is a negligible difference between using a continuous and a discrete-time model in the simulations. Both models yield approximately the same results.

4.5 SUMMARY

This chapter does not present any original contribution. Its main purpose is to provide a benchmark against which controllers for the regenerative electric actuator can be evaluated and compared.

For cases involving wind excitation, it is shown that proportional feedback control can provide effective control. The reduction in the structure's displacement is, however, accompanied

by an increase in the control force and the stroke length. The use of feedback control generally reduces the damping of the mass damper which, in turn, increases the stroke length. A certain amount of gain variation is found to be tolerable without degrading the response. Critical values of actuator time delay and measurement time delay have to be determined in order to set limits on these quantities. Feedforward control can also be used for wind-excited structures. Critical values for the gain, actuator time delay, and measurement time delay determine the limits of effectiveness for this type of control. Simulations are conducted for a single-degree-of-freedom system and a fixed-base multistory building.

Feedback and feedforward proportional control of the single-degree-of-freedom system under earthquake excitation is found to be ineffective. It is only slightly effective for a base-isolated multistory building. Regeneration can be achieved while under proportional control.

CHAPTER 5

Linear Quadratic Control

5.1 INTRODUCTION

Linear quadratic (LQ) controllers constitute the most prevalent type of structural control. Most of the research effort in past few years were geared towards this type of control for civil structures. No original contributions are being presented in this chapter. Since most of the previous work in active control of structures use this method, the purpose of this chapter is to provide a benchmark against which controllers for the regenerative electric actuator are evaluated.

Since environmental disturbances are seldom known *a priori*, the regulator solution presented in this chapter is used to search for the best closed-loop control law for structures subjected to unknown disturbances. This is done by determining the response of the controlled structure when subjected to some assumed disturbances. The best regulator is one which performs well for most of the assumed excitations and excitations which closely resemble the actual disturbances.

The LQ controller is tested on a single-degree-of-freedom system and on a fixed-base and base-isolated multistory building. Increasing the weight on the displacement produces a reduction in the displacement at the cost of increasing the control force and damper stroke. The LQ controller is shown to be effective for both wind and earthquake excitations. However, peak reduction seems to be a problem in earthquake-excited cases. Various criteria are suggested for choosing the weighting matrices.

To improve control efficiency, limits can be set on the control force to reduce stroke length without compromising the displacement response. This type of controller provides opportunity for regeneration. In some cases with sufficient duration of the excitation, there is even a net gain in the source energy

5.2 FORMULATION OF THE OPTIMAL CONTROL PROBLEM

The state equations of any given system, whether it is linear or nonlinear, can be written in the form

$$\dot{\mathbf{x}}(t) = \mathbf{a}(\mathbf{x}(t), \mathbf{u}(t), t) \tag{5.1}$$

where **a** is an n-vector function of the state $\mathbf{x}(t)$, control $\mathbf{u}(t)$, and time t. To solve the optimal control problem [1], one must find an admissible control $\mathbf{u}^*(t)$ which will force the system to follow an admissible trajectory $\mathbf{x}^*(t)$ which minimizes the performance index

$$J = h(\mathbf{x}(t_f), t_f) + \int_{t_0}^{t_f} g(\mathbf{x}(t), \mathbf{u}(t), t)dt \tag{5.2}$$

and, at the same time, satisfying (5.1). In (5.2), h and g are scalar functions while t_0 and t_f are the initial and final times, respectively. The control $\mathbf{u}^*(t)$ which is found to minimize the performance index J is called an optimal control, while the resulting state trajectory $\mathbf{x}^*(t)$ is called an optimal trajectory [1].

The necessary conditions for an optimal solution can be obtained by first defining the Hamiltonian as

$$\mathcal{H}(\mathbf{x}(t), \mathbf{u}(t), \mathbf{p}(t), t) = g(\mathbf{x}(t), \mathbf{u}(t), t) + \mathbf{p}^T(t)[\mathbf{a}(\mathbf{x}(t), \mathbf{u}(t), t)] \tag{5.3}$$

where $\mathbf{p}(t)$ is an n-vector of Lagrange multipliers or costate variables. Assuming that the admissible controls are bounded, the necessary conditions for optimal control are given by [1]

$$\dot{\mathbf{x}}^*(t) = \frac{\partial \mathcal{H}(\mathbf{x}^*(t), \mathbf{u}^*(t), \mathbf{p}^*(t), t)}{\partial \mathbf{p}} \qquad t_0 \le t \le t_f \tag{5.4}$$

$$\dot{\mathbf{p}}^*(t) = -\frac{\partial \mathcal{H}(\mathbf{x}^*(t), \mathbf{u}^*(t), \mathbf{p}^*(t), t)}{\partial \mathbf{x}} \qquad t_0 \le t \le t_f \tag{5.5}$$

$$\mathcal{H}(\mathbf{x}^*(t), \mathbf{u}^*(t), \mathbf{p}^*(t), t) \le \mathcal{H}(\mathbf{x}^*(t), \mathbf{u}(t), \mathbf{p}^*(t), t) \qquad t_0 \le t \le t_f \tag{5.6}$$

for all admissible $\mathbf{u}(t)$

$$\left[\frac{\partial h(\mathbf{x}^*(t_f), t_f)}{\partial \mathbf{x}} - \mathbf{p}^*(t_f)\right]^T \delta\mathbf{x}_f + \left[\mathcal{H}(\mathbf{x}^*(t_f), \mathbf{u}^*(t_f), \mathbf{p}^*(t_f), t_f) + \frac{\partial h(\mathbf{x}^*(t_f), t_f)}{\partial t}\right]\delta t_f = 0 \tag{5.7}$$

where $\delta\mathbf{x}_f$ and δt_f are variations in the final state and final time, respectively. Note that (5.4) is simply the state equations as given in (5.1). Thus, (5.4) requires that the optimal trajectory and optimal control satisfy the state equations. Equation (5.5) results in what are known as the costate equations. Equation (5.6) is a statement of Pontryagin's minimum principle, i.e., that the optimal control must minimize the Hamiltonian. Equation (5.7) provides a set of boundary condition equations. If the admissible controls are not bounded, then a necessary condition for $\mathbf{u}^*(t)$ to minimize the Hamiltonian is

$$\frac{\partial \mathcal{H}(\mathbf{x}^*(t), \mathbf{u}^*(t), \mathbf{p}^*(t), t)}{\partial \mathbf{u}} = \mathbf{0} \qquad t_0 \le t \le t_f \tag{5.8}$$

The solution of the state and costate equations requires the evaluation of $2n$ constants of integration. To evaluate these constants, the initial conditions contribute n equations

$$\mathbf{x}(t_0) = \mathbf{x}_0 \tag{5.9}$$

and another set of n or $(n+1)$ equations, depending on whether or not t_f is specified, is contributed by (5.7).

5.3 THE LINEAR REGULATOR PROBLEM

The linear regulator problem is a subset of the optimal control problem wherein the optimal control is required to move the system from an initial state to a desired final state. For structural systems, the desired final state is the zero state, i.e., zero displacement and zero velocity. Therefore, to obtain the optimal control for a structural system one must basically solve a linear regulator problem. The performance index is chosen so that it makes it desirable to keep the state as close to zero as possible while using the least control effort.

Suppose that the structural system is described by linear state equations of the form

$$\dot{\mathbf{x}}(t) = \mathbf{A}\mathbf{x}(t) + \mathbf{B}\mathbf{u}(t) + \mathbf{H}\mathbf{w}(t) \tag{5.10}$$

The linear regulator problem is to find the control which will minimize the quadratic performance index

$$J = \frac{1}{2}\int_{t_0}^{t_f} [\mathbf{x}^T(t)\mathbf{Q}\mathbf{x}(t) + \mathbf{u}^T(t)\mathbf{R}\mathbf{u}(t)]dt \tag{5.11}$$

for a fixed final time t_f subject to the constraint of the state equation (5.10). **H** and **Q** are real symmetric positive semi-definite matrices, while **R** is a real symmetric positive definite matrix. If the costate is chosen to be a linear function of the state,

$$\mathbf{p}^*(t) = \mathbf{P}(t)\mathbf{x}(t) \tag{5.12}$$

then the matrix Riccati equation will be given by

$$\left[\dot{\mathbf{P}}(t) + \mathbf{P}(t)\mathbf{A} - \frac{1}{2}\mathbf{P}(t)\mathbf{B}\mathbf{R}^{-1}\mathbf{B}^T\mathbf{P}(t) + \mathbf{A}^T\mathbf{P}(t) + 2\mathbf{Q}\right]\mathbf{x}(t) + \mathbf{P}(t)\mathbf{H}\mathbf{w} = \mathbf{0} \tag{5.13}$$

$$\mathbf{P}(t_f) = \mathbf{0} \tag{5.14}$$

The solution of this form of the Riccati equation requires *a priori* knowledge of the disturbance **w**. For most structural control problems, the excitation **w** is generally unknown and difficult to predict. For cases where **w** = **0** or **w** is a white-noise stochastic process, then the Riccati equation simplifies to

$$\mathbf{PA} + \mathbf{A}^T\mathbf{P} - \mathbf{PBR}^{-1}\mathbf{B}^T\mathbf{P} + \mathbf{Q} = \mathbf{0} \tag{5.15}$$

and the control is given by

$$\mathbf{u}^*(t) = -\mathbf{R}^{-1}\mathbf{B}^T\mathbf{P}\mathbf{x}(t) = -\mathbf{K}\mathbf{x}(t) \tag{5.16}$$

If **w** is nonzero or not white noise, then the regulator solution given by (5.16) can still be used to look for the best closed-loop control law for structures subjected to unknown disturbances, i.e., investigate the response of the controlled structure due to some assumed disturbances. Hence, the LQ regulator is used as a simulation benchmark.

As long as the disturbance is present, the performance index will not converge to a steady-state value because the regulator solution does not take the disturbance into account. If the disturbance is known for the entire control interval, then (5.13) can be solved and a convergent performance index is obtained even in the presence of the disturbance.

Example 5.1 Wind-Excited SDOF Structure with Mass Damper

Consider the single degree-of-freedom structure with mass damper described in Example 4.1. Assume that it is excited by a wind force with parameter p = 9.75 kips and ω = 1 rad/sec. A linear quadratic (LQ) controller is designed using the weighting matrices **Q** = diag(2000,1,1,1) and **R** = 0.1. The gain matrix is obtained as

$$\mathbf{K} = \begin{bmatrix} -128.0780 & 1.8746 & 37.5252 & 5.8866 \end{bmatrix}$$

The displacement of the structure with LQ control is shown in Fig. 5.1.

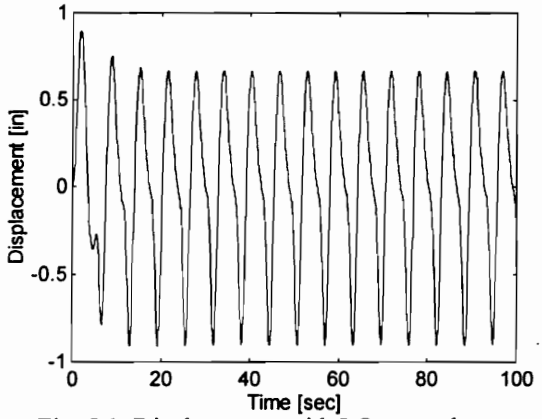

Fig. 5.1 Displacement with LQ control

A comparison of the structure's response with and without LQ control is shown in Table 5.1. There is a 80% reduction in the peak displacement with linear quadratic control applied. This is accompanied by a 35% increase in the maximum stroke-length.

TABLE 5.1 Comparison of Response for Passive and LQ Control

CONTROL TYPE	y_s(peak)	y_s(rms)	z(peak)	z(rms)
Passive	4.6275	1.8895	15.4839	9.3422
LQ Control	0.9148	0.4801	20.8562	10.0273

where y_s is the structure's displacement with respect to the ground (in.) and z is the relative displacement between the structure and the damper (in.).

The control force and the instantaneous power and energy supplied by the regenerative actuator are given by Fig. 5.2. Almost half of the time, the actuator is consuming negative power. This means that the actuator is able to regenerate while under LQ control. The plot for the energy shows that there is a net energy flow directed towards the source after about 20 seconds of the excitation.

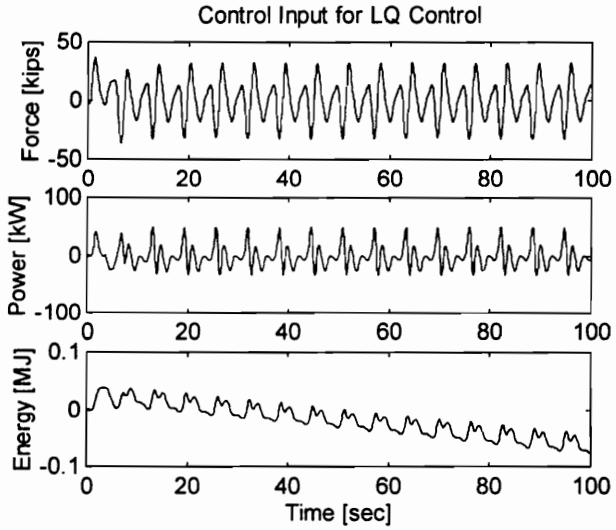

Fig. 5.2 Control input supplied by the actuator

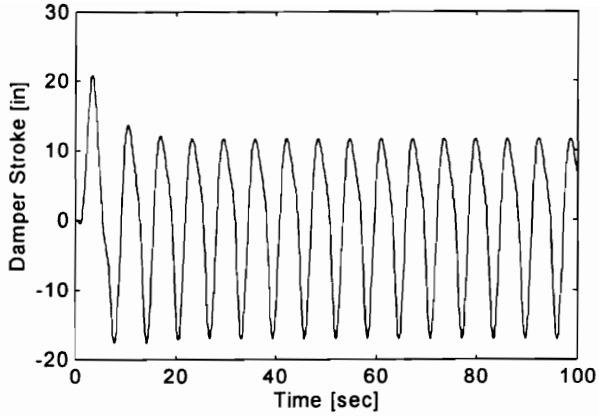

Fig. 5.3 Damper stroke length with linear quadratic control

The damper stroke length is shown in Fig. 5.3. The peak stroke length occurs during the first half-cycle of the wing disturbance. This coincides with the occurrence of the peak displacement. When the stroke velocity and the control force are in the same direction, then motoring action is obtained. Opposing directions for the stroke velocity and control force result in generating action and energy recovery.

The difference between the results for a linear and a nonlinear simulation is shown in Fig. 5.4 while using the LQ controller designed for the linear system. It is seen that the difference between the two simulations is negligible. At the start of the simulation, the difference is zero since the displacement is still within the elastic limit. As long as control is immediately available at the onset of the disturbance, then the displacement is kept within the elastic limits and no significant differences between the linear and nonlinear response is obtained.

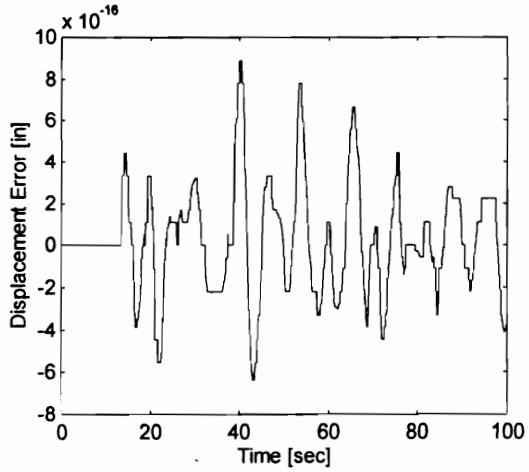

Fig. 5.4 Difference between a linear and a nonlinear simulation

Fig. 5.5 shows the displacement of the structure if a limit is set on the amount of control force, u_{max}, equal to 0, 5, 15, and 37 kips. The saturation of the control force violates the optimality of the original system. However, the introduction of an input nonlinearity that is sector-restricted on the control input-output plane does not destroy the stability of the original system [3].

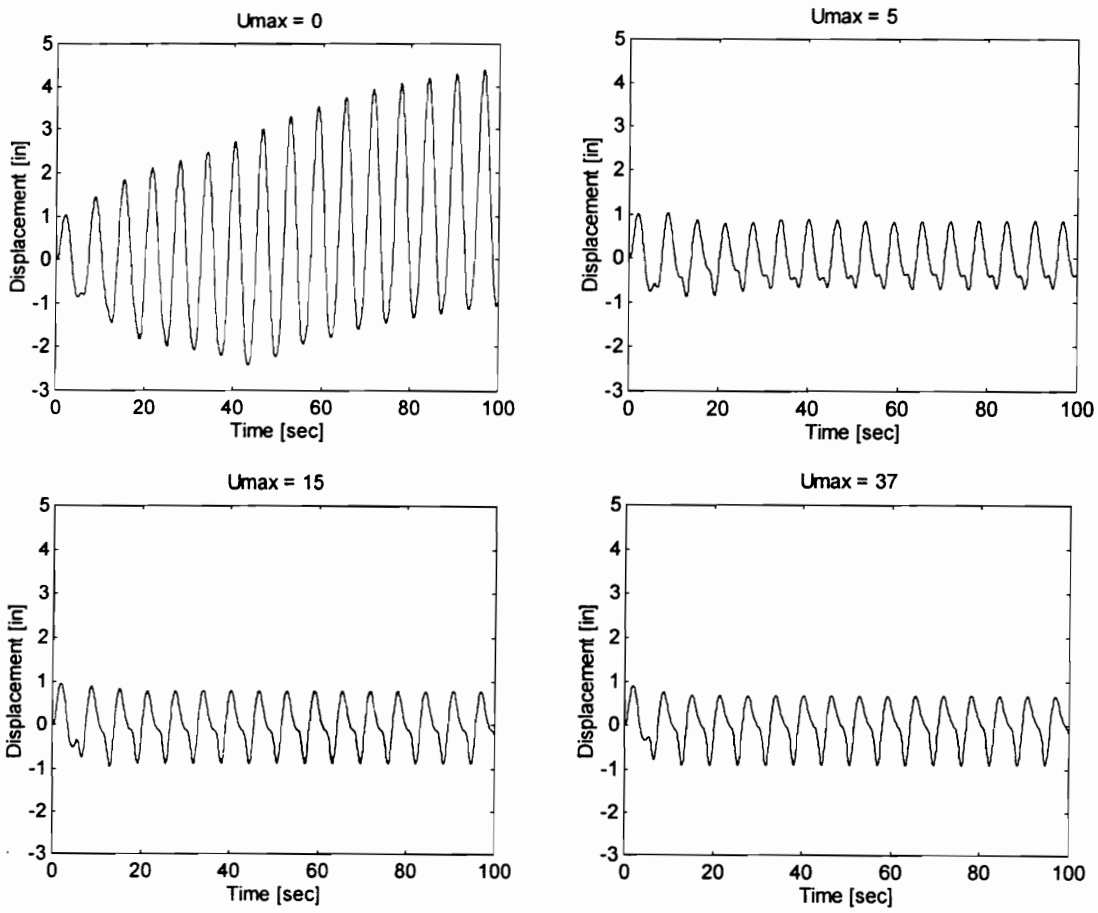

Fig. 5.5 Displacement for various limits (U_{max} kips) on the control force

From these simulations, the sensitivity of the maximum displacement and of the maximum stroke length to limits set on the control force are shown in Fig. 5.6 and Fig. 5.7, respectively. It is noted that increasing the maximum control-force above 5 kips does not produce any appreciable reduction in the maximum displacement. This is indicative of the stability margins for the given controller. However, the larger control force causes a larger stroke length. This would suggest the use of a limit on the control force in order to obtain better efficiency.

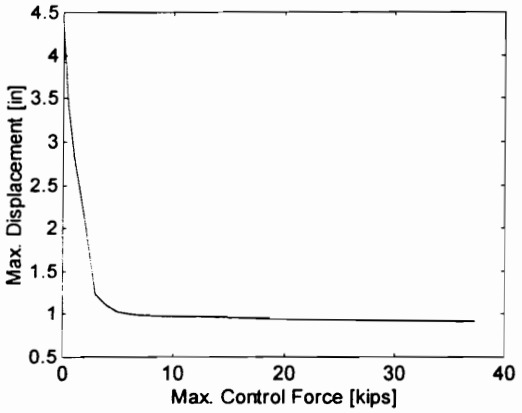

Fig. 5.6 Sensitivity of the maximum displacement to limits on the control force

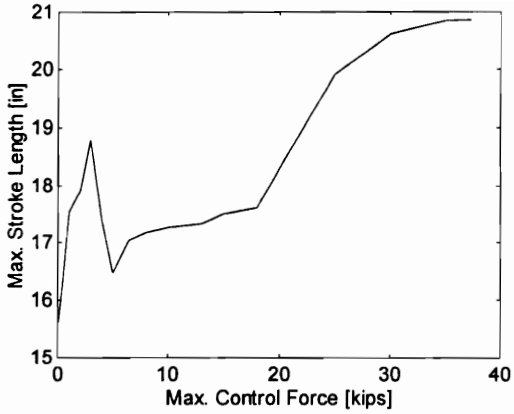

Fig. 5.7 Sensitivity of the maximum stroke length to limits on the control force

The effect of actuator time delay, T_d, on the displacement response is shown in Fig. 5.8. The actuator time delay is not modeled in the control problem. A delay above 0.425 second causes the system to become unstable. This value would correspond to the critical actuator time delay of the controlled system.

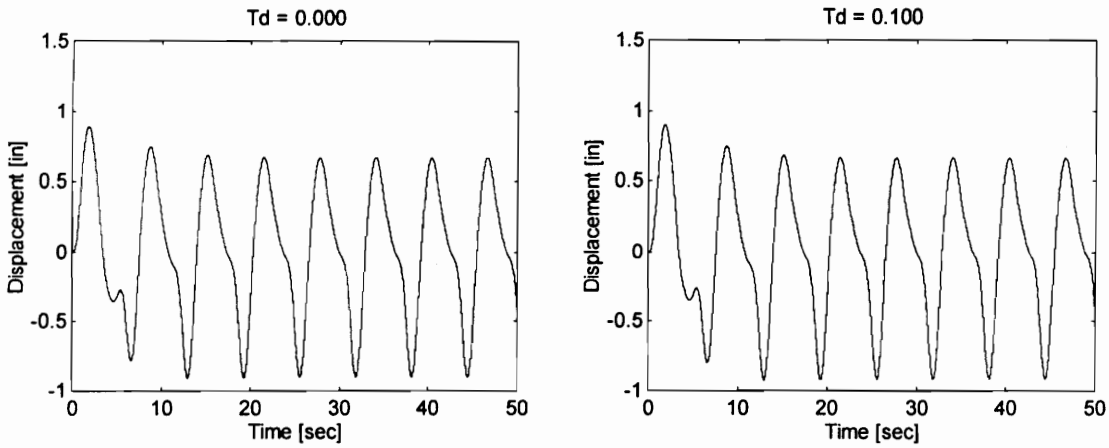

Fig. 5.8 Displacement for various time delays (T_d seconds)

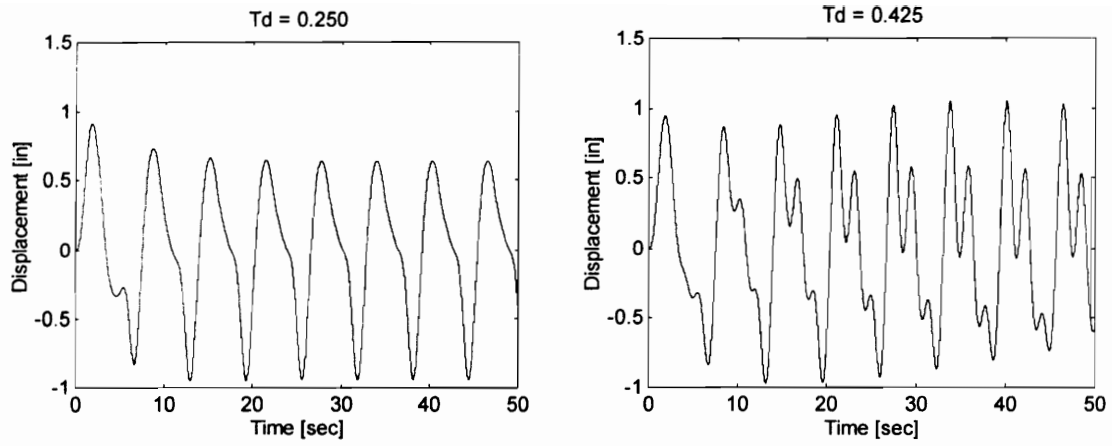

Fig. 5.8 (cont.) Displacement for various time delays (T_d seconds)

The sensitivity of the maximum displacement, maximum control force, and maximum stroke length to variations in the time delay are shown in figures 5.9, 5.10, 5.11, respectively. These figures show that the displacement, control force, and damper stroke start to increase significantly after the critical delay time of 0.35 s is reached.

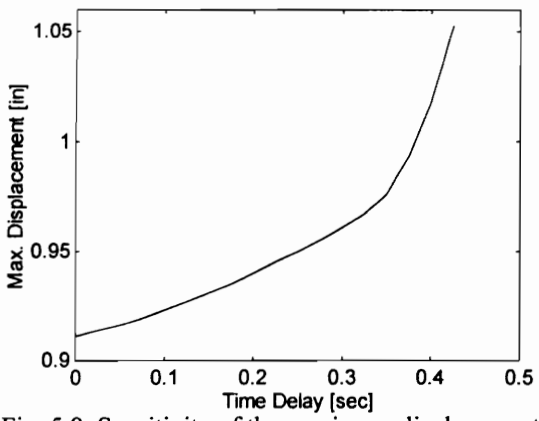

Fig. 5.9 Sensitivity of the maximum displacement to variations in time delay

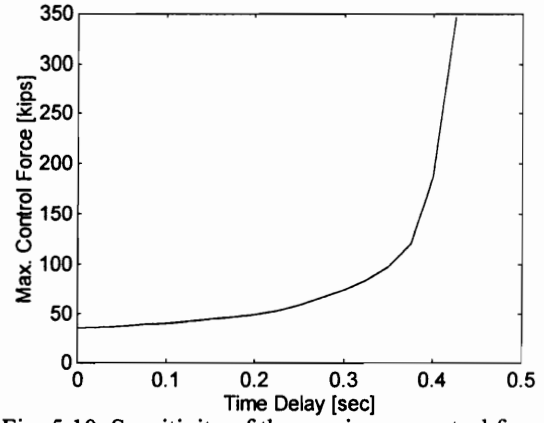

Fig. 5.10 Sensitivity of the maximum control force to variations in time delay

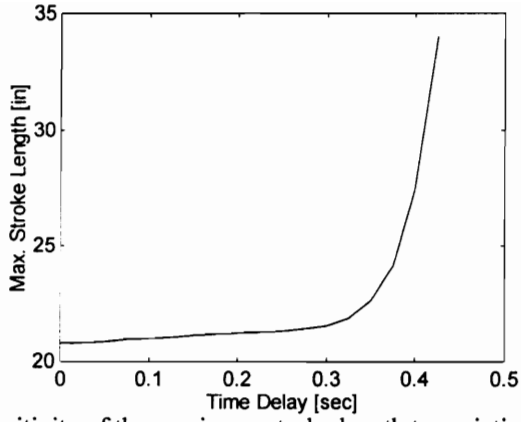

Fig. 5.11 Sensitivity of the maximum stroke length to variations in time delay

The impact of measurement time delay on the displacement of the structure is shown by Fig. 5.12. If the measurement time exceeds 0.75 sec., the system becomes unstable. Again, this corresponds to the critical measurement time delay.

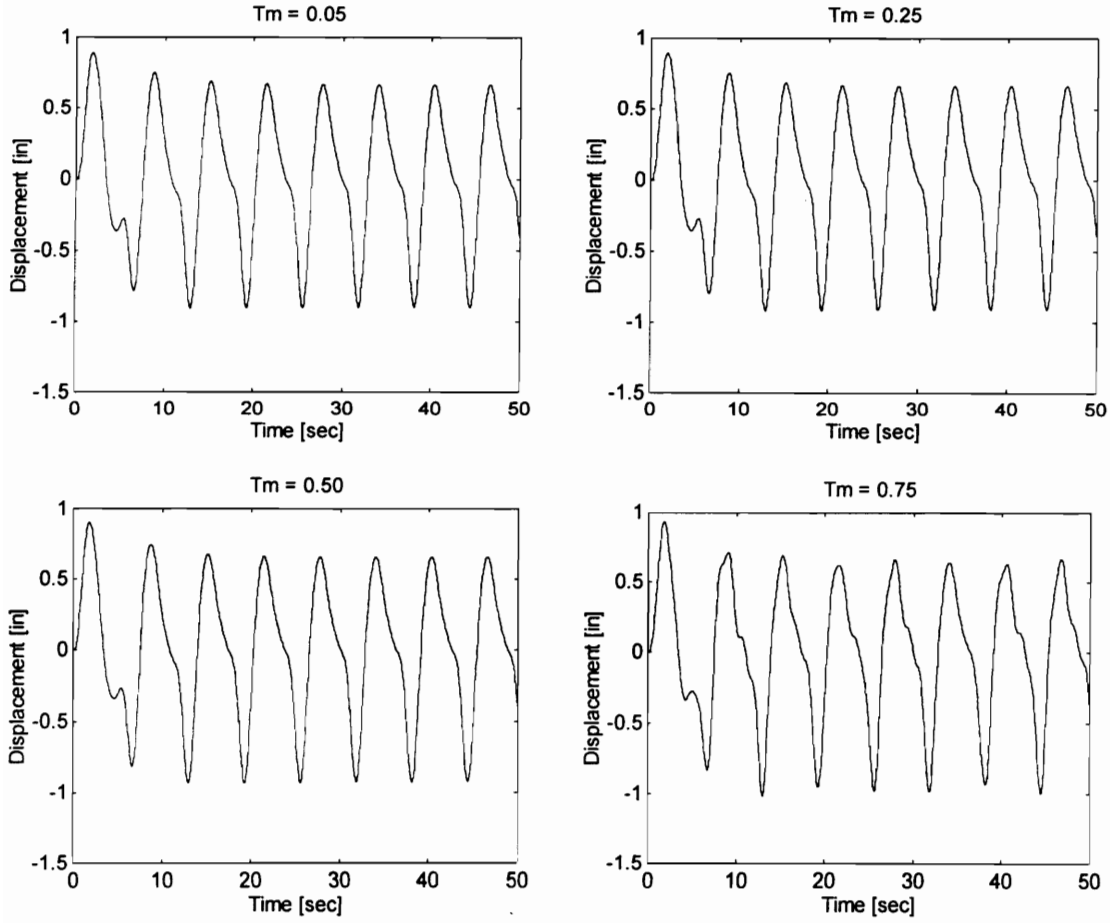

Fig. 5.12 Displacement for various measurement time delays (T_m seconds)

The sensitivity of the maximum displacement, maximum control force, and maximum stroke length to changes in the measurement time delay are given by figures 5.13, 5.14, and 5.15, respectively. The displacement, force, and stroke start to breakaway rapidly after the critical measurement time is reached.

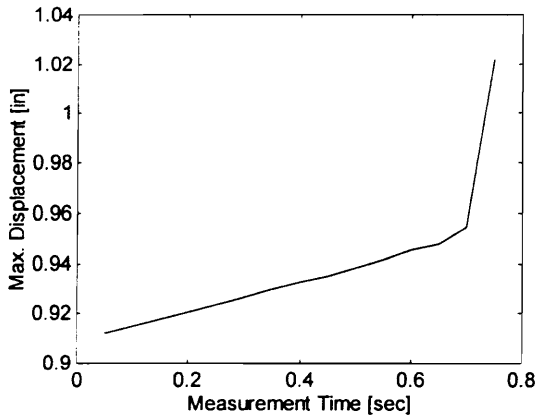

Fig. 5.13 Sensitivity of the maximum displacement to variations in measurement time delay

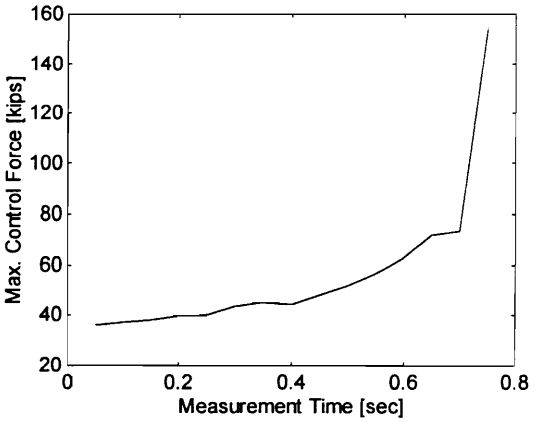

Fig. 5.14 Sensitivity of the maximum control force to variations in measurement time delay

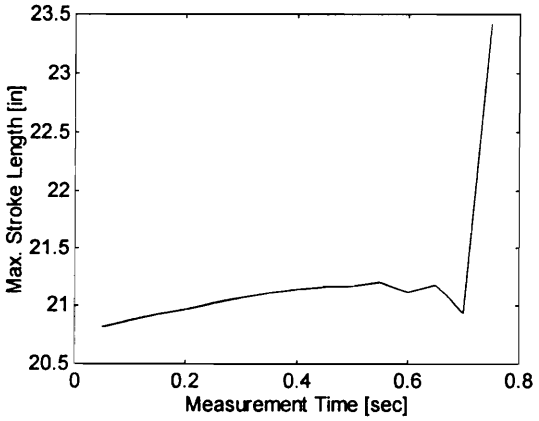

Fig. 5.15 Sensitivity of the maximum stroke length to variations in measurement time delay

The time delays are not modeled for the control derivation. The introduction of time delay will destroy the optimality of the original system. The important thing is that the optimality of the original system allows the introduction of these modifications while maintaining closed-loop stability [3]. However, the properties of the original system cannot resolve all robustness and sensitivity issues. The system eventually becomes unstable once the critical values are reached.

Example 5.2 Earthquake-Excited SDOF Structure with Mass Damper

Using the same LQ controller designed in Example 5.1, the response of the system in Example 5.1 is obtained for an earthquake excitation with a peak acceleration of 17.53 in/sec^2 and having the same shape as Fig. 3.14. The resulting displacement is shown in Fig. 5.16. The controller is unable to reduce significantly the positive peak in the displacement.

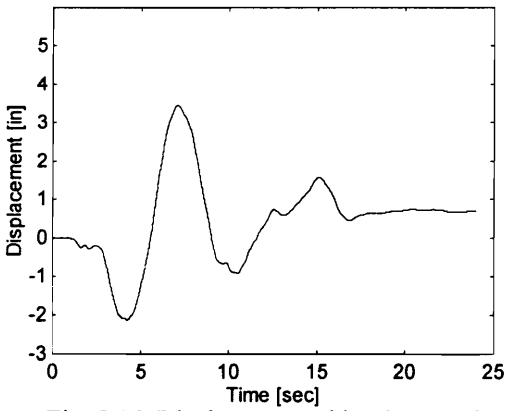

Fig. 5.16 Displacement with LQ control

A comparison of the structure's response with and without LQ is shown in Table 5.2. A 39% reduction in the peak displacement is obtained, while the stroke length increases by 421%. Since the weight on the control force is much smaller than the weight on the displacement, a larger control force is obtained. The larger force requirement produces a larger stroke length.

TABLE 5.2 Comparison of Response for Passive and LQ Control

CONTROL TYPE	y_s(peak)	y_s(rms)	z(peak)	z(rms)
Passive	5.5956	1.8895	15.1441	9.3422
LQ Control	3.4369	1.1349	78.8545	26.8077

where y_s is the structure's displacement with respect to the ground (in.) and z is the relative displacement between the structure and the damper (in.).

The actuator has to provide the control force, power, and energy shown in Fig. 5.17. During the first 10 seconds, the actuator is motoring. The regeneration that occurs at about 10 seconds reduces the net energy requirement from the source.

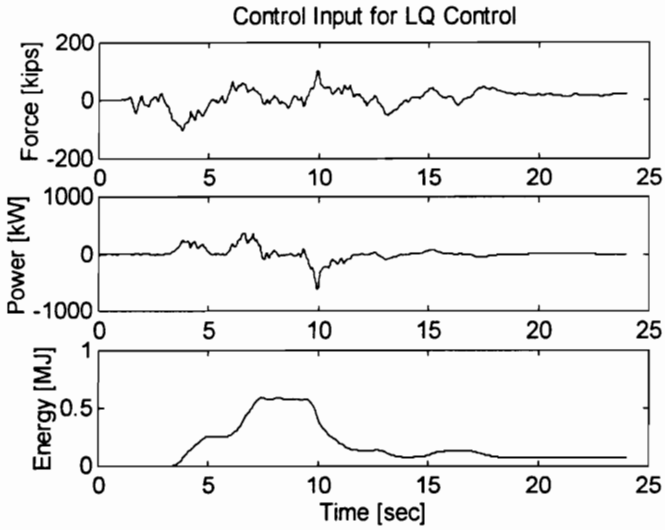

Fig. 5.17 Actuator force, power, and energy

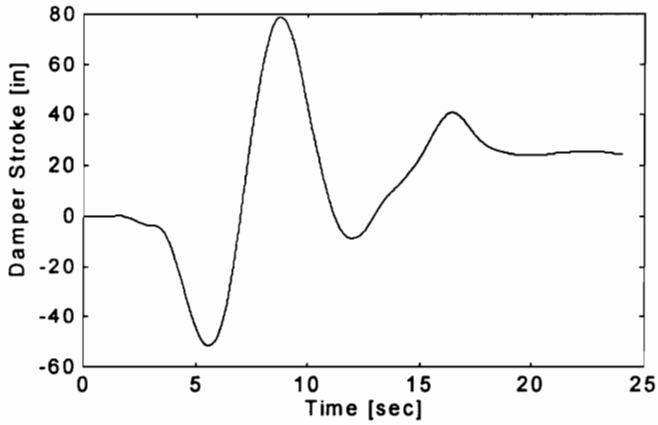

Fig. 5.18 Damper stroke length with linear quadratic control

The damper stroke is shown in Fig. 5.18. The peak occurs in the positive direction. Motoring occurs when the stroke velocity and the control force have the same polarity. Regeneration occurs when the stroke velocity and control force have opposite polarities.

Fig. 5.19 shows the difference between the results of a linear and a nonlinear simulation. The difference is not as negligible as in previous cases. This clearly demonstrates that a nonlinear model has to be used to arrive at more accurate simulation results. Since the controller is unable to restrict the displacement to within the elastic range, the system response becomes nonlinear. Hence, the difference between the two simulations are not quite negligible.

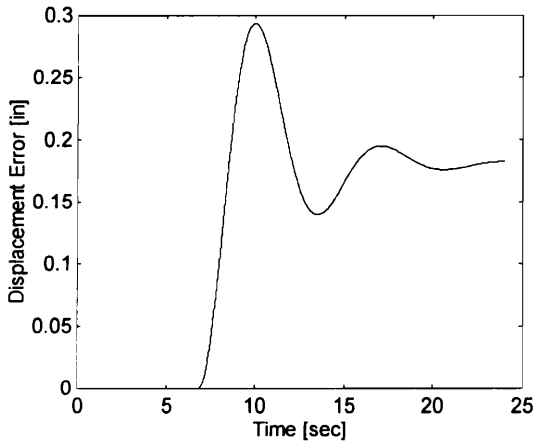

Fig. 5.19 Difference between a linear and a nonlinear simulation

5.4 SELECTION OF THE Q AND R WEIGHTING MATRICES

The choice for the weighting matrices **Q** and **R** has a great impact in shaping the response of a given structure under optimal control. In general, the magnitudes of the elements of **Q** and **R** reflect the relative importance being given to the structural response and the control force when minimizing the performance index. If response reduction is given a higher priority over the control effort, then the elements of the response weighting matrix **Q** are assigned larger values compared to those of **R**. This results in a faster and greater reduction of the response at the expense of larger control forces. One can also interpret this as assigning the structure's safety much more importance than system cost [3]. On the other hand, if the reduction of the control effort is given a higher priority over response reduction then the elements of the control weighting matrix **R** are assigned larger values compared to those of **Q**. This results in a slower and smaller reduction of the response due to smaller control forces. In this case energy requirements are reduced and thus gives system cost a higher priority over safety. Ultimately, a compromise has to be made between the structural response and the required control force in order to choose suitable **Q** and **R** matrices. For most practical cases, response reduction will have greater priority than control effort.

Finding the "best" **Q** and **R** is one of the more difficult steps in LQ control design. When the weighting matrices **Q** and **R** are both assumed to be diagonal matrices, it is found that it is the ratio of the elements of these matrices (and not the individual magnitudes) which influences the response [4]. A trial-and-error approach is usually employed to find the weighting matrices which will give acceptable levels in the responses and control forces.

The equations of motion can be written as

$$\mathbf{M}\ddot{\mathbf{z}} + \mathbf{C}\dot{\mathbf{z}} + \mathbf{K}\mathbf{z} = \mathbf{G}\mathbf{u} + \mathbf{f} - \mathbf{m}\ddot{y}_0 \tag{5.25}$$

where **G** is the actuator influence matrix and **z** is the displacement relative to the ground. The other quantities are as defined in Chapter 3. If the number of actuators equal the number of degrees-of-freedom, then **G** will have full rank. Based on physical considerations, a possible choice for the weighting matrices is one which would lead to a minimization of both the energy of the structure and the quasistatic work done by the controller/actuator [5]. Therefore, if **Q** and **R** are chosen as

$$\mathbf{Q} = \begin{bmatrix} \alpha\mathbf{K} & \mathbf{0} \\ \mathbf{0} & \beta\mathbf{M} \end{bmatrix} \tag{5.26}$$

$$\mathbf{R} = \mathbf{G}^T\mathbf{K}^{-1}\mathbf{G} \tag{5.27}$$

then

$$\tfrac{1}{2}\mathbf{x}^T\mathbf{Q}\mathbf{x} = \alpha\tfrac{1}{2}\mathbf{z}^T\mathbf{K}\mathbf{z} + \beta\tfrac{1}{2}\dot{\mathbf{z}}^T\mathbf{M}\dot{\mathbf{z}} \tag{5.28}$$

where α and β are positive scalar weights. Note that the right-hand side of (5.28) is the weighted sum of the potential (strain) energy and kinetic energy of the system. The work done by the controller/actuator is indirectly weighted by α and β. Minimization of the performance index would result in the reduction of the total energy of the system with the minimum control effort. This approach has the advantage of reducing the number of design parameters.

Other forms of the **Q** matrix that have been suggested include [6]

$$\mathbf{Q} = \begin{bmatrix} \mathbf{K} & \mathbf{0} \\ \mathbf{0} & \mathbf{0} \end{bmatrix} \tag{5.29}$$

which will minimize the potential energy of the structure; and [7]

$$\mathbf{Q} = \begin{bmatrix} \mathbf{0} & \mathbf{0} \\ \mathbf{0} & \mathbf{I} \end{bmatrix} \tag{5.30}$$

Example 5.3 Wind-Excited SDOF Structure with Mass Damper

The displacements given in Fig. 5.20 show the effect of varying the first diagonal element of the **Q** matrix for the system, controller, and excitation described in Example 5.1. Other elements of the **Q** and **R** matrices are kept constant. Increasing the weight on the displacement causes a reduction in the displacement at the expense of larger control forces or increases in the other state variables.

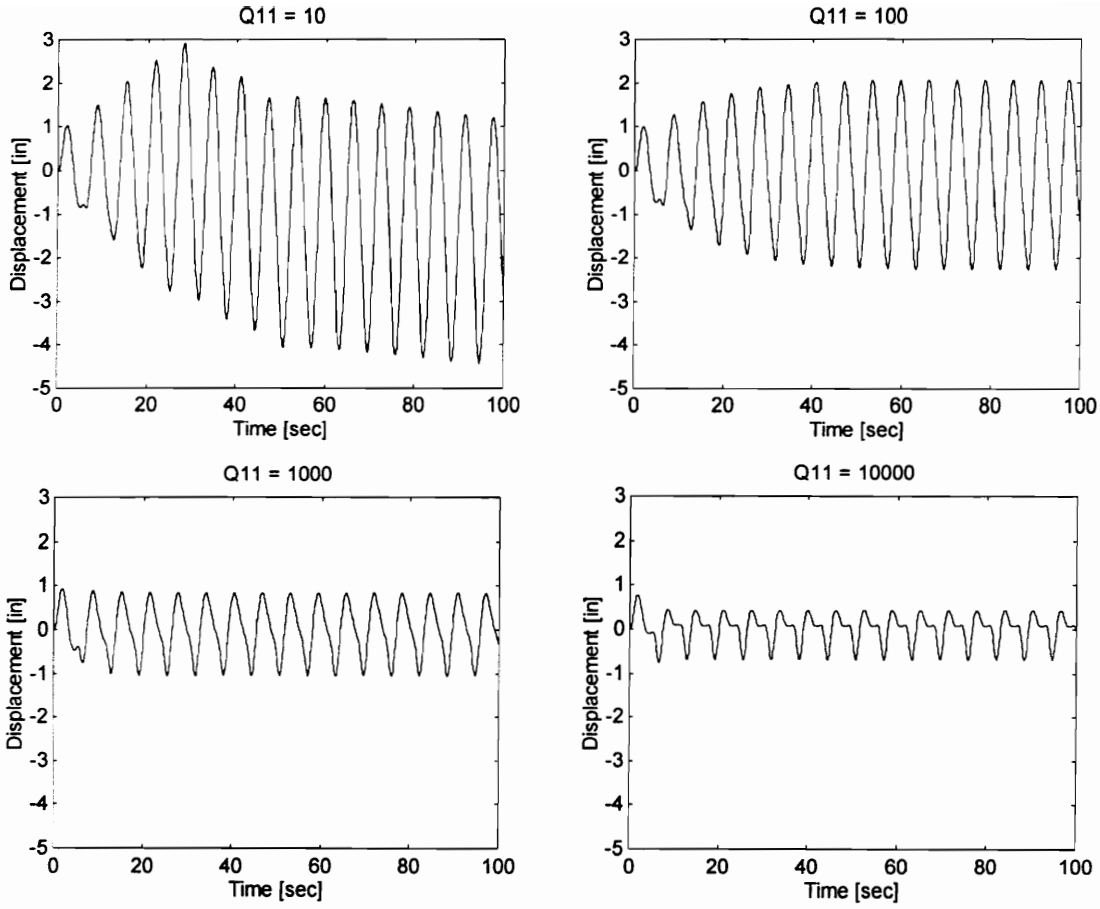

Fig. 5.20 Displacement for various Q11 values

The sensitivity of the maximum displacement, maximum control force, and maximum stroke length to these variations in Q11 are shown in figures 5.21, 5.22, and 5.23, respectively. The reduction in displacement is accompanied by an increase in the required control force and stroke length. The control force starts to increase significantly only after Q11 = 100.

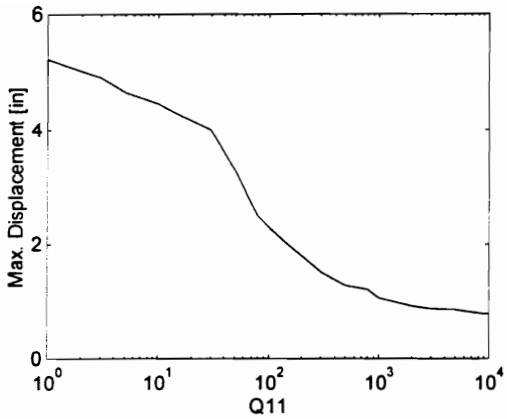

Fig. 5.21 Sensitivity of the maximum displacement to variations in Q11

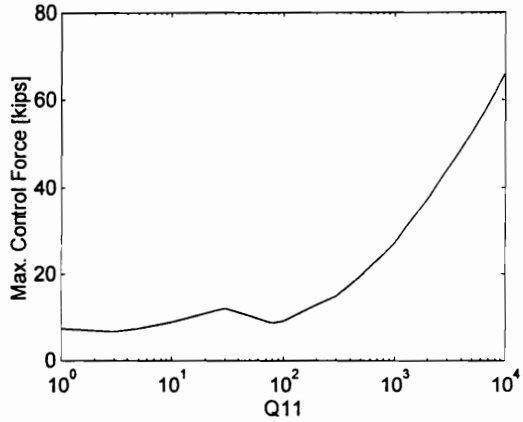

Fig.5.22 Sensitivity of the maximum control force to variations in Q11

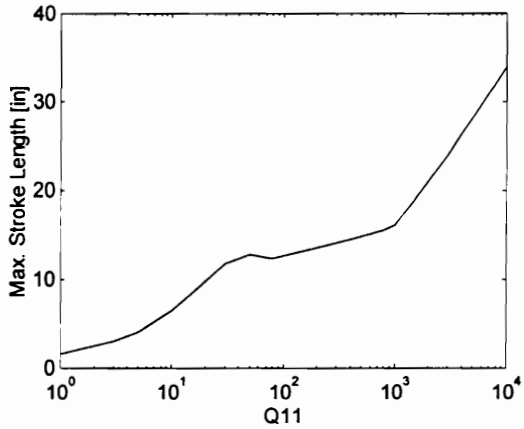

Fig. 5.23 Sensitivity of the maximum stroke length to variations in Q11

On the other hand, if **Q** is fixed and **R** (composed of one element only) is varied, then the displacements shown in Fig. 5.24 are obtained. The bigger weight on the control force causes an increase in the displacement response due to lower cost being assigned to this variable.

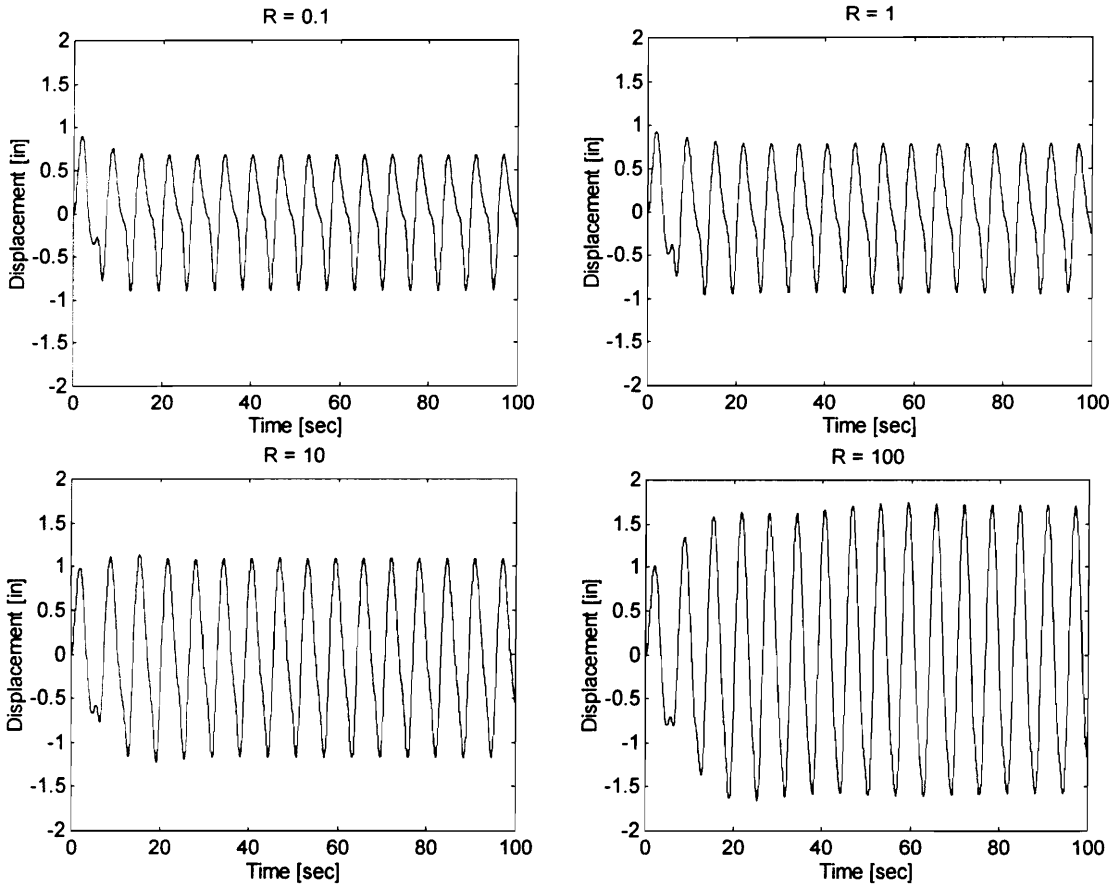

Fig. 5.24 Displacement for various R

The sensitivity of the maximum displacement, maximum control force, and maximum stroke length to variations in **R** are depicted in figures 5.25, 5.26, and 5.27, respectively. The higher cost on the control produces larger displacements. The smaller force requirement also results in a smaller stroke length.

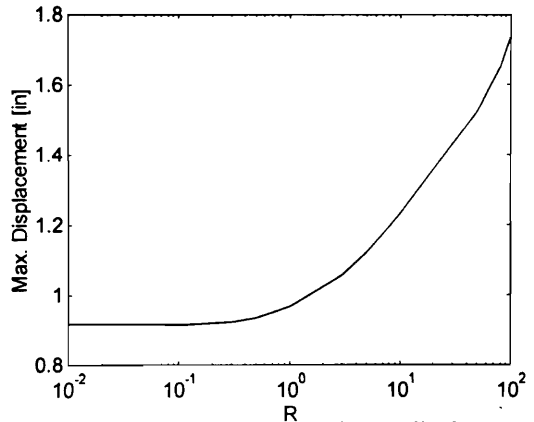

Fig. 5.25 Sensitivity of the maximum displacement to variations in R

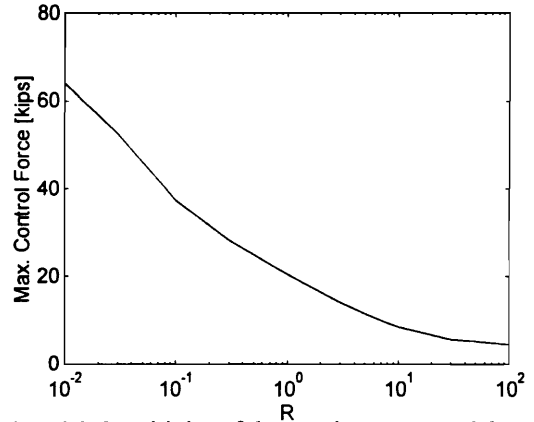

Fig.5.26 Sensitivity of the maximum control force to variations in R

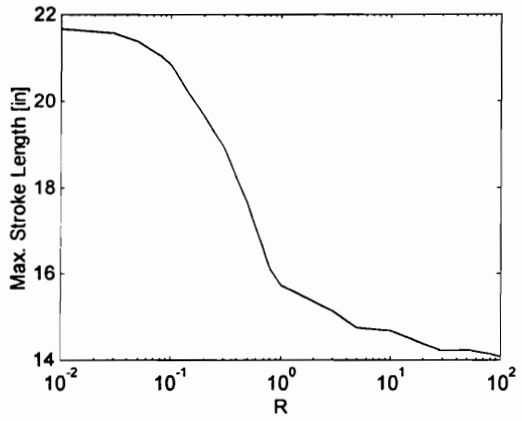

Fig. 5.27 Sensitivity of the maximum stroke length to variations in R

Example 5.4 Linear, Fixed-Base, Eight-Story Building with Mass Damper on the Top Floor

Consider the linear, fixed-base, eight-story building equipped with a mass damper on the top floor, described in Example 4.3. An LQ controller is used to provide active control to the structure while it is being subjected to the same wind excitation. The weighting matrices are chosen as,

$$\mathbf{Q} = \begin{bmatrix} q_{11}\mathbf{I}_{8\times 8} & \mathbf{0}_{8\times 10} \\ \mathbf{0}_{10\times 8} & \mathbf{0}_{10\times 10} \end{bmatrix} \qquad \mathbf{R} = 0.0001$$

where q_{11} is a scalar factor that weighs the interstory displacements. With $q_{11} = 1\times 10^5$, the resulting interstory drifts are shown in Fig.5.28. All interstory displacements reach their peaks during the first cycle of the disturbance.

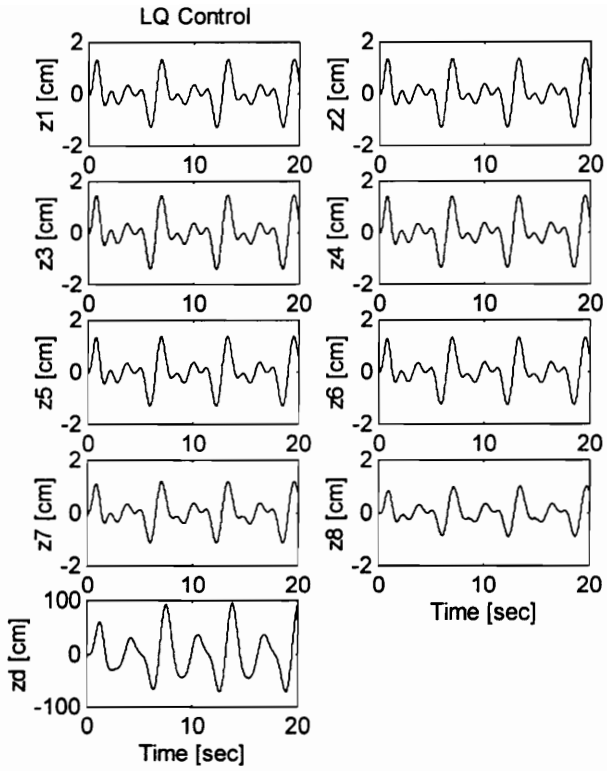

Fig. 5.28 Interstory drifts with LQ control

Table 5.3 gives a comparison of the structure's response without active control and with LQ control. The third story experiences the most interstory displacement. LQ control is able to provide a 29% reduction in this displacement. In order to produce this reduction, the stroke is increased by 287%.

TABLE 5.3 Comparison of Responses with Passive and LQ Control

FLOOR	Z_{pas}	Z_{lq}	R_{pas}	R_{lq}	Y_{pas}	Y_{lq}
1	1.9067	1.3374	0.7100	0.5942	1.9067	1.3374
2	1.9321	1.3574	0.7197	0.6032	3.8388	2.6946
3	2.0803	1.4674	0.7755	0.6522	5.9191	4.1618
4	1.9949	1.4179	0.7447	0.6307	7.9140	5.5797
5	1.8995	1.3703	0.7107	0.6100	9.8134	6.9473
6	1.7791	1.3226	0.6684	0.5893	11.5925	8.2564
7	1.5231	1.2232	0.5773	0.5432	13.1156	9.4428
8	0.9532	1.0252	0.3720	0.4438	14.0672	10.3155
Damper	24.4881	94.8030	9.9176	40.4955	21.3250	98.0185

where Z is the maximum interstory drift (cm), R is the RMS value of the interstory drift (cm), Y is the maximum displacement with respect to the ground (cm), *pas* is a subscript denoting passive control response, and *lq* is a subscript denoting LQ control response.

The force, power, and energy being provided by the actuator are shown in Fig. 5.29. There are instances where the regenerative actuator is able to recover some energy from the excitation. The net energy requirement is, however, still positive. As long as the structure is subjected to the excitation, the net energy keeps increasing because the actuator is consuming more energy than it is able to regenerate.

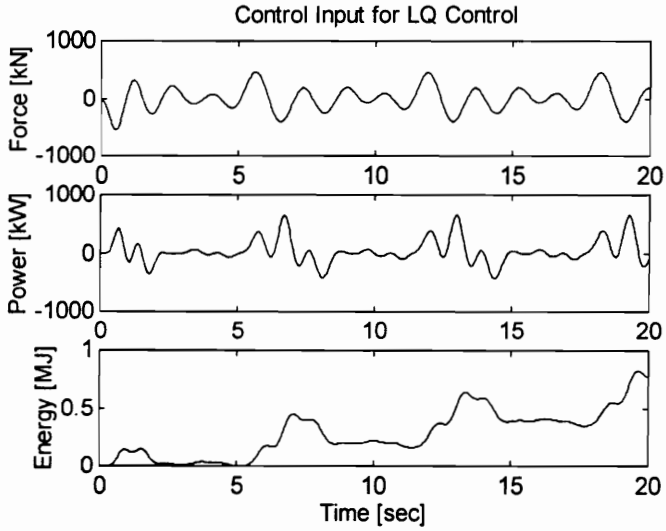

Fig. 5.29 Actuator force, power, and energy

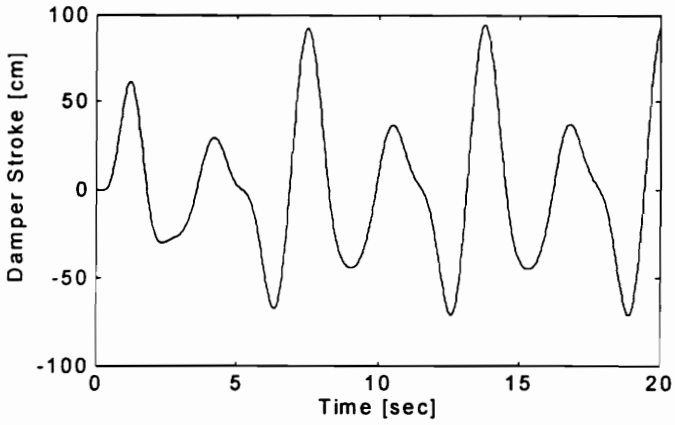

Fig. 5.30 Damper stroke length for linear quadratic control

The damper stroke length is shown in Fig. 5.30. When the stroke velocity and the control force are directed in opposite direction, then regeneration occurs. Motoring action is obtained when the stroke velocity and control force are directed in the same direction.

Varying the value of q_{11} affects the maximum interstory drift, the maximum damper stroke, and the maximum control force as shown in figures 5.31, 5.32, and 5.33. The larger weights on the displacements require larger control forces and, consequently, larger stroke lengths. The larger control forces allow a reduction in the interstory drift. The stroke length starts to increase significantly at about q_{11} = 10000.

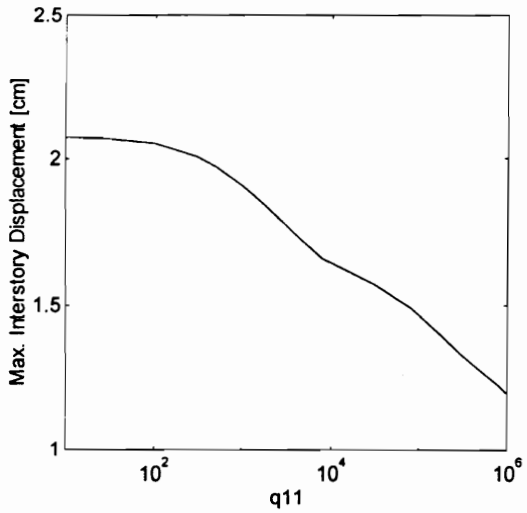

Fig. 5.31 Sensitivity of the maximum interstory drift to variation in q_{11}

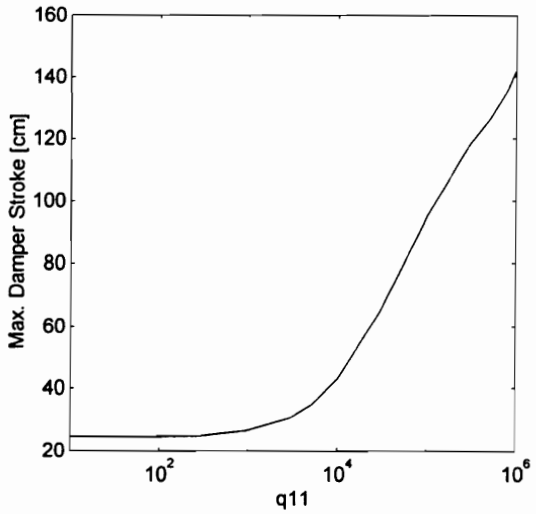

Fig. 5.32 Sensitivity of the maximum damper stroke to variation in q_{11}

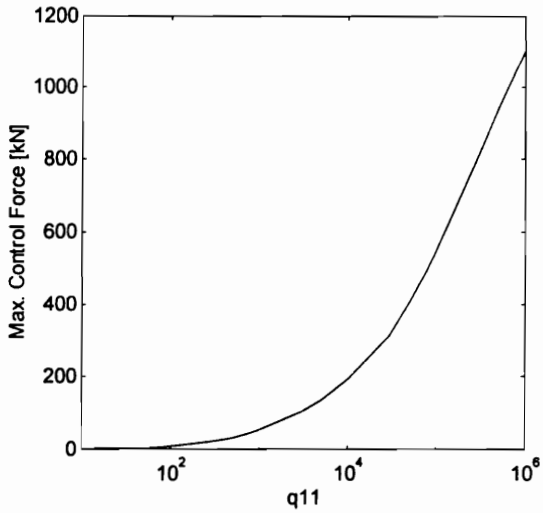

Fig. 5.33 Sensitivity of the maximum control force to variation in q_{11}

Example 5.5 Linear, Base-Isolated, Eight-Story Building with a Mass Damper on the Base Floor

Consider the linear, base-isolated, eight-story building with a mass damper on the base floor, as described in Example 4.4. With the same earthquake excitation, the structure is actively-controlled using an LQ controller. The weighting matrices are chosen as,

$\mathbf{Q} = \text{diag}(1, q_{22}, 1, 1, \ldots, 1)$ $\mathbf{R} = 0.0001$

q_{22} is the weight on the base displacement. It is desired that active control be able to reduce the base displacement which is usually excessive for base-isolated systems. If $q_{22} = 500$, the interstory drifts are shown in Fig. 5.34.

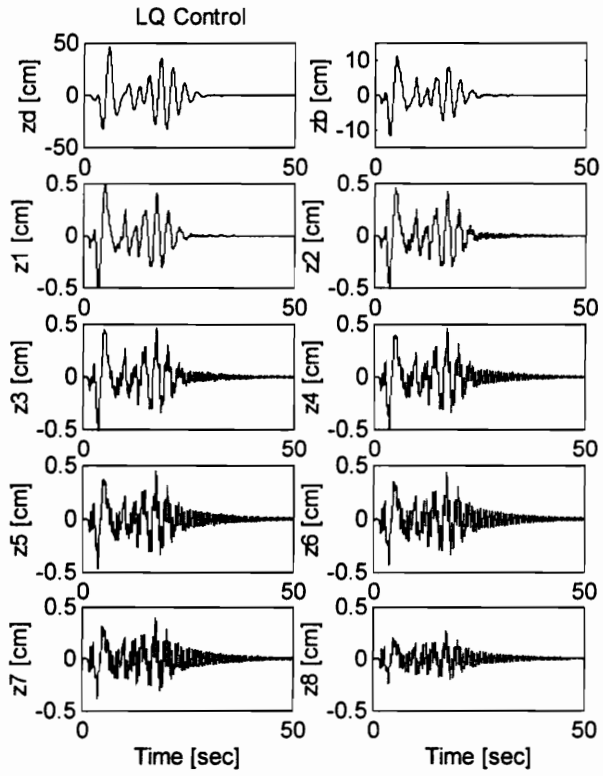

Fig. 5.34 Interstory drifts for LQ control

A comparison of the responses without active control and with LQ control is given in Table 5.4. The first floor experiences the largest interstory drift. LQ control is able to reduce this displacement by 2%, with a 49% increase in the stroke length.

TABLE 5.4 Comparison of Responses with Passive and LQ Control

FLOOR	Z_{pas}	Z_{lq}	R_{pas}	R_{lq}	Y_{pas}	Y_{lq}
Damper	31.4095	46.8333	10.8387	11.5341	35.4893	53.4180
Base	12.5719	11.6045	3.4460	2.8580	12.5719	11.6045
1	0.5401	0.5314	0.1492	0.1293	13.1090	12.1339
2	0.5120	0.5099	0.1399	0.1218	13.5905	12.6288
3	0.5326	0.5310	0.1426	0.1254	14.0548	13.1327
4	0.5094	0.4975	0.1326	0.1180	14.4606	13.6045
5	0.4984	0.4670	0.1250	0.1130	14.8198	14.0576
6	0.4846	0.4457	0.1181	0.1083	15.1363	14.4923
7	0.4349	0.4026	0.1037	0.0964	15.3955	14.8769
8	0.2891	0.2685	0.0681	0.0640	15.5620	15.1245

where Z is the maximum interstory drift (cm), R is the RMS value of the interstory drift (cm), Y is the maximum displacement with respect to the ground (cm), *pas* is a subscript denoting passive control response, and *lq* is a subscript denoting proportional control response

The actuator force, power, and energy are shown in Fig. 5.35. The negative peak in the regenerative actuator's power allows a net energy flow towards the source for the given duration of the excitation. Hence, there is a net gain in source energy.

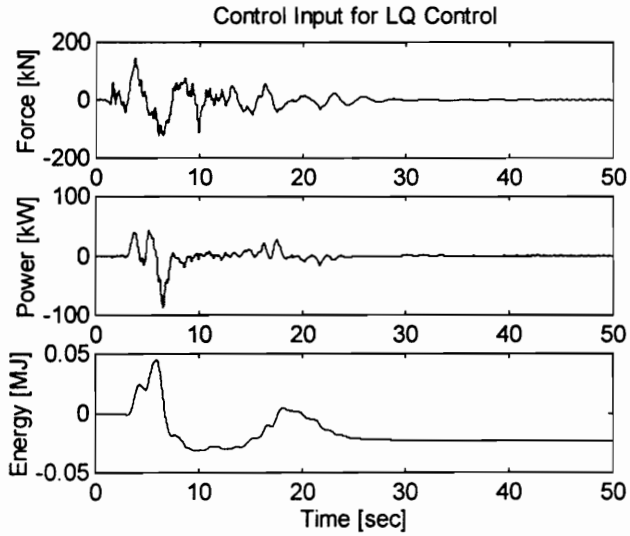

Fig. 5.35 Actuator force, power, and energy

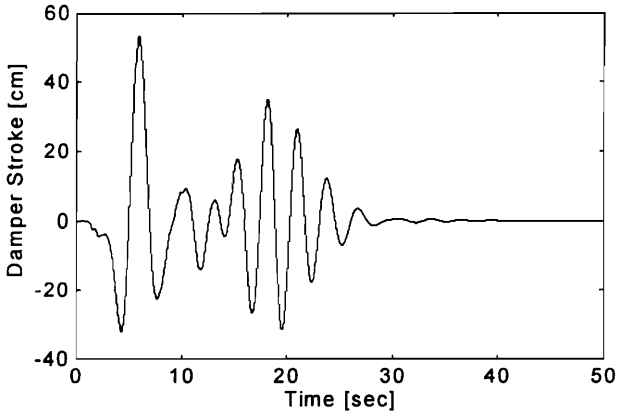

Fig. 5.36 Damper stroke for LQ control

The damper stroke is shown in Fig. 5.36. Motoring occurs when the stroke velocity and the control force are in the same direction. Opposition of the stroke velocity to the control force results in generating action.

The effect that variation in q_{22} has on the maximum interstory drift, maximum base displacement, maximum damper stroke, and maximum control force are shown in figures 5.37, 5.38, 5.39, and 5.40, respectively. Increasing the weight on the base displacement causes a reduction in the base displacement. This is requires an increase in the control force which results in an increase of the stroke length. The minimum interstory displacement occurs at q_{22} = 800, while minimum base displacement occurs at q_{22} = 500. The best compromise would to choose q_{22} between these two values. Increasing q_{22} also produces faster rates of decay in the displacement responses. However, this requires larger control forces and damper strokes.

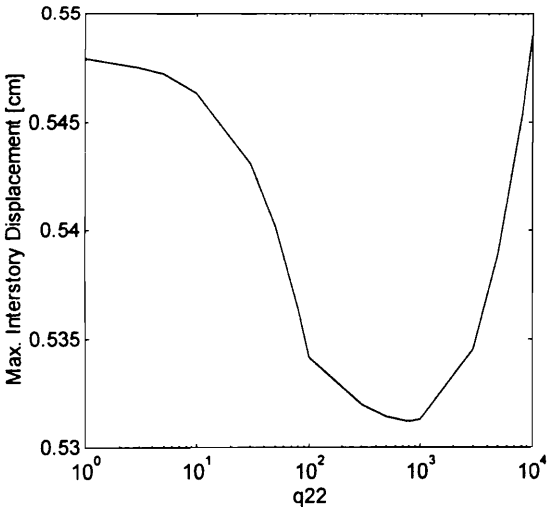

Fig. 5.37 Sensitivity of the maximum interstory drift to variation in q_{22}

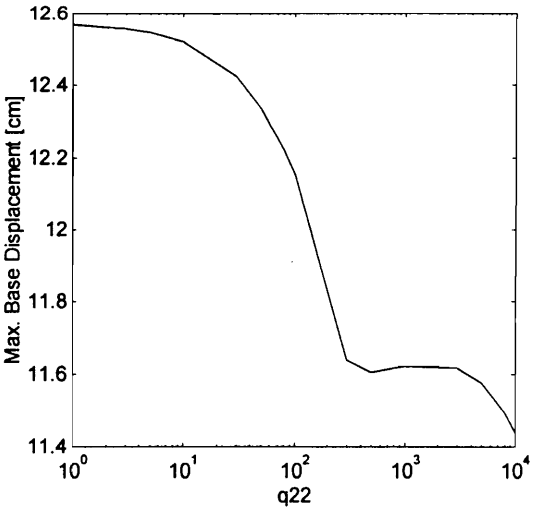

Fig. 5.38 Sensitivity of the maximum base displacement to variation in q_{22}

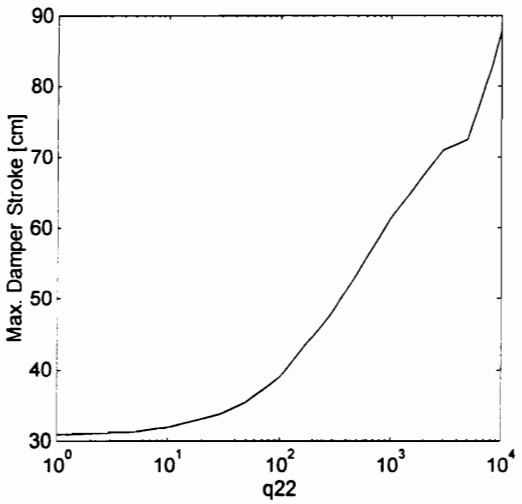

Fig. 5.39 Sensitivity of the maximum damper stroke to variation in q_{22}

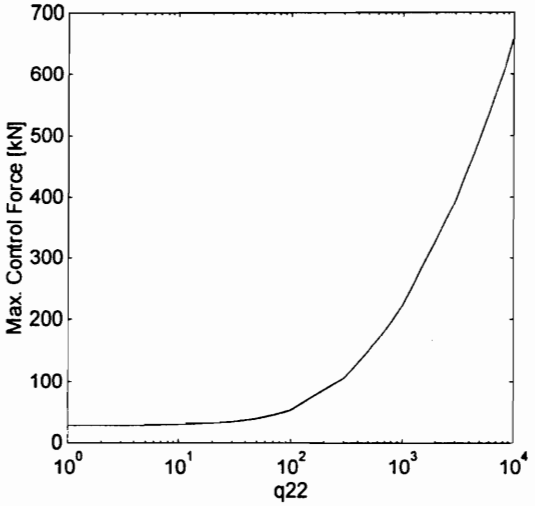

Fig. 5.40 Sensitivity of the maximum control force to variation in q_{22}

5.5 SUMMARY

This chapter does not present any original contribution. The main reason for its inclusion is to provide a benchmark against which controllers for the regenerative electric actuator are evaluated. A majority of the research in structural control have used this control algorithm.

In most structural control problems, the environmental disturbances are often unknown *a priori*. Therefore, the Riccati equation cannot be solved completely. This is also the reason that feedforward LQ control is not implementable. The regulator solution presented in this chapter is used to search for the best closed-loop control law for structures subjected to unknown disturbances. This is done by determining the response of the controlled structure when subjected to some assumed disturbances. The best regulator is one which performs well for most of the assumed excitations and those excitations which closely resemble the actual disturbances.

Simulations are performed for a single-degree-of-freedom system and for a fixed-base and a base-isolated multistory building. Reduction of the displacement response is obtained by increasing the weight on that particular displacement in the weighting matrix. The response reduction is attained at the cost of increasing the control force and the damper stroke. The LQ controller is shown to be effective for both wind and earthquake excitations. However, peak reduction seems to be a problem in earthquake-excited cases. Various criteria are suggested for choosing the weighting matrices.

Critical values in the actuator time delay and measurement time delay limit the extent to which these parameters can be increased without losing stability. Limiting the control force to

reduce stroke length can increase control efficiency without compromising the displacement response. This type of controller is found to provide more opportunities for regeneration. In some cases with sufficient duration in the excitation, there is even a net gain in the source energy.

CHAPTER 6

Sliding Mode Control

This chapter is directed towards the application of sliding mode control (also known as variable structure control) for the active control of structures, with special emphasis on the mitigation of wind- and earthquake-induced motion in tall buildings using regenerative electric actuators. The rationale for using sliding mode control is the fact that regenerative electric actuators use a form of on-off control based on pulse width modulation (PWM). Sliding mode inherently provides a synthesis of this on-off nature of PWM control and guarantees stability for the on-off control law. Due to the limited energy available for active control, saturation of the control force often occurs. Sliding mode control naturally encompasses the nonlinear, on-off nature of control force saturation. At the same time, sliding mode control guarantees stability for the on-off control law. This study is the first of its kind to investigate the applicability of sliding mode control to civil structures. Both linear and nonlinear models of the structure are considered in this study to assess the sliding mode controller's performance during disturbances. It is shown that the controller is able to overcome sensitivity to structural parameter variations, particularly structural stiffness. Systematic procedures for the design of the sliding surface, using both pole-placement and quadratic-minimization methods, are presented together with simulation results obtained by using linear and nonlinear models of the structure. These controllers are also shown to be effective even in the presence of control force saturation. With sliding mode control, the regenerative electric actuator is able to recover energy and store it for later use. This reduces the net energy drawn from the supply by the actuator. In some cases, there is even a net gain in the energy of the supply.

6.1 INTRODUCTION

Sliding mode control or variable structure control uses a high-speed switching control law to drive a system's state onto a specified surface (switching or sliding surface) in the state space, and maintain the state trajectory on this surface [1]. If the state trajectory is above the surface, the controller has one gain and a different gain if the trajectory drops below the surface. The controlled system's behavior can be described as the system dynamics being restricted to this surface. Sliding mode control is characterized by invariance to system parameter variations and to disturbances. This makes it an attractive option in the area of active control of civil structures

where accurate structural models are difficult to obtain. The inaccurate models are further aggravated by nonlinear structural members.

The current in the regenerative electric actuator is controlled by pulse width modulation (PWM) through the on-off application of voltage. Sliding mode control inherently provides a synthesis of this on-off nature of PWM control and guarantees stability for the on-off control law. Due to limitations on the available energy for control, saturation of the control force can occur. Sliding mode control naturally encompasses the nonlinear, on-off nature of control force saturation. While providing a natural synthesis of the on-off nature of control force saturation, it also guarantees stability for the on-off control law.

The idea of applying sliding mode control to civil structures under wind and earthquake excitation was initially proposed in [2] and continued in [3]. The control form proposed in [3] is based on the diagonalization method [4], and preassigns a control structure composed of linear feedback with switched gains. A discontinuous, sliding-mode control law based on an alternative structure for the control are presented in [5] and [6]. In these last two studies, the preassigned control structure is a sum of two components --- the equivalent control and an augmentation to this equivalent control. A similar approach is taken in [7]. Controllers based on continuous sliding mode control [8] are proposed in [9], [10], and [11]. Again, these studies use the augmented-equivalent-control structure. Experimental verifications on scale models are reported in [12] and [13], extending the work done in [9], [10], and [11].

This chapter proposes a new sliding-mode controller for the regenerative electric actuator which will provide active control to civil structures. The control law is based on the diagonalization method and uses a control structure composed of linear feedback with switched gains. The method and results presented in this chapter are based on initial work done in [3].

6.2 VARIABLE STRUCTURE SYSTEMS

Consider the single-input system

$$\dot{\mathbf{x}} = \mathbf{A}\mathbf{x} + \mathbf{b}u \tag{6.1}$$

For state-feedback control, the structure of the state feedback is fixed so that control is a fixed function of the state, i.e.,

$$u = -\mathbf{K}\mathbf{x} \tag{6.2}$$

The constant elements of $\mathbf{K}$ are chosen by using design methods like pole-placement and optimal control. In contrast to this, variable structure systems allow their structure to change by switching at any instant from one to another member of a set of possible continuous functions of the state [14]. One way of describing a control structure which results from a given choice of

feedback function is by drawing a phase plot. Different control structures will give different phase plots. Some of these structures are stable and some are unstable. Therefore, the design of a variable structure system requires the selection of the parameters of each of the structures, and the definition of the switching logic. A motivation for increasing the complexity of the design is the possibility of combining useful properties of each of the control structures by switching from one control structure to another. It is also possible that the resulting variable-structure system possesses new properties not present in any of the control structures used, such as being stable despite the fact that it is composed of unstable control structures. Regenerative electric actuators use a PWM type of control whose synthesis becomes easier with sliding mode control.

6.3 SLIDING MODES

To be more general, the systems that will initially be considered will be nonlinear in the state and linear in the control, i.e.,

$$\dot{\mathbf{x}}(t) = \mathbf{f}(\mathbf{x},t) + \mathbf{B}(\mathbf{x},t)\mathbf{u}(t) + \mathbf{H}\mathbf{w}(\mathbf{x},t) \tag{6.3}$$

where $\mathbf{x} \in \Re^n$, $\mathbf{u} \in \Re^m$, and $\mathbf{B} \in \Re^{n\times m}$. Each component $u_i(t)$ of the discontinuous switched control $\mathbf{u}(t) \in \Re^m$ has the form,

$$u_i = \begin{cases} u_i^+ & \sigma_i(\mathbf{x}) > 0 \\ u_i^- & \sigma_i(\mathbf{x}) < 0 \end{cases} \qquad i = 1,2,\ldots,m \tag{6.4}$$

where $u_i^+ \neq u_i^-$ and $\sigma_i(\mathbf{x}) = 0$ is the ith switching (discontinuity) surface (hyperplane) associated with the $(n - m)$-dimensional switching surface,

$$\sigma(\mathbf{x}) = \left[\sigma_1(\mathbf{x}) \quad \sigma_2(\mathbf{x}) \quad . \quad . \quad . \quad \sigma_m(\mathbf{x})\right]^T = \mathbf{0} \tag{6.5}$$

The switching surface $\sigma(\mathbf{x}) = \mathbf{0}$ is an $(n - m)$-dimensional manifold in $\Re^n$ determined by the intersection of m $(n$-1)-dimensional switching surfaces $\sigma_i(\mathbf{x}) = 0$. Since the design of linear switching surfaces is amenable to techniques used for linear controllers, switching surfaces are chosen to be of the form,

$$\sigma(\mathbf{x}) = \mathbf{S}\mathbf{x}(t) = \mathbf{0} \tag{6.6}$$

where $\mathbf{S}$ is an $m \times n$ matrix.

The state trajectory intercepts the switching surface and remains on the surface for all subsequent time. This phenomenon of the state staying on the switching surface after the trajectory intercepts the surface is called a sliding mode. A sliding mode will exist for a given system if the state velocity vector (derivative of the state vector) is always directed towards the switching surface in the vicinity of the switching surface. It is possible that sliding mode may exist only on the intersection $\sigma(\mathbf{x}) = \mathbf{0}$ and not on the individual $\sigma_i(\mathbf{x}) = 0$.

For sliding motion to occur on the ith hyperplane, it is required that,

$$\lim_{\sigma_i \to 0^+} \dot{\sigma}_i < 0 \tag{6.7}$$

and

$$\lim_{\sigma_i \to 0^-} \dot{\sigma}_i > 0 \tag{6.8}$$

This ensures that the motion of the state trajectory is always directed towards the ith switching surface, once the state is in the vicinity of the surface. Equations (6.7) and (6.8) can be combined to give the equivalent condition for sliding motion to occur as,

$$\sigma_i \dot{\sigma}_i \leq 0 \tag{6.9}$$

in the neighborhood of $\sigma_i(\mathbf{x}) = 0$. When the system is in sliding mode, it satisfies the equations,

$$\sigma_i(\mathbf{x}) = 0 \tag{6.10}$$

and

$$\dot{\sigma}_i(\mathbf{x}) = 0 \tag{6.11}$$

Furthermore, the system gains invariance properties which makes the state trajectory independent of certain system parameters and disturbances. If sliding mode exists on all the switching hyperplanes, then the following will be true during sliding motion:

$$\boldsymbol{\sigma} = \mathbf{0} \tag{6.12}$$

and

$$\dot{\boldsymbol{\sigma}} = \mathbf{0} \tag{6.13}$$

The ideal sliding mode will exist only when the state $\mathbf{x}$ of the controlled system satisfy $\sigma(\mathbf{x}) = 0$ for all time $t \geq t_0$. In order for this to occur, the switching logic must work infinitely fast, with the control oscillating between u_i^+ and u_i^-. However, the switching mechanisms in actual systems have imperfections like time delay or hysteresis. They cause the switching to occur at a finite frequency. The trajectory then oscillates within a neighborhood of the switching surface as a phenomenon called chattering. In cases where the switching frequency is relatively very high compared to the frequency components of the system response, the effect of the switching imperfections and the finite switching frequency can become negligible. As the non-ideal characteristics diminish, the state trajectory will approach the ideal sliding mode on the intersection of the switching surface.

The design of a variable-structure control system can be broken down into three major steps: (a) the design of a switching surface σ where the restricted system will have a desired behavior, (b) the specification of a suitable control function which will ensure sliding motion along the intersection of the switching surfaces σ_i's, and (c) the design of the switched feedback

gains of the control function which will drive the state to the switching surface σ and keep the state on the surface.

6.4 DESIGN OF THE SLIDING SURFACE

A. Method of Equivalent Control

The equivalent control method [15] was formulated to study the system's motion once it is restricted to the switching surface $\sigma(\mathbf{x}) = \mathbf{0}$. Assume that the state trajectory intercepts the switching surface at time t_s and sliding mode is maintained for all $t \geq t_s$. For a sliding mode to exist, it is required that

$$\dot{\sigma}(\mathbf{x}(t)) = \mathbf{0} \quad \text{and} \quad \sigma(\mathbf{x}(t)) = \mathbf{0} \tag{6.14}$$

for all $t \geq t_s$. In order to solve for the equivalent control $\mathbf{u}_{eq}$ which will yield the sliding mode equations for the system, let

$$\dot{\sigma} = \frac{\partial \sigma}{\partial \mathbf{x}} \dot{\mathbf{x}} = \frac{\partial \sigma}{\partial \mathbf{x}} [\mathbf{f}(\mathbf{x},t) + \mathbf{B}(\mathbf{x},t)\mathbf{u}_{eq} + \mathbf{Hw}(\mathbf{x},t)] = \mathbf{0} \tag{6.15}$$

If it is assumed that $\frac{\partial \sigma}{\partial \mathbf{x}} \mathbf{B}$ is nonsingular for all $\mathbf{x}$ and t, then (6.15) can be solved for $\mathbf{u}_{eq}$. Thus,

$$\mathbf{u}_{eq} = -\left[\frac{\partial \sigma}{\partial \mathbf{x}} \mathbf{B}(\mathbf{x},t)\right]^{-1} \frac{\partial \sigma}{\partial \mathbf{x}} [\mathbf{f}(\mathbf{x},t) + \mathbf{Hw}(\mathbf{x},t)] \tag{6.16}$$

If (6.16) is substituted into the original state equations given by (6.3) with the assumption that $\sigma(\mathbf{x}(t_s)) = \mathbf{0}$, the dynamics of the system on the switching surface for all $t \geq t_s$ will be described by

$$\dot{\mathbf{x}} = \left[\mathbf{I} - \mathbf{B}(\mathbf{x},t)\left[\frac{\partial \sigma}{\partial \mathbf{x}} \mathbf{B}(\mathbf{x},t)\right]^{-1} \frac{\partial \sigma}{\partial \mathbf{x}}\right] [\mathbf{f}(\mathbf{x},t) + \mathbf{Hw}(\mathbf{x},t)] \tag{6.17}$$

If a linear switching surface is used, i.e. $\sigma(\mathbf{x}) = \mathbf{Sx}$, then (6.17) reduces to

$$\dot{\mathbf{x}} = \left[\mathbf{I} - \mathbf{B}(\mathbf{x},t)[\mathbf{SB}(\mathbf{x},t)]^{-1}\mathbf{S}\right] [\mathbf{f}(\mathbf{x},t) + \mathbf{Hw}(\mathbf{x},t)] \tag{6.18}$$

where

$$\frac{\partial \sigma}{\partial \mathbf{x}} = \mathbf{S} \tag{6.19}$$

For the linear, time-invariant case without any disturbance,

$$\mathbf{u}_{eq} = -(\mathbf{SB})^{-1}\mathbf{SAx}(t) \tag{6.20}$$

and

$$\dot{\mathbf{x}}(t) = \left[\mathbf{I} - \mathbf{B}(\mathbf{SB})^{-1}\mathbf{S}\right]\mathbf{A}\mathbf{x}(t) \tag{6.21}$$

Therefore, the system's motion on the switching surface is given by (6.17) and the constraint $\sigma(\mathbf{x}) = 0$. The constraint $\sigma(\mathbf{x}) = \mathbf{0}$, which is a constraint on the state variables, will reduce the order of the dynamic equations when the system is on the switching surface. The m algebraic equations given by $\sigma(\mathbf{x}) = \mathbf{0}$ can be used to eliminate m state variables from the n-dimensional dynamic equations (6.17). Thus, the system dynamics is reduced from an nth-order to an $(n-m)$th-order system. This reduction is shown in the design of the sliding surface which is discussed subsequently.

B. Canonical Form for Variable-Structure Controller Design

The system equation given by (6.3) can be expressed as,

$$\dot{\mathbf{x}} = (\mathbf{A} + \Delta\mathbf{A})\mathbf{x} + (\mathbf{B} + \Delta\mathbf{B})\mathbf{u} + \mathbf{v} \tag{6.22}$$

where $\mathbf{v}$ is an external disturbance and $\Delta\mathbf{A}$ and $\Delta\mathbf{B}$ are system perturbations. The system described by (6.22) will possess certain invariance properties if the following matching conditions [16] are met:

$$\begin{aligned} \Delta\mathbf{A} &= \mathbf{B}\tilde{\mathbf{A}} \\ \Delta\mathbf{B} &= \mathbf{B}\tilde{\mathbf{B}} \\ \mathbf{v} &= \mathbf{B}\tilde{\mathbf{v}} \end{aligned} \tag{6.23}$$

Differentiating $\sigma(\mathbf{x}) = 0$ with respect to time t gives,

$$\frac{\partial\sigma}{\partial\mathbf{x}}\left[(\mathbf{A} + \Delta\mathbf{A})\mathbf{x} + (\mathbf{B} + \Delta\mathbf{B})\mathbf{u} + \mathbf{v}\right] = 0 \tag{6.24}$$

From the matching conditions given by (6.23), (6.24) becomes,

$$\frac{\partial\sigma}{\partial\mathbf{x}}\left[\mathbf{A}\mathbf{x} + \mathbf{B}(\tilde{\mathbf{A}}\mathbf{x} + \mathbf{v})\right] + \frac{\partial\sigma}{\partial\mathbf{x}}\mathbf{B}(\mathbf{I} + \tilde{\mathbf{B}})\mathbf{u} = 0 \tag{6.25}$$

Assuming that $\mathbf{I} + \tilde{\mathbf{B}}$ is nonsingular, the equivalent control for the sliding mode is obtained as,

$$\mathbf{u}_{eq} = -(\mathbf{I} + \tilde{\mathbf{B}})^{-1}\left(\frac{\partial\sigma}{\partial\mathbf{x}}\mathbf{B}\right)^{-1}\frac{\partial\sigma}{\partial\mathbf{x}}\left[\mathbf{A}\mathbf{x} + \mathbf{B}(\tilde{\mathbf{A}}\mathbf{x} + \tilde{\mathbf{v}})\right] \tag{6.26}$$

Substituting $\mathbf{u}_{eq}$ in (6.22) yields,

$$\dot{\mathbf{x}} = \mathbf{A}\mathbf{x} + \mathbf{B}\tilde{\mathbf{A}}\mathbf{x} + \mathbf{B}(\mathbf{I} + \tilde{\mathbf{B}})\mathbf{u}_{eq} + \mathbf{B}\tilde{\mathbf{v}} \tag{6.27}$$

or,

$$\dot{\mathbf{x}} = \mathbf{A}\mathbf{x} - \mathbf{B}\left(\frac{\partial \sigma}{\partial \mathbf{x}}\mathbf{B}\right)^{-1}\frac{\partial \sigma}{\partial \mathbf{x}}\mathbf{A}\mathbf{x} \tag{6.28}$$

which is independent of $\Delta\mathbf{A}$, $\Delta\mathbf{B}$, and $\mathbf{v}$.

Since the sliding mode controller is invariant to parameter variations, nonlinearities can be considered as perturbations from a linear model. The controller's invariance to disturbances makes the design of the sliding surface independent of these disturbances. Thus, in designing the sliding hyperplane, it is sufficient to consider the nominal regulator system [17].

$$\dot{\mathbf{x}}(t) = \mathbf{A}\mathbf{x}(t) + \mathbf{B}\mathbf{u}(t) \tag{6.29}$$

where $\mathbf{x}$ is the state n-vector, $\mathbf{u}$ is the control m-vector, and $\mathbf{A}$ and $\mathbf{B}$ have dimensions $n\times n$ and $n\times m$, respectively. It is assumed that $m < n$, $\mathbf{B}$ is of rank m, and $(\mathbf{A},\mathbf{B})$ is completely controllable. The motion of the system in the sliding mode is determined by the defining condition

$$\sigma = \mathbf{S}\mathbf{x}(t) = \mathbf{0} \qquad t \geq t_S \tag{6.30}$$

where t_S is the time of arrival at the sliding mode and $\mathbf{S}$ is an $m\times n$ matrix. To simplify the development of the theory and the design scheme, a particular canonical form is used for the system [5][6]. Assuming that matrix $\mathbf{B}$ has rank m, define a nonsingular linear transformation

$$\mathbf{z}(t) = \mathbf{T}\mathbf{x}(t) \tag{6.31}$$

such that

$$\mathbf{T}\mathbf{B} = \begin{bmatrix} \mathbf{0} \\ \mathbf{B}_2 \end{bmatrix} \tag{6.32}$$

where $\mathbf{T}$ is an orthonormal $n\times n$ transformation matrix ($\mathbf{T}^{-1} = \mathbf{T}^T$) and $\mathbf{B}_2$ is both $m\times m$ and nonsingular. To satisfy (6.32), the first $(n - m)$ rows of matrix $\mathbf{T}$ must form a basis for the $(n - m)$-dimensional subspace orthogonal to the subspace spanned by the vectors of $\mathbf{B}$. $\mathbf{T}$ can be systematically derived by a QR (or QU) decomposition of $\mathbf{B}$, in which $\mathbf{B}$ is decomposed into the form

$$\mathbf{B} = \mathbf{Q}\begin{bmatrix} \mathbf{R} \\ \mathbf{0} \end{bmatrix} \tag{6.33}$$

where $\mathbf{Q}$ is an orthogonal $n\times n$ matrix and $\mathbf{R}$ is a nonsingular, upper-triangular, $m\times m$ matrix. $\mathbf{T}$ can be obtained by rearranging the rows of $\mathbf{Q}^T$.

In terms of the new state variables $\mathbf{z}$, the state equation (6.29) can be written as,

$$\dot{\mathbf{z}}(t) = \mathbf{T}\mathbf{A}\mathbf{T}^{-1}\mathbf{z}(t) + \mathbf{T}\mathbf{B}\mathbf{u}(t) \tag{6.34}$$

If the transformed state $\mathbf{z}$ is partitioned as

$$\mathbf{z} = \begin{bmatrix} \mathbf{z}_1 \\ \mathbf{z}_2 \end{bmatrix} \tag{6.35}$$

where $\mathbf{z}_1$ and $\mathbf{z}_2$ are vectors of length (n - m) and m, respectively, then the matrices $\mathbf{TAT}^{-1}$ and $\mathbf{TB}$ can also be partitioned accordingly such that the transformed state equations become

$$\begin{bmatrix} \dot{\mathbf{z}}_1 \\ \dot{\mathbf{z}}_2 \end{bmatrix} = \begin{bmatrix} \mathbf{A}_{11} & \mathbf{A}_{12} \\ \mathbf{A}_{21} & \mathbf{A}_{22} \end{bmatrix} \begin{bmatrix} \mathbf{z}_1 \\ \mathbf{z}_2 \end{bmatrix} + \begin{bmatrix} \mathbf{0} \\ \mathbf{B}_2 \end{bmatrix} \mathbf{u}(t) \tag{6.36}$$

or

$$\dot{\mathbf{z}}_1(t) = \mathbf{A}_{11}\mathbf{z}_1(t) + \mathbf{A}_{12}\mathbf{z}_2(t) \tag{6.37}$$

$$\dot{\mathbf{z}}_2(t) = \mathbf{A}_{21}\mathbf{z}_1(t) + \mathbf{A}_{22}\mathbf{z}_2(t) + \mathbf{B}_2\mathbf{u}(t) \tag{6.38}$$

$\mathbf{A}_{11}$, $\mathbf{A}_{12}$, $\mathbf{A}_{21}$, and $\mathbf{A}_{22}$ are respectively (n - m)×(n - m), (n - m)×m, m×(n - m), and m×m submatrices. The canonical form of the state equations given by (6.36) is used to determine the control which will ensure the reachability of the sliding mode.

The sliding condition with respect to the new state variables become,

$$\sigma = \mathbf{ST}^{-1}\mathbf{z}(t) \tag{6.39}$$

After partitioning $\mathbf{ST}^{-1}$, the sliding condition can be written as,

$$\sigma = \begin{bmatrix} \mathbf{S}_1 & \mathbf{S}_2 \end{bmatrix} \begin{bmatrix} \mathbf{z}_1 \\ \mathbf{z}_2 \end{bmatrix} \tag{6.40}$$

or

$$\sigma = \mathbf{S}_1\mathbf{z}_1 + \mathbf{S}_2\mathbf{z}_2 \tag{6.41}$$

where $\mathbf{S}_1$ and $\mathbf{S}_2$ are m×(n - m) and m×m submatrices, respectively, and $\mathbf{S}_2$ is nonsingular.

C. Hyperplane Design using Pole-Placement Method[18][19]

With the condition that $\sigma = \mathbf{0}$, (6.41) which defines the sliding condition can be written as,

$$\mathbf{z}_2 = -\mathbf{S}_2^{-1}\mathbf{S}_1\mathbf{z}_1 \tag{6.42}$$

It can be assumed, without loss of generality, that

$$\mathbf{S}_2 = \mathbf{I}_m \tag{6.43}$$

Therefore, it follows from (6.37) that

$$\dot{\mathbf{z}}_1 = \mathbf{A}_{11}\mathbf{z}_1 + \mathbf{A}_{12}\left(-\mathbf{I}^{-1}\mathbf{S}_1\mathbf{z}_1\right) \tag{6.44}$$

or

$$\dot{\mathbf{z}}_1 = \left(\mathbf{A}_{11} - \mathbf{A}_{12}\mathbf{S}_1\right)\mathbf{z}_1 \tag{6.45}$$

The poles of the transformed system are the eigenvalues of the matrix ($\mathbf{A}_{11}$-$\mathbf{A}_{12}\mathbf{S}_1$) and depend on the matrix $\mathbf{S}_1$. Note that (6.45) represents an (n - m)th-order system with state feedback control where $\mathbf{A}_{12}$ is the input matrix and $\mathbf{S}_1$ is the feedback gain matrix. If (**A**,**B**) is a controllable pair, then ($\mathbf{A}_{11}$,$\mathbf{A}_{12}$) is also controllable [20]. Thus, the (n - m) eigenvalues of ($\mathbf{A}_{11}$-$\mathbf{A}_{12}\mathbf{S}_1$) can be placed arbitrarily in the left-hand side of the complex plane by an appropriate choice of the matrix $\mathbf{S}_1$. For controllable systems, the following design procedure is formulated: (a) Determine the transformation matrix **T** in (6.31), (b) Find the matrix $\mathbf{S}_1$ such that the (n - m) eigenvalues of ($\mathbf{A}_{11}$-$\mathbf{A}_{12}\mathbf{S}_1$) have the desired location, and (c) Choose the equation of the switching hyperplane in the space of the original state variables to be,

$$\sigma = [\mathbf{S}_1 \quad \mathbf{I}_m]\mathbf{T}\mathbf{x}(t) = \mathbf{0} \tag{6.46}$$

D. Hyperplane Design using Quadratic Minimization[18][19]

Another way to design the sliding hyperplane is by minimizing the quadratic performance index

$$J = \frac{1}{2}\int_{t_s}^{\infty} \mathbf{x}^T\mathbf{Q}\mathbf{x}dt \tag{6.47}$$

where **Q** is a constant, symmetric, and positive-definite matrix. The objective is to minimize J subject to the state equation (6.37), assuming that $\mathbf{x}(t_s)$ is a known initial condition. This problem can be restated as a linear quadratic regulator problem for the system defined by (6.29). If the matrix $(\mathbf{T}^{-1})^T\mathbf{Q}\mathbf{T}^{-1}$ is partitioned as,

$$\left(\mathbf{T}^{-1}\right)^T\mathbf{Q}\mathbf{T}^{-1} = \begin{bmatrix} \mathbf{Q}_{11} & \mathbf{Q}_{12} \\ \mathbf{Q}_{21} & \mathbf{Q}_{22} \end{bmatrix} \tag{6.48}$$

where

$$\mathbf{Q}_{21}{}^T = \mathbf{Q}_{12} \tag{6.49}$$

then (6.47) can be restated as,

$$J = \frac{1}{2}\int_{t_s}^{\infty} \left(\mathbf{z}_1{}^T\mathbf{Q}_{11}\mathbf{z}_{11} + 2\mathbf{z}_1{}^T\mathbf{Q}_{12}\mathbf{z}_2 + \mathbf{z}_2{}^T\mathbf{Q}_{22}\mathbf{z}_2\right)dt \tag{6.50}$$

Let

$$\mathbf{v} = \mathbf{z}_2 + \mathbf{Q}_{22}{}^{-1}\mathbf{Q}_{12}\mathbf{z}_1 \tag{6.51}$$

$$\mathbf{Q}^* = \mathbf{Q}_{11} - \mathbf{Q}_{12}\mathbf{Q}_{22}{}^{-1}\mathbf{Q}_{12}{}^T \tag{6.52}$$

$$\mathbf{A}^* = \mathbf{A}_{11} - \mathbf{A}_{12}\mathbf{Q}_{22}{}^{-1}\mathbf{Q}_{12}{}^T \tag{6.53}$$

Substituting in the performance index yields,

$$J = \frac{1}{2}\int_{t_s}^{\infty}\left(\mathbf{z}_1{}^T\mathbf{Q}^*\mathbf{z}_1 + \mathbf{v}^T\mathbf{Q}_{22}\mathbf{v}\right)dt \tag{6.54}$$

The state equation (6.37) can be written as,

$$\dot{\mathbf{z}}_1 = \mathbf{A}^*\mathbf{z}_1 + \mathbf{A}_{12}\mathbf{v} \tag{6.55}$$

The problem is now to minimize (6.54) subject to the constraint given by (6.55). These two equations have the form of the standard linear quadratic regulator (LQR) problem. The controllability of $(\mathbf{A}^*,\mathbf{A}_{12})$ is ensured by the controllability of $(\mathbf{A},\mathbf{B})$ [18]. An algebraic Riccati equation can be written for the LQR problem posed by (6.54) and (6.55), i.e.

$$\mathbf{P}\mathbf{A}^* + \mathbf{A}^{*T}\mathbf{P} - \mathbf{P}\mathbf{A}_{12}\mathbf{Q}_{22}{}^{-1}\mathbf{A}_{12}{}^T\mathbf{P} + \mathbf{Q}^* = \mathbf{0} \tag{6.56}$$

Since $\mathbf{Q}$ is required to be positive, then (a) $\mathbf{Q}_{22} > 0$ and $\mathbf{Q}_{22}{}^{-1}$ exists, and (b) $\mathbf{Q}^* > 0$. Thus, a unique and positive-definite Riccati matrix $\mathbf{P}$ is guaranteed. The optimal control $\mathbf{v}$ can then be expressed as,

$$\mathbf{v} = -\mathbf{Q}_{22}{}^{-1}\mathbf{A}_{12}{}^T\mathbf{P}\mathbf{z}_1 \tag{6.57}$$

Substituting (6.57) in (6.51) gives,

$$\mathbf{z}_2 = -\mathbf{Q}_{22}{}^{-1}\left[\mathbf{Q}_{21} + \mathbf{A}_{12}{}^T\mathbf{P}\right]\mathbf{z}_1 \tag{6.58}$$

Comparing (6.58) with (6.42), it is found that

$$\mathbf{S}_1 = \mathbf{Q}_{22}{}^{-1}\left(\mathbf{A}_{12}{}^T\mathbf{P} + \mathbf{Q}_{12}{}^T\right) \tag{6.59}$$

Therefore, the quadratic minimization method can be used as given in the following procedure for designing the sliding hyperplane: (a) Determine the transformation matrix $\mathbf{T}$ in (6.31), (b) Solve the (6.56) for the Riccati matrix $\mathbf{P}$, and (c) Choose the equations for the switching hyperplane in terms of the original state variables as

$$\sigma = \left[\mathbf{Q}_{22}{}^{-1}\left(\mathbf{A}_{12}{}^T\mathbf{P} + \mathbf{Q}_{12}{}^T\right) \quad \mathbf{I}_m\right]\mathbf{T}\mathbf{x}(t) = \mathbf{0} \tag{6.60}$$

6.5 CONTROLLER DESIGN

Assuming that a sliding surface has been designed, the next step will be to determine the switched feedback gains which will drive the state trajectory into the switching surface and eventually maintain the trajectory on the surface. The control function is chosen to have the form

$$u_i = \begin{cases} u_i^+ & \sigma_i(\mathbf{x}) > 0 \\ u_i^- & \sigma_i(\mathbf{x}) < 0 \end{cases} \tag{6.61}$$

where

$$\mathbf{u} = \begin{bmatrix} u_1 & u_2 & \cdots & u_m \end{bmatrix}^T \tag{6.62}$$

$$\sigma(\mathbf{x}) = \begin{bmatrix} \sigma_1(\mathbf{x}) & \sigma_2(\mathbf{x}) & \cdots & \sigma_m(\mathbf{x}) \end{bmatrix}^T \tag{6.63}$$

To ensure that sliding motion will exist simultaneously on the intersection of the m sliding hyperplanes (an n - m subspace), the diagonalization method will be used to design the controller gains. The essential feature of the diagonalization method is the decoupling of motion in the m-dimensional subspace, which is composed of the switching or discontinuity surfaces $\sigma_i(\mathbf{x}) = 0$ (i=1,2,...,m), into m independent first-order motions. If sliding conditions are met on each of the $\sigma_i = 0$ surfaces, a sliding mode is ensured on the manifold $\sigma = \mathbf{0}$. There are two different approaches to the implementation of this method. Method 1 introduces a new control vector $\mathbf{u}^*$ through a nonsingular transformation of the original control vector $\mathbf{u}$. Method 2, in the other hand, requires a nonsingular transformation of σ based on the fact that the equivalent system is invariant to nonsingular transformations of the switching surfaces [21]. Method 1 will used in this study.

Neglecting disturbances, the state equation (6.3) is reduced to,

$$\dot{\mathbf{x}}(t) = \mathbf{f}(\mathbf{x},t) + \mathbf{B}(\mathbf{x},t)\mathbf{u}(t) \tag{6.64}$$

Consider the nonsingular transformation of the original control vector $\mathbf{u}$

$$\mathbf{u}^*(t) = \mathbf{Q}^{-1}(\mathbf{x},t)\left[\frac{\partial \sigma}{\partial \mathbf{x}}\right]\mathbf{B}(\mathbf{x},t)\mathbf{u}(t) \tag{6.65}$$

where $\mathbf{Q}(\mathbf{x},t)$ is an arbitrary $m \times m$ diagonal matrix whose constant elements $q_i(\mathbf{x},t)$ (i=1,2,...,m) satisfy the condition,

$$\inf|q_i| > 0 \qquad \forall t \geq 0, \forall \mathbf{x} \tag{6.66}$$

on the manifold $\sigma = \mathbf{0}$. Although $\mathbf{Q}^{-1}(\mathbf{x},t)$ allows weighting of $\mathbf{u}^*$, $\mathbf{Q}(\mathbf{x},t)$ is usually chosen as an identity matrix. Solving (6.65) for $\mathbf{u}(t)$ and substituting into (6.64) yields,

$$\dot{\mathbf{x}}(t) = \mathbf{f}(\mathbf{x},t) + \mathbf{B}(\mathbf{x},t)\left[\frac{\partial \sigma}{\partial \mathbf{x}}\mathbf{B}(\mathbf{x},t)\right]^{-1}\mathbf{Q}(\mathbf{x},t)\mathbf{u}^*(t) \tag{6.67}$$

For the existence and reachability of a sliding mode, the condition $\sigma^T(\mathbf{x})\dot{\sigma}(\mathbf{x}) < 0$ must be satisfied. Thus,

$$\sigma^T(\mathbf{x})\dot{\sigma}(\mathbf{x}) = \sigma^T(\mathbf{x})\frac{\partial \sigma}{\partial \mathbf{x}}\dot{\mathbf{x}} < 0 \tag{6.68}$$

Substituting (6.67) in (6.68) gives,

$$\sigma^T(\mathbf{x})\dot{\sigma}(\mathbf{x}) = \sigma^T(\mathbf{x})\left[\frac{\partial \sigma}{\partial \mathbf{x}}\mathbf{f}(\mathbf{x},t) + \mathbf{Q}(\mathbf{x},t)\mathbf{u}^*(t)\right] < 0 \tag{6.69}$$

Therefore, the gains u_i^{*+} and u_i^{*-} are chosen such that,

$$q_i(\mathbf{x},t)u_i^{*+} < -\nabla\sigma_i(\mathbf{x})\mathbf{f}(\mathbf{x},t) \qquad \sigma_i(\mathbf{x}) > 0 \tag{6.70}$$

$$q_i(\mathbf{x},t)u_i^{*-} > -\nabla\sigma_i(\mathbf{x})\mathbf{f}(\mathbf{x},t) \qquad \sigma_i(\mathbf{x}) < 0 \tag{6.71}$$

where $\nabla\sigma_i(\mathbf{x})$ is the ith row of $\partial\sigma/\partial\mathbf{x}$. Assuming a linear switching surface $\sigma(\mathbf{x}) = \mathbf{S}\mathbf{x}$,

$$q_i(\mathbf{x},t)u_i^{*+} < -\sum_{j=1}^{n} s_{ij} f_j(\mathbf{x},t) \qquad \sigma_i(\mathbf{x}) > 0 \tag{6.72}$$

$$q_i(\mathbf{x},t)u_i^{*-} > -\sum_{j=1}^{n} s_{ij} f_j(\mathbf{x},t) \qquad \sigma_i(\mathbf{x}) < 0 \tag{6.73}$$

The actual control input is given by,

$$\mathbf{u}(t) = \left[\frac{\partial \sigma}{\partial \mathbf{x}}\mathbf{B}(\mathbf{x},t)\right]^{-1}\mathbf{Q}(\mathbf{x},t)\mathbf{u}^*(t) \tag{6.74}$$

Example 6.1 SDOF Structure with Mass Damper (2DOF System)

Consider the single degree-of-freedom structure with mass damper described in Example 4.1. Assume that the system is being excited by a wind force with parameters p = 9.75 kips and ω = 1 rad/sec. The sliding surface is designed by using (a) the pole-placement method and (b) the quadratic minimization method. To obtain the canonical form, the transformation matrix **T** is chosen (by inspection) as

$$\mathbf{T} = \begin{bmatrix} 1 & 0 & 0 & 0 \\ 0 & 1 & 0 & 0 \\ 0 & 0 & m_s & \dfrac{m_s m_d}{m_s + m_d} \\ 0 & 0 & -\dfrac{1}{m_s} & \dfrac{m_s + m_d}{m_s m_d} \end{bmatrix}$$

The control is of the form

$$u^* = -\mathbf{K}\mathbf{x}$$

where

$$\mathbf{K} = [k_{11} \quad k_{12} \quad k_{13} \quad k_{14}]$$

The actual control is given by

$$u = (\mathbf{SB})^{-1} u^*$$

For the pole-placement method, the equivalent-system poles are chosen to be {-1, -2, -3}. The coefficient matrix of the sliding surface is found to be

$$\mathbf{S} = [8.4465 \quad 3.0023 \quad 252.6342 \quad 5.4442]$$

The elements of the gain matrix are then obtained as

$$k_{1i} = \begin{cases} > \psi_{1i} & \sigma x_i > 0 \\ < \psi_{1i} & \sigma x_i < 0 \end{cases} \qquad i = 1,2,3,4$$

where

$$\Psi = \mathbf{SA} = [\psi_{11} \quad \psi_{12} \quad \psi_{13} \quad \psi_{14}] = [-247.1900 \quad -0.4162 \quad 3.5027 \quad 2.9695]$$

and

$$(\mathbf{SB})^{-1} = 4.1568$$

For the quadratic minimization method, the weighting matrix $\mathbf{Q}$ is chosen as diag(2000,1,1,1). This results in a sliding surface with a coefficient matrix

$$\mathbf{S} = [-16.4580 \quad 0.4905 \quad 13.2634 \quad 0.7506]$$

The elements of the gain matrix are derived as

$$k_{1i} = \begin{cases} > \psi_{1i} & \sigma x_i > 0 \\ < \psi_{1i} & \sigma x_i < 0 \end{cases} \qquad i = 1,2,3,4$$

where

$$\Psi = \mathbf{SA} = [\psi_{11} \quad \psi_{12} \quad \psi_{13} \quad \psi_{14}] = [-12.5128 \quad -0.4162 \quad -0.1671 \quad 0.4576]$$

The results of simulations using the above variable-structure controllers are shown in Fig. 6.1. It is observed that using the pole-placement method to design the switching surface results in smaller displacements at steady-state. However, the peak displacements for both methods are approximately equal. A comparison of the responses for passive and sliding mode control are shown in Table 6.1.

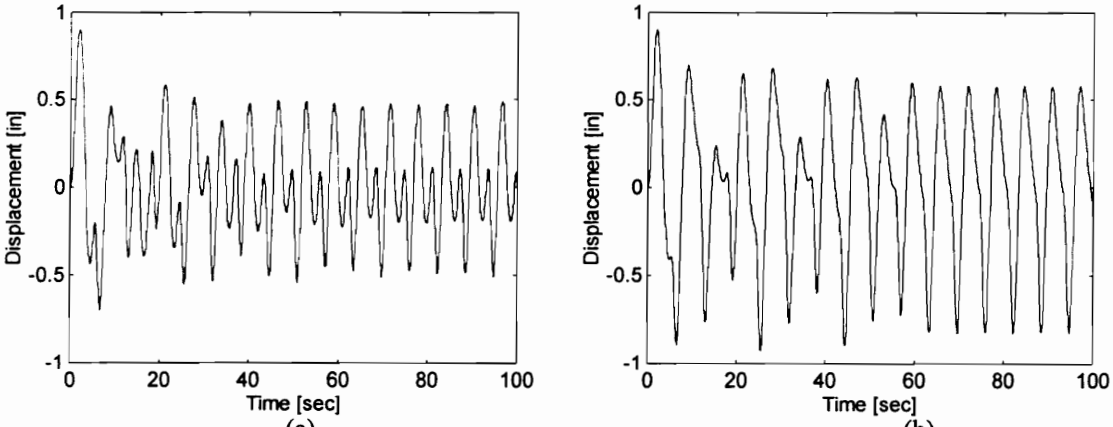

Fig. 6.1 Displacement for (a) SM (P-P) control, and (b) SM (Q-M) control

TABLE 6.1 Comparison of Response for Passive and SM Control

CONTROL TYPE	y_s(peak)	y_s(rms)	z(peak)	z(rms)
Passive	4.6275	1.8895	15.4839	9.3422
SM (P-P) Control	0.9052	0.3037	34.1406	11.9539
SM (Q-M) Control	0.9246	0.4291	33.3344	13.6624

where y_s is the structure's displacement with respect to the ground, in inches; and z is the relative displacement between the structure and the damper, in inches. Table 6.1 shows that sliding-mode control is able to reduce the maximum displacement. There is a 80% reduction in the peak displacement for both the pole-placement method and the quadratic minimization method. However, this reduction in displacement is accompanied by an increase in the actuator's peak stroke-length. The pole-placement method produces a 120% increase in the peak stroke-length, while the quadratic minimization method produces a 115% increase. The larger stroke-lengths for the pole-placement method results in smaller steady-state displacements for this method of switching surface design.

The control input for both design methods are shown in Fig. 6.2 and Fig. 6.3, where the control force is limited to 15 kips. Thus, there is a saturation of the control force. Although other actuators such as hydraulic or pneumatic actuators may not be able to produce the given control, the regenerative electric actuator can easily provide the given control waveform since the force is produced electromagnetically. The plot for the actuator power shows that there are periods of negative power. During these instances, the regenerative electric actuator is able to recover energy from the building or structure instead of simply dissipating it. This reduces the peak energy drawn from the source.

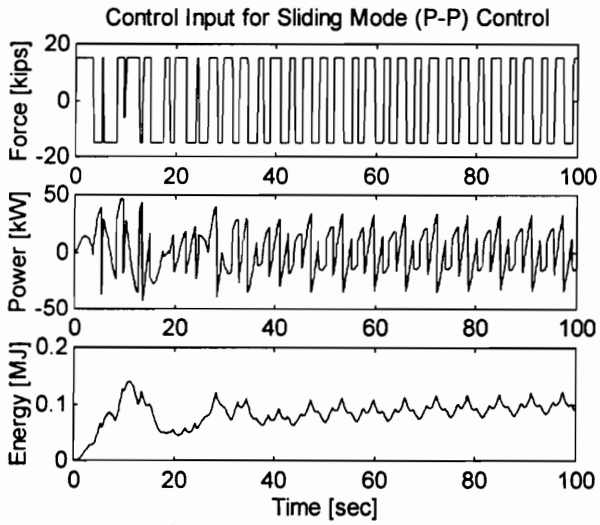

Fig. 6.2 Actuator force, power, and energy for SM (P-P) control

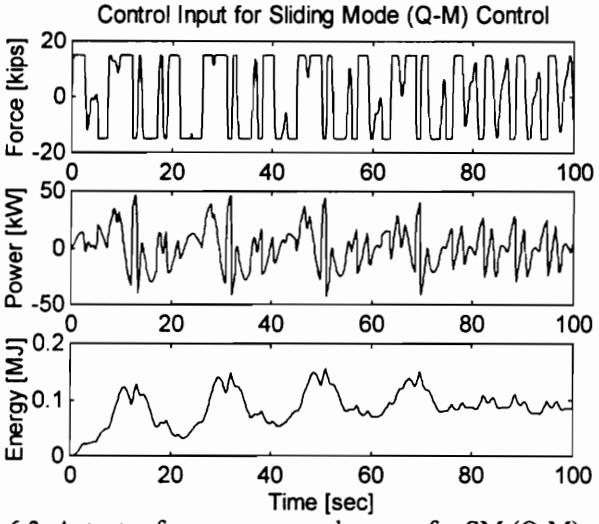

Fig. 6.3 Actuator force, power, and energy for SM (Q-M) control

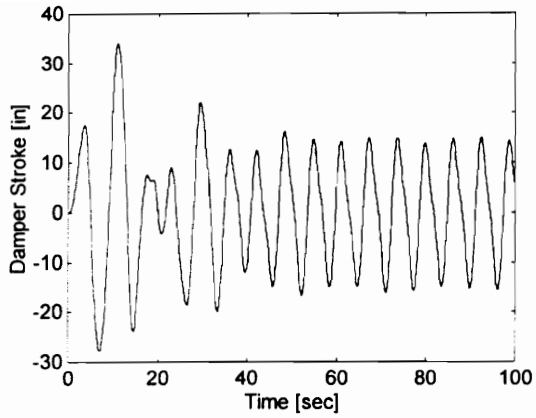

Fig. 6.4 Damper stroke for pole-placement method

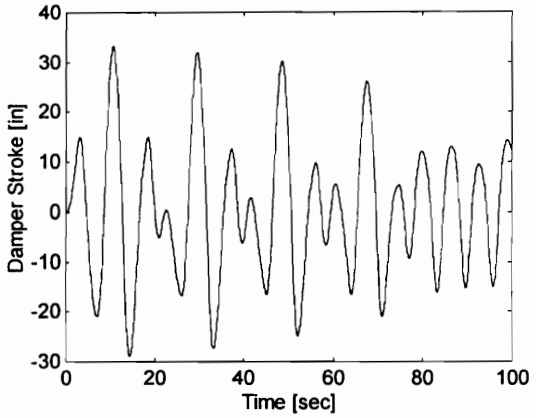

Fig. 6.5 Damper stroke for quadratic minimization method

The damper strokes are shown in Figs. 6.4 and 6.5. Whenever the stroke velocity is in the same direction as the control force, the actuator is operating in motoring mode. On the other hand, the actuator operates as a generator when the stroke velocity is opposite to the control force direction.

The difference between the simulation results for the linear and the nonlinear models is shown in Fig. 6.6. As can be seen, the difference is almost negligible. As long as the desired control input is immediately available at the onset of the disturbance, then a linear model of this system will provide accurate results. It is important that control be applied immediately at the onset of the disturbance in order that the displacement be not driven into the inelastic region of the structure's stiffness. Once the displacement is driven into the inelastic region, significant differences could occur between the linear and nonlinear responses.

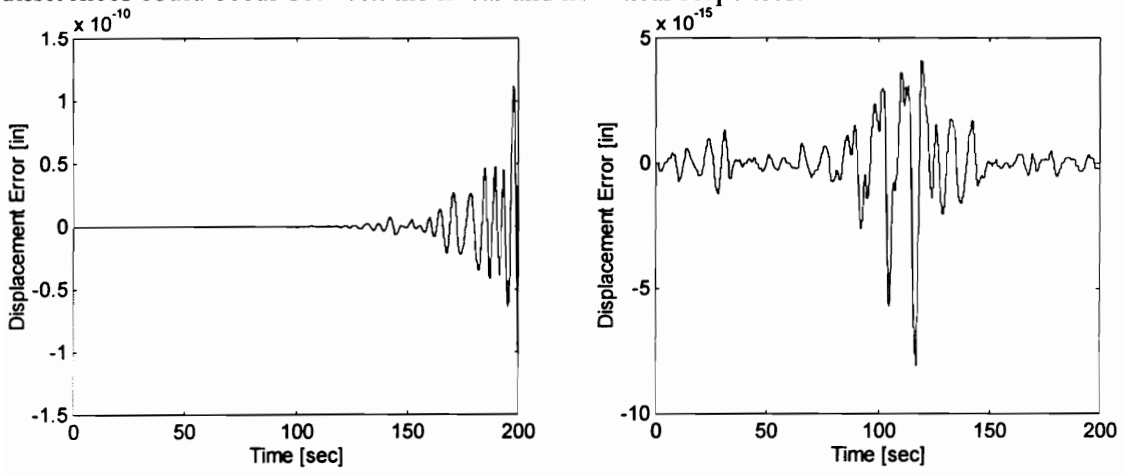

(a) (b)

Fig. 6.6 Difference between responses of the linear and nonlinear models for (a) SM (P-P) and (b) SM (Q-M) control

To show invariance to parameter variation, Fig. 6.7 shows the results of simulations in which a 25% step decrease in k_S occurs at t = 50 seconds. The switching surfaces for the two methods, which are designed using the original value of k_S, are kept the same. The results show that the controller performance is not affected by the change in the structure's stiffness.

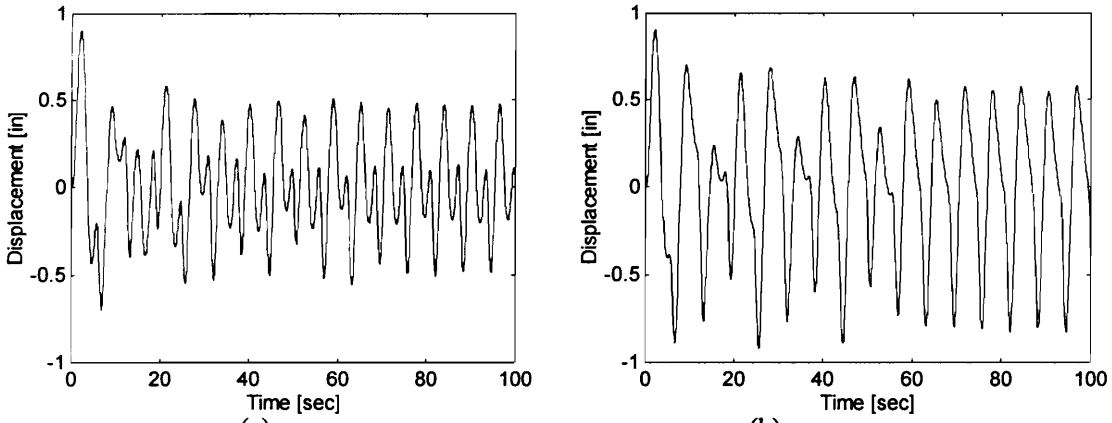

Fig. 6.7 Displacement for a 25% step decrease in k_S with (a) SM (P-P) and (b) SM (Q-M) control

The sensitivity of the maximum displacement to limits set on the control force is shown in Fig. 6.8. Without any limit, the control force required by the pole-placement method is 208 kips, while 64 kips is required by the quadratic minimization method. Hence, the quadratic minimization method requires a smaller control force at the cost of having larger steady-state displacements. The maximum displacement increases at approximately the same rate as the limit on the control force is decreased in both methods. As long as the limit on the control force is above 5 kips for the pole-placement method and 10 kips for the quadratic minimization method, then the peak displacement is always below 1 inch. This shows that control force saturation does not degrade the effectiveness of the sliding mode controllers. Fig. 6.9 shows a plot of the ratio of the maximum displacement to the maximum control force. The plot gives an indication of the effectiveness of increasing the maximum control force in reducing the maximum displacement. For both the pole-placement method and the quadratic minimization, increasing the maximum force above 8 kips does not bring about any significant reduction in the maximum displacement. Increasing the maximum control force above this value is not very effective. If it is desired that the maximum displacement be reduced below 1 inch, then the maximum control force has to increased above 8 kips.

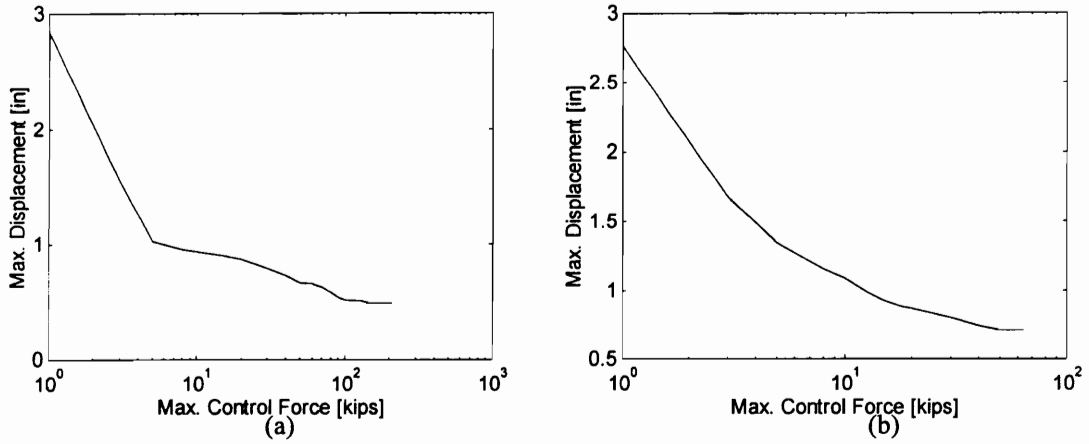

Fig. 6.8 Sensitivity of the maximum displacement to control force limits for (a) SM (P-P) and (b) SM (Q-M) control

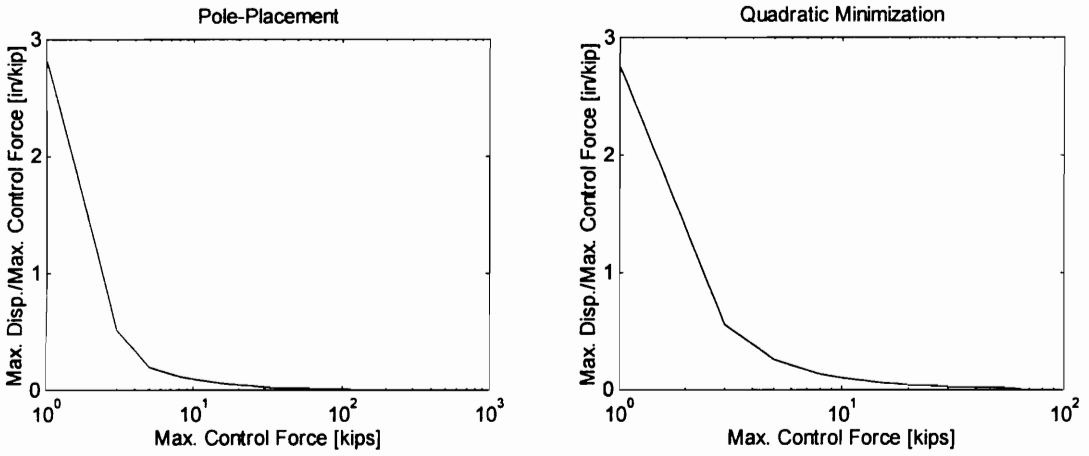

Fig. 6.9 Effectiveness in decreasing the maximum displacement by increasing the maximum control force

Fig. 6.10 shows the sensitivity of the maximum stroke length to limits set on the control force. The limit on the control force has a lesser effect on the stroke-length for the quadratic minimization method than for the pole-placement method. Fig. 6.11 shows a plot of the ratio of the maximum stroke length to the maximum control force. This plot gives a measure of the effectiveness of decreasing the maximum control force in decreasing the maximum damper stroke. It is seen that keeping the control force below 20 kips will give higher effectiveness.

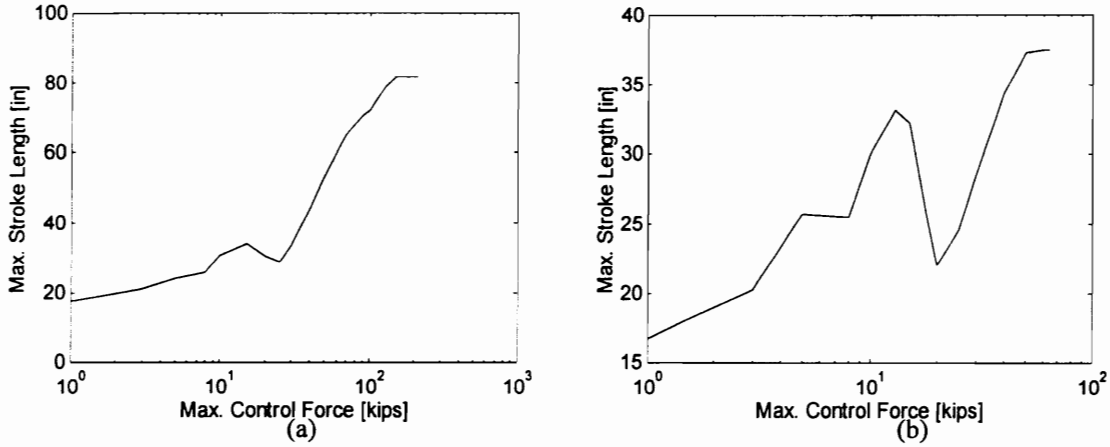

Fig. 6.10 Sensitivity of the maximum stroke length to control force limits for (a) SM (P-P) and (b) SM (Q-M) control

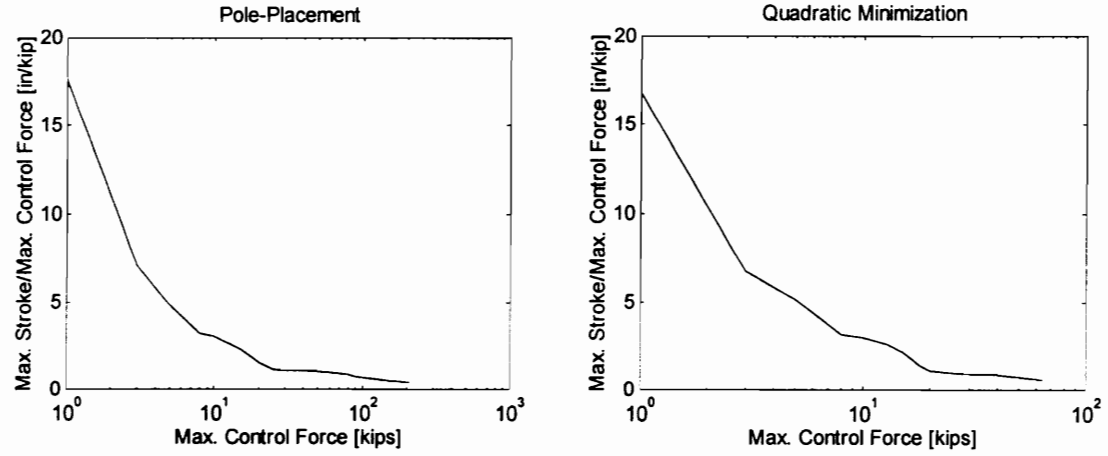

Fig. 6.11 Effectiveness in decreasing the maximum stroke length by increasing the maximum control force

Based on the preceding discussion, it is seen that keeping the maximum control force between 10 and 20 kips will yield the best effectiveness in maximum displacement and maximum stroke reduction. Lower displacements can be obtained by increasing the limit on the control force at the cost of longer stroke lengths.

Example 6.2 Earthquake-Excited SDOF System

The nonlinear single-degree-of-freedom system in Example 6.1 is subjected to the earthquake excitation shown in Fig. 3.14 with a peak acceleration of 17.53 in/sec^2. The excitation lasts until t = 24 sec. The variable-structure controllers designed in Example 6.1 are again used in this example. The simulation results are shown in Fig. 6.12. It is seen that the pole-

placement method for switching surface design produces a smaller peak in the displacement response. Table 6.2 gives a comparison of the response for passive and sliding mode control.

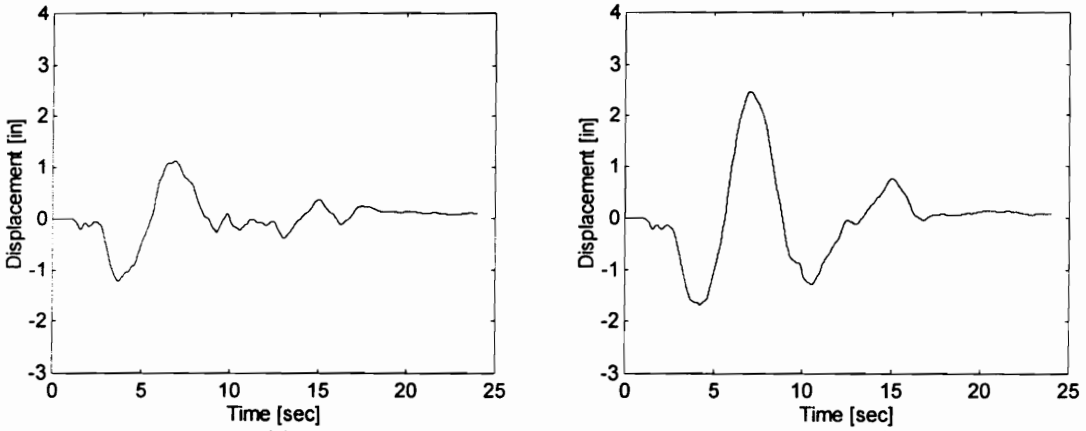

Fig. 6.12 Displacement for (a) SM (P-P) and (b) SM (Q-M) control

TABLE 6.2 Comparison of Response for Passive and SM Control

CONTROL TYPE	y_s(peak)	y_s(rms)	z(peak)	z(rms)
Passive	5.5956	1.8895	15.1441	9.3422
SM (P-P) Control	1.2285	0.4200	188.4835	66.2260
SM (Q-M) Control	2.4529	0.8494	100.6101	34.8416

where y_s is the structure's displacement with respect to the ground, in inches; and z is the relative displacement between the structure and the damper, in inches. The pole-placement method gives a 78% reduction in the maximum displacement compared to only a 56% reduction for the quadratic minimization method. However, this is accompanied by a larger control-force peak (301 kips) than the quadratic minimization method (149 kips). Consequently, there is a higher stroke-length for the pole-placement method due to the larger control force. The control input for sliding mode control with pole-placement and quadratic minimization is shown in figure 6.13 and 6.14. Periods of negative power allow the regenerative electric actuator to recover energy. The energy curves show that the net energy drawn from the source is reduced by regeneration.

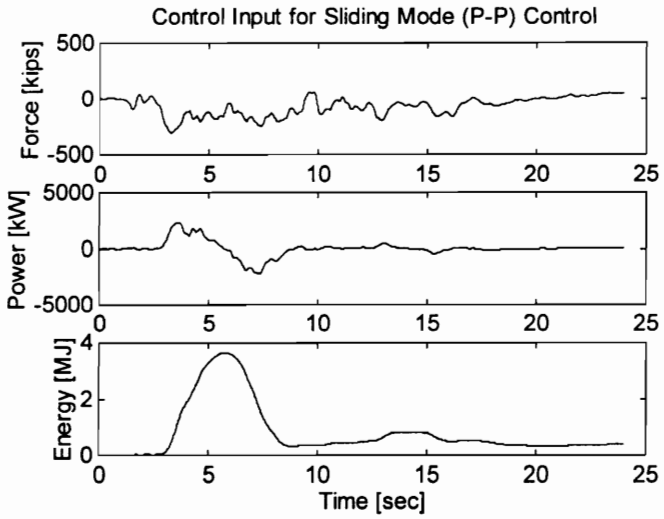

Fig. 6.13 Control input for SM (P-P) control

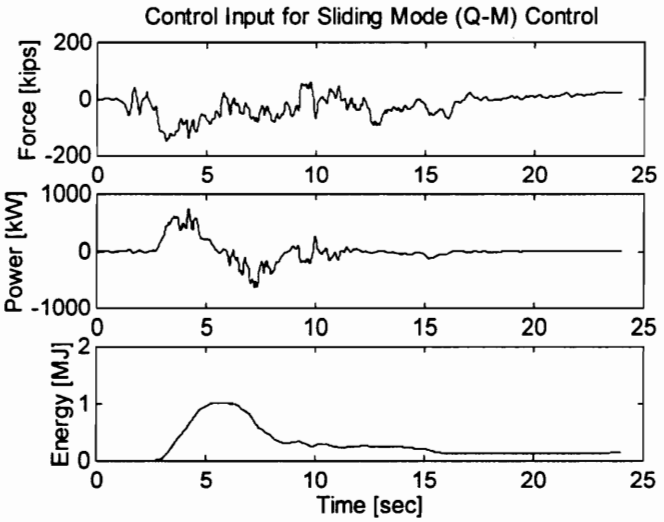

Fig. 6.14 Actuator force, power, and energy for SM (Q-M) control

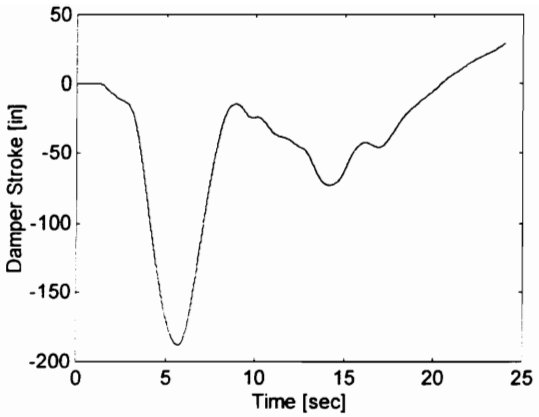

Fig. 6.15 Damper stroke for pole-placement method

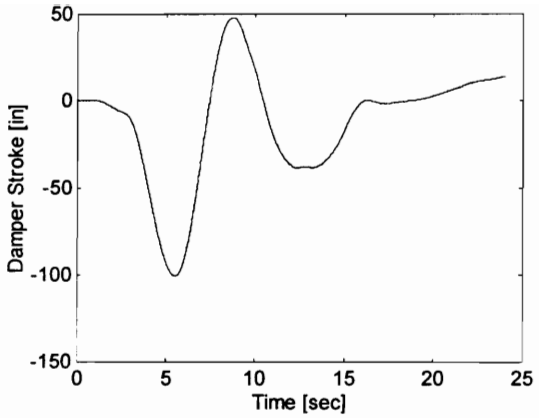

Fig. 6.16 Damper stroke for quadratic minimization method

Figs. 6.15 and 6.16 show the damper strokes for both methods. The peak stroke occurs during negative displacement. Motoring occurs when the stroke velocity is in the same direction as the control force. Regeneration is attained when the control force is directed opposite to the stroke velocity.

The difference between simulations using a linear and a nonlinear model is shown in Fig. 6.17. Again, the error introduced by assuming a linear model is almost negligible for this system. Since the structure undergoes larger displacements for the quadratic minimization method, it drives the structure's stiffness more into inelastic behavior. This results in a slightly larger difference between the linear and nonlinear simulations, as compared to what is obtained for the pole-placement method.

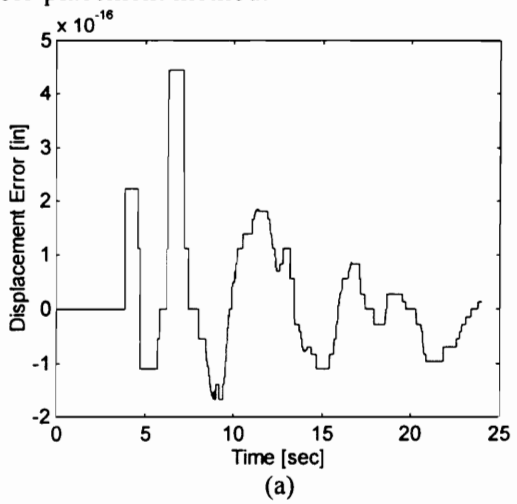

(a)

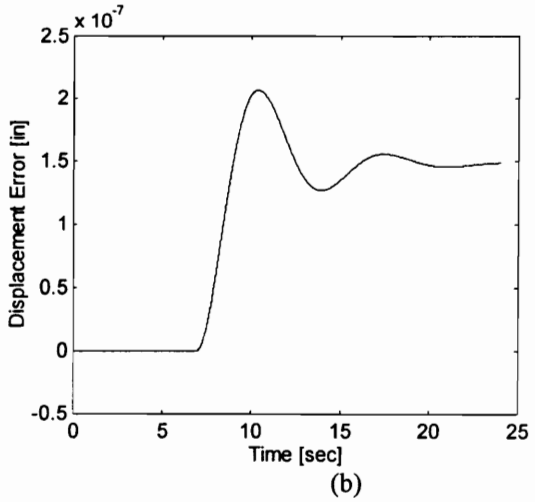

(b)

Fig. 6.17 Difference between responses of linear and nonlinear model for (a) SM (P-P) and (b) SM (Q-M) control

Putting a limit on the control force has the effect shown in Fig. 6.18. Without any limit, the control force for the pole-placement method is almost twice that for the quadratic minimization method. Both methods have approximately equal sensitivity to limits on the control force. As long as the limit on the control force is kept above 70 kips for the pole-placement method and 60 kips for the quadratic minimization method, then the displacement is always below 3 inches. This shows that control force saturation does not degrade the effectiveness of these sliding mode controllers.

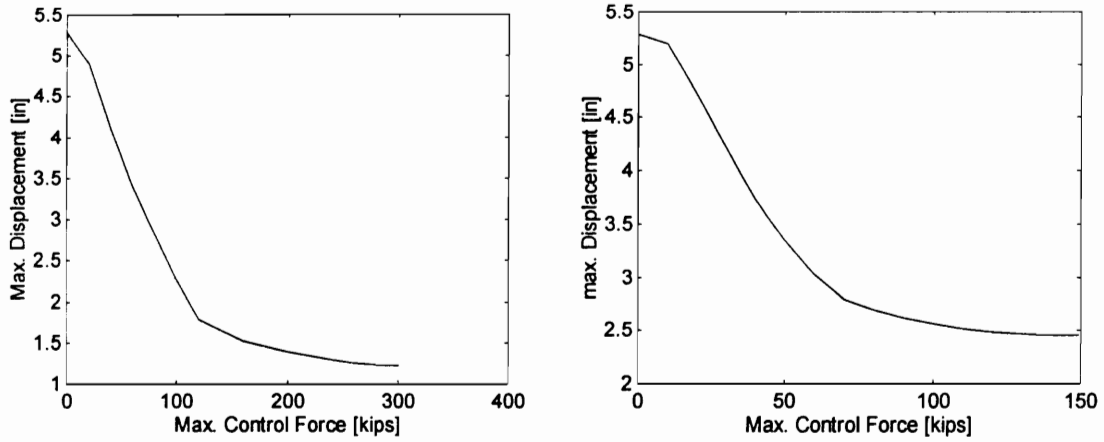

Fig. 6.18 Effect of control force limit for (a) SM (P-P) and (b) SM (Q-M) control

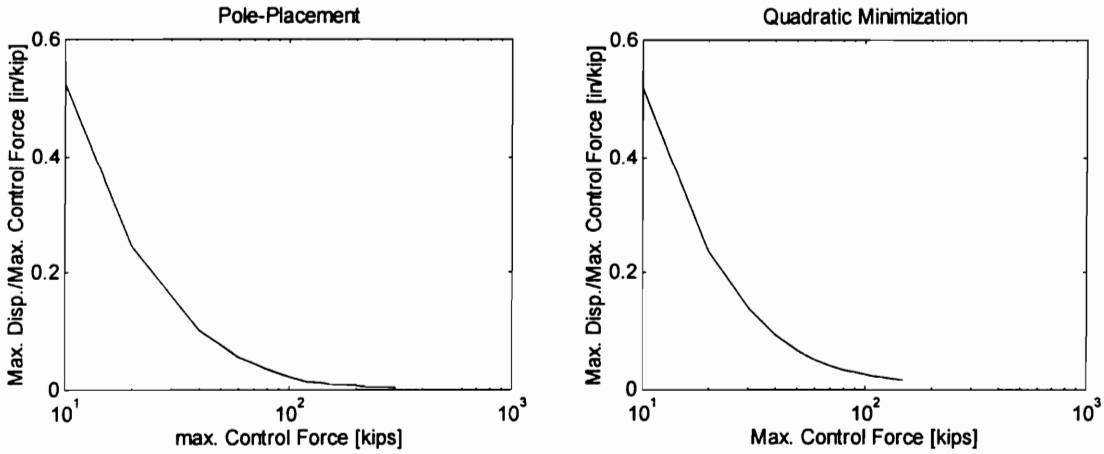

Fig. 6.19 Effectiveness of increasing the maximum control force in reducing the maximum displacement

Fig. 6.19 shows a plot of the ratio of the maximum displacement to maximum control force. Increasing the maximum control force above 100 kips does not produce any significant reduction in the displacement. Increasing the control force above 100 kips is not as effective in reducing the maximum displacement as for control force limits set at lower values. Therefore, a control

force limit of 100 kips is desirable. However, if maximum displacements lower than 3 inches is desired then the control force has to be increased above 100 kips.

Example 6.3 Linear, Fixed Base, Eight-Story Building with Mass Damper on the Top Floor

The fixed-base, eight-story building with a mass damper on the eight floor as described in Example 4.3, is equipped with a sliding mode controller to provide active control. The quadratic-minimization method is used to design the controller parameters. The weighting matrix **Q** used in the quadratic-minimization method is chosen to have the form

$$\mathbf{Q} = \begin{bmatrix} q_{11}\mathbf{I}_{9\times 9} & \mathbf{0} \\ \mathbf{0} & \mathbf{I}_{9\times 9} \end{bmatrix}$$

where q_{11} is a scalar factor. With q_{11} = 800, the interstory drifts are shown in Fig. 6.20. The peak interstory displacement occurs after several cycles of the disturbance have elapse.

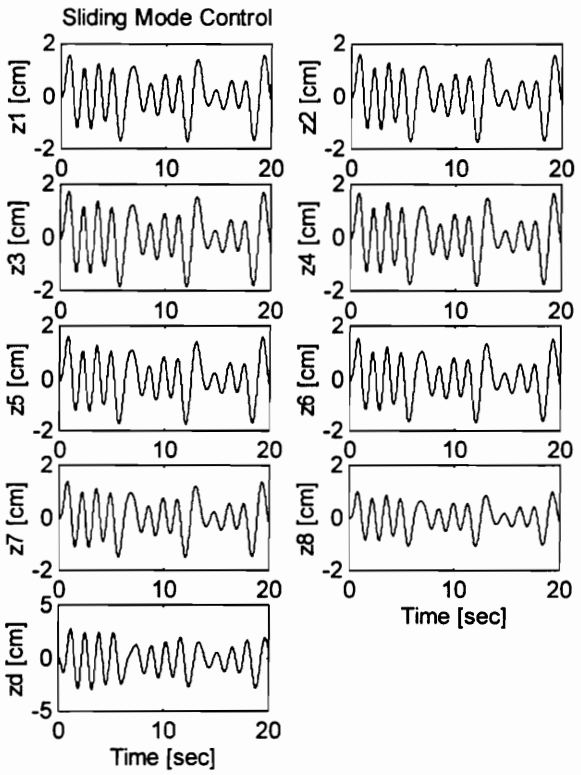

Fig. 6.20 Interstory drifts for sliding mode control (Q-M) with q_{11} = 800

The comparison shown in Table 6.3 is between the responses for passive and sliding mode control. The third floor experiences the largest interstory displacement. The maximum

displacement for this floor is reduced by 9% with sliding mode control. The displacement of the top floor with respect to the ground is reduced by 6 %. In contrast to previous cases considered, the damper stroke in this particular case is reduced by 88% instead of being increased.

TABLE 6.3 Comparison of Responses with Passive and Sliding Mode Control

FLOOR	Z_{pas}	Z_{sm}	R_{pas}	R_{sm}	Y_{pas}	Y_{sm}
1	1.9067	1.7172	0.7100	0.7849	1.9067	1.7172
2	1.9321	1.7439	0.7197	0.7973	3.8388	3.4611
3	2.0803	1.8865	0.7755	0.8630	5.9191	5.3476
4	1.9949	1.8245	0.7447	0.8353	7.9140	7.1721
5	1.8995	1.7618	0.7107	0.8076	9.8134	8.9339
6	1.7791	1.6902	0.6684	0.7766	11.5925	10.6241
7	1.5231	1.5164	0.5773	0.7003	13.1156	12.1405
8	0.9532	1.0810	0.3720	0.5072	14.0672	13.2206
Damper	24.4881	2.9734	9.9176	1.4094	21.3250	14.0991

where Z is the maximum interstory drift (cm), R is the RMS value of the interstory drift (cm), Y is the maximum displacement with respect to the ground (cm), *pas* is a subscript denoting passive control response, and *sm* is a subscript denoting SM control response.

The force, power and energy being supplied by the actuator is shown in Fig. 6.21. It is noted that the net energy transfer is from the structure to the actuator supply source. Most of the time, the actuator is regenerating. The amount of energy that can be recovered will be determined by the energy capacity of the storage device.

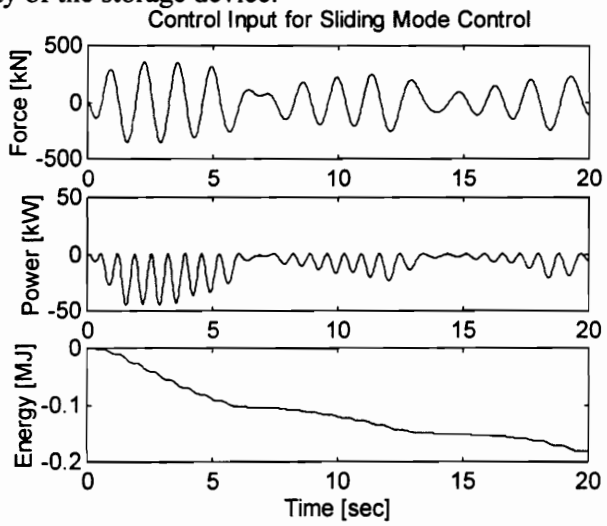

Fig. 6.21 Actuator force, power, and energy for q_{11} = 800

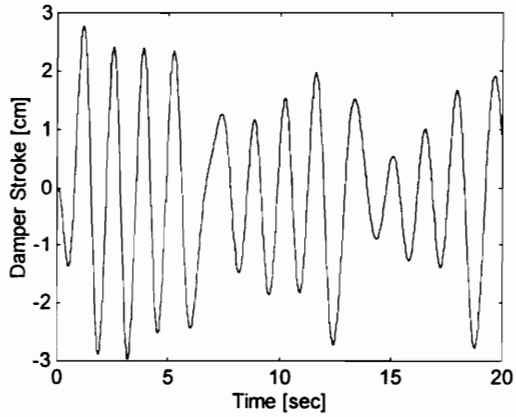

Fig. 6.22 Damper stroke for q_{11} = 800

The damper stroke is shown in Fig. 6.22. The relative polarities of the stroke velocity and the control force determine whether the actuator operates as a motor or as a generator. If they have the same polarity, the actuator is operating as a motor. Otherwise, it is operating as a generator.

The effect of varying q_{11} on the maximum interstory drift is shown in Fig. 6.23. Increasing q_{11} reduces the interstory displacement. Fig. 6.24 shows the ratio of the maximum interstory displacement to q_{11}. This plot provides a measure of the effectiveness of increasing q_{11} in reducing the maximum interstory drift. It is seen that above q_{11}= 10 there is no significant reduction in the maximum interstory drift. This can also be deduced from the almost-constant effectiveness shown in Fig. 6.24 after q_{11}= 10.

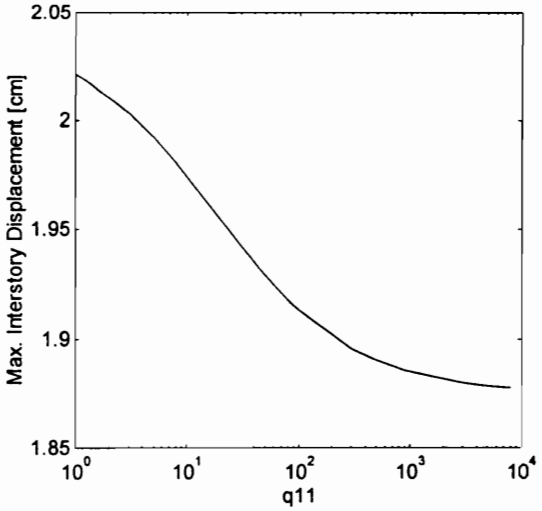

Fig. 6.23 Sensitivity of the maximum interstory displacement to variations in q_{11}

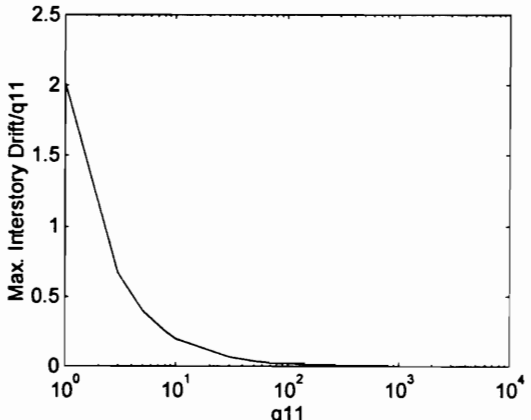

Fig. 6.24 Effectiveness of increasing q_{11} in decreasing the maximum interstory displacement

Fig. 6.25 shows the sensitivity of the maximum damper stroke to variations in q_{11}. After q_{11} = 800, the damper stroke tends to increase slightly. This value is a critical value. Increasing q_{11} above this critical value can lead to instability. Fig. 6.26 shows the ratio of the maximum stroke to q_{11}. It provides a measure of the effectiveness of increasing q_{11} in reducing the maximum stroke length. Above q_{11} = 10, the effectiveness is almost constant. This means that no significant reduction in the maximum stroke length can be obtained above this value. Based on stroke length, the best choice for q_{11} is between 10 and 800.

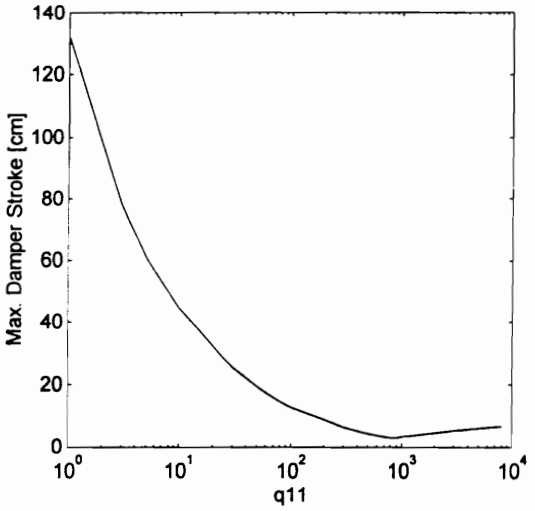

Fig. 6.25 Sensitivity of the maximum damper stroke to variations in q_{11}

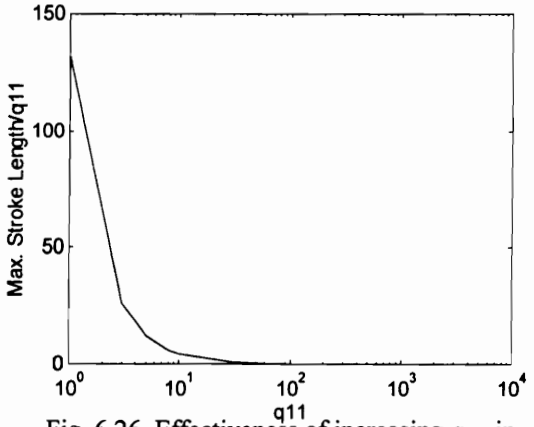

Fig. 6.26 Effectiveness of increasing q_{11} in decreasing the maximum damper stroke

Fig. 6.27 shows the sensitivity of the maximum control force to variations in q_{11}. The maximum control force tends to increase slightly above q_{11} = 800. Increasing q_{11} above 8000 causes the control to be extraordinarily large. This means that q_{11} = 800 is a critical value for q_{11}, above which the system tends to be unstable. Fig. 6.28 gives the ratio of the maximum control force to q_{11}. This plot gives a measure of the effectiveness of increasing q_{11} in decreasing the maximum control force. It is observed that above q_{11} = 10, the increase in q_{11} is not as effective in reducing the control force as for values below q_{11} = 10. Based on the maximum control force, the best range of values for q_{11} is between 10 and 800.

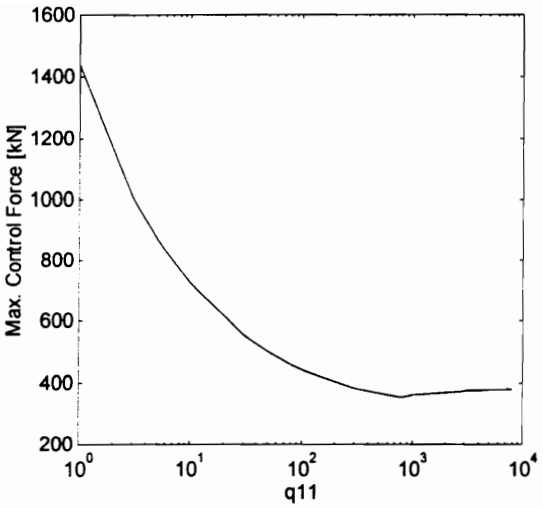

Fig. 6.27 Sensitivity of the maximum control force to variations in q_{11}

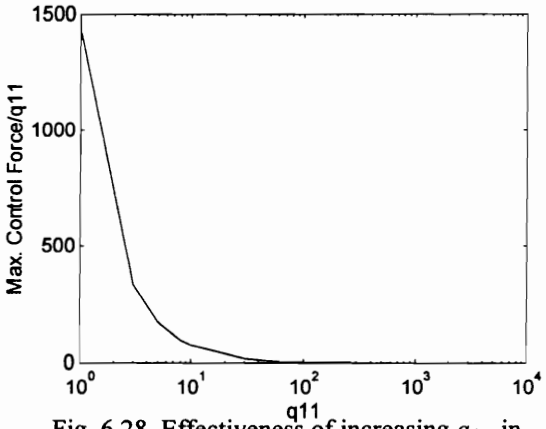

Fig. 6.28 Effectiveness of increasing q_{11} in decreasing the maximum control force

Example 6.4 Linear, Base-Isolated, Eight-Story Building with Mass Damper on the Base Floor

In Example 4.4, a base-isolated, eight-story building with a mass damper installed on the base floor was considered. A sliding mode controller is designed to provide active control to the structure. The sliding surface is designed using the quadratic-minimization method, with the weighting matrix **Q** chosen to have the form

$$\mathbf{Q} = \text{diag}(1, q_{22}, 1, 1, \ldots, 1)$$

With $q_{22} = 10$, the interstory drifts are shown in Fig. 6.29. It is seen that it takes some time for the displacements to decay to zero, even after the disturbance goes to zero at about 25 seconds. Using a larger q_{22} will cause a faster rate of decay at the cost of larger control forces and longer damper strokes.

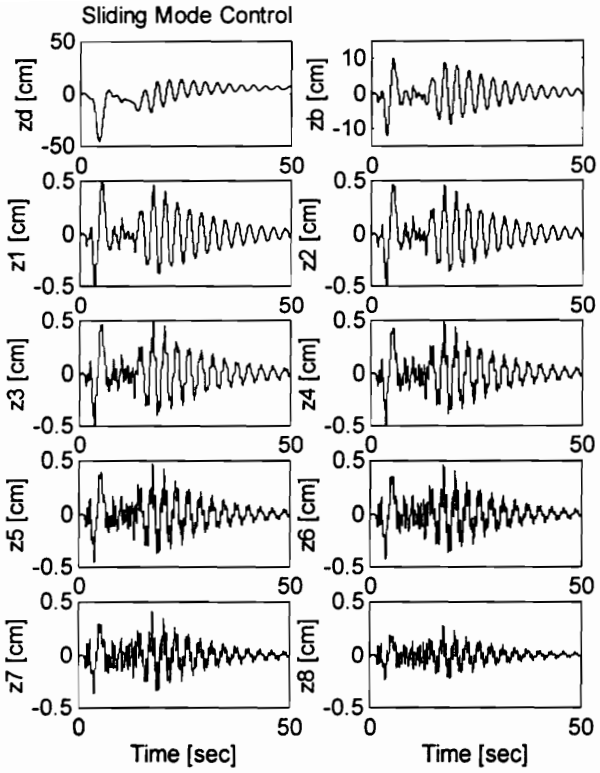

Fig. 6.29 Interstory drifts for sliding mode control with $q_{22} = 10$

A comparison of the responses for passive and sliding mode control is given in Table 6.4. The first story undergoes the largest interstory drift. This displacement is reduced by 4% with sliding mode control, while the base displacement is reduced by 4%. On the other hand, the damper stroke is increased by 34%.

TABLE 6.4 Comparison of Responses with Passive and SM Control

FLOOR	Z_{pas}	Z_{sm}	R_{pas}	R_{sm}	Y_{pas}	Y_{sm}
Damper	31.4095	45.5523	10.8387	10.0140	35.4893	47.59
Base	12.5719	12.1154	3.4460	3.5261	12.5719	12.12
1	0.5401	0.5183	0.1492	0.1642	13.1090	12.63
2	0.5120	0.4964	0.1399	0.1537	13.5905	13.11
3	0.5326	0.5171	0.1426	0.1562	14.0548	13.61
4	0.5094	0.4912	0.1326	0.1444	14.4606	14.08
5	0.4984	0.4812	0.1250	0.1352	14.8198	14.53

6	0.4846	0.4686	0.1181	0.1268	15.1363	14.95
7	0.4349	0.4218	0.1037	0.1106	15.3955	15.32
8	0.2891	0.2815	0.0681	0.0722	15.5620	15.56

where Z is the maximum interstory drift (cm), R is the RMS value of the interstory drift (cm), Y is the maximum displacement with respect to the ground (cm), *pas* is a subscript denoting passive control response, and *sm* is a subscript denoting sliding-mode control response.

The force, power, energy being provided by the actuator is shown in Fig. 6.30. The peak force occurs during the earlier part of the disturbance when the peak displacements also occur. After 5 seconds, the actuator is essentially regenerating. Therefore, there is a net gain in source energy after 50 seconds.

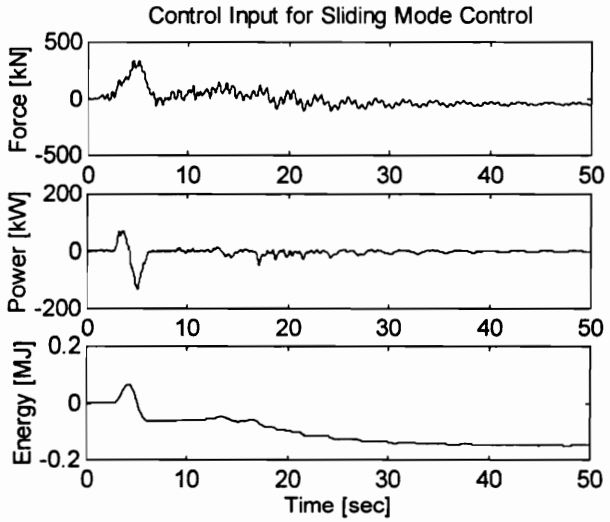

Fig. 6.30 Actuator force, power, and energy for $q_{22} = 10$

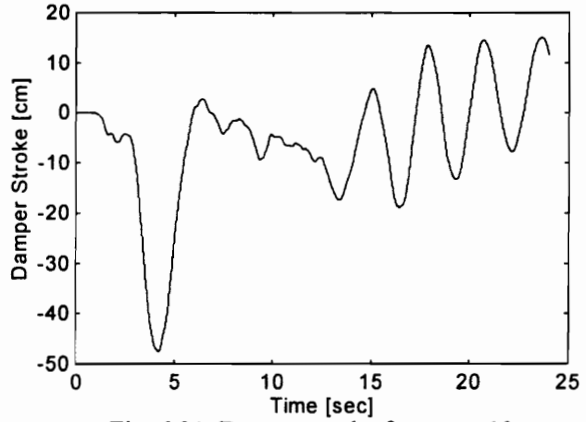

Fig. 6.31 Damper stroke for $q_{22} = 10$

The damper stroke is shown in Fig. 6.31. The relative polarities of the stroke velocity and control force determine whether the actuator is operating as a motor or as a generator. If the velocity and force are in the same direction, then the actuator is operating as motor. If the velocity and force are in opposite directions, then the actuator is operating as generator.

Varying q_{22} affects the maximum interstory drift as shown in Fig. 6.32. Increasing q_{22} has the effect of decreasing the interstory displacement. Choosing a larger q_{22} also produces a faster rate of decay in the interstory drifts. Fig. 6.33 shows a plot of the ratio of the maximum interstory drift to q_{22}. This plot gives a measure of the effectiveness of increasing q_{22} in reducing the maximum interstory displacement. From this plot, it is observed that the effectiveness is almost unchanged after q_{22} = 10. Therefore, this would be a desirable value based on the effectiveness in reducing the interstory drift.

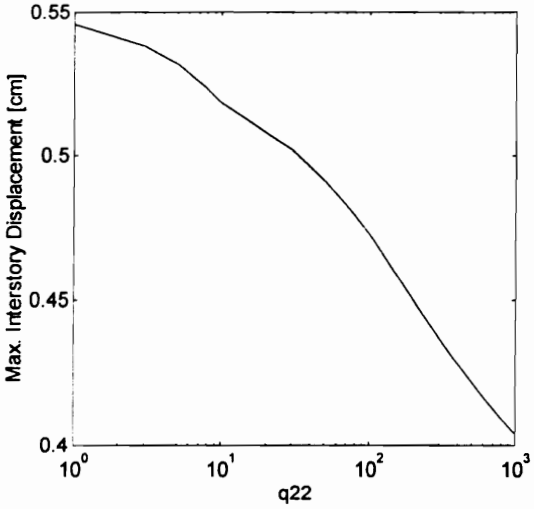

Fig. 6.32 Sensitivity of the maximum interstory drift to variations in q_{22}

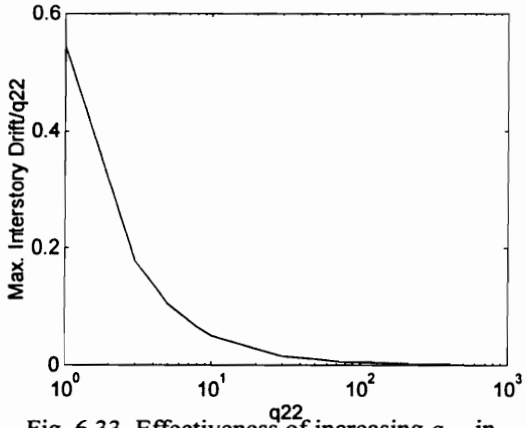

Fig. 6.33 Effectiveness of increasing q_{22} in reducing the maximum interstory drift

Fig. 6.34 shows the sensitivity of the maximum base displacement to variations in q_{22}. The increase in q_{22} has the opposite effect on the base displacement as compared to its effect on the interstory drift. Increasing q_{22}. causes an increase in the maximum base displacement. Fig. 6.35 shows a plot of the ratio of the maximum base displacement to q_{22}. It provides a measure of the effectiveness of decreasing q_{22} in reducing the base displacement. Lower values of q_{22} produce larger reductions in the maximum base displacement for every decrease in q_{22}. This effectiveness starts to increase below q_{22} = 10. Therefore, lower values of q_{22} is desired for lower base displacements.

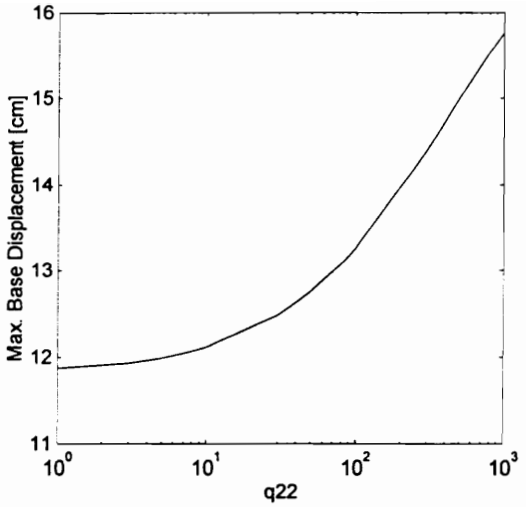

Fig. 6.34 Sensitivity of the maximum base displacement to variations in q_{22}

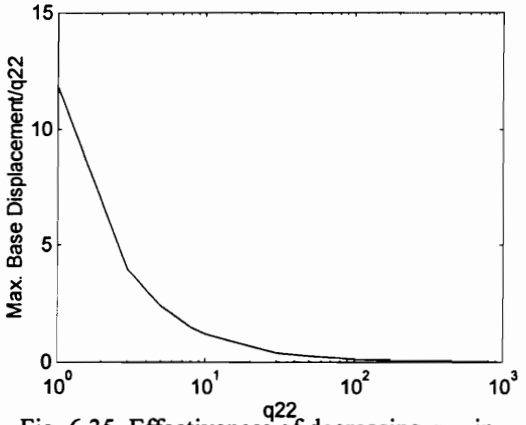

Fig. 6.35 Effectiveness of decreasing q_{22} in reducing the maximum base displacement

Fig. 6.36 shows the sensitivity of the maximum damper stroke to variations in q_{22}. The effectiveness of decreasing q_{22} in reducing the maximum damper stroke is shown in Fig.6.37. It is observed that below q_{22} = 10 there is a larger reduction in the maximum damper stroke per unit decrease in q_{22}. Therefore, it is desirable to chose a value below q_{22} = 10 for lower stroke lengths.

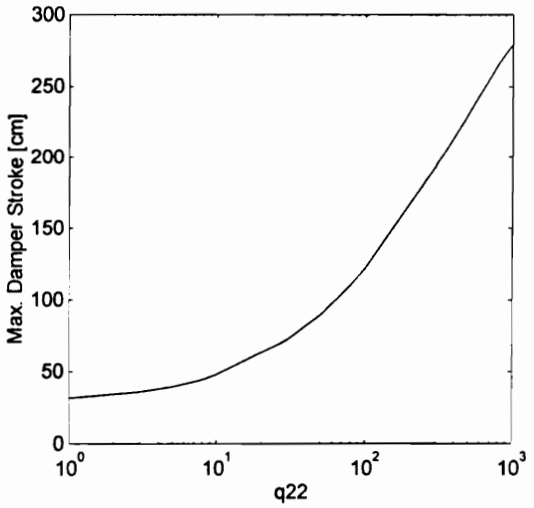

Fig. 6.36 Sensitivity of the maximum damper stroke to variations in q_{22}

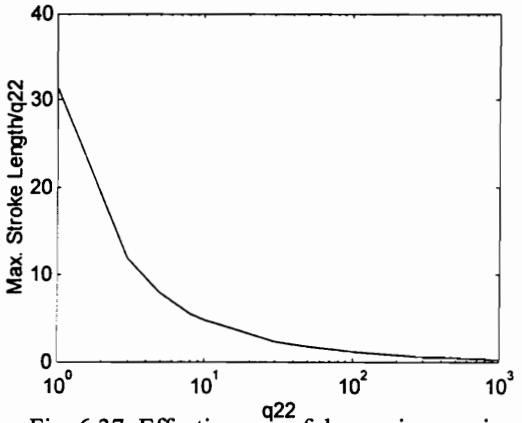

Fig. 6.37 Effectiveness of decreasing q_{22} in reducing the damper stroke length

The sensitivity of the maximum control force to variations in q_{22} is shown in Fig. 6.38. Increasing q_{22} also increases the maximum control force. Fig. 6.39 shows a measure of the

effectiveness of decreasing q_{22} in reducing the maximum control force. Below q_{22}. = 10, an decrease in q_{22}. produces the most reduction in the maximum control force. Thus, it is desirable to have lower q_{22}.

From the preceding discussion, it is desirable to have lower q_{22} for lower base displacement, stroke length, and control force. However, this also increases the interstory displacement. If interstory drift reduction is more important, then a larger q_{22} must be chosen at the cost of larger control forces, base displacements, and damper strokes.

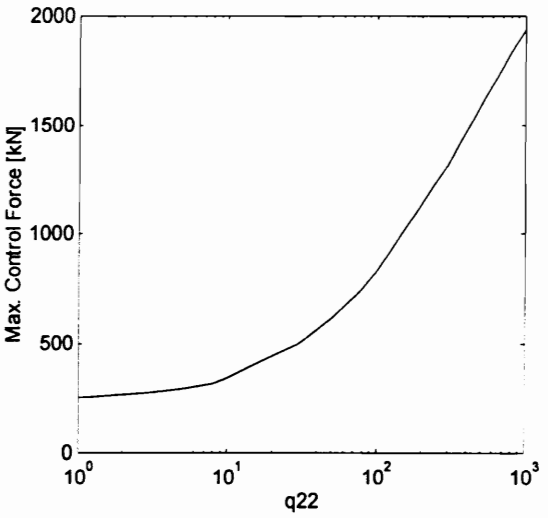

Fig. 6.38 Sensitivity of the maximum control force to variations in q_{22}

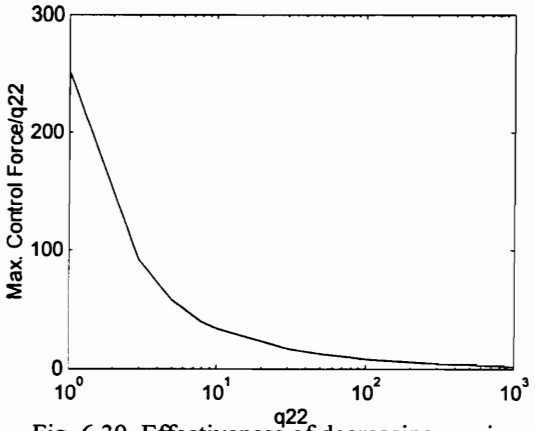

Fig. 6.39 Effectiveness of decreasing q_{22} in decreasing the maximum control force

The base displacement can be reduced by choosing a different weighting matrix. For example, choosing the weighting matrix as

$$\mathbf{Q} = \begin{bmatrix} 100\mathbf{I} & \\ & \mathbf{I} \end{bmatrix}$$

reduces the base displacement to 11.7525 inches, as compared to 11.8617 inches for q_{22} = 1 in the previous choice for the form of **Q**. However, the interstory drift increases from 0.5458 inch to 0.5502 inch and the peak control force increases from 32 kips to 208 kips.

6.6 SUMMARY

This chapter investigates the applicability of sliding mode control (also known as variable structure control) for the active control of structures, with special emphasis on the mitigation of wind- and earthquake-induced motion in tall buildings using regenerative electric

actuators. The rationale for using sliding mode control is the fact that regenerative electric actuators use a form of on-off control based on pulse width modulation (PWM). Sliding mode inherently provides a synthesis of this on-off nature of PWM control and guarantees stability for the on-off control law. Due to the limited energy available for active control, saturation of the control force often occurs. Sliding mode control naturally encompasses the nonlinear, on-off nature of control force saturation. At the same time, sliding mode control guarantees stability for the on-off control law. This study is the first of its kind to propose the application of sliding mode control to civil structures. Sliding mode control is proposed as a candidate controller for the regenerative electric actuator because of its invariance to parameter variations and disturbances. The sliding mode controller being proposed has a form obtained through the diagonalization method, and has a structure which is composed of linear feedback with switched gains. To assess the sliding mode controller's performance during disturbances, both linear and nonlinear models of the structure are considered in this study . It is shown that the controller is able to overcome sensitivity to structural parameter variations, particularly structural stiffness. Systematic procedures for the design of the sliding surface, using both pole-placement and quadratic-minimization methods, are presented together with simulation results obtained by using linear and nonlinear models of the structure. These controllers are also shown to be effective even in the presence of control force saturation. With sliding mode control, the regenerative electric actuator is able to recover energy and store it for later use. This reduces the net energy drawn from the supply by the actuator. In some cases, there is even a net gain in the energy of the electrical supply.

CHAPTER 7

Neural Network Control

A new direct-control scheme for neural network control of civil structures using regenerative electric actuators is proposed. This allows on-line control of the structure without the need for either an accurate model of the system or a specific learning stage. Unlike the controllers that have previously been considered, the neural network controller is able to address changes in system parameters and changes in the operating point and external disturbances. A modified backpropagation algorithm is used to train the neural network. Since the error at the output of the neural network controller will be unknown in the direct-control scheme, the error at the system output is instead backpropagated through the system by considering the system as an additional layer of the neural network. Simulations are conducted for wind and earthquake excitation using a two-layer network composed of neurons with tangent-sigmoid activation functions. It is shown that the controller can tolerate large variations in the input scaling factor, output gain factor, and maximum control force. It is also equally effective for both linear and nonlinear models of the structure.

7.1 INTRODUCTION

One of the important problems in control systems is the inverse problem of determining the input which will produce a desired output. The design of a controller based on a linear approximation of the plant characteristics has certain inescapable disadvantages: (1) The model becomes computationally prohibitive for complex and highly dynamic plants, (2) The control quality is very sensitive to the quality of the linear approximation, and (3) The model has difficulty in adapting to time-varying plant parameters. Therefore, an adaptive controller that learns to control the system interactively and autonomously while in operation is required. Because of their ability to learn actual relevant control and plant data, neural networks have become a promising approach to controlling complicated, multidimensional, and dynamic systems [1].

The use of a neural network controller trained off-line is proposed in [2] and [3] for application in the active control of civil structures. This chapter proposes a new neural-network control scheme for use with a regenerative electric actuator providing structural control. This neural network controller can be trained on-line and is able to adapt itself to variations in the

system parameters. The method and results presented in this chapter are based on work done in [4] and [5].

7.2 LEARNING ARCHITECTURE

Learning control is a control method which determines the inputs required to control or improve the transient behavior of a dynamic system, given that prior knowledge of the controlled system may not be available. The problem is to develop a learning control algorithm which will always produce a smaller error on successive trials. One of the possible solutions to the learning control problem is to use neural networks to determine the control inputs [6][7].

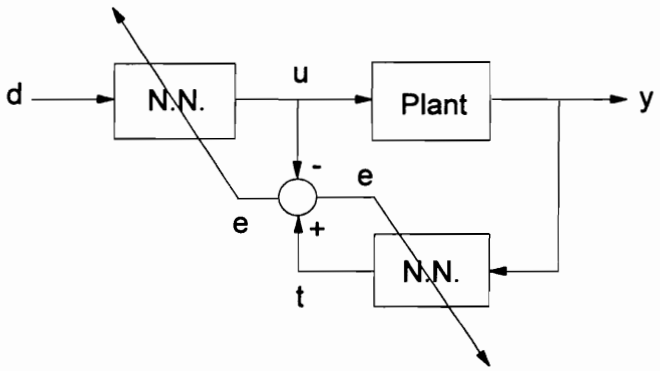

Fig. 7.1 Indirect learning architecture

Three learning control architectures for neural networks have been proposed [8][9]. In the indirect learning architecture shown in Fig. 7.1, the desired plant output d is propagated through a neural network to produce the plant input u. The actual plant output y is then used as an input to a copy of the controlling network. The difference between the outputs of the controlling network and its copy is the indirect or training error which is used to adapt both networks to drive this error to zero. A disadvantage of this architecture is that the networks tend to settle to a solution that maps all desired responses to a single plant input. This input is in turn mapped by the plant to an output that gives zero training error but obviously a non-zero total error. To overcome this problem, the generalized learning architecture shown in Fig. 7.2 trains the neural network by using different u's as inputs to the plant and teaches the neural controller to map the corresponding output y's back to the u's. Disadvantages of this learning strategy are: (1) The controller is inoperative during the learning phase, (2) It cannot delimit its operating range to the relevant one, and (3) The plant is assumed to be a static physical process.

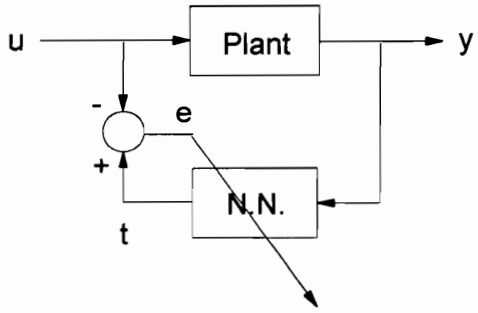

Fig. 7.2 Generalized learning architecture

The above disadvantages can be avoided by using the specialized learning architecture shown in Fig. 7.3. Training involves using the desired responses d's as input to the network. The network then learns to find the plant inputs u's that drive the system outputs y's to the desired d's by using the error between the desired and actual responses of the plant. Thus, the network (1) specifically learns in the region of interest, and (2) may be trained on-line, fine-tuning itself while performing its function. As a result, the controller learns continuously and is able to control plants with time-varying characteristics. Therefore, a specialized learning architecture is used in this study.

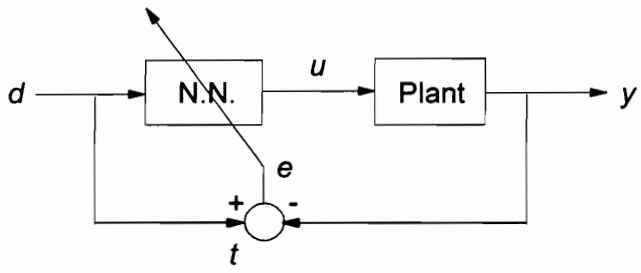

Fig. 7.3 Specialized learning architecture

7.3 TRAINING ALGORITHM

The back-propagation algorithm cannot be directly applied to the specialized learning architecture because of the location on the plant. It was proposed [8] that the plant can be thought of as an additional, although unmodifiable, layer [1]. In the specialized controller architecture shown in Fig. 7.4, the error signal at the system output can be propagated back through the plant using the partial derivatives of the plant at its operating point. The error back-propagating rule can then be used to adjust the weights in all layers except the virtual output layer (the plant).

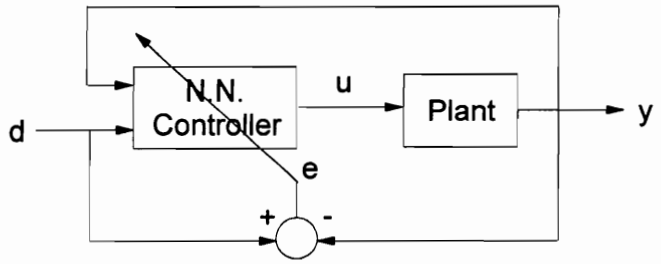

Fig. 7.4 Controller architecture

During the forward pass of the back-propagation algorithm, an activation of the input is propagated through the network and the plant to yield an output. The output layer (the plant) can be thought of as consisting of units that use a linearized transfer function, while the layers of the neural network controller consists of units having a chosen activation function. Therefore, the connection weight between controller output u_k and the plant output y_q can be expressed as

$$w_{qk} = \frac{\partial y_q}{\partial u_k} \tag{7.1}$$

During the backward pass of the algorithm, the differences between the desired and the actual outputs are propagated back through the plant and the network. By starting at the controller's output layer, each layer of the neural network controller is successively adjusted by using these back-propagated differences. The generalized delta-rule [10] can be used to evaluate the error e_q and the weighted sum n_q of the inputs to the plant's output units. Hence,

$$e_q = (d_q - y_q)\frac{\partial a_q}{\partial n_q} \tag{7.2}$$

$$n_q = \sum_k \frac{\partial y_q}{\partial u_k} u_k \tag{7.3}$$

where a_q is the output of neuron unit q. However, the transfer function of each plant neuron unit is simply equal to unity. Therefore, the error at a plant output can be written as

$$e_q = d_q - y_q \tag{7.4}$$

These errors are, in turn, used to calculate the errors in the output units of the controller. Therefore, the error in unit k is given by

$$e_k = f'(n_k)\sum_s e_s w_{ks} \tag{7.5}$$

where s denotes all units in the succeeding layer connected to unit k. f' is the derivative of unit k's activation function. Substituting (7.1) and (7.4) in (7.5), the error in the output units of the controller becomes

$$e_k = f'(n_k)\left\{\sum_q (d_q - y_q)\frac{\partial y_q}{\partial u_k}\right\} \tag{7.6}$$

Using the generalized delta-rule, the weight adjustments in the controller output layer are obtained as

$$\Delta w_{ij} = \eta e_j a_i \tag{7.7}$$

where η is the learning rate. This update equation is also used in all preceding network layers.

In general, the partial derivatives $\partial y_q/\partial u_k$ depend on the plant's operating point, and therefore, these are essentially unknown. An approximation can be obtained by using changes between iterations. Thus,

$$\left.\frac{\partial y_q}{\partial u_k}\right|_i \approx \left.\frac{\Delta y_q}{\Delta u_k}\right|_i = \frac{{y_q}^i - {y_q}^{i-1}}{{u_k}^i - {u_k}^{i-1}} \tag{7.8}$$

The on-line numerical estimation of the Jacobian may cause fast variations in the instantaneous estimates [11] which directly influence the updating of the weights of the neural network controller. Averaging can minimize these variations but will result in slow or ineffective learning.

The errors in the controller's output layer can be approximated as,

$$e_k \approx f'(n_k)\left\{\sum_q (d_q - y_q)\text{sign}\left(\frac{\partial y_q}{\partial u_k}\right)\right\} \tag{7.9}$$

by using $\text{sign}(\partial y_q/\partial u_k)$ instead of $\partial y_q/\partial u_k$. The neural network will create a distributed representation of the numerical values of these partial derivatives by incorporating these values into the weights of the neural network controller [1]. One can use the approximation

$$\text{sign}\left(\frac{\partial y_q}{\partial u_k}\right) \approx \text{sign}\left(\frac{\Delta y_q}{\Delta u_k}\right) \tag{7.10}$$

at each iteration. Therefore, the sign is evaluated in every update cycle.

Since the system layer does not get updated, convergence could become slow in some cases. To solve this problem, a gain factor, which is proportional to the Jacobian's inverse, is introduced between the neural network and the system as shown in Fig. 7.5. This gain can either be kept constant or be updated on-line [12].

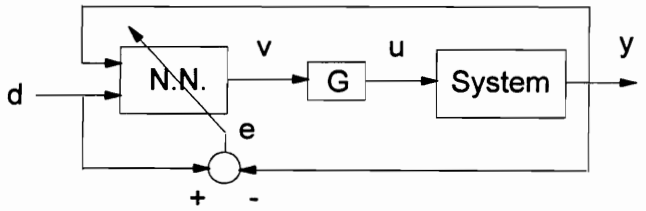

Fig. 7.5 Modified control scheme

A typical structure of the neural network controller that will be used in subsequent examples is shown in Fig. 7.6. In the figure, d_s is the desired structural displacement (zero), y_s is the actual displacement, and $\dot{y}_s$ is the structure's velocity. K_i is an input scaling factor and $K_O = G$ is the output gain factor.

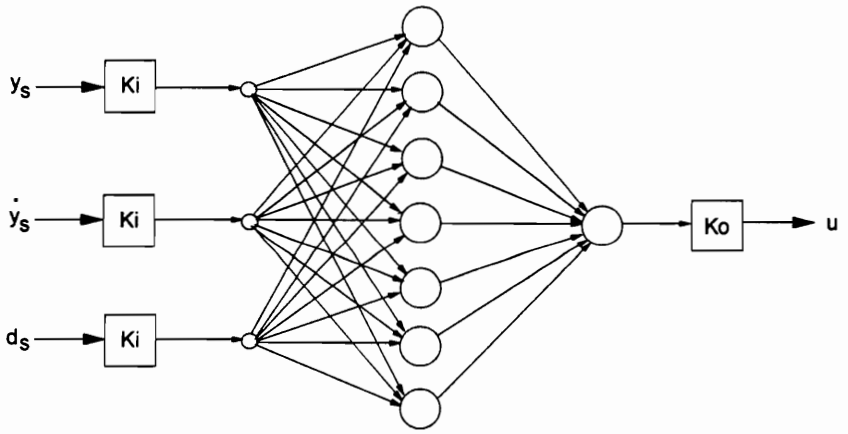

Fig. 7.6 Neural network structure

Example 7.1 SDOF Structure with Mass Damper under Wind Excitation

Using a nonlinear model, the single-degree-of-freedom system described in Example 4.1 is subjected to a wind force with parameters p = 9.75 kips and ω = 1.0 rad/sec. A two-input, two-layer neural network is chosen as the controller. The two inputs are the building displacement and the desired displacement (zero). The fully-interconnected network has seven neurons in the

first layer and a single neuron in the second (controller output) layer. The activation function used for all neuron units is a hyperbolic-tangent sigmoid given by

$$f(n_k) = \tanh\left(\frac{n_k}{2}\right) = \frac{1-\exp(-n_k)}{1+\exp(-n_k)}$$

All weights are initially set to 1.0.

Several network structures were considered by varying the number of layers and the number of neurons per layer. It is found that a two-layer network is sufficient for the given test system. In general, a learning rate of 1.0 results in faster learning times. Using K_i = 0.05 and K_o = 15, the resulting displacement, stroke length, and control input are shown in figures 7.7, 7.8, and 7.9, respectively. The input scaling factor is found by trial and error, while the output gain factor is set equal to the peak force required by the linear-quadratic controller used in previous simulations for the same system. A time step of 0.10 second is used in the simulation.

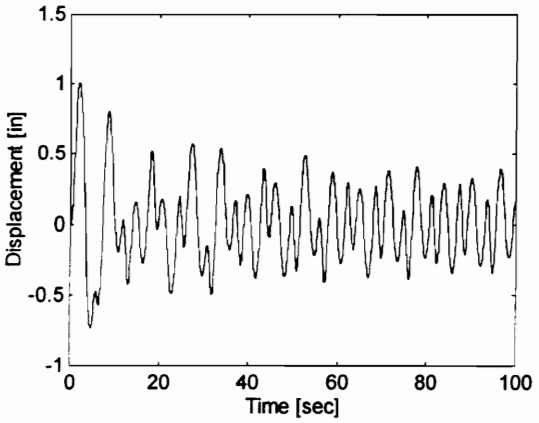

Fig. 7.7 Displacement with neural network control

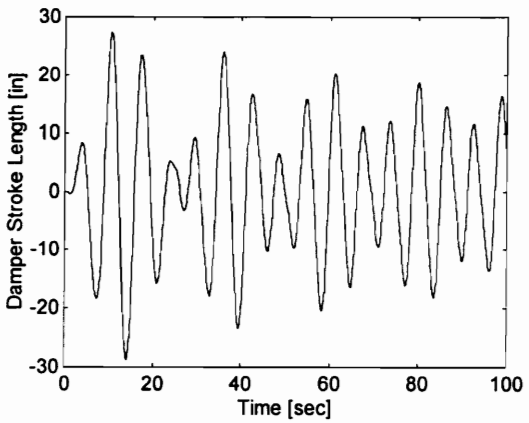

Fig. 7.8 Damper stroke length with NN control

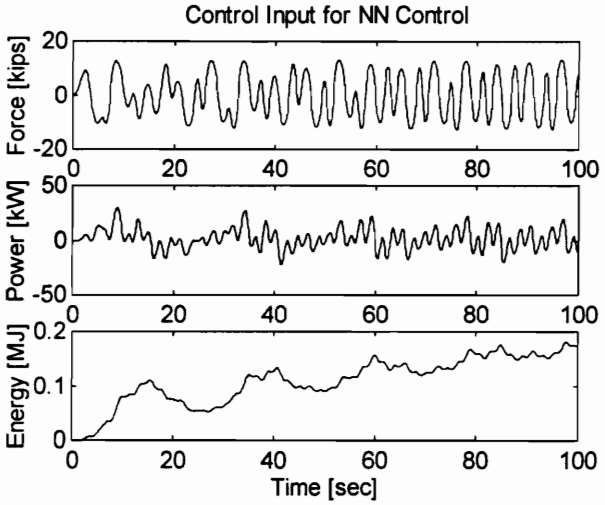

Fig. 7.9 Actuator force, power, and energy for NN control

The plot for the actuator power shows that there are periods of negative power. This means that the regenerative electric actuator is able to recover energy from the excitation. This reduces the peak energy drawn from the actuator supply. The peak energy is reduced from 0.4485 MJ to 0.1815 MJ by regeneration. Without regeneration, the negative power is simply dissipated as heat.

The damper stroke is shown in Fig. 7.8. If the stroke velocity is in the same direction as the control force, then the regenerative actuator is operating as a motor. If the stroke velocity is opposite to control force direction, then the actuator is regenerating.

A comparison of the results with the passive case is shown in Table 7.1.

TABLE 7.1 Comparison of Response

PARAMETER	Passive	Neural Network Control
Max. displacement [in]	4.6275	1.0078
Max. stroke [in]	15.4839	28.8394
Max. control force [kips]	0	13.1444
Max. power [kW]	0	29.5657

Neural network control provides a 78% reduction in the peak displacement. This reduction is achieved at the cost of an 86% increase in the stroke length.

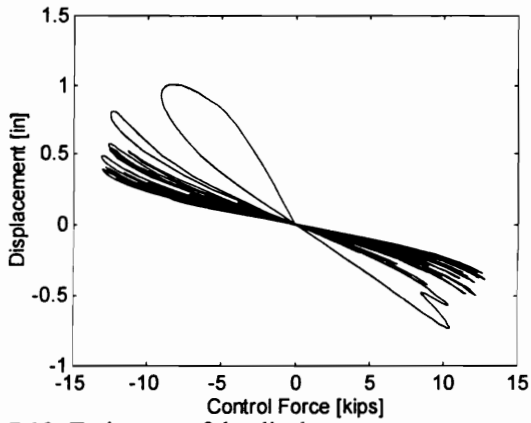

Fig. 7.10 Trajectory of the displacement versus control force

A plot of the displacement versus control force is shown in Fig. 7.10. The plot shows that $\partial y_q / \partial u_k$ is mostly negative. There are a few points with positive $\partial y_q / \partial u_k$ when the network

is initially untrained. As the network becomes trained, $\partial y_q / \partial u_k$ remains negative most of the time.

The sensitivity of the peak displacement and control force to variations in the output gain factor is shown in figures 7.11 and 7.12, respectively. The input scaling factor is fixed at 0.05. Increasing K_O above 10 does not produce any significant reduction in the peak displacement. On the other hand, increasing K_O simply causes a proportional increase in the peak control force. Therefore, choosing an output gain near 10 would give the best trade-off for minimizing the displacement-peak with the least control force. Increasing the gain above 10 also produces a slight increase in the peak of the displacement waveform at steady-state.

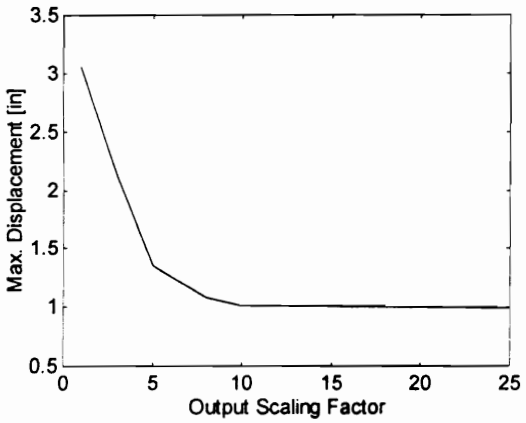

Fig. 7.11 Sensitivity of the maximum displacement to variation in the output gain

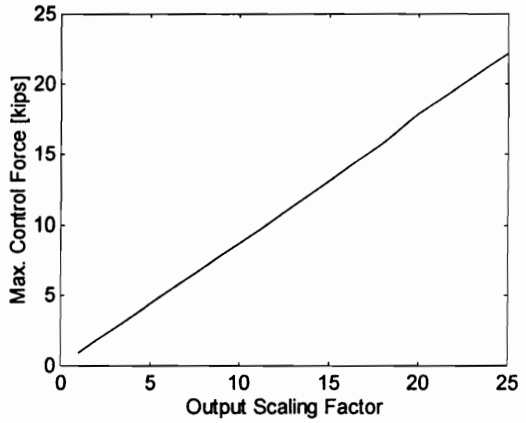

Fig. 7.12 Sensitivity of the maximum control force to variation in the output gain

The effect of varying the input scaling factor on the maximum displacement and control force are shown in figures 7.13 and 7.14, respectively. The output gain is fixed at 15. Increasing the scaling factor above 0.04 does not produce any significant reduction in the peak displacement. However, the peak control force is increased by larger values of this scaling factor. The effective gain being applied on the input to generate the control is proportionately increased by increasing the input scaling factor K_i. Therefore, choosing the input scaling factor to be about 0.04 gives optimum results. The peaks of the displacement at steady-state are unaffected by an increase in the input scaling factor.

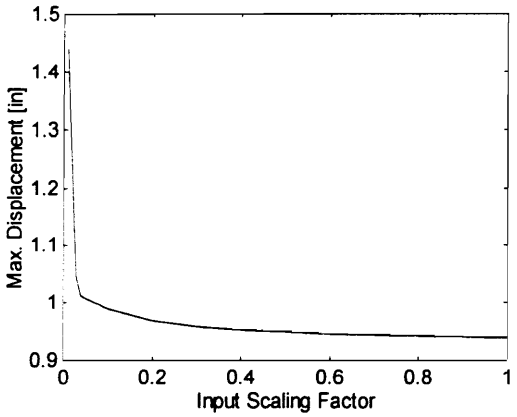

Fig. 7.13 Sensitivity of the maximum displacement to variation in the input scale factor

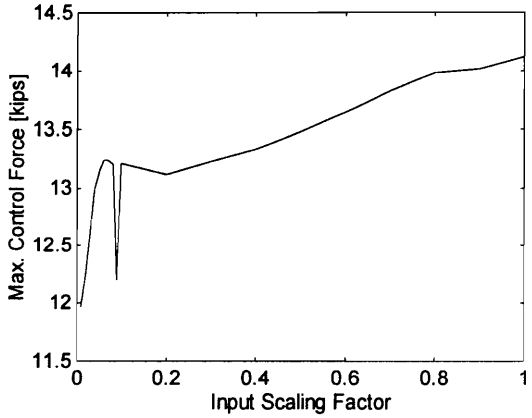

Fig. 7.14 Sensitivity of the maximum control force to variation in the input scale factor

The sensitivity of the maximum displacement and control force to variations in the learning rate is shown in figures 7.15 and 7.16, respectively. No significant reduction in the peak displacement is obtained if the learning rate is increased above 0.30. Increasing the learning rate from 0.8 to 2.0 does not cause any significant increase in the control force. Higher learning rates result in an increase in the displacement and control force.

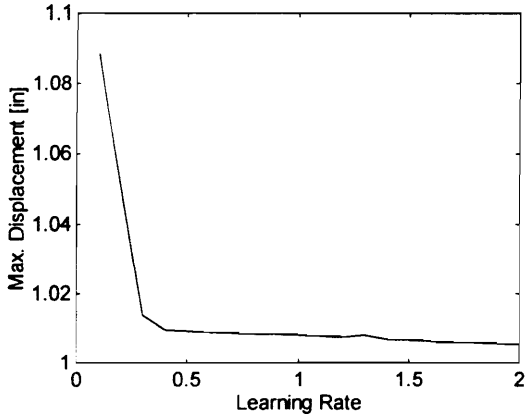

Fig. 7.15 Sensitivity of the maximum displacement to variation in the learning rate

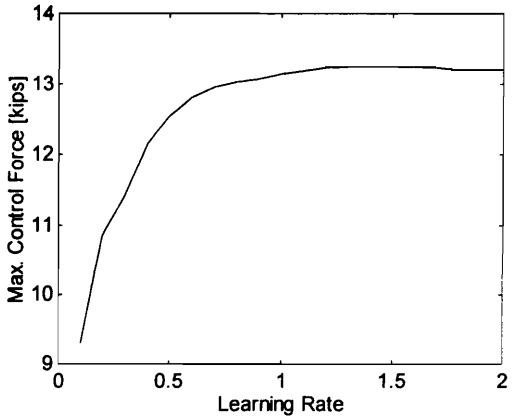

Fig. 7.16 Sensitivity of the maximum control force to variation in the learning rate

The difference between the results when using a linear and a nonlinear model is shown in Fig. 7.17. The error introduced by assuming a linear model is negligible. Again, it is assumed that control is applied at the instant that the disturbance occurs. This keeps the displacement within the elastic limits of the structure's stiffness at all times. As long as the structure's stiffness remain elastic, the structure's response closely approximates a linear system.

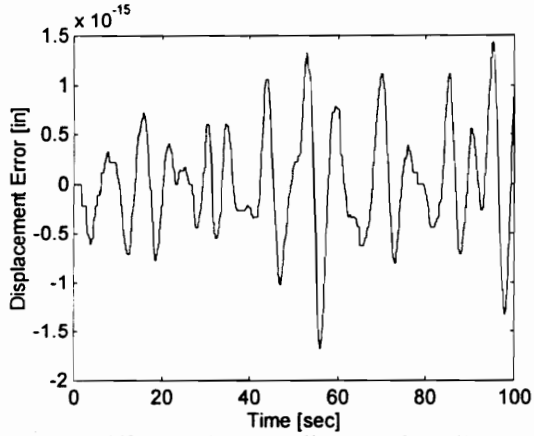

Fig. 7.17 Difference between linear and nonlinear results

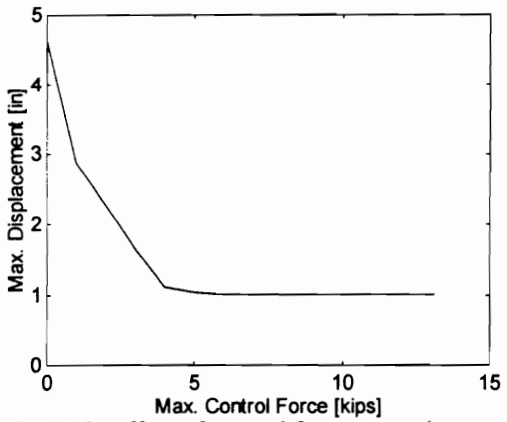

Fig. 7.18 Effect of control force saturation on the maximum displacement

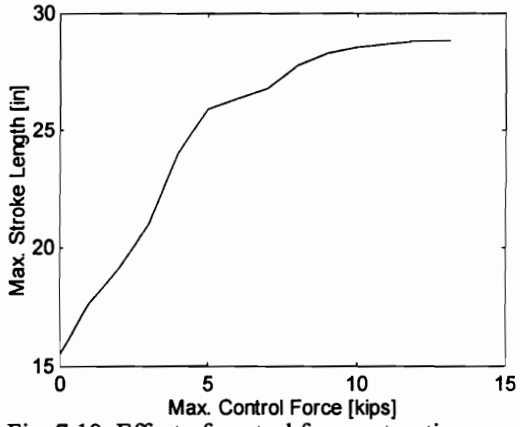

Fig. 7.19 Effect of control force saturation on the maximum stroke length

Fig. 7.18 shows that increasing the limit on the control force above 5 kips does not decrease the maximum displacement significantly. The maximum displacement is basically not affected as the maximum control force is increased from 5 to 13 kips. At the same time, the maximum stroke length shown in Fig. 7.19 does not increase significantly for a maximum control force of above 5 kips. Without any limit, the peak control force requirement is 13.14 kips. All simulations started with an untrained network, with all weights set equal to 1. Choosing a limit of 5 kips will be desirable for this system and excitation.

Example 7.2 Nonlinear SDOF System under Earthquake Excitation

The nonlinear single-degree-of freedom system used in Example 7.1 is subjected to the ground acceleration shown in Fig. 3.4 with the peak acceleration of 17.53 in/sec^2. The input scaling factor is chosen as K_i = 0.05 and the output gain is chosen as K_o = 150. As before, the choice for K_o is based on the peak control force required by a linear quadratic controller which is

designed for the same system and excitation. The same neural network used in Example 7.1 is used in this study, with the structure's velocity as an additional input as depicted in Fig. 7.6. The time increment is 0.01 second and the activation function is chosen to be a hyperbolic-tangent sigmoidal function. The learning rate is set at 0.03. The results of the simulations are shown in Fig. 7.20 and Fig. 7.21. Compared to previous controllers, there is a slower decay of the displacement with neural network control. Other controllers usually have almost-zero displacement after 25 seconds. While previous controllers have a positive peak-displacement, neural network control produces a negative peak-displacement. This can be attributed to the training which occurs during the earlier portions of the disturbance. Using a faster learning rate will cause an increase in the peak displacement and control force.

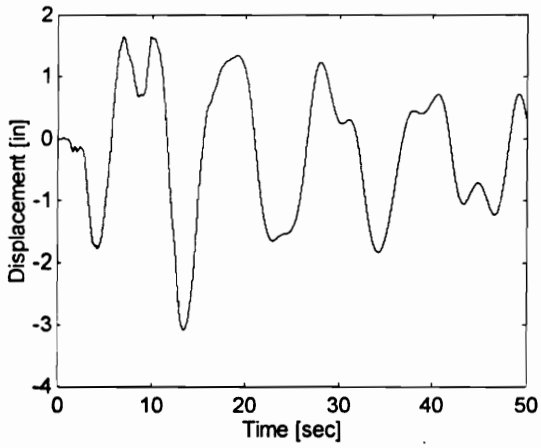

Fig. 7.20 Displacement with NN control

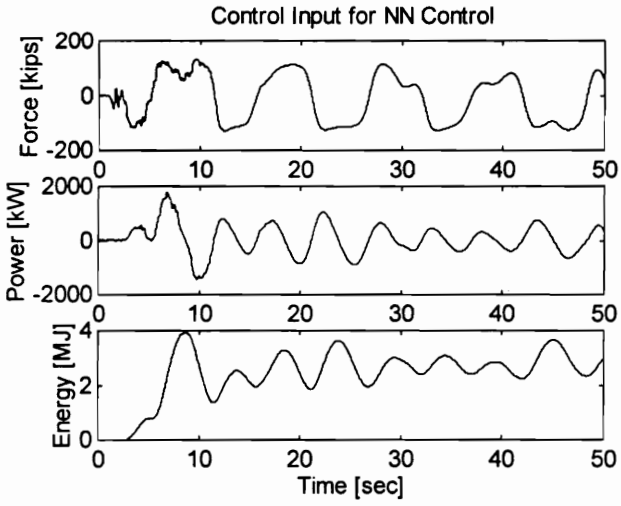

Fig. 7.21 Actuator input for NN control

The plots for the actuator power and energy shows that it is able to regenerate during periods of negative power, thereby reducing the peak energy requirement. The peak power requirement for this type of control is relatively bigger than for previous types of control. Table 7.2 shows a comparison of the results with neural network control to those results obtained without active control. Neural network control is able to reduce the peak displacement by 45%, with a 1155% increase in the stroke length. The power requirement is relatively larger than for previous controllers. However, the peak energy requirement is reduced by 52% from 8.2382 MJ to 3.9187 MJ through regeneration.

TABLE 7.2 Comparison of Response

PARAMETER	Passive	NN Control
Max. displacement [in]	5.5956	3.0893
Max. stroke [in]	15.1441	190.0026
Max. control force [kips]	0	132.9180
Max. power [kW]	0	1783.7
Max. energy [MJ]	0	3.9187

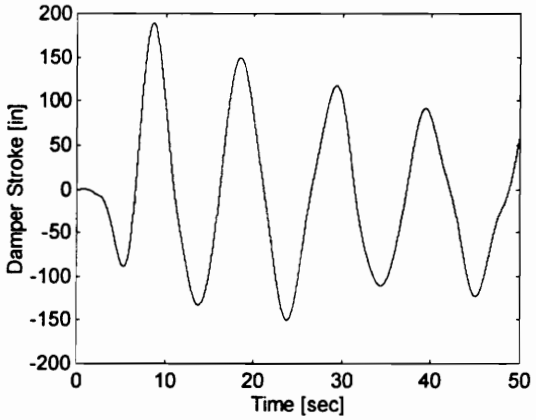

Fig. 7.22 Damper stroke for neural network control

The damper stroke is shown in Fig. 7.22. If the stroke velocity is in the same direction as the control force, then the actuator is operating as a motor. If the stroke velocity and control force are opposite in directions, then the actuator is regenerating.

7.4 SUMMARY

A new direct-control scheme for neural network control of civil structures using regenerative electric actuators is proposed for the first time. This allows on-line control of the structure without the need for either an accurate model of the system or a specific learning stage. Since the controller learns on-line, it is able to address uncertainties and variations in the system parameters and in the operating point. All previous controllers are fixed after the design is completed. Since the design is based on the parameters of the system, any variation in these parameters will render the design incorrect. The neural network controller is able to adapt to any parameter variation.

A modified backpropagation algorithm is used to train the neural network. Since the error at the output of the neural network controller will be unknown in the direct-control scheme, the error at the system output is instead backpropagated through the system by considering the system as an additional layer of the neural network. Simulations are conducted for wind and earthquake excitation using a two-layer network composed of neurons with tangent-sigmoid activation functions. The sensitivity of the neural network controller to variations in the input scaling factor, output gain factor, and learning rate are determined. The effect of control force saturation is also investigated. A comparison is made between the results of simulations using a linear and a nonlinear model. Based on simulation results, the controller is shown to be effective even in the presence of variations in both system and controller/actuator parameters. The regenerative actuator is able to recover energy and reduce the peak energy requirement for control.

CHAPTER 8

Adaptive Fuzzy Control

A new on-line, direct-control scheme for active control of civil structures using an adaptive fuzzy controller is proposed. The advantage of using an adaptive fuzzy controller is that it does not require an accurate model of the system. The controller learns the system dynamics by adapting its parameters on-line. A modified gradient descent method is used as the adaptation mechanism. In order to adapt the parameters of the fuzzy system, the error at the output of the fuzzy controller must be known. In the proposed direct-control scheme, this error is unknown. Thus, it is proposed that the updating be based on the output error of the system directly. The update equations are derived for the controller. Simulations are performed for a structure with a regenerative electric actuator.

8.1 INTRODUCTION

There has been a rapid growth in the use of fuzzy logic in a wide variety of consumer products and industrial systems. Fuzzy logic represents one of the model-free approaches to the problems of system identification and control. The control of vibrations in civil structures due to environmental forces can be viewed as a mapping problem between the controller inputs and controller output. Fuzzy logic systems have been proven to be universal approximators [1] and hence are good candidates for solving complex control problems. Some of the advantages of fuzzy logic systems are that they can be nonlinear, can be adaptive, can admit a high degree of parallel implementation, and can tolerate uncertainty in the system. More importantly, human experience and expertise about the system and its performance can be incorporated into the design of a fuzzy controller.

There has been a number of attempts at using fuzzy control for the active control of civil structures. Nonadaptive fuzzy controllers for civil structure are presented in [2],[3], and [4]. Genetic algorithms are proposed in [5] for self-tuning inference rules and their parameters. Neuro-fuzzy control is suggested in [6] and [7] to improve the performance of a neural network controller.

This chapter presents a novel adaptive-fuzzy control scheme for use with a regenerative electric actuator providing active control to civil structures. The gradient descent method is the

adaptation mechanism through which the parameters of the fuzzy controller are updated. The method and some of the results presented in this chapter are also reported in [8].

8.2 ADAPTIVE FUZZY CONTROL

The basic objective of adaptive control is to maintain consistent system performance in the presence of variations or uncertainties in system parameters or operating conditions. In contrast to nonadaptive fuzzy controllers, the adaptive fuzzy controller achieves better performance by adjusting itself to the changing operating condition. It requires lesser information about the system because the adaptation mechanism is able to learn the dynamics of the system while it is operating. However, this type of control results in a nonlinear and time-varying control system which is also more expensive to implement.

Aside from the fuzzy controller itself, the adaptive fuzzy control system also includes a process monitor and an adaptation mechanism [9]. The process monitor determines changes in the system characteristics and passes the information to the adaptation mechanism. The adaptation mechanism updates the controller parameters in order to address these changes in the system characteristics. The process monitor can be in the form of a performance measure which evaluates how well the controller is able to adjust to the system changes, or a parameter estimator which continuously updates a model of the system. Parameter estimation usually requires an on-line identification of a system model. Performance assessment can be based on overshoot, rise time, settling time, frequency of oscillations of the transient, integral of the squared error, integral of the absolute value of the error, gain and phase margins, etc. A parameter that can be adjusted is the scaling factor which map controller input and output values onto the universe of discourse. Altering the scaling factor has a similar effect as gain tuning in PID controllers. Parameter adjustment can also be achieved by altering the shapes of the fuzzy sets or membership functions. The IF-THEN rules constitute another set of parameters which can be adjusted by the adaptation mechanism. An existing set of rules can be continuously modified or, starting from an empty rule-set, rules can be gradually constructed and/or deleted as the controller learns the system dynamics.

Adaptive fuzzy control can be classified into three types: indirect, direct, and combined indirect/direct [10]. In indirect adaptive control, the fuzzy controller is initially constructed from a collection of IF-THEN rules describing the input-output behavior of the system. The fuzzy controller in direct adaptive control is initially constructed from IF-THEN rules describing control action. The combined indirect/direct fuzzy controller makes use of both system and control information.

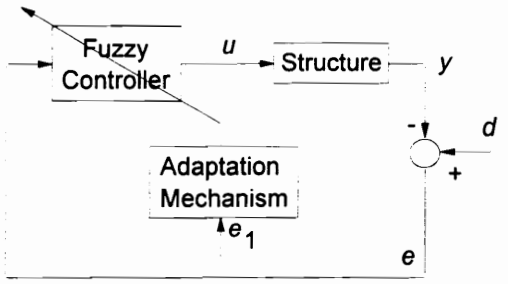

Fig. 8.1 Adaptive Fuzzy Control System

8.3 CONTROL SCHEME

Fig. 8.1 shows the proposed scheme for an adaptive fuzzy controller to be used in the active control of civil structures. In it, $y=[y_S \quad \dot{y}_S]^T$, $d=[0 \quad 0]^T$, $e=d-y=[e_1 \quad e_2]^T$, and y_S is the structural displacement. The structure's displacement and velocity are measured quantities. The difference between the desired (zero) and the measured displacement and velocity are errors which then become inputs to the fuzzy controller. The fuzzy controller is composed of a fuzzifier, a rule-base, an inference engine, and a defuzzifier as shown in Fig. 8.2. The fuzzifier is the structural system-to-fuzzy system interface which performs a mapping of real-valued variables into fuzzy variables. The fuzzy rule-base consists of a collection of fuzzy rules which can be developed by using IF-THEN rules based on available knowledge. These can be fine-tuned by training the fuzzy system to match controller input-output pairs. A selected set of training pairs can also be used to determine the fuzzy system parameters. In the fuzzy inference engine, fuzzy logic principles are used to combine the IF-THEN rules of the rule-base into a desired mapping. The defuzzifier is the fuzzy-system-to-structural-system interface which performs a mapping from fuzzy variables in to real-valued variables. The adaptation mechanism modifies the parameters of the fuzzy system based on the errors in displacement.

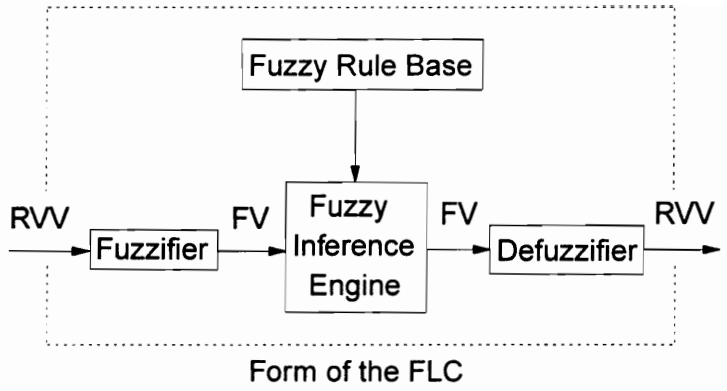

Fig. 8.2 Form of the fuzzy logic controller

The following steps are taken to implement the adaptive fuzzy controller described in the preceding paragraphs: (1) Obtain a nonadaptive fuzzy controller based on input-output pairs obtained for an existing controller. (2) Modify the parameters of the fuzzy controller to obtain an improvement over the existing controller. Some intuition may be required in order to determine the direction in which certain parameters should be varied. In the worst case, where no such intuition is forthcoming, run several test simulations to observe the effect that varying different parameters have on the controller performance. (3) Adapt the fuzzy controller parameters using some performance criterion. The current value of the performance criterion can be attributed to different parameters of the fuzzy controller.

8.4 ADAPTATION MECHANISM

If a reliable set of controller input-output data is available, then the membership functions used in the fuzzy controller can be tuned using an optimization procedure. The gradient descent algorithm is one of the simplest solution to such an optimization problem. This iterative algorithm seeks to decrease the value of an objective function with each iteration. This is due to the fact that the objective function at any point decreases most rapidly in the direction of the negative gradient vector of its parameters at that particular point.

The squared-error at the output of the fuzzy logic controller shown in Fig. 8.1 can be written as,

$$E_u = \frac{1}{2}(u_d - u)^2 \tag{8.1}$$

where u_d is the desired output of the fuzzy controller and u is the actual output of the fuzzy controller. For the typical adaptive-fuzzy controller [10], this squared-error is used to adapt the parameters of the membership functions. This is the objective function which is to be minimized by the fuzzy controller. For the scheme shown in Fig. 8.1, the main problem is the evaluation of (u_d - u) because the appropriate control u_d is not known. Only the system squared-error

$$E_y = \frac{1}{2}(d - y)^2 \tag{8.2}$$

which is implicitly related to E_u, can be measured at the output of the structural system. To solve the problem, it is proposed that the system squared-error E_y be used as the objective function which has to be minimized by the fuzzy controller instead of E_u. Let

$$e_y = (d - y) = (0 - y) = -y \tag{8.3}$$

The gradient of the error with respect to the fuzzy controller parameters θ is,

$$\frac{\partial E_y}{\partial \theta} = -e_y \frac{\partial y}{\partial \theta} \tag{8.4}$$

Using the chain rule,

$$\frac{\partial E_y}{\partial \theta} = -e_y \frac{\partial y}{\partial u} \cdot \frac{\partial u}{\partial \theta} \tag{8.5}$$

To apply the gradient-descent method, the update equation is given by

$$\theta(k+1) = \theta(k) - \eta \frac{\partial E_y}{\partial \theta} \tag{8.6}$$

where η is a learning rate. For this study, the fuzzy system is chosen to have a product inference engine, a singleton fuzzifier, a center average defuzzifier, and Gaussian membership functions. If x_1 and x_2 are the inputs to the fuzzy controller and u is the corresponding output, then

$$u = \frac{\sum_{i=1}^{M} (\mu_{1i})(\mu_{2i})\bar{u}_i}{\sum_{i=1}^{M} (\mu_{1i})(\mu_{2i})} \tag{8.7}$$

where

$$\mu_{1i} = \exp\left\{-\frac{1}{2}\left(\frac{x_1 - \bar{x}_{1i}}{\sigma_{1i}}\right)^2\right\} \tag{8.8}$$

$$\mu_{2i} = \exp\left\{-\frac{1}{2}\left(\frac{x_2 - \bar{x}_{2i}}{\sigma_{2i}}\right)^2\right\} \tag{8.9}$$

It is assumed that there are M rules, i.e., $i = [1,M]$, and μ_{1i} and μ_{2i} are the degrees of membership of the first and second input, respectively, for rule i. The fuzzy controller parameters which can be adapted are: the center of the output membership function for rule i, $\bar{u}_i$; the center of the 1st-input membership function for rule i, $\bar{x}_{1i}$; the center of the 2nd-input membership function for rule i, $\bar{x}_{2i}$; the spread of the 1st-input membership function for rule i, σ_{1i}; and the spread of the 2nd-input membership function for rule i, σ_{2i}. To facilitate the derivation of the update equations, let

$$Z_i = \mu_{1i}\mu_{2i} \tag{8.10}$$

$$b = \sum_{i=1}^{M} Z_i \tag{8.11}$$

$$a = \sum_{i=1}^{M} \bar{u}_i Z_i \tag{8.12}$$

Therefore, the control can be expressed as,

$$u = \frac{a}{b} \tag{8.13}$$

Based on the gradient descent method, the update equation for the center of the output membership function for rule i is given by,

$$\bar{u}_i(k+1) = \bar{u}_i - \eta \frac{\partial E_y}{\partial \bar{u}_i(k)} \tag{8.14}$$

Substituting (8.5) into (8.14),

$$\bar{u}_i(k+1) = \bar{u}_i(k) + \eta e_y \frac{\partial y}{\partial u} \cdot \frac{\partial u}{\partial \bar{u}_i(k)} \tag{8.15}$$

However, the partial derivative of u with respect to $\bar{u}_i$ is,

$$\frac{\partial u}{\partial \bar{u}_i} = \frac{\partial u}{\partial a} \cdot \frac{\partial a}{\partial \bar{u}} = \frac{1}{b} \cdot Z_i \tag{8.16}$$

Therefore, (8.15) can written as,

$$\bar{u}_i(k+1) = \bar{u}_i(k) + \eta e_y \frac{\partial y}{\partial u} \cdot \frac{Z_i}{b} \tag{8.17}$$

The update equation for the center of the *j*th input's membership function for rule *i* is given by,

$$\bar{x}_{ji}(k+1) = \bar{x}_{ji}(k) - \eta \frac{\partial E_y}{\partial \bar{x}_{ji}(k)} \qquad j = [1,2] \tag{8.18}$$

Substituting (8.5) into (8.18),

$$\bar{x}_{ji}(k+1) = \bar{x}_{ji}(k) + \eta e_y \frac{\partial y}{\partial u} \cdot \frac{\partial u}{\partial \bar{x}_{ji}(k)} \qquad j = [1,2] \tag{8.19}$$

However, the partial derivative of *u* with respect to $\bar{x}_{ji}$ is,

$$\frac{\partial u}{\partial \bar{x}_{ji}} = \frac{\partial u}{\partial Z_i} \cdot \frac{\partial Z_i}{\partial \bar{x}_{ji}} = \frac{1}{b}(\bar{u}_i - u) \cdot Z_i \frac{\left(x_j - \bar{x}_{ji}\right)}{\sigma_{ji}^2} \tag{8.20}$$

Combining (8.19) and (8.20), $\bar{x}_{ji}(k+1)$ is,

$$\bar{x}_{ji}(k+1) = \bar{x}_{ji}(k) + \eta e_y \frac{\partial y}{\partial u} \cdot \frac{(\bar{u}_i - u)}{b} \cdot \frac{Z_i\left(x_j - \bar{x}_{ji}\right)}{\sigma_{ji}^2} \qquad j = [1,2] \tag{8.21}$$

The update equation for spread of the *j*th input's membership function for rule *i* is given by

$$\sigma_{ji}(k+1) = \sigma_{ji}(k) - \eta \frac{\partial E_y}{\partial \sigma_{ji}(k)} \qquad j = [1,2] \tag{8.22}$$

Substituting (8.5) into (8.22),

$$\sigma_{ji}(k+1) = \sigma_{ji}(k) + \eta e_y \frac{\partial y}{\partial u} \cdot \frac{\partial u}{\partial \sigma_{ji}} \qquad j = [1,2] \tag{8.23}$$

However, the partial derivative of *u* with respect to σ_{ji} is,

$$\frac{\partial u}{\partial \sigma_{ji}} = \frac{\partial u}{\partial Z_i} \cdot \frac{\partial Z_i}{\partial \sigma_{ji}} = \frac{1}{b}(\bar{u}_i - u) \cdot Z_i \frac{(x_j - \bar{x}_{ji})^2}{\sigma_{ji}^3} \tag{8.24}$$

Substituting (8.24) into (8.23) gives the update of the spread as,

$$\sigma_{ji}(k+1) = \sigma_{ji}(k) + \eta e_y \frac{\partial y}{\partial u} \cdot \frac{(\bar{u}_i - u)}{b} \cdot \frac{Z_i (x_j - \bar{x}_{ji})^2}{\sigma_{ji}^3} \qquad j = [1,2] \tag{8.25}$$

Since the learning rate in each update equation can be chosen carefully, the exact partial derivatives in (8.15), (8.19), and (8.23) are not required in the update equations. If the signs of these partial derivatives are determined, the gradient descent algorithm can reach the minima by traveling in the proper local direction of greatest error reduction. The direction is determined by the polarities of the partial derivatives. Thus, the following approximations can be made:

$$\frac{\partial y}{\partial u} \approx \text{sign}\left(\frac{\partial y}{\partial u}\right) \tag{8.26}$$

$$(\bar{u}_i - u)(x_j - \bar{x}_{ji}) \approx \text{sign}\left[(\bar{u}_i - u)(x_j - \bar{x}_{ji})\right] \tag{8.27}$$

$$(\bar{u}_i - u) \approx \text{sign}(\bar{u}_i - u) \tag{8.28}$$

Noting that Z_i, b, and σ_{ji} are always positive, then the update equations can be approximated as

$$\bar{u}_i(k+1) = \bar{u}_i(k) + \eta e_y \cdot \text{sign}\left(\frac{\partial y}{\partial u}\right) \tag{8.29}$$

$$\bar{x}_{ji}(k+1) = \bar{x}_{ji}(k) + \eta e_y \cdot \text{sign}\left(\frac{\partial y}{\partial u}\right) \cdot \text{sign}\left[(\bar{u}_i - u)(x_j - \bar{x}_{ji})\right] \qquad j = [1,2] \tag{8.30}$$

$$\sigma_{ji}(k+1) = \sigma_{ji}(k) + \eta e_y \cdot \text{sign}\left(\frac{\partial y}{\partial u}\right) \cdot \text{sign}(\bar{u}_i - u) \qquad j = [1,2] \tag{8.31}$$

The signum functions in the above equations have to be evaluated during each update. Equation (8.26) can be approximated [11] in each update as,

$$\text{sign}\left(\frac{\partial y}{\partial u}\right) \approx \text{sign}\left(\frac{\Delta y}{\Delta u}\right) \tag{8.32}$$

To avoid being stuck in a local minimum, a momentum factor m_c can be included in the update equation such that

$$\hat{\theta}(k+1) = m_c \theta(k) + (1 - m_c)\theta(k+1) \tag{8.33}$$

In the next update,

$$\theta(k) = \hat{\theta}(k) \tag{8.34}$$

Example 8.1

Consider the single-degree-of-freedom system with mass damper under wind excitation described in Example 4.1. To obtain a nonadaptive fuzzy controller, controller input-output pairs are recorded for simulations using a proportional controller. The controller inputs are the structure's displacement and velocity. The control output is u. Fifty data pairs are selected, determining the centers of the membership functions for the inputs and the output. It should be noted that this method for determining the centers of the membership functions is not unique. If knowledge on the behavior of the system is available, some linguistic rules can be formed rather than relying completely on the controller input-output data. The widths of membership functions are assumed to be 0.10. In this particular example, only the centers of the membership functions are adapted on-line. A learning rate of 0.01 and a momentum factor of 0.95 are used in the simulation.

The resulting displacement and damper stroke length are shown in Fig. 8.3 and Fig. 8.4. Since the training data is obtained from results for a simulation using proportional control using displacement feedback, then the response obtained closely resembles that obtained for proportional control. Since the controller is undergoing adaptation during the first few cycles of the disturbance, it cannot effectively reduce the peak that occurs during this period.

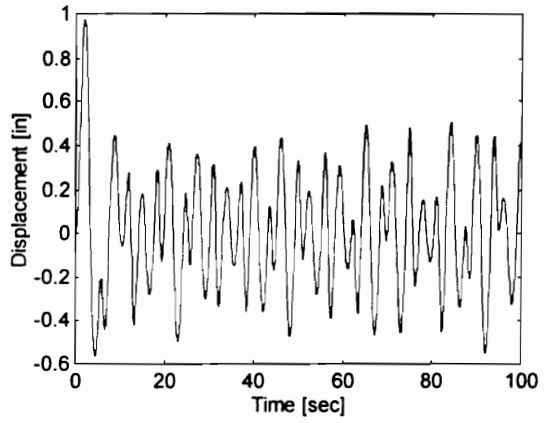

Fig. 8.3 Displacement with adaptive fuzzy control

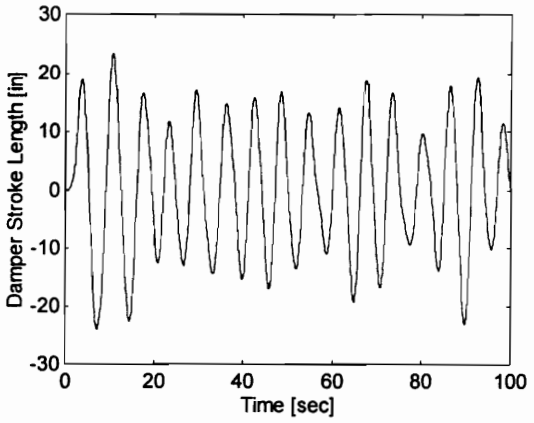

Fig. 8.4 Stroke length with adaptive fuzzy control

TABLE 8.1
Comparison of Responses

PARAMETER	Passive	Adaptive Fuzzy Control
Max. displacement [in]	4.4035	0.9760
Max. stroke length [in]	15.4733	23.9320
Max. control force [kips]	0	37.9155
Max. actuator power [kW]	0	35.4019

A comparison of the response with and without adaptive fuzzy control is shown in Table 8.1. There is a 78% reduction of the peak displacement with adaptive fuzzy control. However, this is accompanied by a 55% increase in the damper stroke length. In order to provide the necessary control force to the structure, the stroke length has to increase accordingly.

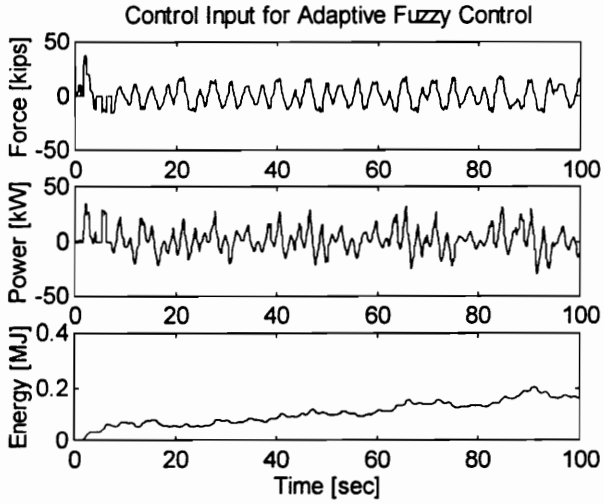

Fig. 8.5 Actuator force, power, and energy for adaptive fuzzy control

The regenerative electric actuator provides the control input shown in Fig. 8.5. Since the maximum displacement occurs during the first few cycles of the excitation and the controller is initially based on a proportional controller, the maximum force also occurs at this time. The periods of negative power enables the regenerative actuator to store energy and reduce the peak energy required from the supply. The peak energy requirement is reduced from 0.4789 MJ to 0.2048 MJ for the given duration of the disturbance. This translates to a reduction of 57% in the required electrical source capacity.

8.5 SUMMARY

A new on-line, direct-control scheme for active control of civil structures using an adaptive fuzzy controller is proposed. The adaptive fuzzy-control approach does not require an accurate model of the system in order to function. It is able to achieve this by adapting the fuzzy controller parameters on-line. A modified gradient descent method is used as the adaptation mechanism. In order to adapt the parameters of the fuzzy system, the error at the output of the fuzzy controller must be known. In the proposed direct-control scheme, this error is unknown. Thus, it is proposed that the updating be based on the output error of the system directly. The update equations are derived for the controller. Simulations are performed for a structure equipped with a regenerative electric actuator, while under wind excitation.

CHAPTER 9

Comparison of Controllers

The preceding chapters investigated the feasibility of various controllers for application in structures with regenerative electric actuators. In these studies, actuator dynamics are neglected because they are very much faster than the dynamics of the structure and the damper. This chapter compares the different controllers based on various criteria. The major factors that have to be considered when choosing a controller for the regenerative electric actuator include maximum displacement, stroke length, control force, actuator power, and actuator energy. Control force saturation has to be considered to obtain the most effective type of control. The final decision in choosing a controller for the regenerative electric controller has to consider all of the above-mentioned factors. A compromise may be required if conflicting objectives have to be satisfied.

9.1 DISPLACEMENT, DAMPER STROKE, AND CONTROL FORCE

A. Single-Degree-of-Freedom System under Wind Excitation

For the single-degree-of-freedom structure under wind excitation, Table 9.1 shows a comparison of the maximum displacement, maximum damper stroke, and maximum control force for different controllers.

TABLE 9.1 Comparison of Maximum Displacement, Stroke, and Control Force

CONTROL TYPE	Max. Displacement [cm]	Max. Stroke [cm]	Max. Control Force [kN]	Displacement-Force Ratio [cm/kN]
Passive	11.7538	39.3291	0	-
Proportional	2.4803	66.1388	65.1550	0.0381
Linear Quadratic	2.3236	52.9747	165.8796	0.0140
Sliding Mode (P-P)	2.2992	86.7171	66.7230	0.0344
Sliding Mode (Q-M)	2.3485	84.6694	66.7230	0.0352
Neural Network	2.5598	73.2521	58.4689	0.0438
Adaptive Fuzzy	2.4790	60.7873	168.6557	0.0147

The maximum displacement occurs during the first cycle of the displacement waveform. It is during this time that the controller and actuator is trying to build up the necessary counter-force to mitigate the effect of the disturbance. Table 9.1 shows that the minimum peak-displacement is obtained when using the sliding mode controller which is designed by the pole-placement method. An 80% reduction in the maximum displacement is obtained when using this type of control. The sliding mode controller is able to issue a larger control command even if the displacement response is still small during the first few cycles of the disturbance. Therefore, it is able to limit the peak displacement to a lower value as compared to the other controllers.

The largest maximum-displacement value results from using the neural network controller. This is due to the fact that the network is initially untrained. It takes a few training cycles before it learns the system dynamics and issue the correct control command. It is during these early training cycles that the peak displacement occurs. Thus, it is unable to limit the peak displacement as well as the other controllers.

The large displacement that occur during the first few cycles of the excitation causes the controller to issue a large control command. This produces the peak in the control force waveform. Table 9.1 shows that the neural network controller has the minimum peak-control-force. Since the network is still undergoing training during the early cycles of the disturbance, it does not command a proportionately large force for the large displacement that occurs.

The sliding mode and proportional controllers produce peaks in the control force that are comparable to that produced by the neural network controller. The control force for the sliding mode controllers is limited to 67 kN, based on the peak value obtained for the proportional controller. Despite the limit set on the control force, the sliding mode controller still produces the smaller peak-displacement. The linear quadratic controller has a larger control force due to the smaller weight placed on the control as compared to the displacement response.

Due to the more abrupt changes in the control command for the sliding mode controller, the maximum stroke length for these controllers are larger than those for the other controllers. Other controllers have a gradual change in the control command as compared to the sliding mode controllers. Consequently, the stroke lengths for these controllers are smaller. The sliding mode controller which is designed by using the pole-placement method experiences the largest increase in the damper stroke of about 120%. The linear quadratic controller produces the least increase in damper stroke of 35%. This increase in damper stroke is greatly dependent on the weight placed on the stroke length.

The displacement-force ratio is the ratio of the maximum displacement to the maximum control force. This provides a measure of the effectiveness of the control force. A larger value

means that there is a greater reduction in the maximum displacement per unit of force being applied. The neural network, sliding mode, and proportional controllers have comparable effectiveness. These controllers have approximately the same peak control force providing the same amount of reduction in the displacement peak. The larger control forces required by the linear quadratic and adaptive fuzzy controllers make the displacement-force ratio smaller for these controller types.

Based on the maximum displacement, stroke length, and control force, the proportional and sliding mode controllers provide the best control for the single-degree-of-freedom system under the given magnitude of wind excitation.

B. Single-Degree-of-Freedom System under Earthquake Excitation

For the single-degree-of-freedom system under earthquake excitation, Table 9.2 shows a comparison of the maximum displacement, maximum stroke, and maximum control force for different controllers.

TABLE 9.2 Comparison of Maximum Displacement, Stroke, and Control Force

CONTROL TYPE	Max. Displacement [cm]	Max. Stroke [cm]	Max. Control Force [kN]	Displacement-Force Ratio [cm/kN]
Passive	14.2128	38.4660	0	-
Linear Quadratic	8.7297	200.2904	553.5109	0.0158
Sliding Mode (P-P)	4.0284	373.1494	667.2300	0.0061
Sliding Mode (Q-M)	6.2304	255.5497	664.7141	0.0094
Neural Network	7.8468	482.6066	591.2458	0.0132

The maximum displacement occurs during the first few cycles of the displacement waveform. During this period, the actuator and damper is trying to build up the necessary counter-force. The damper's inertia causes the delay in the generation of sufficient force. Table 9.2 shows that the minimum peak-displacement is obtained when using the sliding mode controller which is designed by the pole-placement method. A 72% reduction in the maximum displacement is obtained when using this type of control. The sliding mode controller is able to issue a larger control command even if the displacement response is still small during the first few cycles of the disturbance. Therefore, it is able to limit the peak displacement to a lower value as compared to the other controllers.

The linear quadratic controller produces the largest peak-displacement, with a reduction of only 39%. The largest weight is given to the displacement response. Since the displacement is small at the start of the disturbance, the control force generated during this period is relatively smaller. Therefore, larger peaks in the displacement are obtained.

The large displacement that occurs during the first few cycles of the excitation eventually causes the controller to issue a large control command. This produces the peak in the control force waveform. Table 9.2 shows that the linear quadratic controller has the minimum peak-control-force. This simply means that the effective gain applied to the displacement to generate part of the control is smaller for the linear quadratic controller than for the other controllers. The sliding mode controllers require the largest control force peak but have lower displacement-force ratios. This is due to the fact that the sliding mode controller produces smaller peaks in the displacement while using control forces that are comparable in magnitude to those used by other controllers.

The damper stroke and velocity are not used as inputs to the neural network controller. Therefore, the resulting peak in the damper stroke is largest for this type of controller. All the other controllers use a feedback of the damper stroke and velocity. Thus, these controllers are able to minimize the damper stroke.

Based on the maximum displacement, stroke, and control force, the sliding mode controller is able to provide the best control for the single-degree-of-freedom system under the given magnitude of earthquake excitation.

C. Fixed-Base, Multidegree-of-Freedom System under Wind Excitation

For the fixed-base, multidegree-of-freedom system under wind excitation, Table 9.3 shows a comparison of the maximum displacement, damper stroke length, and control force for various types of control.

TABLE 9.3 Comparison of Maximum Displacement, Stroke, and Control Force

CONTROL TYPE	Max. Interstory Displacement [cm]	Max. Stroke [cm]	Max. Control Force [kN]	Displacement-Force Ratio [cm/kN]
Passive	2.0803	24.4881	0	-
Proportional	1.4422	225.2129	904.8419	0.0016
Linear Quadratic	1.4674	94.8030	546.8642	0.0027
Sliding Mode	1.8865	2.9734	354.1092	0.0053

In all cases, the maximum interstory displacement occurs at the third floor. The eighth floor experiences the largest displacement with respect to the ground. For the given excitation, the peak displacement occurs during the first or second cycle of the disturbances waveform. Table 9.3 shows that proportional control results in the minimum peak in the interstory displacement, producing a 31% reduction in the peak interstory drift. However, the required control force is very much greater than in the other two control types. This is due to the fact that the feedback quantity in the proportional controller is the displacement of the eighth floor with respect to the ground. This quantity definitely undergoes a larger variation than the interstory drifts used in the linear quadratic and sliding mode controllers.

Table 9.3 shows that for the given system and excitation, larger control forces result in longer stroke lengths. Due to the smaller control force required by the sliding mode controller, the displacement-control force ratio is the larger value for this type of controller. Based on the maximum damper stroke and control force, the sliding mode controller provides the best control. If smaller interstory displacements are desired, then proportional control gives better results at the cost of larger control forces.

D. Base-Isolated, Multidegree-of-Freedom System under Earthquake Excitation

For the base-isolated, multidegree-of-freedom system being subjected to earthquake excitation, Table 9.4 gives the maximum displacement, damper stroke length, and control force for various controllers.

TABLE 9.4 Comparison of Maximum Displacement, Stroke, and Control Force

CONTROL TYPE	Max. Interstory Drift [cm]	Max. Base Displacement [cm]	Max. Stroke [cm]	Max. Control Force [kN]	Displacement-Force Ratio [cm/kN]
Passive	0.5401	12.5719	35.4893	0	-
Proportional	0.5185	11.6516	67.6722	116.5160	0.0044
Linear Quad.	0.5314	11.6045	53.4180	147.0765	0.0036
Sliding Mode	0.5183	12.1154	47.5925	339.6541	0.0015

The maximum interstory displacement occurs in the first floor for the linear quadratic and sliding mode controllers. For proportional control, the maximum interstory displacement occurs in the third floor. Table 9.4 shows that proportional and sliding mode control give the minimum peak in

interstory displacements, reducing the peak by 4%. However, linear quadratic control gives the smallest peak in the base displacement by reducing it by 8%.

For the given system and excitation, the peak stroke length is inversely affected by the peak control force. Proportional control has the longest stroke length but requires the smallest peak force. On the other hand, sliding mode control has the shortest stroke length but requires a the largest peak in the control force.

If the primary objective is to reduce the interstory drift, then proportional control gives the most reduction in the peak displacement for the least control force. If the primary objective is to reduce the base displacement, then sliding mode control gives the best result at the cost of higher peaks in the control force.

9.2 POWER AND ENERGY

A. Single-Degree-of-Freedom System under Wind Excitation

For the single-degree-of-freedom system under wind excitation, Table 9.5 gives a comparison of the actuator power and energy for different controllers. The peak energy is determined for a disturbance duration of 100 seconds.

TABLE 9.5 Comparison of Power and Energy

CONTROL TYPE	Max. Power [kW]	Max. Energy with Regen. [MJ]	Max. Energy without Regen. [MJ]	Reduction in Max. Energy
Proportional	22.3242	0.1788	0.2902	38%
Linear Quadratic	50.4336	0.0398	0.6941	94%
Sliding Mode (P-P)	46.9538	0.1407	0.8603	84%
Sliding Mode (Q-M)	47.3990	0.1572	0.7104	78%
Neural Network	29.5657	0.1815	0.4485	60%
Adaptive Fuzzy	35.4019	0.2048	0.4789	57%

The energy values are the energy required by the actuator from the electrical source. These values are reduced through the use of a regenerative electric actuator. Instead of dissipating energy as heat, the regenerative electric actuator recovers the energy during periods of negative power and stores it for later use. The lower energy requirement translates to a lower ampere-hour rating for a battery bank which acts as the electrical source for the actuator and as the energy storage device.

The maximum actuator power determines the peak power rating of the actuator. The nominal power rating of the actuator is lower than the given maximum power. Table 9.5 shows that a proportional controller requires the least power. However, the amount of energy saved by the actuator through regeneration is only 38%. On the other hand, the linear quadratic controller requires the maximum peak-power but is able to reduce the peak energy requirement by 94%. It is observed that the higher the maximum power, the greater is the recovered energy.

B. Single-Degree-of-Freedom System under Earthquake Excitation

For the single-degree-of-freedom system under earthquake excitation, Table 9.6 gives a comparison of the actuator power and energy for different controllers. The maximum energy is determined for a disturbance duration of 24 seconds.

TABLE 9.6 Comparison of Power and Energy

CONTROL TYPE	Max. Power [kW]	Max. Energy with Regen. [MJ]	Max. Energy without Regen. [MJ]	Reduction in Max. Energy
Linear Quadratic	608.8404	0.6408	0.8285	23%
Sliding Mode (P-P)	1469.7	2.3613	3.3416	29%
Sliding Mode (Q-M)	751.0914	1.0193	1.1535	12%
Neural Network	1783.7	3.9187	8.2382	52%

The linear quadratic controller requires an actuator with the smallest power rating. However, the peak energy requirement is reduced by only 23%. If it is desired that more energy be recovered, then a larger actuator rating is required by using a neural network controller. Despite having the lowest power requirement, it is noted that linear quadratic control does not necessarily result in the lowest percentage in energy reduction as is observed for wind excitation.

C. Fixed-Base, Multidegree-of-Freedom System under Wind Excitation

For the fixed-base, multidegree-of-freedom system subjected to a wind excitation, Table 9.7 gives a comparison of the actuator power and energy for various controllers. The maximum energy is determined for a disturbance duration of 20 seconds.

TABLE 9.7 Comparison of Power and Energy

CONTROL TYPE	Max. Power [kW]	Max. Energy with Regen. [MJ]	Max. Energy without Regen. [MJ]	Reduction in Max. Energy
Proportional	2701.1	10.1141	58.3865	83%
Linear Quadratic	654.9221	0.8237	8.5644	90%
Sliding Mode (P-P)	45.1081	0	0.0002728	100%

For this particular system and excitation, sliding mode control requires the least power rating for the actuator and recovers 100% of the energy expended for control through regeneration. The zero energy peak means that the actuator is in generation-mode all of the time. Proportional control has the largest peak in power and reduces the energy requirement by the lowest amount among the three controllers being considered. Based on maximum power and energy, sliding mode control is desirable for this particular system and disturbance.

D. Base-Isolated, Multidegree-of-Freedom System under Earthquake Excitation

For the base-isolated, multidegree-of-freedom system subjected to an earthquake excitation, Table 9.8 gives a comparison of the actuator power and energy for various controllers. The maximum energy is determined for a disturbance duration of 24 seconds.

TABLE 9.8 Comparison of Power and Energy

CONTROL TYPE	Max. Power [kW]	Max. Energy with Regen. [MJ]	Max. Energy without Regen. [MJ]	Reduction in Max. Energy
Proportional	115.4689	0.2176	1.3873	84%
Linear Quadratic	88.3408	0.0451	0.5280	91%
Sliding Mode (P-P)	133.7742	0.0659	0.0937	30%

Table 9.8 shows that linear quadratic control has the minimum power requirement and the largest reduction in the energy requirement of the actuator. Based on the maximum power and energy, linear quadratic control is desirable for this particular system and excitation.

9.3 CONTROL FORCE SATURATION

A. Single-Degree-of-Freedom System under Wind Excitation

For the single-degree-of-freedom system under wind excitation, Fig. 9.1 shows a comparison of the effect of control force limits on the maximum displacement for different controllers. The effectiveness of increasing the control force limit to obtain smaller peaks in the displacement is determined by the slope of the plot. Larger negative slopes indicate that increasing the control limit will produce larger reductions in the maximum displacement. Near-zero slopes indicate that increasing the control limit will not produce any significant reduction in the peak displacement.

Proportional and adaptive fuzzy control allow a control force maximum of about 5 kN without any significant increase in the displacement maximum. Of course, further reduction of the control limit will eventually degenerate into the equivalent of an uncontrolled case. For these two controllers, it would be desirable to keep the control limit at a low value. Increasing the control force limit does not produce any reduction in the peak displacement. However, the control limit must not be placed so near zero because variations in the system or controller parameters might result into that of the uncontrolled case.

For linear quadratic and neural network control, increasing the control force limit above 20 kN does not produce any significant reduction in the maximum displacement. Therefore, it would be desirable to fix the control limit at 20 kN for these two controllers. To take into account any variation in system or controller parameters, it would be prudent to choose a control limit which is slightly above 20 kN. This will avoid the possibility of increasing the maximum displacement above 2.5 cm.

Only the sliding mode controllers possess the ability to decrease the maximum displacement by increasing the control limit above 20 kN. The plot for the pole-placement method has approximately a constant slope above 20 kN. Therefore, choosing a control limit anywhere between 20 and 120 kN will result in the same control effectiveness. For the quadratic minimization method, the slope of the plot is slightly higher near 20 kN and gradually decreasing until 70 kN. After 70 kN, the slope remains essentially constant. Choosing the control limit to be at or near 20 kN would not be desirable since the maximum displacement is slightly above 2.5 cm. Choosing the control limit at or near 50 kN would keep the displacement within 2.5 cm. As in the linear quadratic and neural network controller, it would be wise to select a control limit which is slightly above the "knee" of the plot. If it is desired that the maximum displacement be reduced below 2.5 cm, choosing a sliding mode controller will produce the desired reduction.

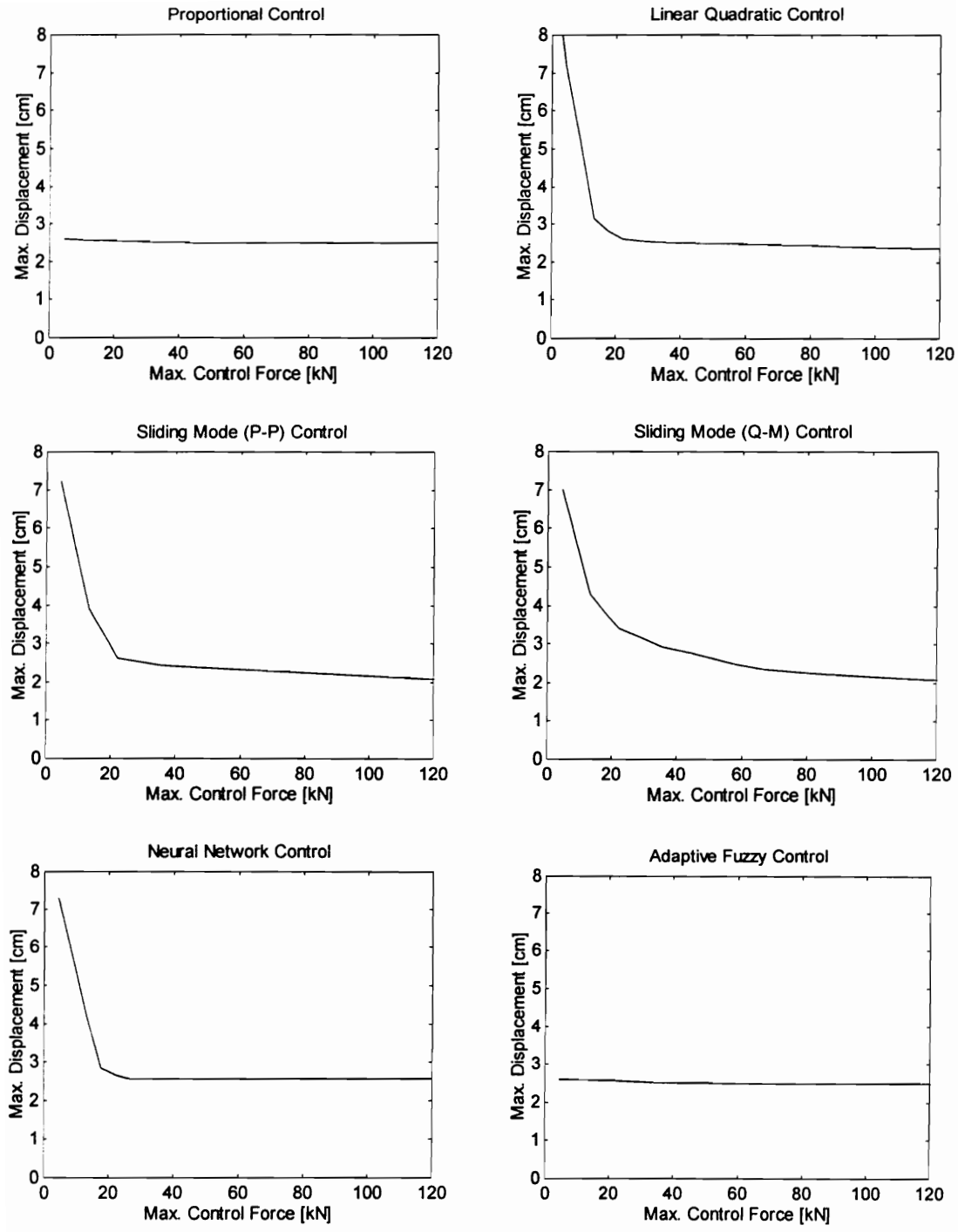

Fig. 9.1 Comparison of the effect of limiting the control force on the maximum displacement

B. Single-Degree-of-Freedom System under Earthquake Excitation

For the single-degree-of-freedom system under earthquake excitation, Fig. 9.2 shows a comparison of the effect of control force limits on the maximum displacement for various control types. For the linear quadratic controller, increasing the control limit above 300 kN does not produce any significant reduction in the maximum displacement which remains at about 9 cm. Similarly, increasing the control limit above 300 kips for the neural network controller does not produce any significant reduction in the maximum displacement. In this case, the maximum displacement remains at about 8 cm. To avoid the possibility of getting a significant increase in the displacement due to parameter variations, it would be advisable to choose a control limit above the "knee" of the plot. Although the linear quadratic controller has a higher peak displacement, the displacement waveform decays faster for this type of control as compared to neural network control. Thus, the linear quadratic controller has a slight advantage over neural network control.

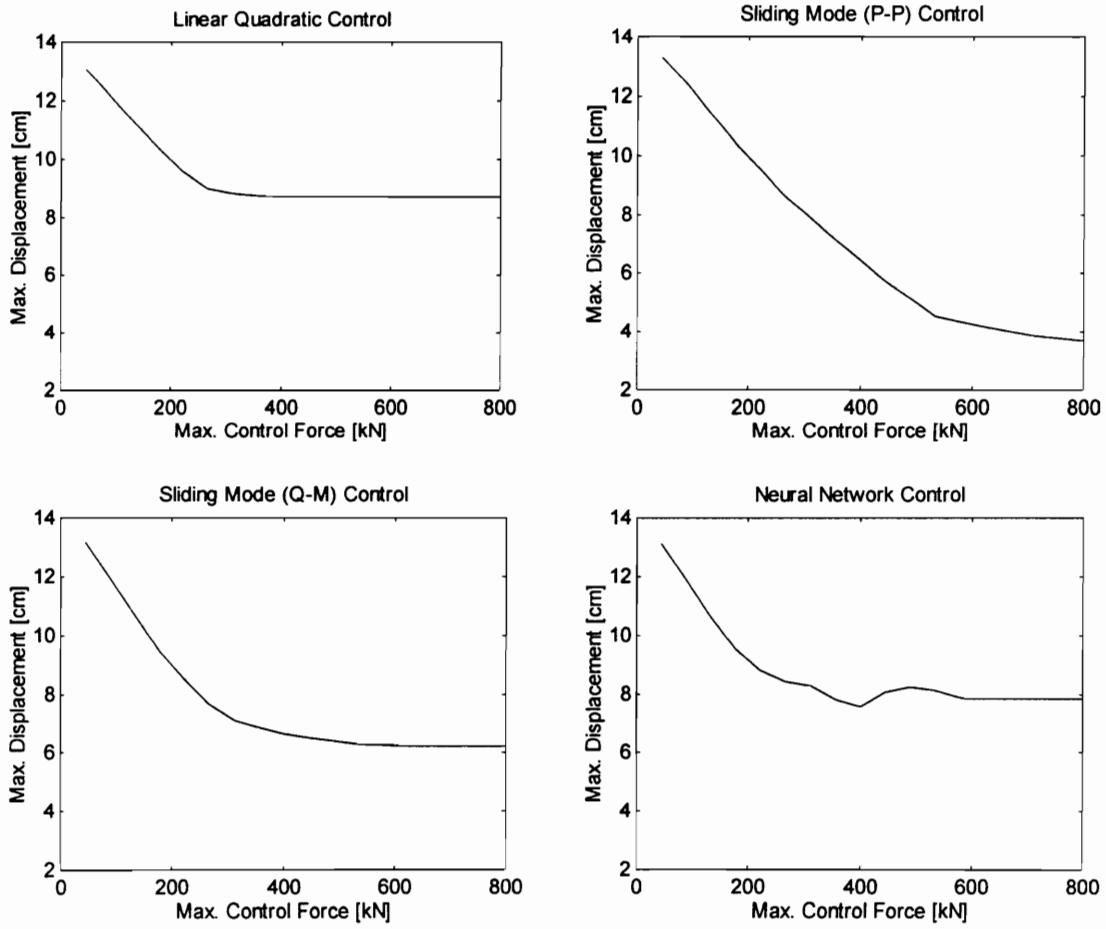

Fig. 9.2 Comparison of the effect of limiting the control force on the maximum displacement

Only the sliding mode controller is able to reduce the peak displacement below 8 cm. The slope of the plot for the quadratic minimization method approaches zeros at about 600 kN. Therefore, increasing the control limit above 600 kN will not result in any significant reduction of the maximum displacement. The peak displacement remains essentially constant at about 6.3 cm. The slope of the plot for the pole-placement method remains nonzero even above a control limit of 600 kN. Therefore, it is advantageous to set higher control limits for this controller. This will result in smaller peaks in the displacement. Maximum displacements below 6.3 cm can even be obtained, which is not possible for the other controller types.

9.4 SOME CONSIDERATIONS IN CONTROLLER IMPLEMENTATION

The proportional controllers that were considered made use of only one input. Although it makes proportional control easier to implement, the appropriate feedback quantity must be chosen carefully. For fixed-base systems, the displacement of the top floor with respect to the ground is usually a likely candidate. A base-isolated structure usually behaves like a rigid body, with minimal interstory displacements. Therefore, the base floor displacement is a possible choice in base-isolated systems.

For linear quadratic and sliding mode control, a full state feedback is required. This requires a measurement of displacements and velocities. Depending on the model used, these displacements can be interstory displacements or displacements with respect to ground. Compared to proportional control, a larger amount of information is required for these two types of control. An estimation of some quantities may be resorted to if these are not directly available.

For neural network and adaptive fuzzy control, increasing the number of input variables will require a longer training time. Since these controllers are trained on-line, it is important that the updating of the controller parameters be done in a short time as possible. On the other hand, more inputs could provide a better mapping of the controller inputs and output. Therefore, a compromise has to be made between faster update times and more accurate mappings.

9.5 SUMMARY

The major factors that have to be considered when choosing a controller for the regenerative electric actuator include maximum displacement, stroke length, control force, actuator power, and actuator energy. Control force saturation has to be considered to obtain the most effective type of control.

Based on the maximum displacement, stroke length, and control force, the proportional and sliding mode controllers provide the best control for the single-degree-of-freedom system

under the given magnitude of wind excitation. For the same system under a given earthquake excitation, the sliding mode controller is able to provide the best control based on the maximum displacement, stroke, and control force.

Based on the maximum damper stroke and control force, the sliding mode controller provides the best control for multistory fixed-base system under wind excitation. If smaller interstory displacements are desired, then proportional control gives better results at the cost of larger control forces.

If the primary objective is to reduce the interstory drift in the multistory base-isolated system under earthquake excitation, then proportional control gives the most reduction in the peak displacement for the least control force. If the primary objective is to reduce the base displacement, then sliding mode control gives the best result at the cost of higher peaks in the control force.

For the single-degree-of-freedom system, choosing a controller based on the actuator power and energy requires a compromise between using smaller ratings for the actuator and recovering a larger amount of energy through regeneration.

Based on maximum power and energy of the regenerative actuator, sliding mode control is desirable for the fixed-base multistory system subjected to a wind disturbance. On the other hand, linear quadratic control is desirable for the base-isolated multistory system under an earthquake disturbance based on the maximum power and energy of the actuator.

For the single-degree-of-freedom system subjected to wind excitation, choosing a control force limit above 20 kN keeps the maximum displacement at or below 2.5 cm. If further reduction is desired, using a sliding mode controller will result in smaller peaks. The pole-placement can produce greater reduction in the peak displacement if a larger control force is available. If the same system is subjected to an earthquake excitation, choosing the control limit above 300 kN will keep the maximum displacement at or below 9 cm. If smaller peaks in the displacement is desired, sliding mode control can produce the desired effect. The pole-placement method can produce the largest reduction if larger control forces are available.

The final decision when choosing a controller for the regenerative electric controller has to consider all of the above-mentioned factors. A compromise may be required if conflicting objectives have to be satisfied.

CHAPTER 10

Regenerative Electric Actuators

10.1 INTRODUCTION

A novel technique is investigated for utilizing the motion caused by environmental forces on a civil structure to generate electrical energy when the structure's response is within safety limits. When strong winds and earthquakes occur, the utility power source which supply energy to the actuator in an active control system is usually not reliable. It is during these instances that active control is needed most. With a regenerative electric actuator, the recovered energy is used to reduce the peak oscillations of the structure by applying forces (through actuators which use the recovered energy) counter to the environmental forces even if the utility power is not available. To achieve this, a tuned mass damper is used as the intermediary for the energy transfer between the structure and the actuator. The actuator proposed for this study is a permanent-magnet brushless DC machine which can provide a higher instantaneous torque in a compact frame size. This study is the first of its kind to propose and investigate active control of civil structures using regenerative electric actuators.

The actuator can either operate in the passive mode, 4-quadrant mode, or in the 2-quadrant generation mode. In the 4-quadrant mode, the performance of various controllers are compared based on the maximum displacement, stroke, control torque, actuator power, and source energy. Motor and generator action can both occur in the 4-quadrant mode. It is desired that the controller require a smaller actuator power rating so that the cost of the machine will be lower. A lower actuator energy is desired so that the capacity of the electrical source will be lower. Furthermore, a lower energy requirement means that a lower capacity for the energy storage device is needed. In majority of the test cases, sliding mode control often has the lowest power and energy requirement. The use of regenerative electric actuators reduce the required source capacity as compared to using non-regenerative actuators which simply dissipate energy as heat. The amount of reduction is often significant. This can translate to savings in equipment cost. Single-degree-of-freedom and multidegree-of-freedom structures are simulated. In the 2-quadrant generation mode, the system response must always fall within the safety margins of the structure. The amount of energy that can be recovered is limited by the power rating of the actuator and the energy capacity of the electrical source and the storage device.

The dynamics of the electrical subsystem can be incorporated into actuator-structure system to determine transient behavior of the entire system. It is shown that the actual torque closely follows the command torque. This is one of the advantages of using an electrical actuator. More accurate models of the electrical source and storage device can also be included in the simulation to determine the variation of the voltage at the terminals of the source. In this study, the variation of the terminal voltage of the source is determined by representing the source as an ideal voltage source in series with a source resistance.

Preliminary results of this study are also reported in [1]. In this chapter, the equations of motion are derived for the combined system with the actuator. In order to obtain a preliminary estimate of the system response, it is initially assumed that the commanded control T_e* is also the actual control T_e. It is shown in a later section that this assumption is valid, due to the faster time constants of the electrical subsystem compared to those of the mechanical subsystem.

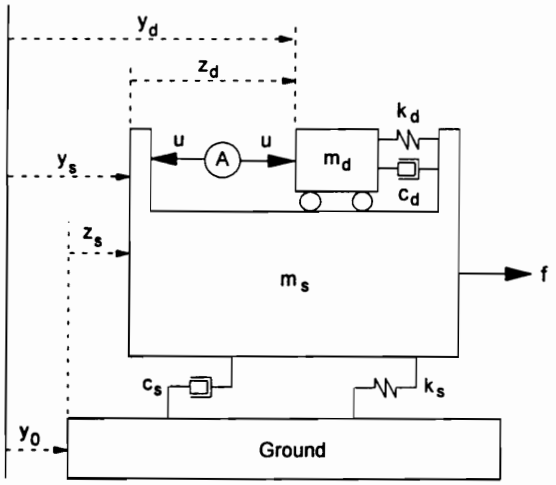

Fig. 10.1 Single-Degree-of-Freedom Structure with Mass Damper

10.2 MODES OF OPERATION

The actuator can operate in either passive mode, 4-quadrant mode, or 2-quadrant generation mode. In the passive mode, there is no torque or force exerted by the actuator. The actuator's mass and damping simply contribute to the damper's mass and damping. In the 4-quadrant mode, the actuator acts as a motor or a generator. Using a feedback of the system response, a controller (e.g., sliding mode, neural network, fuzzy) determines the control force magnitude and direction which will mitigate the structure's motion due to an external disturbance. To gain a physical insight into motoring and generating action, consider the single-

degree-of-freedom structure with mass damper shown in Fig. 10.1. The actuator can mitigate the oscillation of the structure by exerting a force on the damper in the positive or the negative direction. A force exerted on the damper in the positive direction will be transmitted to the structure through the damper stiffness and damping as a push in the positive direction. A force exerted on the damper in the negative direction will be transmitted to the structure as a pull in the negative direction through the damper stiffness and damping. When the structure is moving in a particular direction, the force exerted on the damper must be in the opposite direction in order to reduce the structure's displacement. Assume that the damper is moving in the positive direction (positive velocity). Motoring action occurs when the actuator applies a control force in the positive direction, i.e., in the same direction as the velocity. Generating action occurs when the actuator applies a control force in the negative direction, opposite to the direction of motion. In motoring action, the actuator is imparting kinetic energy to the damper by pushing on the damper. On the other hand, the actuator is absorbing some of the kinetic energy of the damper during generating action as the actuator is being pulled by the damper.

In the 2-quadrant generation mode, the actuator operates strictly as a generator. The controller produces a control force of a specified magnitude, whose polarity is opposite to the direction of motion. Thus, the controller output can have two possible values of the same magnitude but different polarities. The controller has to monitor the structure's response, making sure that it is always within the safety limits.

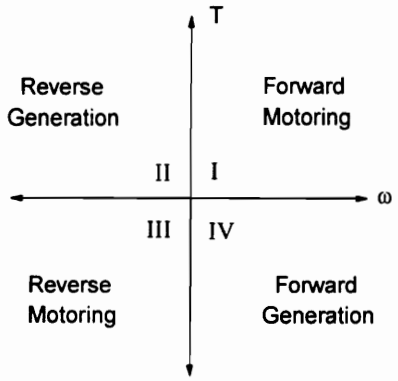

Fig. 10.2 Quadrants of operation for the regenerative electric actuator

Fig. 10.2 shows the four possible quadrants of operation for the regenerative electric actuator. Positive torque corresponds to positive force, while positive angular velocity corresponds to positive linear velocity. In forward motoring, both torque and velocity are positive. Reverse motoring has both negative torque and negative velocity. Forward generation

has positive torque but with negative velocity, while reverse generation has negative torque with positive velocity. Positive velocity means that the damper is moving in the positive direction. In the 4-quadrant mode, the actuator can operate in any of the four quadrants of operation. In the 2-quadrant generation mode, the actuator can operate in either quadrant II or IV.

10.3 BASIC CONTROL SCHEME

Fig. 10.3 shows the basic scheme of the proposed active/semi-active structural control system. The building-TMD system is being subjected to an external excitation f. Sensors measure the response y of the building-TMD and sends the measurements to the controller. The controller then forms a command input T_e^* to the actuator subsystem. The actuator can be switched to operate in either passive mode, 4-quadrant mode, or 2-quadrant generating mode. In 4-quadrant mode, the actuator applies the required control force to the building-TMD system. It should be noted that depending on the polarities of the torque and the stroke velocity, the actuator can consume or generate energy while in the 4-quadrant mode. In contrast to pneumatic or hydraulic actuators which dissipate energy as heat during periods of negative power, the regenerative electric actuator is able to store the recovered energy. If the external disturbance is such that the resulting displacements are well within safety limits, then the actuator can be switched to operate entirely in the 2-quadrant generation mode. The torque command is chosen such that it will have a polarity opposite to that of the stroke velocity. Thus, the actuator power will always be negative. During regeneration, the actuator converts the building-TMD motion to electrical energy for storage in battery or capacitor banks. If the battery bank is used as the electrical supply source for the actuator, regeneration will reduce the required energy capacity of the battery bank.

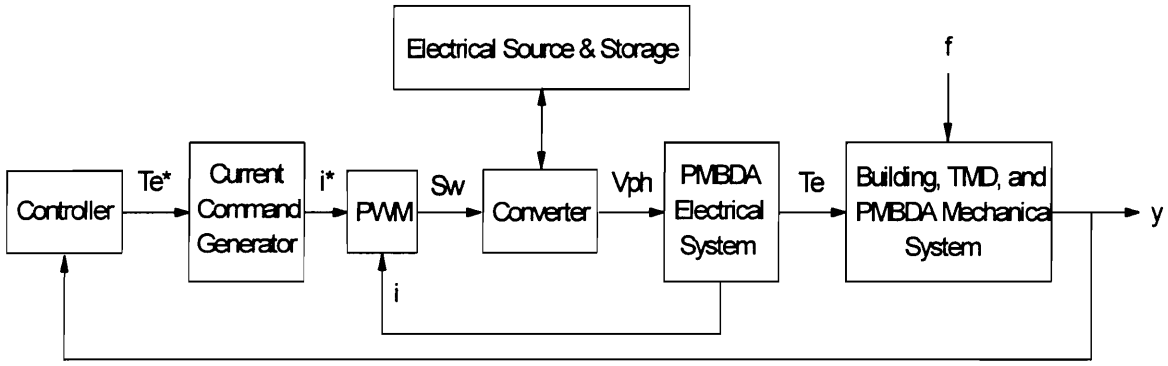

Fig. 10.3 Basic control scheme

10.4 SYSTEM MODELING

Consider the single-degree-of-freedom structural model with a mass damper, as shown in Fig. 10.1. In previous chapters, the mechanical dynamics of the actuator are neglected in order to obtain a faster estimate of the system response. This section incorporates the mechanical equations of the regenerative actuator with the mechanical equations of the structure-and-damper system. To facilitate the derivations, it is initially assumed that the stiffness k_s is linear. The equations of motion are given by,

$$m_s\ddot{z}_s + c_s\dot{z}_s + k_s z_s - c_d\dot{z}_d - k_d z_d = f - u - m_s\ddot{y}_0 \tag{10.1}$$

$$m_d(\ddot{z}_s + \ddot{z}_d) + c_d\dot{z}_d + k_d z_d = u - m_d\ddot{y}_0 \tag{10.2}$$

All quantities are as previously defined in Chapter 3. The actuator is a regenerative electric actuator. The actuator has to counteract the mechanical losses and provide the linear control force u. Similar to the concept of referring quantities to one side of a transformer, the control force u is reflected as the load torque T_L on the actuator. Thus, the control can be written as,

$$u = n_t T_L \tag{10.3}$$

where n_t is the linear-rotational transformation ratio which is determined by the mechanism through which rotational torque is converted to linear force, and vice versa. The actuator torque equation is given by

$$T_L = T_e - J\dot{\omega} - B\omega \tag{10.4}$$

where T_e is electromagnetic torque, J is the moment of inertia, and B is the damping coefficient. The rotational quantities are related to the linear quantities such that

$$\omega = n_t\dot{z}_d \tag{10.5}$$

$$\dot{\omega} = n_t\ddot{z}_d \tag{10.6}$$

The equations of motion are then modified as,

$$m_s\ddot{z}_s + c_s\dot{z}_s + k_s z_s - c_d\dot{z}_d - k_d z_d = f - n_t\left[T_e - Jn_t\ddot{z}_d - Bn_t\dot{z}_d\right] - m_s\ddot{y}_0 \tag{10.7}$$

$$m_d(\ddot{z}_s + \ddot{z}_d) + c_d\dot{z}_d + k_d z_d = n_t\left[T_e - Jn_t\ddot{z}_d - Bn_t\dot{z}_d\right] - m_d\ddot{y}_0 \tag{10.8}$$

Rearranging terms in (10.7) and (10.8), the equations of motion are rewritten as,

$$m_s\ddot{z}_s + c_s\dot{z}_s + k_s z_s - Jn_t{}^2\ddot{z}_d - \left[c_d + Bn_t{}^2\right]\dot{z}_d - k_d z_d = f - n_t T_e - m_s\ddot{y}_0 \tag{10.9}$$

$$m_d\ddot{z}_s + \left[m_d + Jn_t{}^2\right]\ddot{z}_d + \left[c_d + Bn_t{}^2\right]\dot{z}_d + k_d z_d = n_t T_e - m_d\ddot{y}_0 \tag{10.10}$$

or

$$m_s\ddot{z}_s + c_s\dot{z}_s + k_s z_s - J_1\ddot{z}_d - c_1\dot{z}_d - k_d z_d = f - n_t T_e - m_s\ddot{y}_0 \tag{10.11}$$

$$m_d\ddot{z}_s + m_1\ddot{z}_d + c_1\dot{z}_d + k_d z_d = n_t T_e - m_d\ddot{y}_0 \tag{10.12}$$

where

$$J_1 = Jn_t{}^2 \tag{10.13}$$

$$c_1 = c_d + Bn_t{}^2 \tag{10.14}$$

$$m_1 = m_d + Jn_t{}^2 \tag{10.15}$$

From (10.12), one can get the expression

$$\ddot{z}_d = \frac{1}{m_1}\left[n_t T_e - m_d\ddot{y}_0 - m_d\ddot{z}_s - c_1\dot{z}_d - k_d z_d\right] \tag{10.16}$$

Substituting (10.16) into (10.11) and moving terms to the right hand side yields

$$\begin{aligned} m_s\ddot{z}_s = {} & -c_s\dot{z}_s - k_s z_s + \frac{J_1}{m_1}\left[n_t T_e - m_d\ddot{y}_0 - m_d\ddot{z}_s - c_1\dot{z}_d - k_d z_d\right] \\ & + c_1\dot{z}_d + k_d z_d + f - n_t T_e - m_s\ddot{y}_0 \end{aligned} \tag{10.17}$$

Rearranging terms in (10.17) gives

$$\begin{aligned} \left[m_s + \frac{J_1}{m_1}m_d\right]\ddot{z}_s = {} & -c_s\dot{z}_s - k_s z_s + \left[1 - \frac{J_1}{m_1}\right]c_1\dot{z}_d + \left[1 - \frac{J_1}{m_1}\right]k_d z_d \\ & + f - n_t\left[1 - \frac{J_1}{m_1}\right]T_e - \left[m_s + \frac{J_1}{m_1}m_d\right]\ddot{y}_0 \end{aligned} \tag{10.18}$$

or

$$m_2\ddot{z}_s = -c_s\dot{z}_s - k_s z_s + \left[1-\frac{J_1}{m_1}\right]c_1\dot{z}_d + \left[1-\frac{J_1}{m_1}\right]k_d z_d + f - n_t\left[1-\frac{J_1}{m_1}\right]T_e - m_2\ddot{y}_0 \quad (10.19)$$

where

$$m_2 = m_s + \frac{J_1}{m_1}m_d \quad (10.20)$$

From (10.19), one can solve for

$$\ddot{z}_s = \frac{1}{m_2}\left[-c_s\dot{z}_s - k_s z_s + \left(1-\frac{J_1}{m_1}\right)c_1\dot{z}_d + \left(1-\frac{J_1}{m_1}\right)k_d z_d + f - n_t\left(1-\frac{J_1}{m_1}\right)T_e - m_2\ddot{y}_0\right] \quad (10.21)$$

Substituting (10.21) into (10.12) results in,

$$\begin{aligned}&\frac{m_d}{m_2}\left[-c_s\dot{z}_s - k_s z_s + \left(1-\frac{J_1}{m_1}\right)c_1\dot{z}_d + \left(1-\frac{J_1}{m_1}\right)k_d z_d + f - n_t\left(1-\frac{J_1}{m_1}\right)T_e - m_2\ddot{y}_0\right] \\ &\quad + m_1\ddot{z}_d + c_1\dot{z}_d + k_d z_d = n_t T_e - m_d\ddot{y}_0\end{aligned} \quad (10.22)$$

Rearranging terms in (10.22) will yield,

$$\begin{aligned}&m_1\ddot{z}_d + \left[1+\frac{m_d}{m_2}\left(1-\frac{J_1}{m_1}\right)\right]c_1\dot{z}_d + \left[1+\frac{m_d}{m_2}\left(1-\frac{J_1}{m_1}\right)\right]k_d z_d - \frac{m_d}{m_2}c_s\dot{z}_s - \frac{m_d}{m_2}k_s z_s = \\ &\quad -\frac{m_d}{m_2}f + n_t\left[1+\frac{m_d}{m_2}\left(1-\frac{J_1}{m_1}\right)\right]T_e\end{aligned} \quad (10.23)$$

Finally, from (10.21) and (10.23), the structure and damper accelerations are obtained as,

$$\ddot{z}_s = -\frac{c_s}{m_2}\dot{z}_s - \frac{k_s}{m_2}z_s + \frac{1}{m_2}\left(1-\frac{J_1}{m_1}\right)c_1\dot{z}_d + \frac{1}{m_2}\left(1-\frac{J_1}{m_1}\right)k_d z_d - \frac{1}{m_2}n_t\left(1-\frac{J_1}{m_1}\right)T_e + \frac{1}{m_2}f - \ddot{y}_0 \quad (10.24)$$

$$\ddot{z}_d = \frac{m_d}{m_1 m_2} c_s \dot{z}_s + \frac{m_d}{m_1 m_2} k_s z_s - \frac{1}{m_1}\left[1 + \frac{m_d}{m_2}\left(1 - \frac{J_1}{m_1}\right)\right] c_1 \dot{z}_d - \frac{1}{m_1}\left[1 + \frac{m_d}{m_2}\left(1 - \frac{J_1}{m_1}\right)\right] k_d z_d + \frac{1}{m_1} n_t \left[1 + \frac{m_d}{m_2}\left(1 - \frac{J_1}{m_1}\right)\right] T_e - \frac{m_d}{m_1 m_2} f \tag{10.25}$$

Let

$$\mathbf{x} = \begin{bmatrix} x_1 & x_2 & x_3 & x_4 \end{bmatrix}^T = \begin{bmatrix} z_s & z_d & \dot{z}_s & \dot{z}_d \end{bmatrix}^T \tag{10.26}$$

$$\mathbf{w} = \begin{bmatrix} f & \ddot{y}_0 \end{bmatrix}^T \tag{10.27}$$

then the state-space equation for the system is given by,

$$\dot{\mathbf{x}} = \mathbf{A}\mathbf{x} + \mathbf{B}T_e + \mathbf{H}\mathbf{w} \tag{10.28}$$

where

$$\mathbf{A} = \begin{bmatrix} 0 & 0 & 1 & 0 \\ 0 & 0 & 0 & 1 \\ -\frac{k_s}{m_2} & \frac{1}{m_2}\left(1 - \frac{J_1}{m_1}\right) k_d & -\frac{c_s}{m_2} & \frac{1}{m_2}\left(1 - \frac{J_1}{m_1}\right) c_1 \\ \frac{m_d}{m_1 m_2} k_s & -\frac{1}{m_1}\left\{1 + \frac{m_d}{m_2}\left(1 - \frac{J_1}{m_1}\right)\right\} k_d & \frac{m_d}{m_1 m_2} c_s & -\frac{1}{m_1}\left\{1 + \frac{m_d}{m_2}\left(1 - \frac{J_1}{m_1}\right)\right\} c_1 \end{bmatrix} \tag{10.29}$$

$$\mathbf{B} = \begin{bmatrix} 0 \\ 0 \\ -\frac{1}{m_2} n_t \left(1 - \frac{J_1}{m_1}\right) \\ \frac{1}{m_1} n_t \left\{1 + \frac{m_d}{m_2}\left(1 - \frac{J_1}{m_1}\right)\right\} \end{bmatrix} \tag{10.30}$$

$$\mathbf{H} = \begin{bmatrix} 0 & 0 \\ 0 & 0 \\ \dfrac{1}{m_2} & -1 \\ -\dfrac{m_d}{m_1 m_2} & 0 \end{bmatrix} \tag{10.31}$$

To take into account a structure with a nonlinear stiffness force, the nonlinear motion equations can be written as,

$$\begin{bmatrix} \dot{x}_1 \\ \dot{x}_2 \\ \dot{x}_3 \\ \dot{x}_4 \end{bmatrix} = \begin{bmatrix} \dot{z}_s \\ \dot{z}_d \\ \ddot{z}_s \\ \ddot{z}_d \end{bmatrix} = \mathbf{A} \begin{bmatrix} \alpha z_s + (1-\alpha) D_y v \\ z_d \\ \dot{z}_s \\ \dot{z}_d \end{bmatrix} + \mathbf{B} T_e + \mathbf{H}\mathbf{w} \tag{10.32}$$

$$\dot{x}_5 = \dot{v} = \frac{1}{D_y} \left\{ \lambda \dot{z}_s - \beta v |\dot{z}_s| |v|^{\eta-1} - \gamma \dot{z}_s |v|^{\eta} \right\} \tag{10.33}$$

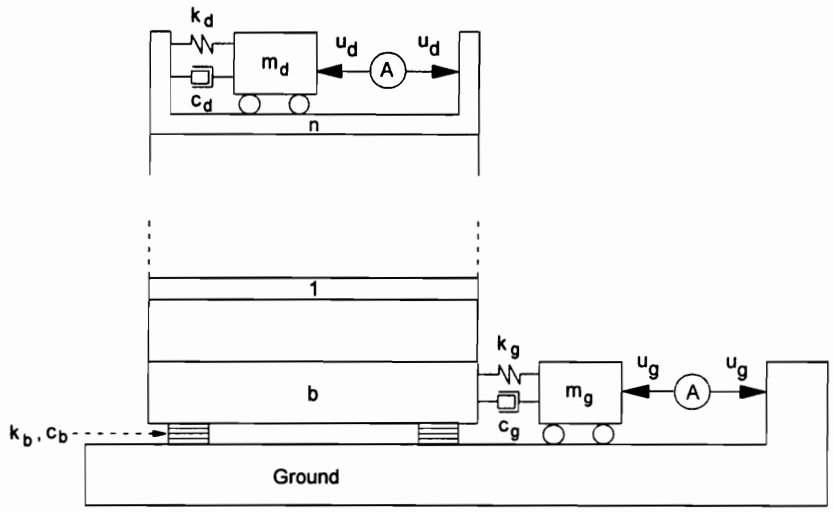

Fig, 10.4 Multidegree-of-freedom structure with REAs

Consider the multistory structure shown in Fig. 10.4. In terms of the interstory drifts, the multidegree-of-freedom equations are given by,

$$m_g\left(\ddot{y}_0+\ddot{z}_b+\ddot{z}_g\right)+c_g\dot{z}_g+k_g z_g=-u_g \tag{10.34}$$

. . . .

$$m_n(\ddot{y}_0+\ddot{z}_b+\ddot{z}_1+...+\ddot{z}_n)+c_n\dot{z}_n+k_n z_n-c_d\dot{z}_d-k_d z_d=f_n+u_d \tag{10.35}$$

$$m_d(\ddot{y}_0+\ddot{z}_b+\ddot{z}_1+...+\ddot{z}_n+\ddot{z}_d)+c_d\dot{z}_d+k_d z_d=-u_d \tag{10.36}$$

where

$$u_g=n_{tg}\left[T_{eg}-J_g n_{tg}\left(-\ddot{z}_b-\ddot{z}_g\right)-B_g n_{tg}\left(-\dot{z}_b-\dot{z}_g\right)\right] \tag{10.37}$$

$$u_d=n_{td}\left[T_{ed}-J_d n_{td}(-\ddot{z}_d)-B_d n_{td}(-\dot{z}_d)\right] \tag{10.38}$$

All structural parameters are as defined in Chapter 3. Substituting (10.37) and (10.38) into (10.34), (10.35), and (10.36) will result in the motion equations being expressed as,

$$m_g\left(\ddot{y}_0+\ddot{z}_b+\ddot{z}_g\right)+c_g\dot{z}_g+k_g z_g=-n_{tg}T_{eg}-J_g n_{tg}{}^2\ddot{z}_b-J_g n_{tg}{}^2\ddot{z}_g -B_g n_{tg}{}^2\dot{z}_b-B_g n_{tg}{}^2\dot{z}_g \tag{10.39}$$

. . . .

$$m_n(\ddot{y}_0+\ddot{z}_b+\ddot{z}_1+...+\ddot{z}_n)+c_n\dot{z}_n+k_n z_n-c_d\dot{z}_d-k_d z_d= f_n+n_{td}T_{ed}+J_d n_{td}{}^2\ddot{z}_d+B_d n_{td}{}^2\dot{z}_d \tag{10.40}$$

$$m_d(\ddot{y}_0+\ddot{z}_b+\ddot{z}_1+...+\ddot{z}_n+\ddot{z}_d)+c_d\dot{z}_d+k_d z_d= -n_{td}T_{ed}-J_d n_{td}{}^2\ddot{z}_d-B_d n_{td}{}^2\dot{z}_d \tag{10.41}$$

Rearranging terms in (10.39), (10.40), and (10.41) yields,

$$\left(m_g+J_g n_{tg}{}^2\right)\ddot{z}_g+\left(m_g+J_g n_{tg}{}^2\right)\ddot{z}_b+\left(c_g+B_g n_{tg}{}^2\right)\dot{z}_g+B_g n_{tg}{}^2\dot{z}_b+k_g z_g= -n_{tg}T_{eg}-m_g\ddot{y}_0 \tag{10.42}$$

. . . .

$$m_n(\ddot{z}_b+\ddot{z}_1+...+\ddot{z}_n)-J_d n_{td}{}^2\ddot{z}_d+c_n\dot{z}_n-\left(c_d+B_d n_{td}{}^2\right)\dot{z}_d+k_n z_n-k_d z_d= f_n+n_{td}T_{ed}-m_n\ddot{y}_0 \tag{10.43}$$

$$m_d(\ddot{z}_b+\ddot{z}_1+...+\ddot{z}_n)+\left(m_d+J_d n_{td}{}^2\right)\ddot{z}_d+\left(c_d+B_d n_{td}{}^2\right)\dot{z}_d+k_d z_d= -n_{td}T_{ed}-m_d\ddot{y}_0 \tag{10.44}$$

The matrix equations describing the structural system without the dynamics of the regenerative electric actuator can now be modified by using the above equations.

Example 10.1

Consider the single-degree-of-freedom structure with a mass damper described in Example 4.1. In that particular example, a single-degree-of-freedom structure with a mass damper is subjected to a wind disturbance. The same wind excitation is also applied in the present simulation. A regenerative electric actuator is used to provide control to the system. It is assumed that the actuator has the following parameters: J = 0.1 kg-m^2 and B = 5.34×10^{-4} kN-sec/rad. A ball-screw with a pitch p of 3.3 mm/rev is used to couple the actuator to the damper. One can also use other types of linear-to-rotational transformations. The best efficiency will be obtained if a linear electrical machine is used as the actuator. For a ball screw mechanism, the transformation ratio is given by

$$n_t = \frac{2\pi e}{p}$$

where e is the efficiency of the ball screw.

For the 4-quadrant mode, three types of control are considered: proportional, linear quadratic, and sliding mode control. A proportional controller with a gain K = 15 is used. The LQ controller is designed using the weighting matrices $\mathbf{Q}$ = diag(2000,1,1,1) and $\mathbf{R}$ = 0.1. This results in the gain matrix $\mathbf{K} = [-108.2373 \quad 3.1268 \quad 82.6489 \quad 4.99192]$. To design the sliding mode controller, the quadratic minimization method is used with $\mathbf{Q}$ = diag(2000,1,1,1). This results in $\Psi = \mathbf{SA} = [26.0162 \quad 0.4202 \quad 34.0752 \quad -0.9640]$. With the wind excitation being characterized by the parameters p = 9.75 kips and ω = 1.0 rad/sec, Fig. 10.5 shows a comparison the resulting displacements for the different types of control.

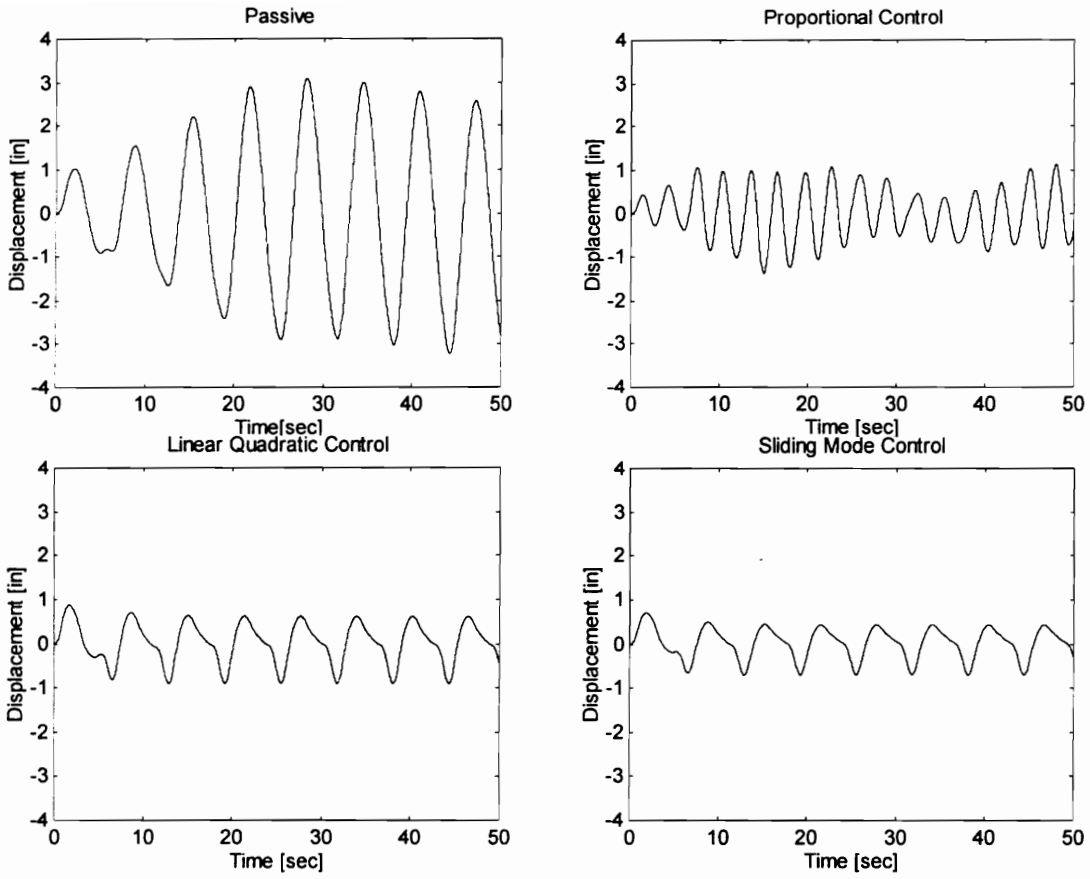

Fig. 10.5 Comparison of displacements for various types of control

If no control is applied, the plot for the passive system is obtained. Fig. 10.5 shows that all three controllers are able to produce remarkable reductions in the displacement. The peak displacement for proportional control occurs after several cycles of the excitation has elapsed. On the other hand, the peak displacement occurs during the first cycle for linear quadratic and sliding mode control. Table 10.1 gives a comparison of the peak responses for the three controllers.

TABLE 10.1 Comparison of Maximum Responses

CONTROL TYPE	Max. Displacement [in]	Max. Damper Stroke [in]	Max. Control Torque [kips-in]	Displacement-Control Ratio
Passive	3.2340	3.0590	0	-
Proportional	1.3654	147.6482	20.4829	0.0667
Linear Quadratic	0.9114	21.4440	3.3567	0.2715
Sliding Mode	0.6987	39.2330	2.7080	0.2580

Table 10.1 shows that sliding mode control produces the most reduction in the peak displacement of about 78%. This type of control also requires the least control torque. The longer stroke length for proportional control compared to the other types of control makes it an undesirable controller. The displacement-control ratio is the ratio of the maximum displacement over the maximum control torque. This quantity can provide one with a measure of the control's effectiveness in reducing the peak displacement. Table 10.1 shows that linear quadratic control has the best displacement-control ratio. Sliding mode control also provides a comparable control effectiveness. Based on the maximum displacement and maximum torque, sliding mode control would be a better controller due to its lower control torque requirement.

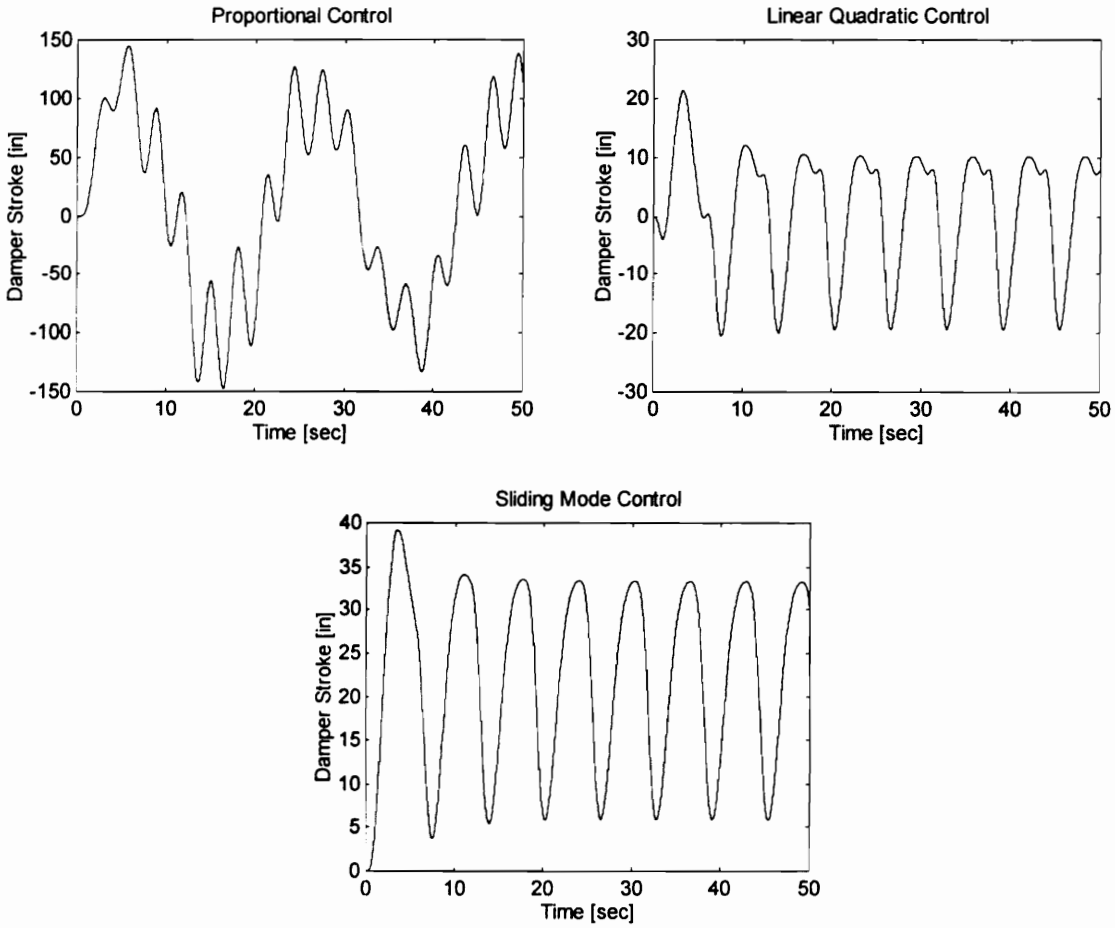

Fig. 10.6 Comparison of damper stroke lengths

Fig. 10.6 shows a comparison of the damper stroke waveforms for the different controllers. Proportional control gives the longest stroke length, while linear quadratic control yields the shortest stroke length. Sliding mode control has an unsymmetrical stroke length. This

can be attributed to the unsymmetrical switched gains used for the controller. Based on damper stroke length, linear quadratic control would be the best choice for the controller.

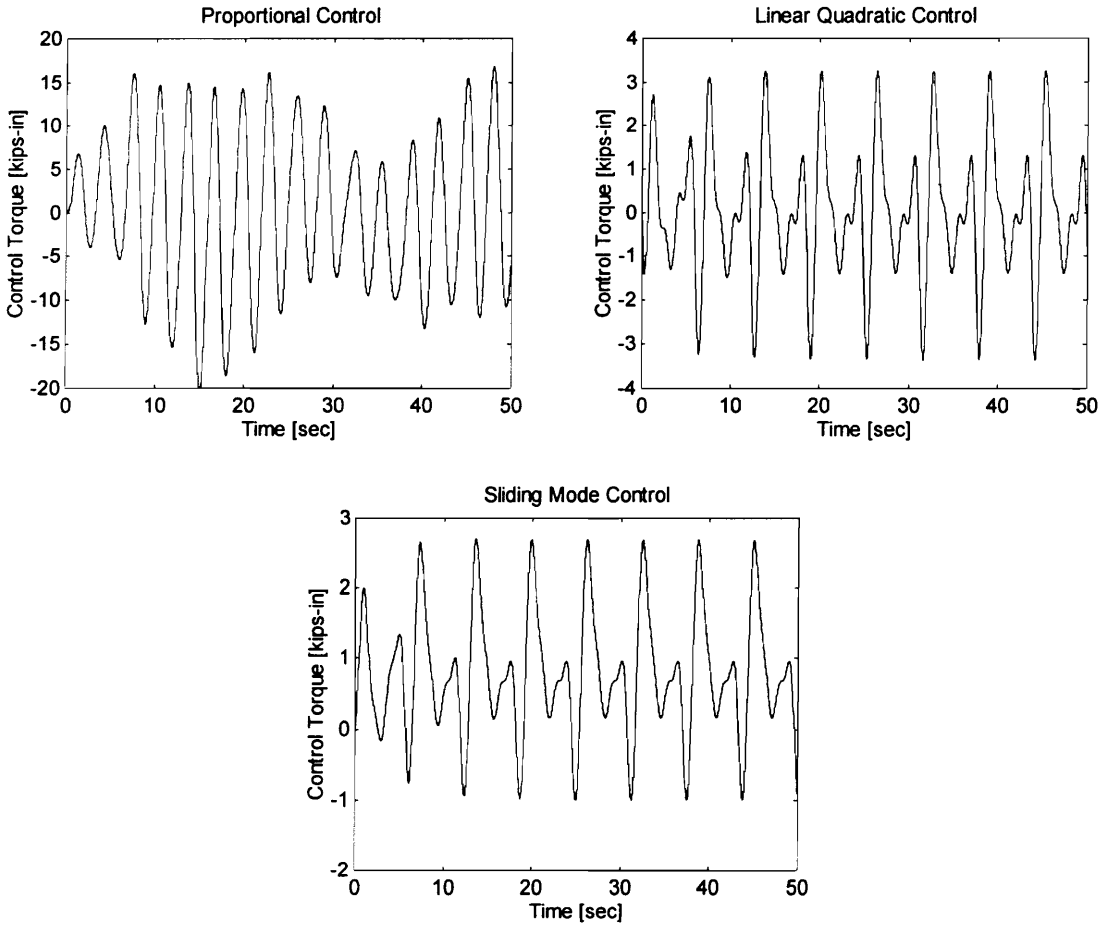

Fig. 10.7 Comparison of control torques for various controllers

Fig. 10.7 shows a comparison of the control torques required by various controllers. Proportional control requires the largest torque, while sliding mode requires the least amount of control torque. Linear quadratic and sliding mode control have similar torque waveforms due to the use of the same **Q** weighting matrix.

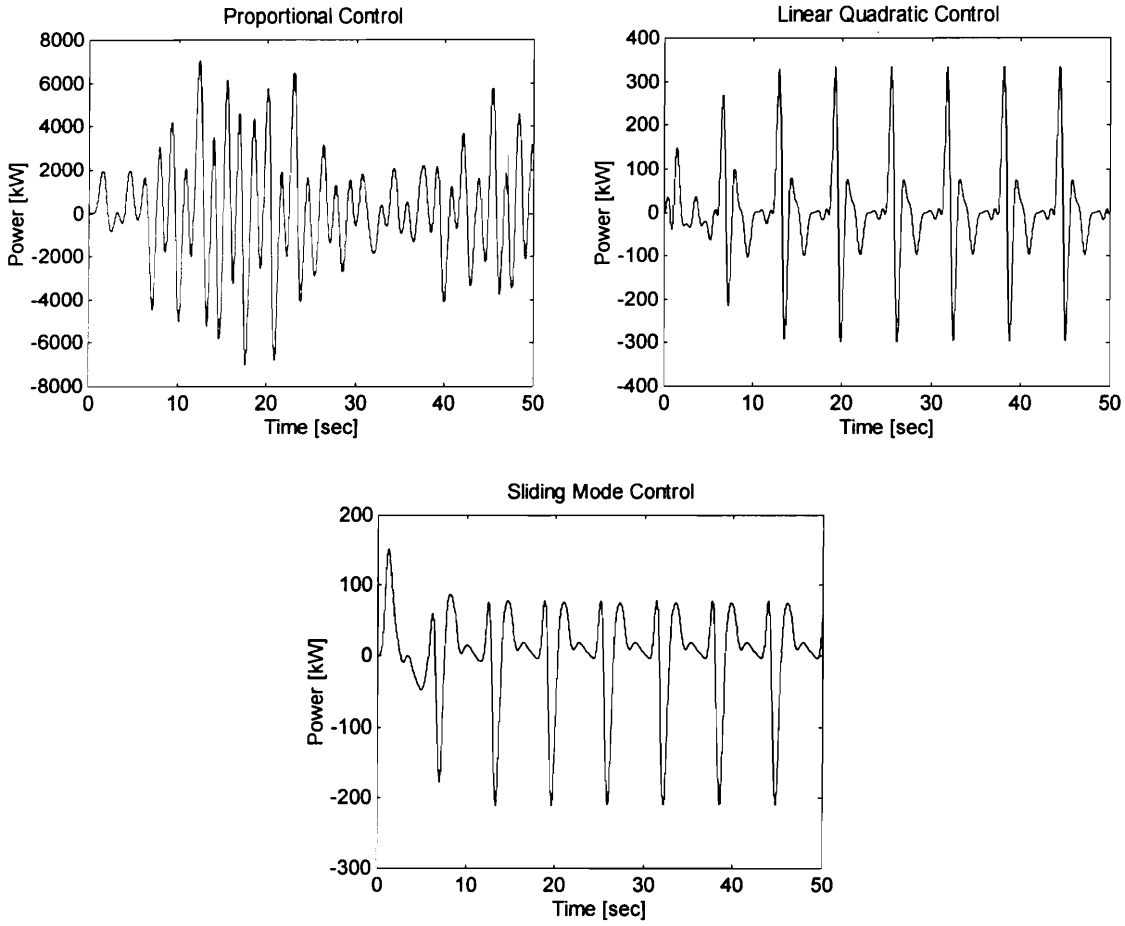

Fig. 10.8 Comparison of actuator powers for various controllers

Fig. 10.8 shows a comparison of the instantaneous power being provided by the regenerative actuator for the three control types. Note that there are periods of negative power. These correspond to periods of regeneration while the actuator is being operated in the 4-quadrant mode. Due to the large control torques required by the proportional controller, the resulting power requirement is also substantial. The sliding mode controller requires the least control torque and hence, the least power for the actuator. Therefore, the actuator rating for this type of control will also be smaller. Based on the required rating for the actuator, the sliding mode controller will be the better choice.

Fig. 10.9 shows the net energy drawn from the source for the three types of control. The upper curve is a plot of the energy drawn if there is no regeneration. The lower curve is a plot of the net energy drawn from the source with regeneration, i.e., with the use of a regenerative electric actuator. Without regeneration, the energy is dissipated as heat by a non-regenerative actuator during the periods of negative power.

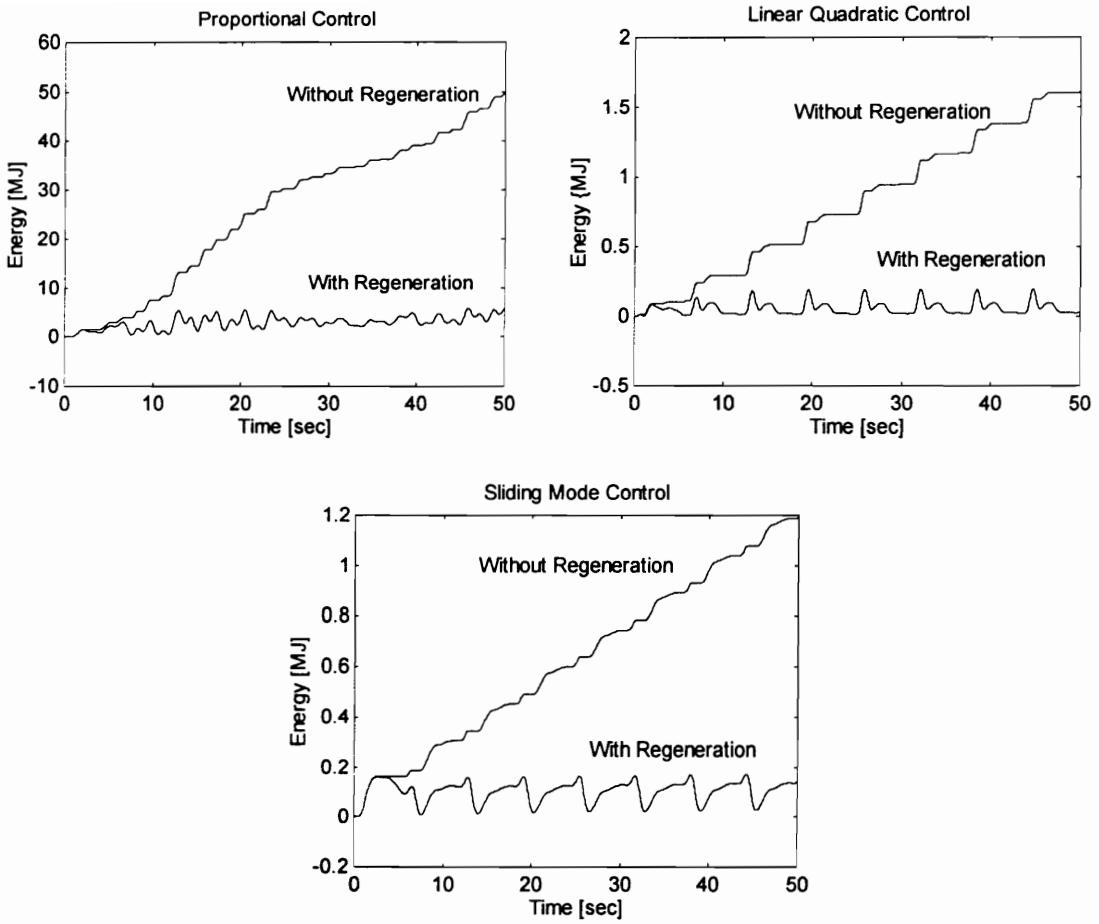

Fig. 10.9 Comparison of actuator energy with and without regeneration for various controllers

The large control forces required by the proportional controller make its energy requirement also enormous. With regeneration, there is an 88% reduction in the peak energy requirement for proportional control during the given 50-second duration of the disturbance. Linear quadratic control also achieves an 88% reduction in the energy peak during the given duration, while sliding mode control produces an 86% reduction. Note that a longer duration of the disturbance will allow more recovery of energy and will result in greater percentage reduction in the energy peak. A lower energy peak translates into a lower energy capacity for the electrical source. Therefore, regeneration reduces the required energy capacity of the electrical supply. Among the three controllers, sliding mode control will be the best choice since it requires the least energy for the actuator.

Example 10.2

The single-degree-of-freedom structure and regenerative actuator described in Example 10.1 is operated in the 2-quadrant generation mode. A wind excitation characterized by p = 5 kips and ω = 1.1 rad/sec. is assumed to be acting on the structure. During regeneration, a torque command is specified. This torque command will determine the amount of energy that is recovered. For a torque command of 5.65 kN-m, the resulting displacement, actuator power, and actuator energy are shown in Figs. 10.10, 10.11, and 10.12.

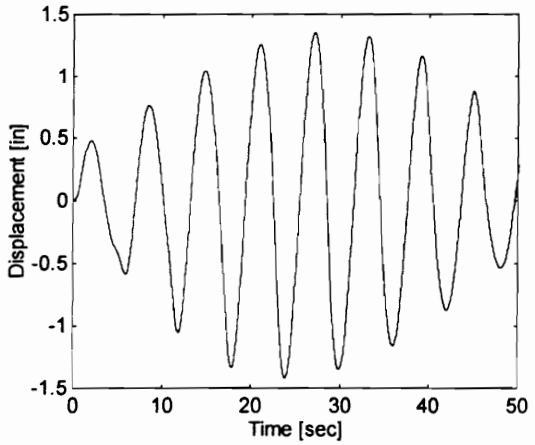

Fig. 10.10 Displacement with regeneration

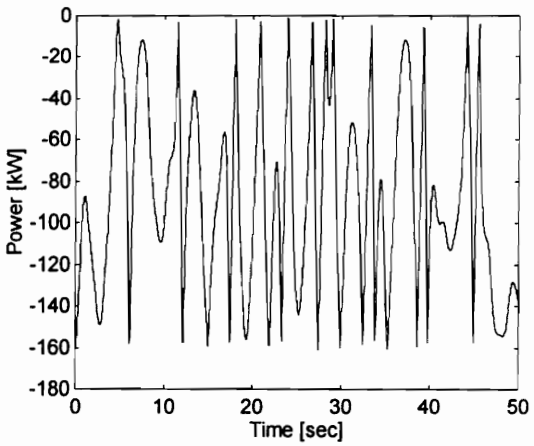

Fig. 10.11 Actuator power during regeneration

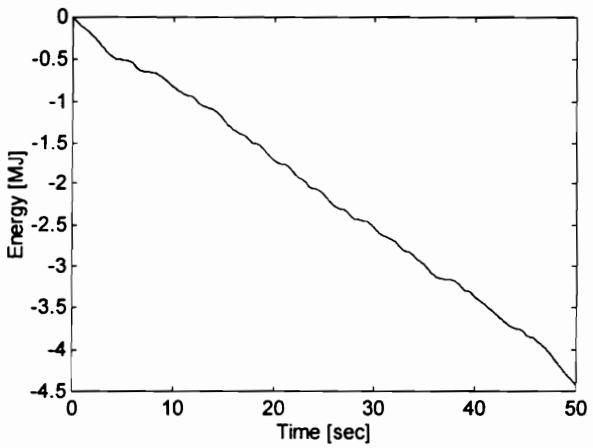

Fig. 10.12 Recovered energy during regeneration

The displacement shown in Fig. 10.10 is assumed to be well within the safety limits of the structure. This criterion has to be satisfied before the actuator is operated in generation mode. Other criteria, like maximum acceleration, can also be specified. The peak power in Fig. 10.11 will be determined by the rating of the actuator. A higher power rating for the actuator means

that a higher torque command can be specified. This also means that more energy as shown in Fig. 10.12 can be recovered. The maximum amount of energy that can be recovered is determined by the capacity of the storage device. Therefore, the amount of energy has to be monitored in order that the storage capacity is not exceeded.

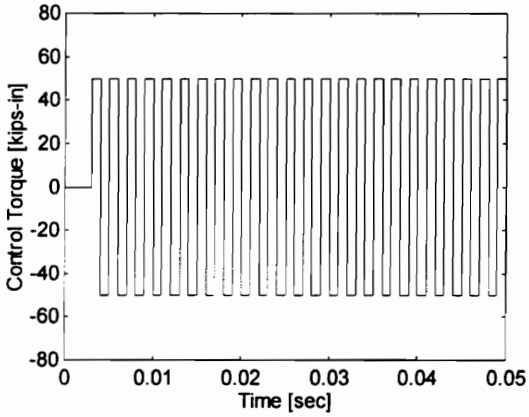

Fig. 10.13 Control torque during regeneration

Fig. 10.13 shows the control torque required for regeneration. The polarity of the control torque is determined by the polarity of the stroke velocity. The commanded torque is not necessarily the optimum value which will mitigate the structure's motion. That is why it is necessary to monitor the structure's response to make sure that it is always within safety limits.

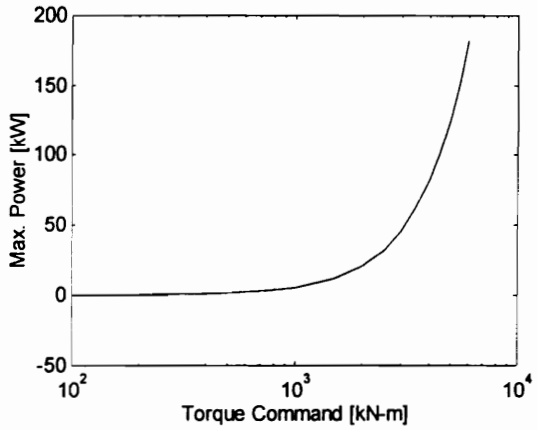

Fig. 10.14 Effect of torque command on the maximum power

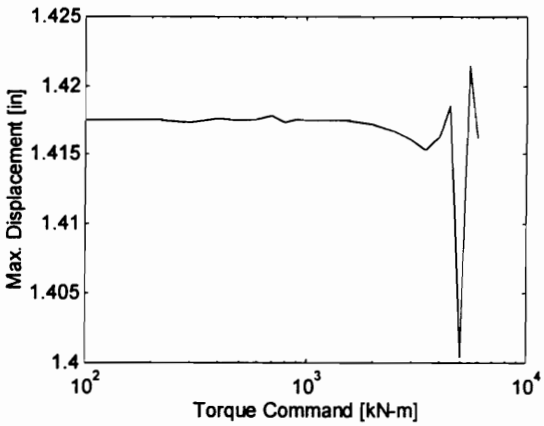

Fig.10.15 Effect of torque command on the maximum displacement

Figs. 10.14 and 10.15 show the maximum power and maximum displacement as a function of the torque command. For a given actuator rating, Fig. 10.14 gives the corresponding limit on the torque command that can be issued. To increase the amount of energy that is recovered, the torque command can be increased in order to increase the power. The maximum

power and energy will be determined by the power rating of the actuator and the energy capacity of the storage device. For the given range of torque commands, the maximum displacement shown in Fig. 10.15 is more or less constant and unaffected by the torque command. These simulations assume that the actual torque follows the torque command closely. Otherwise, there will be periods of positive power when the polarity of the torque is the same as the polarity of the velocity (motoring action). This will decrease the amount of recovered energy.

Example 10.3

The structural system and regenerative actuator described in Example 10.1 is operated in 4-quadrant mode while under an earthquake excitation with a peak acceleration of 17.53 in/sec^2. The shape of the earthquake excitation is as given in Fig. 3.14. The linear quadratic and sliding mode controllers designed in Example 10.1 are also used in this simulation. Fig. 10.16 shows a comparison of the resulting displacement for these two types of control.

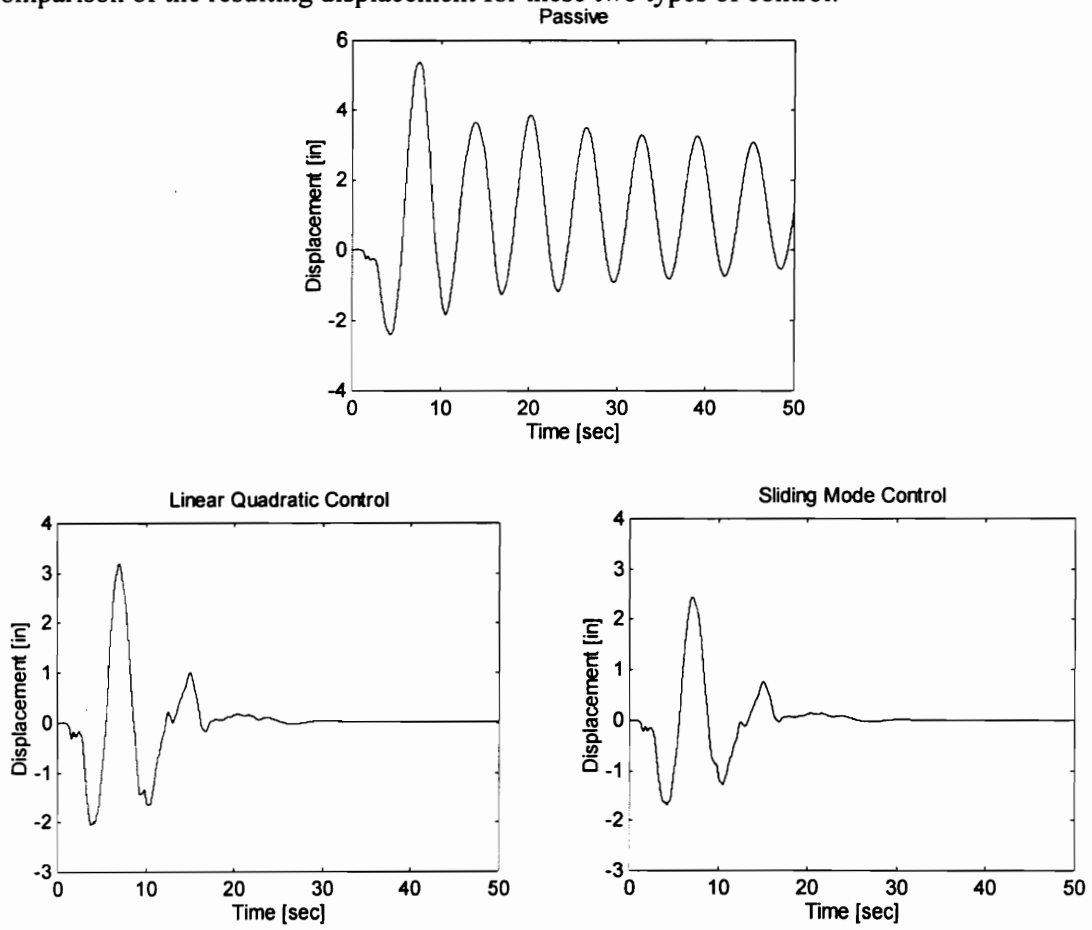

Fig. 10.16 Comparison of displacements for different types of control

Without any form of active control, the displacement shown for the passive case will be obtained. Fig. 10.13 shows that in the passive case it takes a relatively long time for the displacement to decay to zero if no active control is applied. If control is applied, these displacement decay to zero in approximately 30 seconds. The resulting displacements for linear quadratic and sliding mode control have basically the same shape, except for the peak values. This can be attributed to the use of the same weighting matrix **Q** in both methods. A comparison of the peak response values is given in Table 10.2

TABLE 10.2 Comparison of Maximum Responses

CONTROL TYPE	Max. Displacement [in]	Max. Damper Stroke [in]	Max. Control Torque [kips-in]	Displacement-Control Ratio
Passive	5.3970	7.4091	0	-
Linear Quadratic	3.2060	73.8032	33.0407	0.0970
Sliding Mode	2.4501	100.9051	5.6919	0.4305

Sliding mode control is able to achieve a larger reduction in the peak displacement. There is a 55% reduction in the peak, while linear quadratic control reduces the peak displacement by only 41%. However, there is a 1262% increase in the stroke length for sliding mode control, as compared to 896% for linear quadratic control, with both increases being measure with respect to the damper stroke for passive control. Despite the longer stroke length, sliding mode control requires a very much smaller control torque. This is reflected in the displacement-control ratio. Thus, sliding mode control is more effective in reducing the peak displacement. Based on the maximum displacement and control torque, sliding mode control will be a better choice for the controller.

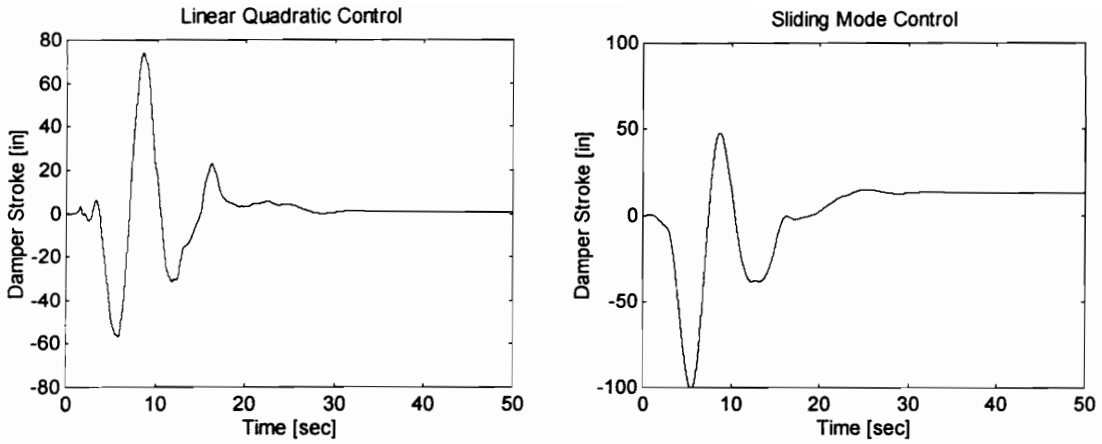

Fig. 10.17 Comparison of damper stroke lengths for the two controllers

Fig. 10.17 shows a comparison of the damper stroke lengths for the two controllers being considered. The peak damper stroke for linear quadratic controller occurs during negative displacement, while peak damper stroke for the sliding mode controller occurs during positive displacement. Based on stroke lengths, both controllers have approximately the same performance.

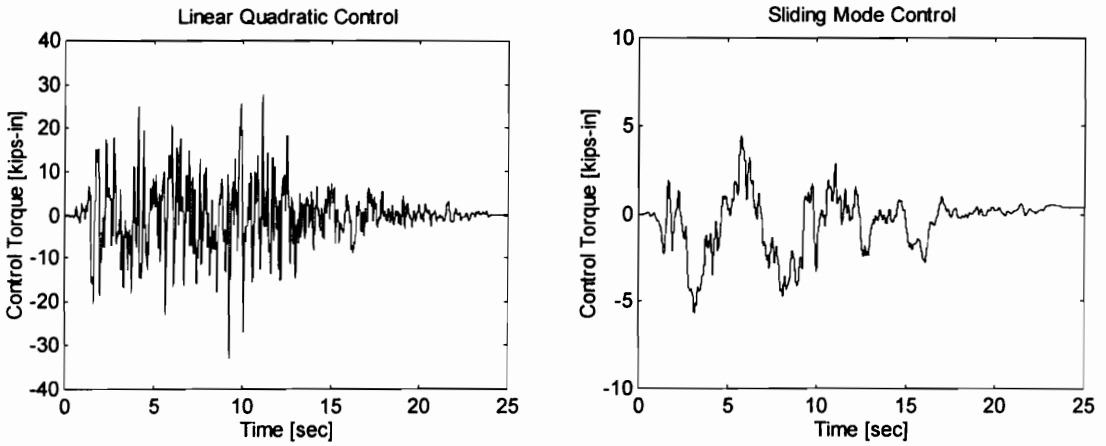

Fig. 10.18 Comparison of control torques for the two controllers

A comparison of the control torque required by the two controllers being considered is shown in Fig. 10.18. The control torque for linear quadratic control is larger than that for sliding mode control. It also has more high-frequency components. Based on the control torque, the sliding mode controller is better because it requires a smaller magnitude of torque and a smoother torque waveform.

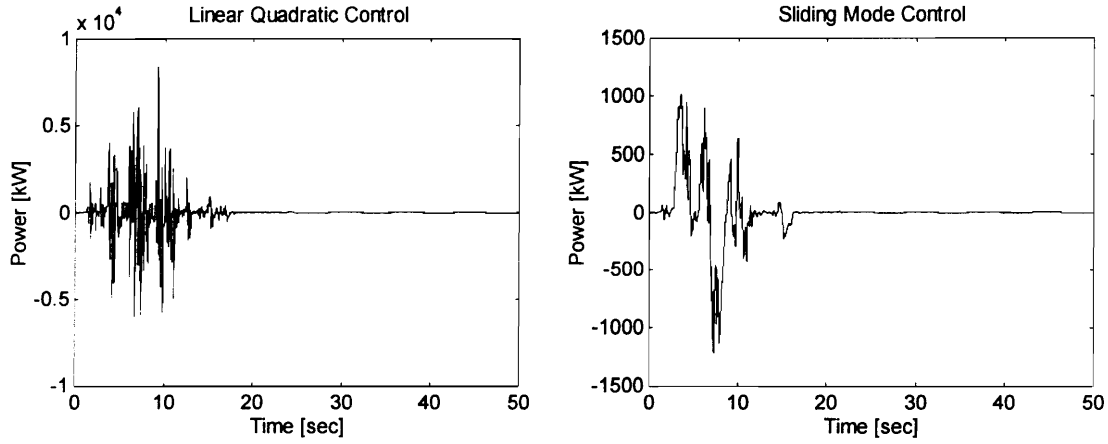

Fig. 10.19 Comparison of actuator powers

Fig.10.19 shows a comparison of the instantaneous actuator power for both types of control. Periods of negative power allow the actuator to regenerate. The larger control torque required by the linear quadratic controller result in a larger power consumption. The smaller power requirement for sliding mode control will allow the use of an actuator with a smaller power rating. Therefore, a sliding mode controller is the better choice based on actuator power rating.

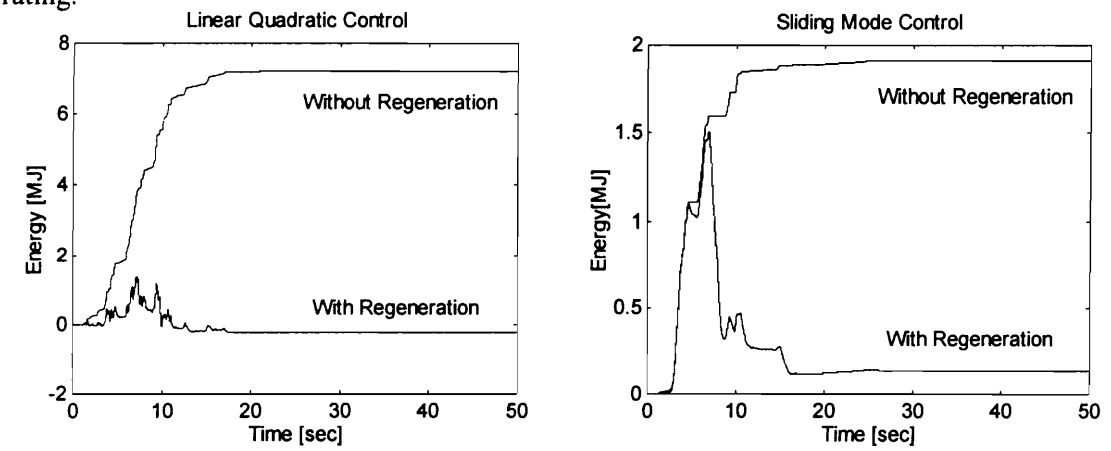

Fig. 10.20 Comparison of actuator energy with and without regeneration for two controllers

Fig. 10.20 shows a plot of the actuator energy with and without regeneration for the two types of control. The upper plot is the energy drawn from the electrical source if there is no regeneration. The lower plot is the energy drawn from the source when a regenerative electric actuator is used. Due to the higher control torques required by the linear quadratic controller, the energy requirement is also higher as compared to that of the sliding mode controller. For the given disturbance duration of 50 seconds, linear quadratic control produces an 81% reduction in

the peak energy requirement. Sliding mode control reduces the maximum energy by only 22%. Since the peak energy requirements are approximately the same for both controllers with a regenerative actuator, either controller can be used if the choice is solely based on the required energy capacity of the electrical source and storage device.

Example 10.4

The single-degree-of-freedom system is operated in 2-quadrant generation mode while being subjected to an earthquake excitation with a peak acceleration of 8.76 in/sec^2. The excitation has the same shape shown in Fig. 3.14. For a torque command of 1000 kN-m, the resulting displacement, actuator power, and actuator energy are shown in Figs. 10.21 , 10.22, and 10.23.

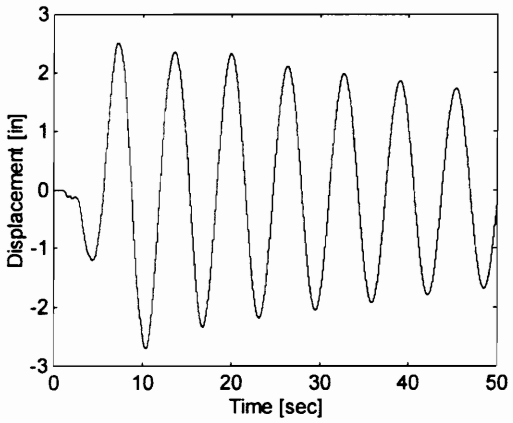

Fig. 10.21 Displacement with regeneration

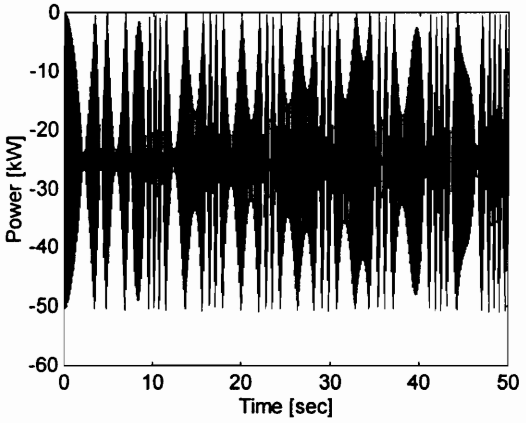

Fig. 10.22 Actuator power with regeneration

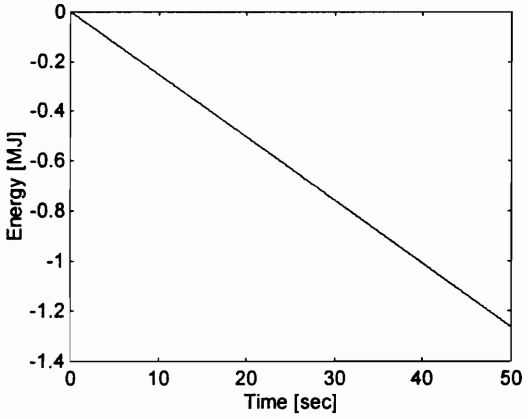

Fig. 10.23 Recovered energy with regeneration

It is assumed that the displacement shown in Fig. 10.21 is within the safety limits of the structure. Additional criteria can be imposed for regeneration to insure that structural integrity and occupant comfort are maintained. The peak power that can be attained in Fig. 10.22 is determined by the torque command. The amount of energy recovered is, in turn, dependent on the power that can be handled by the actuator. The power rating of the actuator will determine the maximum torque command that can be given. The energy capacity of the storage device will limit the amount of energy that can be recovered.

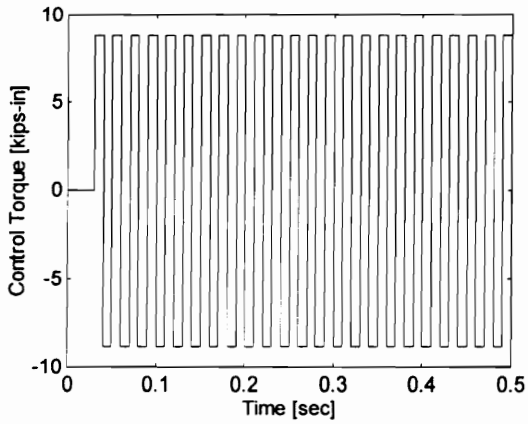

Fig. 10.24 Control torque during regeneration

Fig. 10.24 shows the required control torque for 2-quadrant regeneration. The polarity of the torque command is opposite to the polarity of the stroke velocity. The structure's response has to be constantly monitored because the control torque is not necessarily the optimum value for response mitigation.

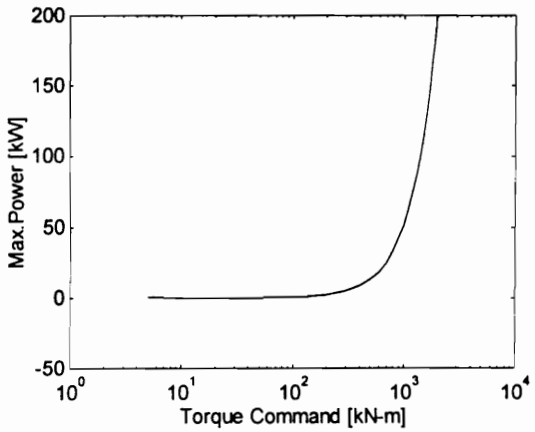

Fig. 10.25 Effect of torque command on the maximum power

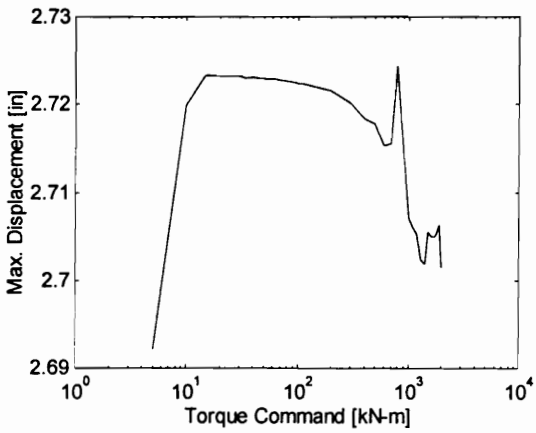

Fig.10.26 Effect of torque command on the maximum displacement

For the given system and excitation, Fig. 10.25 shows the relationship between the maximum power and the torque command. Fig.10.26 shows the effect of the torque command on the maximum displacement. The actuator power can be increased by increasing the torque command. The maximum torque command will be determined by the power rating of the actuator. In addition, the safety limits have to be continuously satisfied in order to keep on regenerating. The accumulated energy have to be monitored in order not to exceed the capacity of the storage device. For the given range of torque commands, the maximum displacement appears to have minimal variation. Choosing a torque command below 10 kN-m or above 1000 kN-m yields lower peak-displacements.

Example 10.5

Consider the fixed-base, multidegree-of-freedom system described in Example 4.3. A regenerative electric actuator with parameters J = 3 kg-m^2 and B = 0.01688 N-m/rad/sec is used to provide active control to the structure. The same wind excitation used in Example 4.3 is used in the present simulation for 4-quadrant mode. Three controller types are considered: proportional, linear quadratic, and sliding mode. The proportional controller uses a gain K = 40 on the displacement of the 8th floor with respect to the ground. The linear quadratic controller is designed by using the weighting matrices

$$\mathbf{Q} = \begin{bmatrix} 5\mathbf{I}_{8\times 8} & \mathbf{0}_{8\times 10} \\ \mathbf{0}_{10\times 8} & \mathbf{0}_{10\times 10} \end{bmatrix} \qquad \mathbf{R} = 0.0001$$

The sliding mode controller is designed by using the quadratic minimization method with the weighting matrix chosen as

$$\mathbf{Q} = \begin{bmatrix} 100\mathbf{I}_{9\times 9} & \mathbf{0} \\ \mathbf{0} & \mathbf{I}_{9\times 9} \end{bmatrix}$$

TABLE 10.3 Comparison of Maximum Responses

CONTROL TYPE	Max. Interstory Drift [cm]	Max. Damper Stroke [cm]	Max. Control Torque [kN-m]	Displacement-Control Ratio	Max. Power [kW]
Passive	2.1351	11.2405	0	-	0
Proportional	1.7066	88.1034	4.3355	0.3936	1394.5
Linear Quad.	1.4738	69.8386	4.4434	0.3317	954.8924
Sliding Mode	1.8850	3.6047	1.6739	1.1261	0.2080

Table 10.3 gives a comparison of the maximum responses for the different control types. Linear quadratic control gives the largest reduction in the peak displacement of 31%. However, it requires the largest control torque. In terms of control effectiveness, sliding mode control has the highest displacement-control ratio because it has the lowest control torque. The low control torque also makes the required power rating for the actuator a low value. Furthermore, sliding mode control reduces the damper stroke instead of increasing it. Based on the maximum responses, sliding mode control provides the best results. Its only drawback is the higher interstory drift.

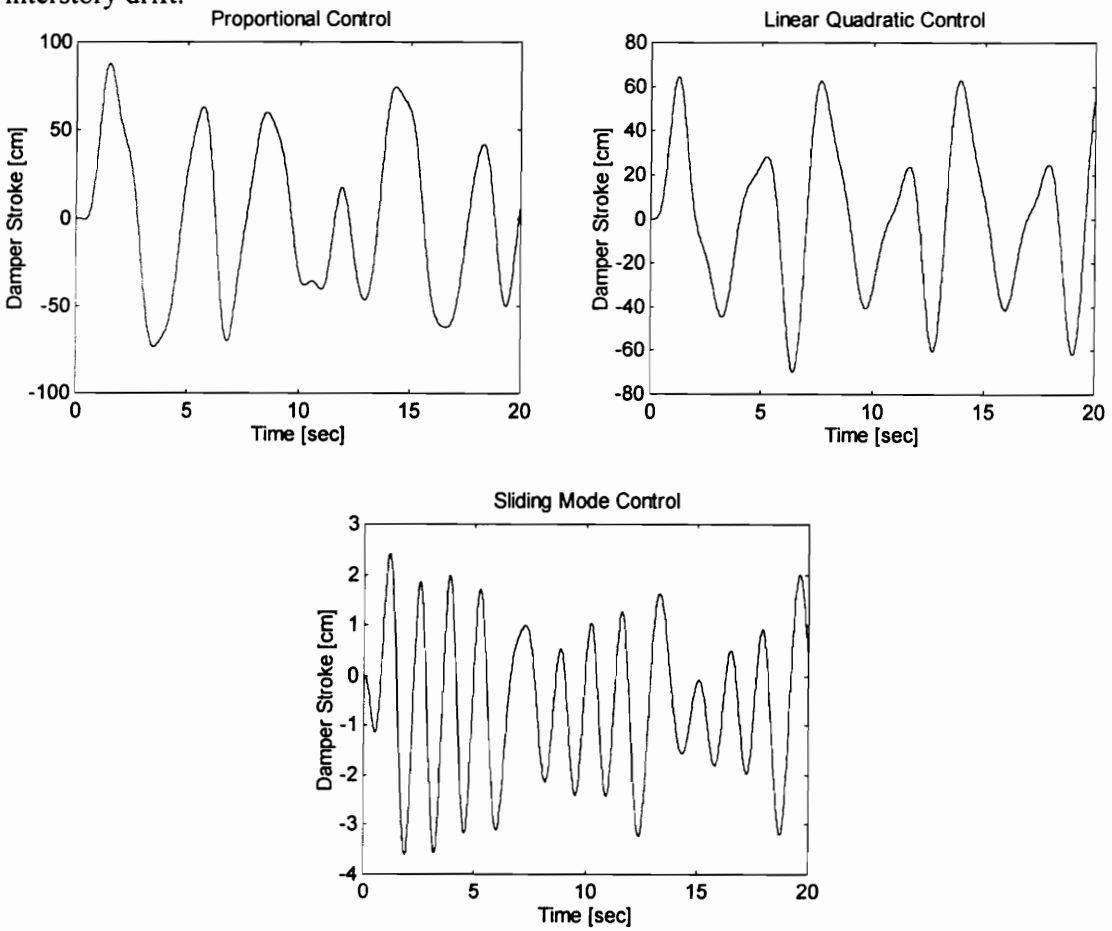

Fig. 10.27 Damper stroke lengths for various controllers

Fig. 10.27 compares the damper stroke lengths for the three controllers being considered. Proportional control has the longest stroke length, while sliding mode control has the shortest stroke length. Therefore, sliding mode control would be the better controller for having the shortest stroke length.

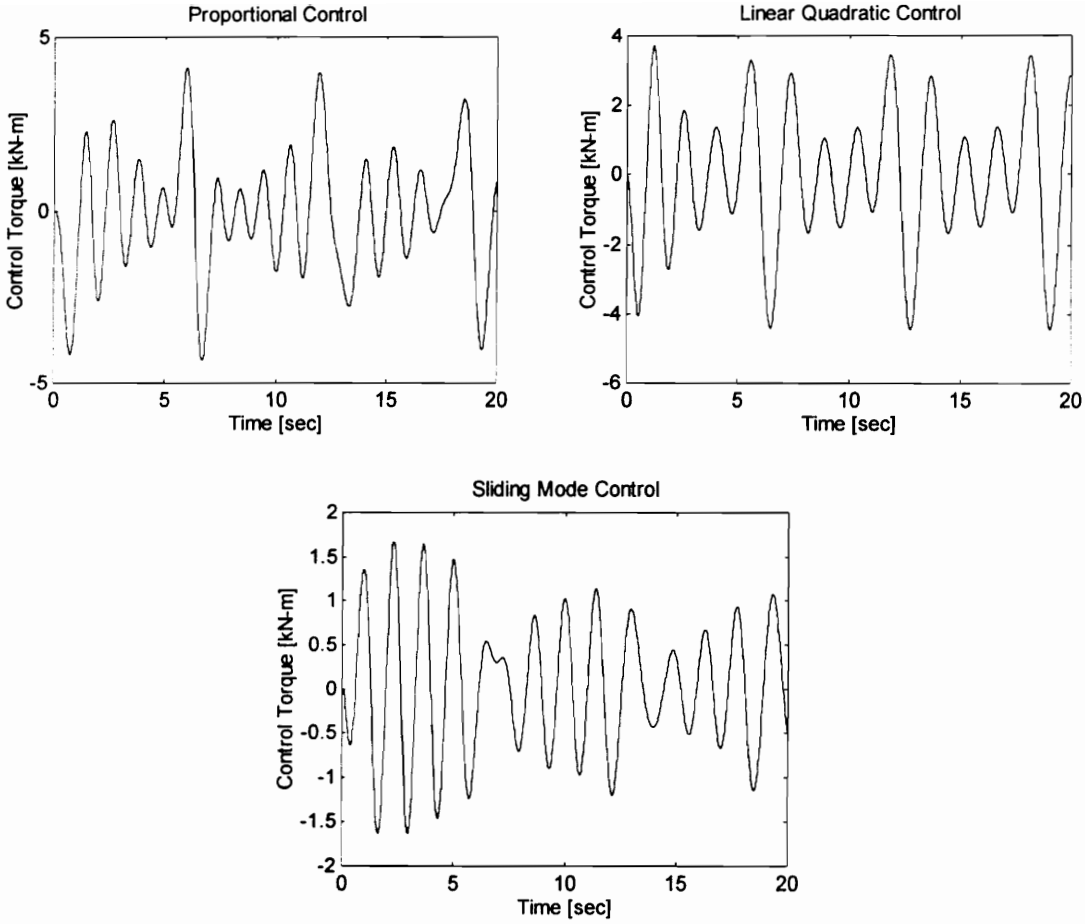

Fig. 10.28 Comparison of control torques for various controllers

Fig. 10.28 shows a comparison of the required control torque for various controllers. Proportional control requires the most amount of control torque, while sliding mode control uses the least amount of control torque. Although the torque magnitudes are relatively close, sliding mode control is the better controller for having the smallest torque requirement.

Fig. 10.29 shows a comparison of the energy requirement for the different controllers. The upper curve corresponds to the energy requirement without regeneration, while the lower curve is obtained when a regenerative actuator is used.

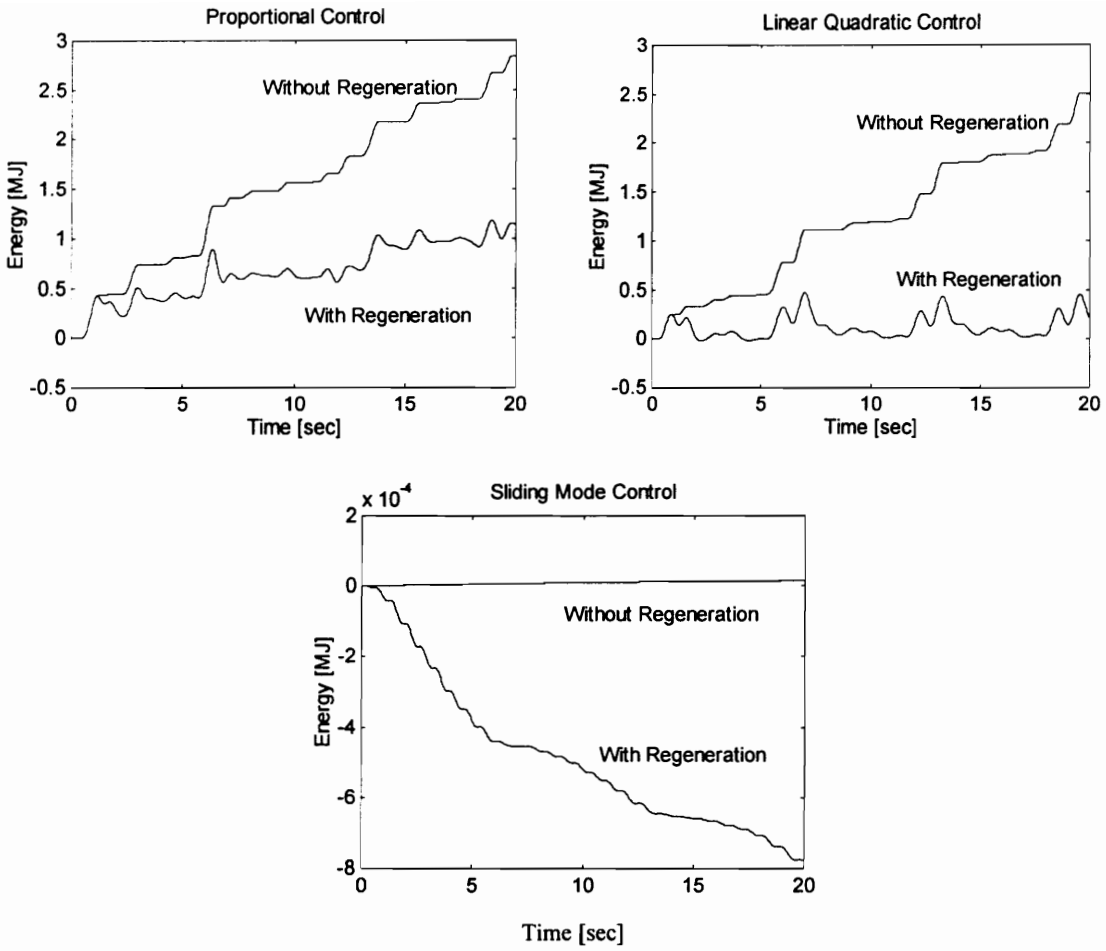

Fig. 10.29 Comparison of actuator energy with and without regeneration for various controllers

Fig. 10.29 shows that proportional control will require the most energy. The higher control torques for the proportional and linear quadratic controllers result in the much higher actuator energies as compared to the sliding mode controller. For 20-second duration of the disturbance, proportional control reduces the peak energy through regeneration by 58%, while linear quadratic control is able to reduce it by 81%. With sliding mode control, the actuator is most of the time regenerating. The small control torque required by sliding mode control makes the required energy small, too. Therefore, sliding mode control will provide the best control based on a smaller power rating of the actuator and a smaller capacity for the electrical source.

Example 10.5

Consider the base-isolated, multidegree-of-freedom system described in Example 4.4. A regenerative electric actuator with parameters J = 3 kg-m^2 and B = 0.01688 N-m/rad/sec is used to provide active control to the structure. The same earthquake excitation used in Example 4.4 is used in the present simulation for 4-quadrant mode. Three controller types are considered: proportional, linear quadratic, and sliding mode. The proportional controller uses a gain K = 2 on the displacement of the base floor with respect to the ground. The linear quadratic controller is designed by using the weighting matrices

$\mathbf{Q}$ = diag(1,300,1,...,1) $\mathbf{R}$ = 0.0001

The sliding mode controller is designed by using the quadratic minimization method with the weighting matrix chosen as

$\mathbf{Q}$ = diag(1,6,1,...,1)

TABLE 10.4 Comparison of Maximum Responses

CONTROL TYPE	Max. Interstory Drift [cm]	Max. Base Displacement [cm]	Max. Damper Stroke [cm]	Max. Control Torque [kN-m]	Displacement-Control Ratio	Max. Power [kW]
Passive	0.5591	11.9108	36.7615	0	-	0
Proportional	0.5468	11.5771	49.6540	0.2315	2.3620	0.1221
Linear Quad.	0.5019	10.9518	66.1756	14.1020	0.0356	13.3137
Sliding Mode	0.5388	11.6605	28.2114	1.2125	0.4444	0.3933

Table 10.4 gives a comparison of the maximum responses for the different control types. Linear quadratic control gives the largest reduction in the peak displacement of 10%. However, it requires the largest control torque. In terms of control effectiveness, proportional control has the highest displacement-control ratio because it has the lowest control torque. The low control torque also makes the required power rating for the actuator a low value. Sliding mode control reduces the damper stroke instead of increasing it. Based on the maximum responses, sliding mode control provides the best results. Its only drawback is the higher interstory drift.

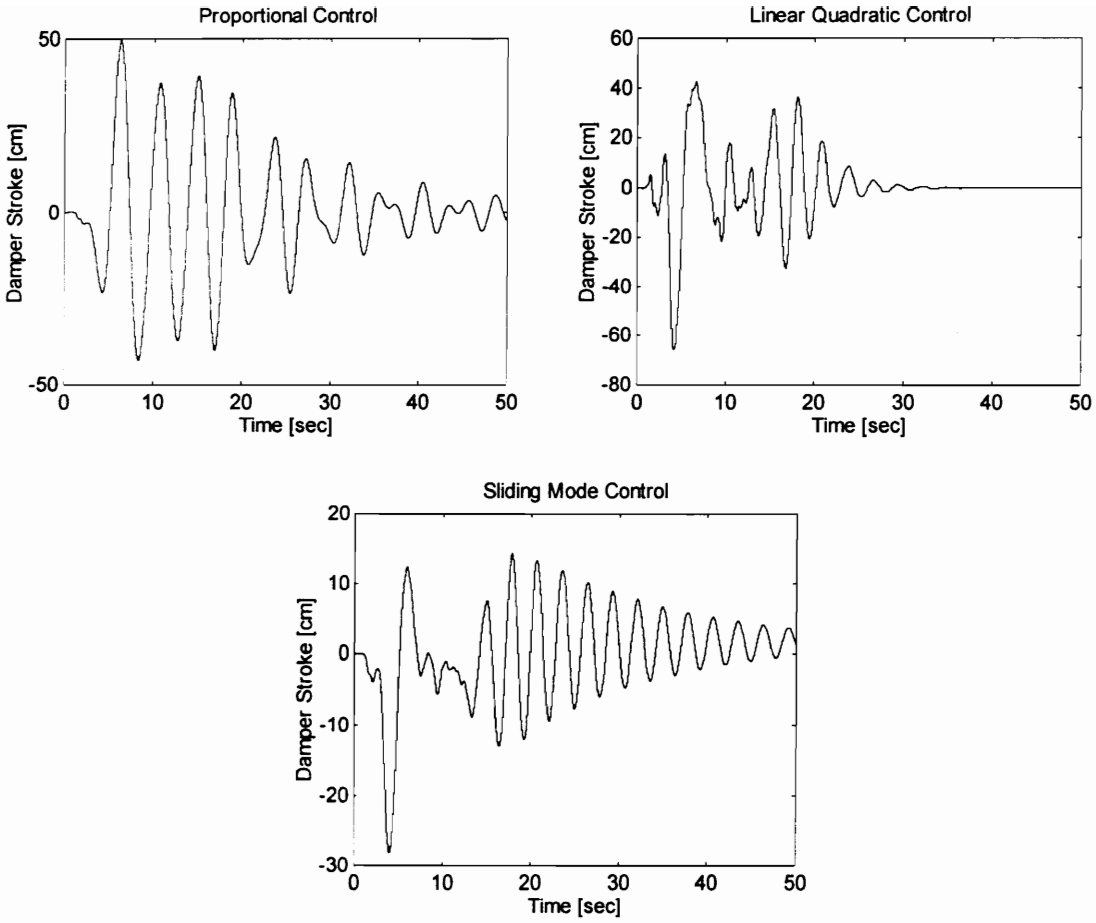

Fig. 10.30 Comparison of damper strokes for the three controllers

The damper stroke lengths for the three controllers being considered are compared in Fig. 10.30. Proportional control has the longest stroke, while sliding mode control yields the shortest stroke length. However, linear quadratic control produces the fastest decay in the damper displacement. Based on stroke length, either a linear quadratic or a sliding mode controller will provide the better performance.

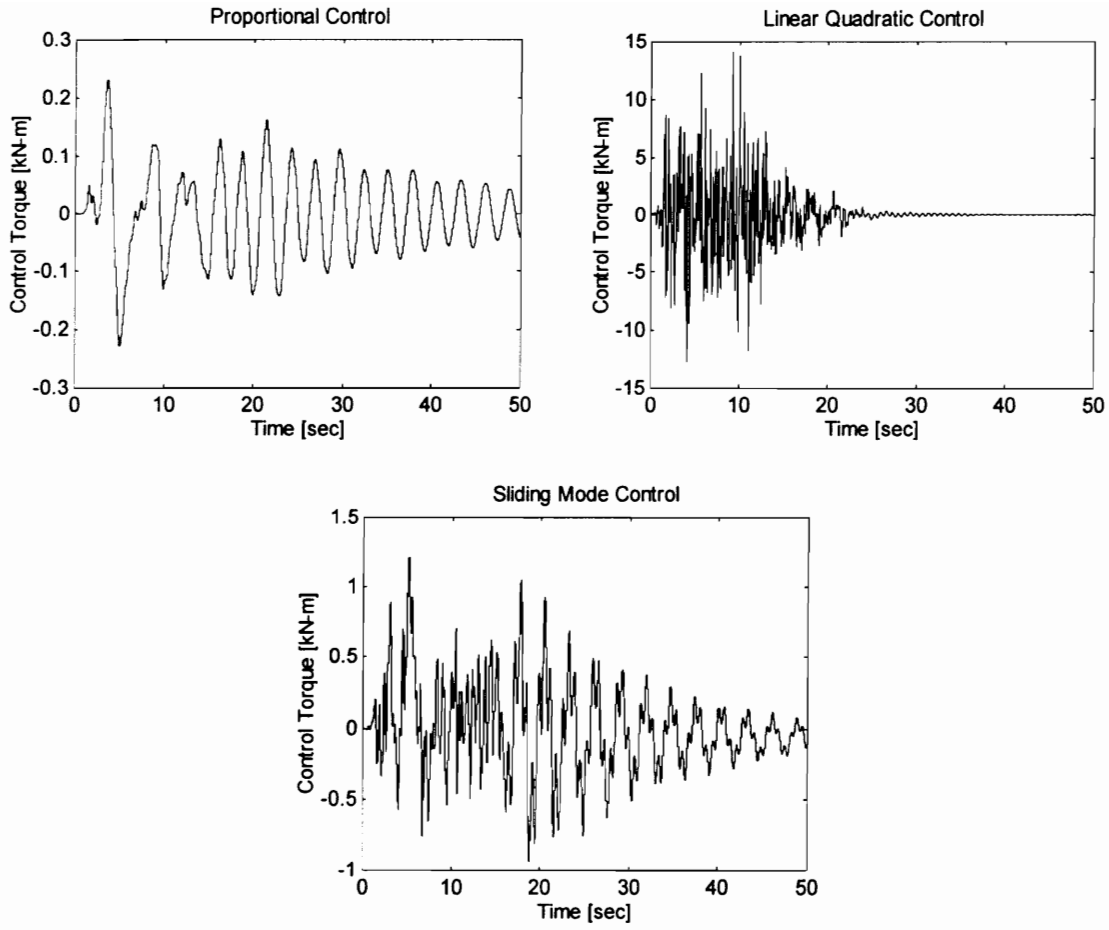

Fig. 10.31 Comparison of control torques for the three controllers

A comparison of the control torques required by the three controllers is shown in Fig. 10.31. Proportional control requires the smallest peak torque but has a slower rate of decay in the stroke length. On the other hand, linear quadratic control requires the most torque but has a faster rate of decay for the stroke length. Based on the control torque, either of the three controllers can be chosen. The choice will be compromise between smaller control torques and faster rates of decay for the stroke length.

Fig. 10.32 shows a comparison of the energy requirement for the different controllers. The upper curve corresponds to the energy requirement without regeneration, while the lower curve is obtained when a regenerative actuator is used.

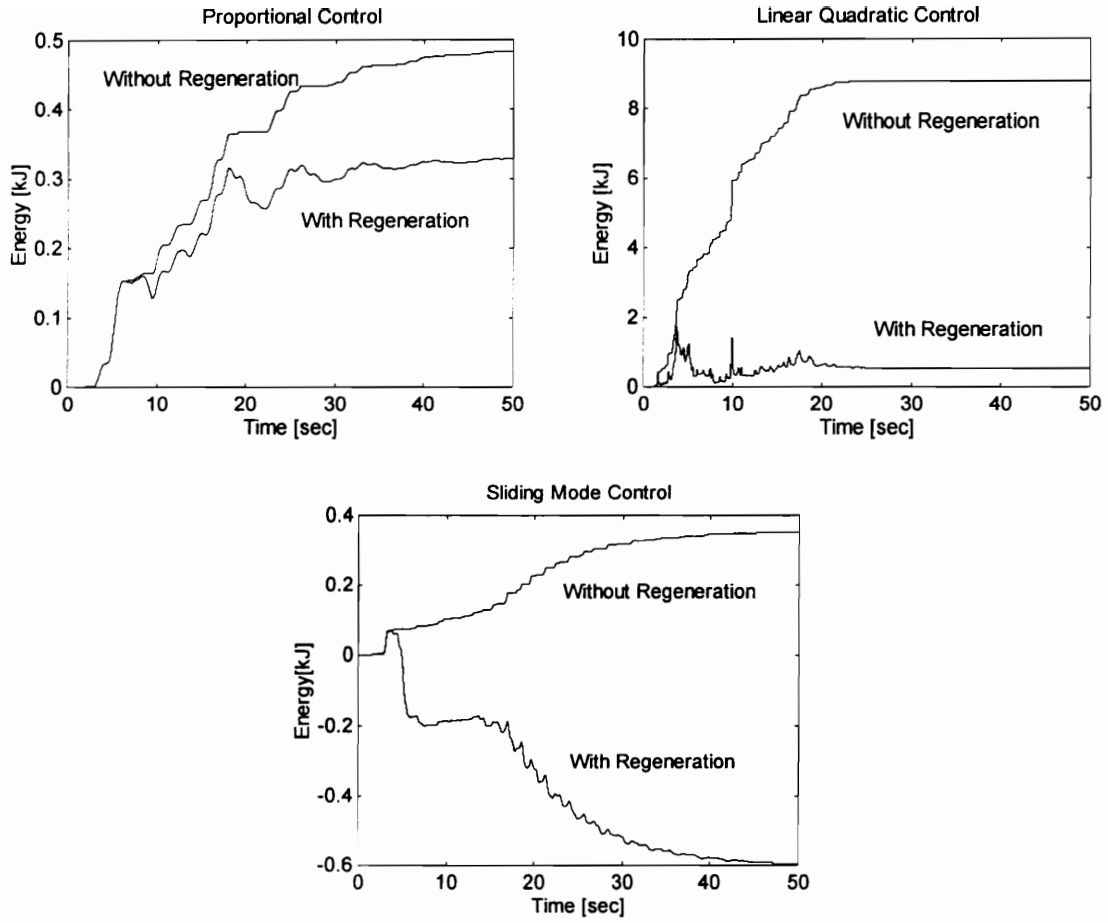

Fig. 10.32 Comparison of actuator energy with and without regeneration for different controllers

Fig. 10.32 shows that linear quadratic control will require the most energy. The higher control torques for the linear quadratic controller result in the much higher actuator energies as compared to the proportional and sliding mode controllers. For the 50-second duration of the disturbance, proportional control reduces the peak energy through regeneration by 32%, while linear quadratic and sliding mode control are able to reduce it by 80%. With sliding mode control, the actuator is most of the time regenerating. The small control torque required by sliding mode control makes the required energy small, too. Therefore, sliding mode control will provide the best control based on a smaller power rating of the actuator and a smaller capacity for the electrical source.

10.5 SELECTION OF THE ELECTRIC ACTUATOR

The use of an AC machine as the actuator is not pursued because it requires external excitation for four-quadrant operation. On the other hand, the use of a DC machine with commutators is limited by saturation and commutation problems due to the high currents. Therefore, a permanent-magnet brushless DC machine is chosen as the regenerative electric actuator (REA) because this machine-type has a higher peak-to-rated torque ratio. Furthermore, this machine has a more compact frame-size compared to other machine types. This makes it attractive for installation or retrofitting in structures with limited space. The machine can either be a rotational machine or a linear machine.

10.6 MODELING OF THE PERMANENT-MAGNET BRUSHLESS DC MACHINE

The model used in this section is based on [2]. Since the flux distribution in a PM brushless DC machine is nonsinusoidal, no advantage would be gained in using the *d-q* reference frame to formulate the machine model. Thus, the stator *a-b-c* reference frame is used. It is assumed that iron and stray losses and rotor induced-currents due to stator harmonic fields are negligible.

The voltage equations for the stator windings are given by

$$\begin{bmatrix} v_{as} \\ v_{bs} \\ v_{cs} \end{bmatrix} = \begin{bmatrix} R_s & 0 & 0 \\ 0 & R_s & 0 \\ 0 & 0 & R_s \end{bmatrix} \begin{bmatrix} i_{as} \\ i_{bs} \\ i_{cs} \end{bmatrix} + \frac{d}{dt} \begin{bmatrix} L_{aa} & L_{ab} & L_{ac} \\ L_{ba} & L_{bb} & L_{bc} \\ L_{ca} & L_{cb} & L_{cc} \end{bmatrix} \begin{bmatrix} i_{as} \\ i_{bs} \\ i_{cs} \end{bmatrix} + \begin{bmatrix} e_{as} \\ e_{bs} \\ e_{cs} \end{bmatrix} \tag{10.45}$$

where v_{as}, v_{bs}, and v_{cs} are the *a*, *b*, and *c* phase voltages, respectively, and i_{as}, i_{bs}, and i_{cs} are the *a*, *b*, and *c* phase currents, respectively. R_s is the stator phase resistance, and L_{ii} and L_{ij} are the self- and mutual inductances, respectively. Since the flux distribution in a permanent-magnet brushless DC machine is trapezoidal, the induced emf's e_{as}, e_{bs}, and e_{cs} are also trapezoidal with a peak value

$$E_p = K_b \omega_r \tag{10.46}$$

K_b is the induced-emf constant and ω_r is the electrical rotor speed. Fig. 10.33 shows the induced emf for phase *a*. Phases *b* and *c* have the same shape but shifted +120° and -120°.

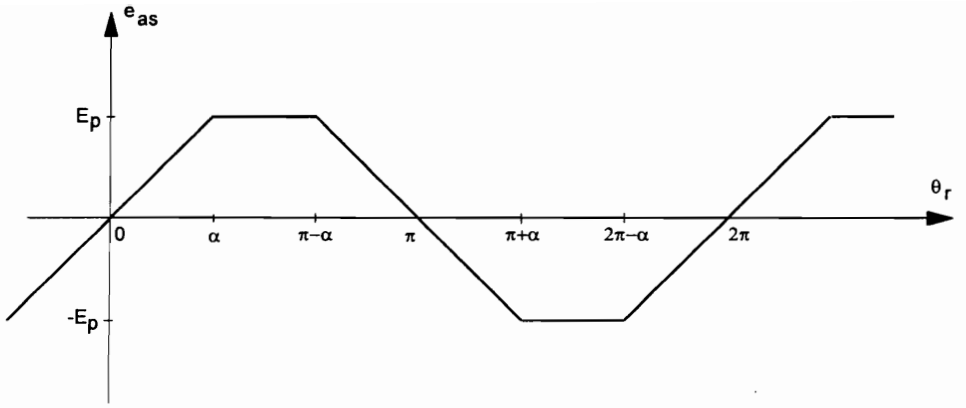

Fig. 10.33 Phase-*a* induced emf

Assuming that the rotor reluctance is independent of rotor position and that the three phases are symmetric,

$$L_{aa} = L_{aa} = L_{aa} = L \tag{10.47}$$

$$L_{ab} = L_{ba} = L_{ac} = L_{ca} = L_{bc} = L_{cb} = M \tag{10.48}$$

Substituting into the voltage equations,

$$\begin{bmatrix} v_{as} \\ v_{bs} \\ v_{cs} \end{bmatrix} = \begin{bmatrix} R_s & 0 & 0 \\ 0 & R_s & 0 \\ 0 & 0 & R_s \end{bmatrix} \begin{bmatrix} i_{as} \\ i_{bs} \\ i_{cs} \end{bmatrix} + \begin{bmatrix} L & M & M \\ M & L & M \\ M & M & L \end{bmatrix} \frac{d}{dt} \begin{bmatrix} i_{as} \\ i_{bs} \\ i_{cs} \end{bmatrix} + \begin{bmatrix} e_{as} \\ e_{bs} \\ e_{cs} \end{bmatrix} \tag{10.49}$$

Furthermore, for a 3-wire connection,

$$i_{as} + i_{bs} + i_{cs} = 0 \tag{10.50}$$

Thus, the voltage equation can be rewritten as

$$\begin{bmatrix} v_{as} \\ v_{bs} \\ v_{cs} \end{bmatrix} = \begin{bmatrix} R_s & 0 & 0 \\ 0 & R_s & 0 \\ 0 & 0 & R_s \end{bmatrix} \begin{bmatrix} i_{as} \\ i_{bs} \\ i_{cs} \end{bmatrix} + \begin{bmatrix} (L-M) & 0 & 0 \\ 0 & (L-M) & 0 \\ 0 & 0 & (L-M) \end{bmatrix} \frac{d}{dt} \begin{bmatrix} i_{as} \\ i_{bs} \\ i_{cs} \end{bmatrix} + \begin{bmatrix} e_{as} \\ e_{bs} \\ e_{cs} \end{bmatrix} \tag{10.51}$$

The electromagnetic torque can be expressed as

$$T_e = \frac{1}{\omega_m}\left[e_{as}i_{as} + e_{bs}i_{bs} + e_{cs}i_{cs}\right], \text{ N-m} \tag{10.52}$$

or

$$T_e = \frac{P}{2}\frac{1}{\omega_r}\left[e_{as}i_{as} + e_{bs}i_{bs} + e_{cs}i_{cs}\right], \text{ N-m} \tag{10.53}$$

where P is the number of poles and ω_m is the mechanical speed. The induced emf's can be expressed as,

$$e_{as} = f_{as}(\theta_r)K_b\omega_r \tag{10.54}$$

$$e_{bs} = f_{bs}(\theta_r)K_b\omega_r \tag{10.55}$$

$$e_{cs} = f_{cs}(\theta_r)K_b\omega_r \tag{10.56}$$

where $f(\theta_r)$ is a position-dependent function having the same shape as the corresponding emf but with a peak magnitude of 1. The electromagnetic torque can now be written as

$$T_e = \frac{P}{2}K_b\left[f_{as}(\theta_r)i_{as} + f_{bs}(\theta_r)i_{bs} + f_{cs}(\theta_r)i_{cs}\right] \tag{10.57}$$

The mechanical equations for the machine are given by,

$$J\frac{d\omega_r}{dt} + B\omega_r = \frac{P}{2}(T_e - T_L) \tag{10.58}$$

$$\frac{d\theta_r}{dt} = \omega_r \tag{10.59}$$

where J is the rotor moment of inertia, B is the damping coefficient, and T_L is the load torque. The electrical and mechanical equations can be combined in state-space form as

$$\dot{\mathbf{x}} = \mathbf{A}\mathbf{x} + \mathbf{B}\mathbf{u} \tag{10.60}$$

where

$$\mathbf{x} = \begin{bmatrix} i_{as} & i_{bs} & i_{cs} & \omega_r & \theta_r \end{bmatrix}^T \tag{10.61}$$

$$\mathbf{A} = \begin{bmatrix} -\frac{R_s}{L_l} & 0 & 0 & -\frac{K_b}{L_l}f_{as}(\theta_r) & 0 \\ 0 & -\frac{R_s}{L_l} & 0 & -\frac{K_b}{L_l}f_{bs}(\theta_r) & 0 \\ 0 & 0 & -\frac{R_s}{L_l} & -\frac{K_b}{L_l}f_{cs}(\theta_r) & 0 \\ \left(\frac{P}{2}\right)^2\frac{K_b}{J}f_{as}(\theta_r) & \left(\frac{P}{2}\right)^2\frac{K_b}{J}f_{as}(\theta_r) & \left(\frac{P}{2}\right)^2\frac{K_b}{J}f_{as}(\theta_r) & -\frac{B}{J} & 0 \\ 0 & 0 & 0 & 1 & 0 \end{bmatrix} \tag{10.62}$$

$$\mathbf{B} = \begin{bmatrix} \frac{1}{L_l} & 0 & 0 & 0 \\ 0 & \frac{1}{L_l} & 0 & 0 \\ 0 & 0 & \frac{1}{L_l} & 0 \\ 0 & 0 & 0 & -\frac{P}{2J} \\ 0 & 0 & 0 & 0 \end{bmatrix} \tag{10.63}$$

$$\mathbf{u} = \begin{bmatrix} v_{as} & v_{bs} & v_{cs} & T_L \end{bmatrix}^T \tag{10.64}$$

$$L_l = L - M \tag{10.65}$$

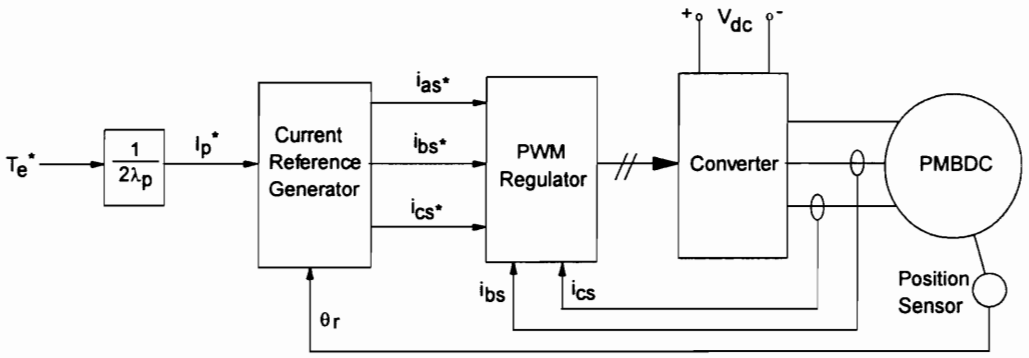

Fig. 10.34 PM brushless DC torque-drive scheme

10.7 DRIVE SCHEME FOR THE PM BRUSHLESS DC MACHINE

Fig. 10.34 shows the torque-drive scheme for the permanent-magnet brushless DC machine. This scheme is adapted from a portion of the speed-control drive described in [2]. The absolute rotor position is obtained through a position sensor. The current magnitude command I_p^* is generated from the torque command T_e^*. Then the current magnitude command and the absolute rotor position are used to generate the stator phase-current commands. These are compared with the actual phase currents to determine the current errors. Only two currents need to be measured because

$$i_{as} = -i_{bs} - i_{cs} \tag{10.66}$$

for 3-wire, three-phase systems. Pulse width modulation (PWM) or hysteresis logic is used to generate the switching logic signals for the converter switches, based on the current errors.

Regeneration is achieved by generating a torque of opposite polarity to that of motoring torque. In order to do this, the directions of the currents in the machine windings must be reversed. Hence, the emf and the phase current waveforms are in-phase during motoring and 180° out-of-phase during regeneration. In order to produce regenerating torque, the sequence in which converter switches are gated ON must be changed from that which is used during motoring.

Example 10.6

The entire system composed of the structure, mass damper, and actuator, under wind excitation, is simulated for the torque command shown in Fig. 10.35. The actuator is a 50 kW, 500 V permanent-magnet brushless DC machine. Other machine parameters are: R_s = 0.11 Ω, L_l = 50 μH, K_b = 0.24588 V-sec/rad. The PWM frequency is set at 25 kHz. The resulting electromagnetic torque is shown in Fig. 10.36.

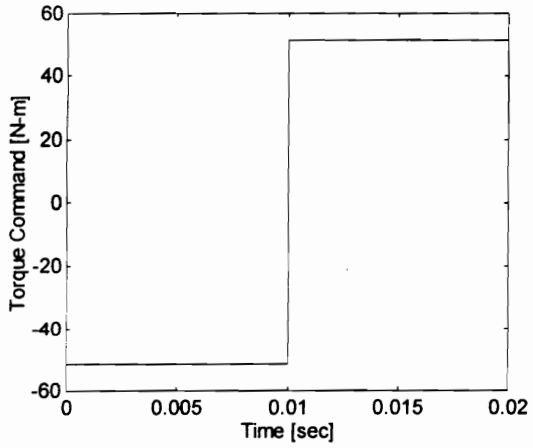

Fig. 10.35 Torque command T_e*

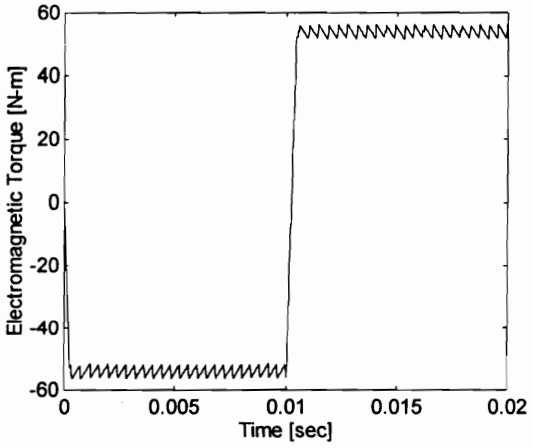

Fig. 10.36 Electromagnetic torque T_e

Thus, the assumption that the actual torque closely follows the commanded torque is validated. The torque ripple is a consequence of the PWM control of the phase currents. The rise time in the torque waveform will be dependent on the machine inductances. The phase currents are shown in Fig. 10.37.

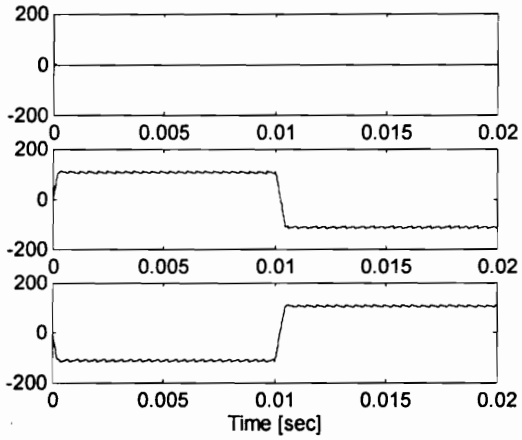

Fig. 10.37 Phase currents [A]

The phase current in phase *a* remains zero due to the rotor position. At this position the current command for phase *a* is equal to zero for either a positive or negative torque command.

10.8 TERMINAL VOLTAGE OF THE ELECTRICAL SOURCE

In all previous simulations, it has been assumed that the terminal voltage of the electrical source supplying the actuator is constant. This assumption may not be true if the power drawn by the actuator approaches the rating of the electrical source. To get a better estimate of the terminal voltage, a more accurate model of the source must be used. If a battery bank is used, it can be represented as an ideal voltage source in series with a source resistance. It should be noted that this source resistance is generally not constant and can be affected by the temperature or the operating current. The value of equivalent resistance will depend on the type of battery used. If a capacitor bank is used as a storage device, then we can model it as a capacitance in parallel with a resistance. In these applications, the capacitor bank must have a large capacitance in order to maintain the voltage near its nominal value.

Example 10.7

Consider the single-degree-of-freedom system being subjected to a wind disturbance. The same regenerative electric actuator and sliding mode controller used in Example 10.1 is also used in this simulation. Assume that the electrical source can be modeled as ideal voltage source in series with a source resistance. The source resistance is assumed to 0.1 ohm. The line current is shown in Fig. 10.38. The resulting terminal voltage of the source is given by Fig. 10.39.

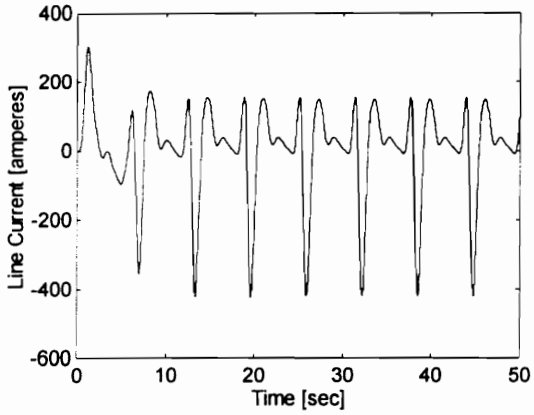

Fig. 10.38 Line current for sliding mode control

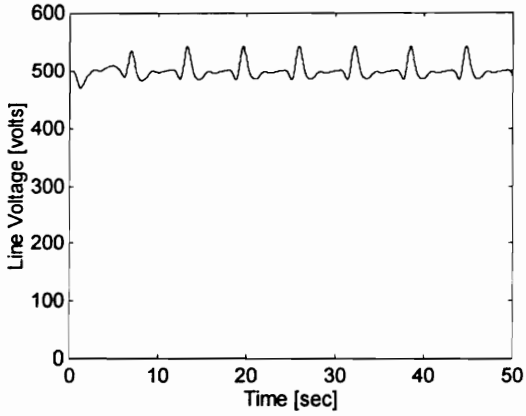

Fig. 10.39 Line voltage for sliding mode control

There is 15% peak-to-peak ripple in the terminal voltage shown in Fig. 10.39. To reduce the fluctuations in the voltage, the source resistance (or equivalent battery resistance) must be reduced by using a different type of battery or a different configuration for the battery bank. Capacitors can also be installed. During regeneration, the terminal voltage must be protected against overvoltage. If the voltage approaches the limit, then the torque command must be reduced.

10.9 SUMMARY

This chapter presents the first study of its kind to investigate active control of civil structures using regenerative electric actuators (REA). This novel technique utilizes the motion caused by environmental forces on a structure to generate electrical energy when the structure's response is within the safety limits. The rationale for this type of active control is that the utility power supply which provides power to an actuator is usually not reliable during episodes of strong winds or earthquakes. The recovered energy is used to reduce the peak oscillations of the structure by applying control forces to counter the environmental forces. To achieve this, a tuned mass damper is used as the intermediary for the energy transfer between the structure and the actuator. The electric actuator proposed for use in this scheme is a permanent-magnet brushless DC machine (PMBDC). The rationale for choosing a PMBDC for this application is provided. The combined system consisting of the structure, TMD, and actuator is simulated and analyzed for both wind and earthquake forces. Based on the results obtained, it is shown that the proposed strategy is both a viable and reliable alternative for active control of civil structures.

The actuator can either operate in the passive mode, 4-quadrant mode, or in the 2-quadrant generation mode. In the 4-quadrant mode, the performance of various controllers are

compared based on the maximum displacement, stroke, control torque, actuator power, and source energy. It is desired that the controller require a smaller actuator power rating so that the cost of the machine will be lower. A lower actuator energy is desired so that the capacity of the electrical source will be lower. Furthermore, a lower energy requirement means that a lower capacity for the energy storage device is needed. In majority of the test cases, sliding mode control often has the lowest power and energy requirement. A major advantage of using regenerative electric actuators is the reduction in the required energy capacity for the electrical source. The amount of reduction in the peak energy requirement depends on the choice for the controller. Single-degree-of-freedom and multidegree-of-freedom structures are simulated. In the 2-quadrant regeneration mode, the system response must always fall within the safety margins of the structure. The amount of energy that can be recovered is limited by the power rating of the actuator and the energy capacity of the electrical source and the storage device.

To obtain a better estimate of the transient behavior of the entire system, the dynamics of the electrical subsystem can be incorporated into actuator-structure system. It is shown that the actual torque closely follows the command torque. This is one of the advantages of using an electrical actuator, i.e., to provide accurate and controllable damping to the structure. To determine the terminal voltage of the source, the source is modeled as an ideal source behind a source resistance. More accurate models of the electrical source and storage device can also be included in the simulation to determine the variation of the voltage at the terminals of the source.

CHAPTER 11

Conclusions and Recommendations

11.1 CONCLUSIONS

A novel technique is investigated for utilizing the motion caused by environmental forces on a civil structure to generate electrical energy when the structure's response is within safety limits. When strong winds and earthquakes occur, the utility power source which supply energy to the actuator in an active control system is usually not reliable. It is during these instances that active control is needed most. With a regenerative electric actuator, the recovered energy is used to reduce the peak oscillations of the structure by applying forces (through actuators which use the recovered energy) counter to the environmental forces even if the utility power is not available. To achieve this, a tuned mass damper is used as the intermediary for the energy transfer between the structure and the actuator. The use of a regenerative electric actuator allows a precise control of the amount of damping being provided by the actuator. Another advantage of using regenerative electric actuators is the reduction of the required energy capacity of the electrical source. This translates into lower energy ratings for the electrical source, and lower equipment and maintenance costs. This study is the first of its kind to propose and investigate active control of civil structures using regenerative electric actuators.

Although no original contribution is being claimed for proportional control, it can be used as a benchmark against which controllers for the regenerative electric actuator are evaluated. The effect of variations in gain, actuator time delay, and measurement time delay on the structural response is investigated. Differences between the results of a linear and a nonlinear simulation and the effect of control force saturation are also studied.

For wind excitation, it is shown that proportional feedback control can provide effective control. However, the reduction in the structure's displacement is accompanied by an increase in the control force and the stroke length. The use of feedback control generally reduces the damping of the mass damper which, in turn, increases the stroke length. A certain amount of gain variation can be tolerated without any significant increase in the displacement. Critical values of the actuator time delay and measurement time delay have to be determined. Feedforward control can also be used for wind-excited structures. Critical values for the gain, actuator time delay, and measurement time delay determine the limits of effectiveness for this type of control.

Simulations are conducted for a single-degree-of-freedom system , a fixed-base multistory building, and a base-isolated multistory building.

Feedback and feedforward proportional control of the single-degree-of-freedom system under earthquake excitation is not effective. It is only slightly effective for a base-isolated multistory building. It is shown that regeneration can be achieved while under proportional control.

Although no original contribution is being claimed for linear quadratic (LQ) control, it provides a benchmark against which controllers for the regenerative electric actuator are evaluated. Since environmental disturbances are seldom known *a priori*, the regulator solution presented is used to search for the best closed-loop control law for structures subjected to unknown disturbances. This is done by determining the response of the controlled structure when subjected to some assumed disturbances. The best regulator is one which performs well for most of the assumed excitations and those excitations which closely resemble the actual disturbances.

The LQ controller is tested on a single-degree-of-freedom system and on a fixed-base and a base-isolated multistory building. Increasing the weight on the displacement produces a reduction in the displacement at the cost of increasing the control force and damper stroke. The LQ controller is shown to be effective for both wind and earthquake excitations. However, peak reduction seems to be a problem in earthquake-excited cases. Various criteria are suggested for choosing the weighting matrices.

To improve control efficiency, limits can be set on the control force to reduce stroke length without compromising the displacement response. The linear quadratic controller provides opportunity for regeneration. In some cases with sufficient duration of the excitation, there is even a net gain in the source energy

This study is the first of its kind to investigate the applicability of sliding mode control to civil structures, with special emphasis on the mitigation of wind- and earthquake-induced motion in tall buildings using regenerative electric actuators. The rationale for using sliding mode control is the fact that regenerative electric actuators use a form of on-off control based on pulse width modulation (PWM). Sliding mode control provides a synthesis of this on-off nature of PWM control and guarantees stability for the on-off control law. Furthermore, sliding mode control naturally fits the nonlinear, on-off nature of control force saturation which is always present in the active control of civil structures. Again, sliding mode provides a natural synthesis of the on-off nature of control force saturation and guarantees stability for the on-off control law.

Both linear and nonlinear models of the structure are considered in this study to assess the sliding mode controller's performance during disturbances. It is shown that the controller is

able to overcome sensitivity to structural parameter variations, particularly structural stiffness. Systematic procedures for the design of the sliding surface, using both pole-placement and quadratic-minimization methods, are presented together with simulation results obtained by using linear and nonlinear models of the structure. These controllers are also shown to be effective even in the presence of control force saturation. With sliding mode control, the regenerative electric actuator is able to recover energy and store it for later use. This reduces the net energy drawn from the supply by the actuator. In some cases, there is even a net gain in the energy of the supply.

A new direct-control scheme for neural network control of civil structures using regenerative electric actuators is proposed. This allows on-line control of the structure without the need for either an accurate model of the system or a specific learning stage. Unlike the controllers that have previously been considered, the neural network controller is able to address changes in system parameters and changes in the operating point and external disturbances. A modified backpropagation algorithm is used to train the neural network. Since the error at the output of the neural network controller will be unknown in the direct-control scheme, the error at the system output is instead backpropagated through the system by considering the system as an additional layer of the neural network. Simulations are conducted for wind and earthquake excitation using a two-layer network composed of neurons with tangent-sigmoid activation functions. It is shown that the controller can tolerate large variations in the input scaling factor, output gain factor, and maximum control force. It is also equally effective for both linear and nonlinear models of the structure.

A new on-line, direct-control scheme for active control of civil structures using an adaptive fuzzy controller is proposed. The advantage of using an adaptive fuzzy controller is that it does not require an accurate model of the system. The controller learns the system dynamics by adapting its parameters on-line. It is proposed that a modified gradient descent method be used as the adaptation mechanism. In order to adapt the parameters of the fuzzy system, the error at the output of the fuzzy controller must be known. In the proposed direct-control scheme, this error is unknown. Thus, it is proposed that the updating be based on the output error of the system directly. The update equations are derived for the controller. Simulations are performed for a structure with a regenerative electric actuator.

After investigating the feasibility of various controllers for application in structures with regenerative electric actuators, a comparison is made of the different controllers based on various criteria. The major factors that have to be considered when choosing a controller for the regenerative electric actuator include maximum displacement, stroke length, control force,

actuator power, and actuator energy. Control force saturation has to be considered to obtain the most effective type of control.

Based on the maximum displacement, stroke length, and control force, the proportional and sliding mode controllers provide the best control for the single-degree-of-freedom system under the given magnitude of wind excitation. For the same system under a given earthquake excitation, the sliding mode controller is able to provide the best control based on the maximum displacement, stroke, and control force.

Based on the maximum damper stroke and control force, the sliding mode controller provides the best control for multistory fixed-base system under wind excitation. If smaller interstory displacements are desired, then proportional control gives better results at the cost of larger control forces.

If the primary objective is to reduce the interstory drift in the multistory base-isolated system under earthquake excitation, then proportional control gives the most reduction in the peak displacement for the least control force. If the primary objective is to reduce the base displacement, then sliding mode control gives the best result at the cost of higher peaks in the control force.

For the single-degree-of-freedom system, choosing a controller based on the actuator power and energy requires a compromise between using smaller ratings for the actuator and recovering a larger amount of energy through regeneration.

Based on maximum power and energy of the regenerative actuator, sliding mode control is desirable for the fixed-base multistory system subjected to a wind disturbance. On the other hand, linear quadratic control is desirable for the base-isolated multistory system under an earthquake disturbance based on the maximum power and energy of the actuator.

For the single-degree-of-freedom system subjected to wind excitation, choosing a control force limit above 20 kN keeps the maximum displacement at or below 2.5 cm. If further reduction is desired, using a sliding mode controller will result in smaller peaks. The pole-placement can produce greater reduction in the peak displacement if a larger control force is available. If the same system is subjected to an earthquake excitation, choosing the control limit above 300 kN will keep the maximum displacement at or below 9 cm. If smaller peaks in the displacement is desired, sliding mode control can produce the desired effect. The pole-placement method can produce the largest reduction if larger control forces are available.

The final decision, when choosing a controller for the regenerative electric actuator, has to consider all of the above-mentioned factors. A compromise may be required if conflicting objectives have to be satisfied.

The actuator proposed for this study is a permanent-magnet brushless DC machine which can provide a higher instantaneous torque in a compact frame size. The actuator can either operate in the passive mode, 4-quadrant mode, or 2-quadrant generation mode. In the motoring mode, the performance of various controllers are compared based on the maximum displacement, stroke, control torque, actuator power, and source energy. It is desired that the controller require a smaller actuator power rating so that the cost of the machine will be lower. A lower actuator energy is also desired so that the capacity of the electrical source will be lower. Furthermore, a lower energy requirement means that a lower capacity for the energy storage device is needed. In majority of the test cases, sliding mode control often has the lowest power and energy requirement. The use of regenerative electric actuators reduce the required source capacity as compared to using non-regenerative actuators which simply dissipate energy as heat. The amount of reduction is often significant. This can translate to savings in equipment and maintenance costs. Single-degree-of-freedom and multidegree-of-freedom structures are simulated. In the regeneration mode, the system response must always fall within the safety margins for the structure. The amount of energy that can be recovered is limited by the power rating of the actuator and the energy capacity of the electrical source and energy storage device.

The dynamics of the electrical subsystem can be incorporated into the actuator-structure system to determine the transient behavior of the entire system. The equations of motion are derived for the combined system. In order to obtain a preliminary estimate of the system response, it is initially assumed that the commanded control T_e^* is also the actual control T_e. It is shown that this assumption is valid, due to the faster time constants of the electrical subsystem compared to those of the mechanical subsystem. This is one of the advantages of using an electrical actuator. More accurate models of the electrical source and storage device can also be included in the simulation to determine the variation of the voltage at the terminals of the source. In this study, the electrical source is modeled as an ideal voltage source in series with a source resistance.

The study shows that the use of regenerative electric actuators is a viable and a reliable alternative for active control of civil structures.

11.2 RECOMMENDATIONS FOR FUTURE WORK

The following are recommendations for possible investigation in future studies:

(1) Apply REA to multiple dampers in a single structure.

(2) Investigate the application of REA for structural motion in two-dimension.

(3) Consider other adaptation mechanisms for adaptive fuzzy control of REA.

(4) Investigate the applicability of other adaptive control methods for REA.

(5) Investigate the use of power capacitors, inductors, and other energy storage devices as alternative energy sources.

References

CHAPTER 2

[1] T. Kobori, "Technology development and forecast of Dynamic Intelligent Building (D.I.B.)," in *Intelligent Structures,* K. P. Chong, S. C. Liu, and J. C. Li (Eds.), London: Elsevier Applied Science, 1990, pp. 42-59.

[2] M. Sakamoto and T. Kobori, "Practical applications of active and hybrid response control systems," *Proceedings of the International Workshop on Structural Control,* Honolulu, Hawaii, August 1993, pp. 432-446.

[3] R. E. Klein and M. D. Healey, "Semi-active control of wind induced oscillations in structures," *Structural Control: Proceedings of the Second International Symposium on Structural Control,* Waterloo, Canada, July 15-17, 1985, pp. 354-369.

[4] J. J. Connor, Jr. and B. A. Klink, "A methodology for motion based design," *Proceedings of the First World Conference on Structural Control,* Vol. 3, Los Angeles, California, August 1994, pp. FA1-49 - FA1-58.

[5] T. Kobori, "State-of-the-art of seismic response control research in Japan," *Proceedings of the U.S. National Workshop in Structural Research,* Los Angeles, California, October 1990, pp. 1-21.

[6] M. D. Symans, M. C. Constantinou, D. P. Taylor, and K. D. Garnjost, "Semi-active fluid viscous dampers for seismic response control," *Proceedings of the First World Conference on Structural Control,* Vol. 3, Los Angeles, California, August 1994, pp. FA4-3 - FA4-12.

[7] H. Iemura *et al.*, "Comparison of passive, active and hybrid control techniques on earthquake response of flexural structures," *Proceedings of the U.S.-Italy-Japan Workshop/Symposium on Structural Control and Intelligent Systems,* Sorrento and Genoa, Italy, July 1992, pp.117-125.

[8] J. J. Connor Jr. and B. A. Klink, "A methodology for motion based design," *Proceedings of the First World Conference on Structural Control,* Vol. 3, Los Angeles, California, August 1994, pp. FA1-49 - FA1-58.

[9] S. Okamoto and Y. Kitagawa, "State-of-the-arts of Japanese structural control research and BRI roles in the future," *Proceedings of the International Workshop on Structural Control,* Honolulu, Hawaii, August 1993, pp.385-392.

[10] R. K. Miller *et al.*, "Active vibration control of large civil structures," *Journal of Engineering Mechanics,* ASCE, Vol. 114, No. 9, September 1988, pp.1542-1570.

[11] M. Q. Feng, "Application of hybrid sliding isolation system to buildings," *Journal of Engineering Mechanics,* ASCE, Vol. 119, No. 10, October 1993, pp.2090-2108.

[12] J. Rodellar, A. H. Barbat, and N. Molinares, "Response analysis of buildings with a new nonlinear base isolation system," *Proceedings of the First World Conference on Structural Control,* Vol. 2, Los Angeles, California, August 1994, pp. TP1-31 - TP1-40.

[13] J. N. Yang, A. Danielians, and S.C. Liu, "Aseismic hybrid control system for building structures under strong earthquake," in *Intelligent Structures,* K. P. Chong, S. C. Liu, and J. C. Li (Eds.), London: Elsevier Applied Science, 1990, pp.179-195.

[14] H. Kitamura *et al.*, "Structural response control technologies of Tansei Corporation," *Proceedings of the U.S. National Workshop on Structural Control Research*, Los Angeles, CA., October 25-26, 1990, pp. 141-150.

[15] S. Kawamura *et al.*, "Hybrid isolation system using friction-controllable sliding bearings," in *Intelligent Structures 2: Monitoring and Control*, Y.K. Wen (Ed.), London: Elsevier Applied Science, 1992, pp. 264-278.

[16] M. Q. Feng, "Application of hybrid isolation system to buildings," *Journal of Engineering Mechanics*, ASCE, Vol. 119, No. 110, October 1993, pp. 2090-2108.

[17] K. Seto, "Recent developments in Japan relevant to control theory and its application in structural control, *Proceedings of the International Workshop on Structural Control,* Honolulu, Hawaii, August 1993, pp.447-460.

[18] L. Petti, T. T. Soong, and B. Palazzo, "Hybrid mass dampers for structural control against wind and earthquakes," *Proceedings of the First World Conference on Structural Control,* Vol. 2, Los Angeles, California, August 1994, pp. TP1-110 - TP1-118.

[19] M. Izumi *et al.*, "Buildings with response control systems in Japan," *Proceedings of the International Workshop on Structural Control,* Honolulu, Hawaii, August 1993, pp.268-275.

[20] M. Setareh, "Use of the doubly-tuned mass dampers for passive vibration control," *Proceedings of the First World Conference on Structural Control,* Vol. 1, Los Angeles, California, August 1994, pp. WP4-12 - WP4-21.

[21] K. Maebayashi *et al.*, "Performance of a hybrid mass damper system implemented in a tall building," *Proceedings of the International Workshop on Structural Control,* Honolulu, Hawaii, August 1993, pp.318-328.

[22] M. Sakamoto and T. Kobori, "Practical applications of active and hybrid response control systems," *Proceedings of the International Workshop on Structural Control,* Honolulu, Hawaii, August 1993, pp.432-446.

[23] E. J. Nielsen *et al.*, "Viscoelastic damper overview for seismic and wind applications," *Proceedings of the First World Conference on Structural Control,* Vol. 3, Los Angeles, California, August 1994, pp.FP3-42 - FP3-51.

[24] T. T. Soong, "State-of-the-art of structural control in U.S.A.," *Proceedings of the U.S. National Workshop in Structural Research,* Los Angeles, California, October 1990, pp.48-65.

[25] Y. Fujino *et al.*, "Tuned liquid damper (TLD) for suppressing horizontal motion of structures," *Journal of Engineering Mechanics,* ASCE, Vol. 118, No. 10, October 1992, pp.2017-2030.

[26] A. Kareem, "The next generation of tuned liquid dampers," *Proceedings of the First World Conference on Structural Control,* Vol. 3, Los Angeles, California, August 1994, pp. FP5-19 - FP5-28.

[27] H. P. Gavin, D. S. Ortiz, and R. D. Hanson, "Testing and modeling of a proto-type ER damper for seismic structural response control," *Proceedings of the International Workshop on Structural Control,* Honolulu, Hawaii, August 1993, pp.166-180.

[28] D. P. Tomasula and J. Ghaboussi, "Gravity actuators in structural control," *Proceedings of the First World Conference on Structural Control,* Vol. 2, Los Angeles, California, August 1994, pp. TA1-50 - TA1-59.

[29] A.C. Nerves and R. Krishnan, "A strategy for active control of tall civil structures using regenerative electric actuators," *Proceedings of the 11th ASCE Engineering Mechanics Specialty Conference*, Ft. Lauderdale, FL, May 19-22, 1996, pp. 503-506.

CHAPTER 3

[1] M. Paz, *Structural Dynamics: Theory and Computation*, New York: Van Nostrand Reinhold Company, 1980.

[2] Y.K. Wen, "Methods of random vibration for inelastic structures," *Journal of Applied Mechanics Review,* Vol. 42, No. 2, Feb. 1989, pp. 39-52.

[3] J.C.H. Chang and T.T. Soong, "Structural control using active tuned mass dampers," *Journal of the Engineering Mechanics Division, Proceedings of the American Society of Civil Engineers,* Vol. 106, No. EM6, Dec. 1980, pp. 1091-1098.

CHAPTER 5

[1] D.E. Kirk, *Optimal Control Theory*, Englewood Cliffs, NJ: Prentice-Hall, Inc., 1970.

[2] T.T. Soong, *Active Structural Control: Theory and Practice*, New York, NY: Longman Scientific and Technical, 1990.

[3] B.D.O. Anderson and J.B. Moore, *Optimal Control: Linear Quadratic Methods*, Englewood Cliffs, NJ: Prentice Hall, 1990.

[4] J.N. Yang, "Application of optimal control theory to civil engineering structures," *Journal of the Engineering Mechanics Division*, ASCE, Vol. 101, No. EM6, December 1975, pp. 819-838.

[5] F.Y. Cheng, C.K. Choi, and D.S. Juang, "Developments of optimum design and control of seismic structures," in *Intelligent Structures*, K.P. Chong, S.C. Liu, and J.C. Li (Eds.), London: Elsevier Applied Science, 1990, pp. 264-281.

[5] W.K. Belvin and K.C. Park, "Structural tailoring and feedback control synthesis: an interdisciplinary approach," *Journal of Guidance, Control, and Dynamics*, AIAA, Vol. 13, No. 3, May-June 1990, pp. 424-429.

[7] T.T. Soong *et al.*, "Full-scale implementation of active control I: design and simulation," *Journal of Structural Engineering*, ASCE, Vol. 117, No. 11, November 1991, pp. 3516-3536.

[8] N. Kurata *et al.*, "Shaking table experiment of active variable damping system," *Proceedings of the First World Conference on Structural Control*, Los Angeles, CA, August 3-5, 1994, pp. TP2-108 - TP2-127.

[9] J.N. Yang, A. Akbarpour, and P. Ghaemmaghami, "New optimal control algorithms for structural control," *J. Engineering Mechanics*, ASCE, Vol. 113, No. 9, September 1987, pp. 1369-1386.

CHAPTER 6

[1] R.A. DeCarlo, S.H. Zak, and G.P. Mathews, "Variable structure control of nonlinear multivariable systems: a tutorial," *Proceedings of the IEEE*, Vol. 76, No. 3, March 1988, pp. 212-232.

[2] R. Krishnan *et al.*, "Active Control of Structures using Sliding Mode Control Techniques with Regenerative Electric Actuator," NSF Grant No. BDS-9301574, October 1991.

[3] R. Krishnan, M.P. Singh, and A.C. Nerves, "Mitigation of wind and earthquake effects on structures by sliding mode control," *Proceedings of the First World Conference on Structural Control*, Vol. 1, Los Angeles, CA, August 3-5, 1994, pp. WA2-13-WA2-22.

[4] V.I. Utkin, *Sliding Modes in Control and Optimization*, Berlin: Springer-Verlag, 1992.

[5] J.N. Yang, Z. Li, and J.C. Wu, "A discontinuous control method for civil engineering structures," *Proceedings of the 9th VPI&SU Symposium on Dynamics and Control of Large Structures*, Blacksburg, VA., 1993, pp. 167-180.

[6] J.N. Yang, Z. Li, and J.C. Wu, "Discontinuous nonlinear control of base-isolated buildings," *Proceedings of the International Workshop on Structural Control*, USC, Los Angeles, CA, 1993, pp. 551-563.

[7] M.P. Singh, E.E. Matheu, and K. Ramu, "Active structural control of seismic effects: limitations and potential,"

[8] F.X. Zhou and D.G. Fisher, "Continuous sliding mode," *International Journal of Control*, Vol. 55, No. 2, 1992, pp. 313-327.

[9] J.N. Yang, A.K. Agrawal, and J.C. Wu, "Sliding mode control for structures subjected to seismic loads," *Proceedings of the First World Conference on Structural Control*, Los Angeles, CA, August 3-5, 1994, pp. WA1-13-WA1-22.

[10] J.N. Yang, J.C. Wu, and A.K. Agrawal, "Sliding mode control for nonlinear and hysteretic structures," *Journal of Engineering Mechanics*, ASCE, Vol. 121, No. 12, December 1995, pp. 1330-1339.

[11] J.N. Yang, J.C. Wu, and A.K. Agrawal, "Sliding mode control for seismically excited linear structures," *Journal of Engineering Mechanics*," ASCE, Vol. 121, No. 12, December 1995, pp. 1386-1390.

[12] J.N. Yang *et al.*, "Experimental verification of Hoo and sliding mode control for seismically excited buildings," *Journal of Structural Engineering*, ASCE, Vol. 122, No. 1, January 1996.

[13] J.N. Yang *et al.*, "Control of sliding-isolated building using sliding mode control," *Journal of Structural Engineering*, ASCE, Vol. 122, No. 2, February 1996.

[14] V.I. Utkin, "Variable structure systems with sliding modes," *IEEE Transactions on Automatic Control*, Vol. AC-22, No. 2, April 1977, pp. 212-222

[15] V.I. Utkin, *Sliding Modes in Control and Optimization*, Berlin: Springer-Verlag, 1992.

[16] W. Gao and J.C. Hung, "Variable structure control of nonlinear systems: a new approach," *IEEE Trans. Industrial Electronics*, Vol. 40, No. 1, February 1993, pp. 45-55.

[17] A.S.I. Zinober (ed.), *Variable Structure and Lyapunov Control*, London: Springer-Verlag, 1994.

[18] V.I. Utkin and K.D. Yang, "Methods for constructing discontinuity planes in multidimensional variable structure systems," *Automation and Remote Control*, Vol. 39, No. 10, 1978, pp. 1466-1470.

[19] C.M. Dorling and A.S.I. Zinober, "Two approaches to hyperplane design in multivariable variable structure control systems," *International Journal of Control*, Vol. 44, No. 1, 1986, pp. 65-82.

[20] K.K.D. Young *et al.*, "Asymptotic stability of model reference systems with variable structure control," *IEEE Transactions on Automatic Control*, Vol. AC-21, 1977, pp. 279-281.

[21] V.I. Utkin, *Sliding Modes and Their Application in Variable Structure Systems*, Moscow: Mir Publishers, 1978.

CHAPTER 7

[1] W.H. Schifman and H.W. Geffers, "Adaptive control of dynamic systems by back propagation networks," *Neural Networks*, Vol. 6, 1993, pp. 517-524.

[2] Y.K. Wen *et al.*, "Control of structures using neural networks," *Proc. U.S.-Italy-Japan Workshop/Symp. on Structural Control and Intelligent Systems*, Sorrento, Italy, July 12-15, 1992, pp. 232-251.

[3] J. Ghaboussi and A. Joghataie, "Active control of structures using neural networks," *J. Engineering Mechanics*, ASCE, Vol. 121, No. 4, April 1995, pp. 555-567.

[4] A.C. Nerves and R. Krishnan, "Active control of wind-induced vibrations in tall buildings using neural networks," *Proc. IEEE Conference on Industrial Electronics, Control, and Instrumentation (IECON'94)*, Bologna, Italy, September 5-9, 1994, pp. 1292-1297.

[5] A.C. Nerves, R. Krishnan, and M.P. Singh, "Modeling, simulation, and analysis of active control of structures with nonlinearities using neural networks," *Proc. 10th ASCE Engineering Mechanics Conference*, Vol. 2, Boulder, CO, May 21-24, 1995, pp.1054-1057.

[6] V.C. Chen and Y.H. Pao, "Learning control with neural networks," *Proc. IEEE International Conference on Robotics and Automation*, Vol. 3, 1989, pp.1448-1453.

[7] M.A. Waddoups and K.L. Moore, "Neural networks for iterative learning control," *Proc. American Control Conference*, Vol. 4, Chicago, IL, June 1992, pp. 3049-3051.

[8] D. Psaltis, A. Sideris, and A.A. Yamamura, "A multilayered neural network controller," *IEEE Control Systems Magazine*, Vol. 8, No. 2, April 1988, pp.17-21.

[9] D.H. Nguyen and B. Widrow, "Neural networks for self-learning control systems," *IEEE Control Systems Magazine*, April 1990, pp. 18-23.

[10] D.E. Rumelhart, G.E. Hinton, and R.J. Williams, "Learning internal representations by error propagation," in *Parallel Distributed Processing, Vol 1: Foundations*, Cambridge, MA: MIT Press, 1986.

[11] K.P. Venugopal, A.S. Pandya, and R. Sudhakar, "A recurrent neural network controller and learning algorithm for the on-line learning control of autonomous underwater vehicles," *Neural Networks*, Vol. 7, No. 5, 1994, pp. 833-846.

[12] K.P. Venugopal, R. Sudhakar, and A.S. Pandya, "On-line learning control of autonomous underwater vehicles using feedforward neural networks," *IEEE Journal of Oceanic Engineering*, Vol. 17, No. 4, October 1992, pp. 308-319.

CHAPTER 8

[1] L.X. Wang, *Adaptive Fuzzy Systems and Control*, Englewood Cliffs, NJ: PTR Prentice Hall Inc., 1994.

[2] M. Yamada *et al.*, "Active vibration control using fuzzy theory," *Proc. First World Conf. on Structural Control*, Los Angeles, CA, August 3-5,1994, pp. WP1-13-WP1-20 (Part 2) and WP1-41-WP1-48 (Part1).

[3] M. Iiba *et al.*, "Shaking table test on seismic response control system by fuzzy optimal logic," *Proc. First World Conf. on Structural Control*, Los Angeles, CA, August 3-5,1994, pp. WP1-69-WP1-77.

[4] L. Sun and Y. Goto, "Application of fuzzy theory to variable dampers for bridge vibration control," *Proc. First World Conf. on Structural Control*, Los Angeles, CA, August 3-5,1994, pp. WP1-31-WP1-40.

[5] H. Furuta *et al.*, "Application of genetic algorithms to self-tuning of fuzzy active control for structural vibration," *Proc. First World Conf. on Structural Control*, Los Angeles, CA, August 3-5,1994, pp. WP1-3-WP1-12.

[6] A. Joghataie and J. Ghaboussi, "Neural networks and fuzzy logic in structural control," *Proc. First World Conf. on Structural Control*, Los Angeles, CA, August 3-5,1994, pp. WP1-21-WP1-30.

[7] L. Faravelli and T. Yao, "Application of an adaptive-network-based fuzzy inference system (ANFIS) to active structural control," *Proc. First World Conf. on Structural Control*, Los Angeles, CA, August 3-5,1994, pp. WP1-49-WP1-58.

[8] N. Tripathi, A. Nerves, H. VanLandingham, and R. Krishnan, "An adaptive fuzzy controller for dampening wind-induced building oscillations," *Proc. 10th VPI&SU Symp. on Structural Dynamics and Control*, Blacksburg, VA., May 8-10, 1995.

[9] D. Driankov, H. Hellendorn, and R. Reinfrank, *An Introduction to Fuzzy Control*, Berlin: Springer-Verlag, 1993.

[10] L.X. Wang, *A Course in Fuzzy Systems and Control*, Upper Saddle River, NJ: Prentice Hall PTR, 1997.

[11] D. Psaltis, A. Sideris, and A.A. Yamamura, "A multilayered neural network controller," *IEEE Control Systems Magazine*, Vol. 8, No. 2, April 1988, pp.17-21.

CHAPTER 10

[1] AC. Nerves and R. Krishnan, "A strategy for active control of tall civil structures using regenerative electric actuators," *Proc. 11th Engineering Mechanics Conf.*, ASCE, Y.K. Lin and T.C. Su (Eds.), Ft. Lauderdale, FL, May 19-22, 1996, pp. 503-506.

[2] R. Krishnan, *Electronic Control of Machines*, A book to be published by Prentice-Hall.

Vita

Allan C. Nerves was born in Cebu City, Philippines on August 5, 1961. He received his B.S. degree in electrical engineering and M.S. degree in electrical engineering from the University of the Philippines in 1982 and 1988, respectively.

He joined the Department of Electrical and Electronics Engineering, University of the Philippines, as an Instructor in 1982. He is presently an Assistant Professor in the same department. He has worked in various consulting positions in the National Engineering Center, University of the Philippines. His research interests include electrical machines, motion control, and power systems.

Mr. Nerves is a registered Professional Electrical Engineer in the Republic of the Philippines.